

Johannes Hofer, BSc.

Fluorescence- and Reflection Spectroscopy of Industrially Relevant Minerals for Automatic Sensor Based Sorting Applications

DIPLOMA THESIS

For the academic degree of a Master of Science

granted at the

Graz University of Technology

in cooperation with BINDER + Co AG

Supervisor:

Ao. Univ.-Prof. Dr. Karl GATTERER

Institute of Physical and Theoretical Chemistry

Graz University of Graz

2012

To my family.

Abstract

In the present work reflection- and fluorescence spectra of industrially relevant minerals were recorded and interpreted. Reflection spectra were measured with the Lambda 950 system of Perkin Elmer. The first and second derivatives of the spectra can be used to find spectral features which allow a classification of the materials in optical sorting. As sample set for reflection spectra Bauxite, Magnesite, Talc, Fluorite, Calcite, Chalcedony and Barite were chosen. For all chosen samples reflection data of good quality were obtained.

The measurement of fluorescence emission spectra with the LS 55 system of Perkin Elmer turned out to be more difficult. Because of the fact, that there is a certain pulse to pause ratio of the excitation source, a Xe-flashlamp and many internal data processing steps more operator knowledge is required. As sample set for the fluorescence emission spectra Fluorite, Calcite, Magnesite, Chalcedony, Silicon, CAB 15¹ and a commercially available lead doped glass (referred to as PbO reference glass 1) were chosen.

The illumination situation in the LS 55 instrument was investigated and compared to industrial laser illumination technologies. A semi-quantitative approach for comparing emission intensities of different samples is proposed and compared to a reference system for absolute Quantum Yield detection (Hamamatsu Quantaaurus).

Furthermore a short overview of possible reflection and fluorescence databases on minerals available in the internet, literature on fluorescence of minerals and a short theoretical introduction to the field of solid state chemistry and solid state spectroscopy of minerals and solids are provided.

Zusammenfassung

In der vorliegenden Arbeit wurden Reflektions- und Fluoreszenzspektren von Industriemineralien gemessen und interpretiert. Die Reflektionsspektren konnten leicht mit dem Lambda 950 Reflektionsspektrometer von Perkin Elmer aufgezeichnet werden. Mit Hilfe der ersten und zweiten Ableitungen der Rohspektren konnten einige spektrale Eigenschaften zur Unterscheidung der Mineralien gefunden werden, die ein optisches Sortieren ermöglichen. Als Auswahl an Industriemineralien wurden Bauxit, Magnesit, Talk, Fluorit, Calcit, Chalcedon und Barit verwendet. Für all diese Proben konnten Reflektionsdaten in guter Qualität erhalten werden.

Die Fluoreszenzmessung mit dem LS 55 von Perkin Elmer an den ausgewählten Proben stellte sich als etwas problematischer heraus. Das Puls- zu Pause Verhältnis der Xe-Blitzlampe und geräteinterne Datenprozessierungsschritte müssen bei den Messungen berücksichtigt werden. Fluorit, Calcit, Magnesit, Chalzedon, Silizium, CAB 15² und ein handelsübliches Bleiglas wurden als Proben für die Fluoreszenzmessung verwendet.

Die Beleuchtungsverhältnisse im LS 55 wurden untersucht und mit industrieller Lasertechnologie verglichen. Für den Vergleich der relativen Fluoreszenzintensitäten verschiedener Proben wurde eine semiquantitative Methode vorgeschlagen und mit Ergebnissen einer absoluten Quantenausbeutemessung (Hamamatsu Quantaaurus) verglichen.

Einige im Internet zugängliche Fluoreszenz- und Reflektionsdatenbanken für Mineralien, Literatur zur Mineralienfluoreszenz und eine kurze theoretische Einleitung zu Festkörperchemie und Festkörperspektroskopie an Mineralien anderen Festkörpern sind in der Arbeit zu finden.

¹ CAB 15 is an artificial lead doped calcium aluminum borate glass

² CAB 15 ist ein künstlich hergestelltes mit Blei dotiertes Calcium-Aluminium-Boratglas

Acknowledgements

First of all I want to thank my university advisor Prof. Dr. Karl Gatterer who guided me along this work. Special thanks go to DI Reinhold Huber from the Binder + Co Company who funded the research project.

I also want to thank my partner MA Stéphanie Lüders who always supported me in my studies and helped me with the corrections of the present work and former drafts.

Thanks go to my parents Rosemarie Hofer and Eduard Hofer as well as my brother Manfred Hofer who funded my studies of Technical Chemistry.

Furthermore I want to thank all the personal of the R & D department of the Binder + Co company for their interest in my work. Special thanks go to Ing. Rainer Eixelberger for his introduction to NIR-sensors, Ing. Karl Leitner for detailed information on the illumination situation in optical sorters manufactured by Binder, DI(FH) Reinhard Taucher for special advise on sample systematization and an introduction to the system of optical sorters.

Thank goes to my colleague Georg Weingrill, BSc. from MUL for providing the samples and mineralogical information as well as he Raman-data on the samples for the ongoing project.

The department of Physical and Theoretical Chemistry of the Graz University of Technology provided me a good basement for this interesting work. Special thanks go to Ing. Helmut Eisenkölbl, Herbert Lang and Hilde Freißmuth for continuous support and advice in technical, chemical and practical difficulties of all kinds. Furthermore I want to thank Prof. Günter Grampp for his constructive input on solid state sample positioning in the LS 55 and Prof. Stephan Landgraf for discussions on absolute fluorescence measurements.

I want to thank my colleagues Michael Scherzer, BSc for his fruitful discussions on the method development for solid state fluorescence and Daniel Schloffer, Bsc. for the interest in my work and constructive input in method development during his project laboratory.

Furthermore I want to thank my colleagues Nina Schrödl, BSc. and DI Christian Zelger for continuous support and friendship throughout the studies.

Thanks go to Dr. Ivo Stemmler and Ing. Thomas Schumacher from Perkin Elmer for support services for the L950 and the LS 55 system. I also want to thank Peter Senne from Biolab for his flexibility concerning software issues and trouble shooting.

I also want to thank Dr. Alexander Kiel from Hamamatsu for his measurements on my samples with the Quantaurus QY system and fruitful discussions.

Last but not least I want to thank Dr. Stuart Huckins from Qiagen Germany for his crucial input concerning method development for the LS 55 solid state phosphorescence method.

STATUTORY DECLARATION

I declare that I have authored this thesis independently, that I have not used other than the declared sources/resources, and that I have explicitly marked all material which has been quoted either literally or by content from the used sources.

.....
Graz, date

.....
signature

EIDESSTATTLICHE ERKLÄRUNG

Ich erkläre an Eides statt, dass ich die vorliegende Arbeit selbstständig verfasst, andere als die angegebenen Quellen/Hilfsmittel nicht benutzt, und die den benutzten Quellen wörtlich und inhaltlich entnommene Stellen als solche kenntlich gemacht habe

.....
Graz, am

.....
Unterschrift

Table of Contents

1	INTRODUCTION	15
1.1	Background	15
1.2	Sorting and Beneficiation Technologies	16
1.3	Mineral and Glass Sorting	17
1.4	Minerals	18
1.4.1	Origin and Definitions	18
1.4.2	Chemical Properties, Symmetry and Classification according to Strunz	19
1.5	Solid State Spectroscopy	24
1.5.1	General Introduction	24
1.5.1.1	Quantum mechanical basics and overview on techniques	24
1.5.1.2	Vibrational Spectroscopy and Symmetry Considerations	27
1.5.1.3	Crystal field spectroscopy	32
1.5.1.4	Anharmonic Oscillator and IR-spectra	38
1.5.2	Reflection Spectroscopy with the L950 on Minerals	40
1.5.3	Raman Spectroscopy of Minerals	46
1.5.4	Fluorescence Spectroscopy and Sorting of Minerals	48
1.5.4.1	From Molecular Fluorescence to Solid State Fluorescence	48
1.5.4.2	Mineral Fluorescence	52
1.5.5	The LS 55 – a lab-scale spectrofluorimeter	57
1.6	Spectral Databases	59
1.6.1	Fluorescence databases	60
1.6.2	Reflectance spectroscopy databases	61
1.6.3	Assessment of the Databases	62
2	MATERIALS AND METHODS	64
2.1	Sample Preparation	64
2.2	Reflection Measurement of Minerals	65
2.2.1	Measurement Procedure	65
2.3	Fluorescence Measurements of Minerals	66
2.3.1	Method Development and Measurement Procedure	66
2.4	Illumination situation in the LS 55	69
2.4.1	Fundamentals	69

2.4.2	Manuals and Quotes	72
2.4.3	Xe-flash lamp and the detector	73
2.4.3.1	The lamp	73
2.4.3.2	R955 detector	76
2.4.4	Testo 545 measurements: VIS	77
2.4.5	UVC intensity measurements	84
2.4.6	Actinometer measurements	86
2.4.7	Comparison to other illumination techniques	92
3	RESULTS AND DISCUSSION	94
3.1	Reflection Spectra and Interpretation	94
3.1.1	Bauxite	95
3.1.2	Magnesite	96
3.1.3	Talc	97
3.1.4	Fluorite	98
3.1.5	Calcite	100
3.1.6	Chalcedony	101
3.1.7	Barite	102
3.1.8	Discrimination of minerals via the reflection spectrum	104
3.2	Fluorescence Measurements	109
3.2.1	Parameter Dependence of Intensities	109
3.2.2	Emission Correction Functions	113
3.2.3	Spectra of Minerals and Glasses with Interpretation	121
3.2.3.1	Fluorite – Luminescence Spectra	125
3.2.3.2	Calcite – Luminescence Spectra	129
3.2.3.3	Magnesite – Luminescence Spectra	133
3.2.3.4	Chalcedony – Luminescence Spectra	137
3.2.3.5	Silicon – Luminescence Spectra	141
3.2.3.6	CAB 15 – Luminescence Spectra	145
3.2.3.7	PbO reference glass 1 – Luminescence Spectra	149
3.2.4	Decay curves	153
4	CONCLUSION	155
5	LITERATURE	156
6	APPENDIX	166
6.1	Emission Correction function for the LS 55 with R955 PMT	166

List of figures

FIGURE 1: 14 BRAVAIS LATTICES [126]	20
FIGURE 2: THE ELECTROMAGNETIC SPECTRUM [31]	24
FIGURE 3: ENERGY LEVELS OF A DIATOMIC MOLECULE [37, 74]	27
FIGURE 4: FLOW CHART TO FIND THE PROPER POINT GROUP FOR A MOLECULAR STRUCTURE [46,47]	30
FIGURE 5: D-ORBITALS IN AN OCTAHEDRAL CRYSTAL FIELD [49]	32
FIGURE 6: ENERGY LEVEL SPLITTING OF THE FIVE DEGENERATE STATES OF A D-ELECTRON IN AN OCTAHEDRAL CRYSTAL FIELD [49]	33
FIGURE 7: NOTATION AND ORIGIN OF THE SPLITTINGS OF ENERGY LEVELS IN ATOMS AND IONS [53]	35
FIGURE 8: ORBITAL GRAPHS FOR THE D^5 AND D^6 CONFIGURATION OF Fe^{3+} AND Fe^{2+} , RESPECTIVELY	36
FIGURE 9: TANABE SUGANO DIAGRAMS FOR TWO D-ELECTRON SYSTEMS IN OCTAHEDRAL SYMMETRY (FOR CONVENIENCE THE "G" INDEX IS NOT WRITTEN – ALL STATES ARISING FROM D-SYSTEMS ARE G)	37
FIGURE 10: POTENTIAL CURVE FOR A HARMONIC (GREEN) AND AN ANHARMONIC (BLUE) OSCILLATOR [59]	38
FIGURE 11: THE OPTICAL SYSTEM OF THE L950 SPECTROMETER [63]	40
FIGURE 12: A) THE L950 SPECTROMETER, B) THE INTEGRATING SPHERE DETECTOR MODULE, C) A BAUXITE SAMPLE AT THE DIFFUSE REFLECTION PORT OF THE INTEGRATING SPHERE, D) THE PMT-DETECTOR FOR UV-VIS-DETECTION (LEFT) AND THE INGAAS-DETECTOR FOR NIR-DETECTION (RIGHT)	41
FIGURE 13: INTERACTION OF LIGHT WITH A SAMPLE [66]	42
FIGURE 14: SPECTRALON REFLECTION SPECTRUM [128]	43
FIGURE 15: SAMPLE POSITIONING AT THE L950 INTEGRATING SPHERE REFLECTION PORT A) WITH THE ORIGINAL HOLDER, B) WITH TAPE USING A TEFLON APERTURE WITH 8 MM HOLE DIAMETER	43
FIGURE 16: SCHEMATIC DIAGRAM OF THE CONTROL WINDOW OF UV-WINLAB	44
FIGURE 17: HO-OXIDE REFLECTION SPECTRUM WITH AND WITHOUT PROPER WARM UP TIME AND GAIN SETTINGS	45
FIGURE 18: A) EXAMPLE RAMAN SPECTRUM, B) ENERGY LEVEL SCHEME FOR ELASTIC RAYLEIGH SCATTERING AND INELASTIC ANTI-STOKES AND STOKES RAMAN SCATTERING, C) BASIC SETUP OF A RAMAN SPECTROMETER [129]	46
FIGURE 19: RAMAN SPECTROMETER AT THE MUL: A) RAMAN WORKPLACE, B) SAMPLE POSITIONED IN THE APPARATUS, C) RAMAN SPECTROMETER AT WORK WITH THE GREEN LASER LIGHT SOURCE.	47
FIGURE 20: A) MECHANISM OF PHOSPHORESCENCE AND FLUORESCENCE. THE CRUCIAL FEATURE FOR PHOSPHORESCENCE IS THE INTERSYSTEM CROSSING (ISC) AS A CHANGE FROM SINGLET TO TRIPLET STATE, WHICH IS POSSIBLE BECAUSE OF THE SPIN ORBIT COUPLING. B) JABLONSKI DIAGRAM [130]	49
FIGURE 21: A) BREATHING MODE OF AN OCTAHEDRON [133], B) A DIATOMIC OSILLATOR	49
FIGURE 22: COMBINED DIAGRAM FOR THE SYSTEM Cr^{3+} IN OCTAHEDRAL CRYSTAL FIELD [132]	50
FIGURE 23: ABSORPTION AND EMISSION SPECTRUM OF RUBY (Cr^{3+} IN Al_2O_3) [132]	51
FIGURE 24: DIEKE DIAGRAM FOR RARE EARTH IONS IN CRYSTALS [134]	56
FIGURE 25: A) THE LS 55, B) SOLID SAMPLE HOLDER OF THE LS 55 WITH A FLUORITE SAMPLE MOUNTED	57
FIGURE 26: OPTICAL LAYOUT OF THE LS 55 [135]	58
FIGURE 27: A) POLISHING DEVICE TUG, B) CUTTING MACHINE TUG, C) POLISHING PLACE MUL AND D) CUTTING MACHINE MUL	64
FIGURE 28: ELECTRONICS DIAGRAM FOR THE LS 55 [136]	66
FIGURE 29: DATA HANDLING DIAGRAM	67
FIGURE 30: MEASUREMENT SCHEME OF THE LS 55 (NOT TO SCALE)	68

FIGURE 31: SPECTRAL BRIGHTNESS SENSITIVITY $V(\lambda)$ AS A FUNCTION OF THE WAVELENGTH IN NM; A) LINEAR PRESENTATION B) LOGARITHMIC PRESENTATION [1]	70
FIGURE 32: SPECTRAL OUTPUT OF A CONTINUOUS XE ARC LAMP AND XE FLASH LAMP [109]	74
FIGURE 33: EMISSION SPECTRA FOR THE UV-LAMP NU-4 KL FOR SETTING OF LAMP TO A) 254 NM AND B) 366 NM	74
FIGURE 34: EMISSION SPECTRUM OF A LOW PRESSURE HG-AR-LAMP [111]	75
FIGURE 35: TYPICAL SPECTRAL RESPONSE FOR R928- AND R955-PMT [112]	76
FIGURE 36: MEASUREMENT SURFACE OF TESTO 545 IN THE LS 55	77
FIGURE 37: ILLUMINANCE VALUES FOR SEVERAL SLIT WIDTHS (IN NM) AND WAVELENGTHS AT THE MEASUREMENT SPOT OF LS 55	78
FIGURE 38: ILLUMINANCE VALUES FOR SEVERAL SLIT WIDTHS AT 550 NM	78
FIGURE 39: ILLUMINANCE VALUES FOR THE LS 55 AT REFLECTION POSITION OF THE EXCITATION MONOCHROMATOR	80
FIGURE 40: TESTO 545 RESULTS IN IRRADIANCE	83
FIGURE 41: A) THE UV-LAMP NU-4 KL, B) UVM CP RADIOMETER, C) EXPERIMENTAL SETUP	84
FIGURE 42: IRRADIANCE VS. DISTANCE TO A 4 W UV-LAMP SET AT 254 NM EMISSION WAVELENGTH	85
FIGURE 43: ABSORBANCE OF A) THE ORIGINAL AND B) THE ILLUMINATED ACTINOMETER SOLUTION	87
FIGURE 44: ABSORBANCE VALUES AFTER CORRECTION FOR THE ACTINOMETER EXPERIMENT	88
FIGURE 45: IRRADIANCE VS. SLIT WIDTH	91
FIGURE 46: BAUXITE SAMPLE	95
FIGURE 47: BAUXITE REFLECTION SPECTRUM	95
FIGURE 48: MAGNESITE SAMPLE	96
FIGURE 49: MAGNESITE REFLECTION SPECTRUM	97
FIGURE 50: TALC SAMPLE	97
FIGURE 51: TALC REFLECTION SPECTRUM	98
FIGURE 52: FLUORITE SAMPLE	99
FIGURE 53: FLUORITE REFLECTION SPECTRUM	99
FIGURE 54: CALCITE SAMPLE	100
FIGURE 55: CALCITE REFLECTION SPECTRUM	100
FIGURE 56: CHALCEDONY SAMPLE	101
FIGURE 57: CHALCEDONY REFLECTION SPECTRUM	102
FIGURE 58: BARITE SAMPLE	102
FIGURE 59: BARYT REFLECTION SPECTRUM	103
FIGURE 60: REFLECTION SPECTRA OF 7 MINERALS	104
FIGURE 61: REFLECTION SPECTRA OF 7 MINERALS – 1 ST DERIVATIVE	105
FIGURE 62: REFLECTION SPECTRA OF 7 MINERALS – 2 ND DERIVATIVE	105
FIGURE 63: UV-VIS – REFLECTION SPECTRA OF 7 MINERALS – RAW DATA	106
FIGURE 64: UV-VIS REFLECTION SPECTRA OF 7 MINERALS	106
FIGURE 65: UV-VIS REFLECTION SPECTRA OF 7 MINERALS – 2 ND DERIVATIVE	107
FIGURE 66: NIR REFLECTION SPECTRA OF 7 MINERALS – RAW DATA	107
FIGURE 67: NIR REFLECTION SPECTRA OF 7 MINERALS – 1 ST DERIVATIVE	108
FIGURE 68: NIR REFLECTION SPECTRA OF 7 MINERALS – 2 ND DERIVATIVE	108
FIGURE 69: EMISSION SPECTRA FOR FLUORITE AT DIFFERENT EMISSION SLIT SETTINGS (IN NM)	110
FIGURE 70: OBSERVED AND FITTED PEAK HEIGHT VS. EMISSION SLIT WIDTH RELATION	110
FIGURE 71: RELATIVE FLUORESCENCE INTENSITY SCALE WITH SOME EXAMPLES	112
FIGURE 72: SAMPLES FOR THE COMPARISON OF LUMINESCENCE INTENSITIES UNDER 254 NM EXCITATION: A) CALCITE, B) CHALCEDONY, C) MAGNESITE, D) FLUORITE, E) PBO REFERENCE GLASS 1, F) CAB 15, G) SILICON	112

FIGURE 73: OVERVIEW OF THE EXPERIMENTAL PROCEDURE ACCORDING TO BAM [72]	114
FIGURE 74: BAM-F001 TWISTED AND NON-TWISTED EMISSION SPECTRA	116
FIGURE 75: : A) ZERO DEGREE POSITION – TOP VIEW; B) ZERO DEGREE POSITION – SIDE VIEW; C) TWISTED POSITION – TOP VIEW; D) TWISTED POSITION – SIDE VIEW	116
FIGURE 76: BAM STANDARDS UNDER UV LAMP NU-4 KL	117
FIGURE 77: TECHNICAL EMISSION SPECTRA FOR THE BAM STANDARDS IN SETTING A)	118
FIGURE 78: TECHNICAL EMISSION SPECTRA FOR THE BAM STANDARDS IN SETTING B)	118
FIGURE 79: COMPARISON OF AVAILABLE DETECTION FUNCTIONS FROM THE CALIBRATION EXPERIMENT	119
FIGURE 80: RESULTING CORRECTION FUNCTION OF CALIBRATION EXPERIMENTS	120
FIGURE 81: XRF ANALYZER CALIBRATED WITH LEAD CRYSTAL OF KNOWN PBO-CONTENT	121
FIGURE 82: SAMPLES FOR THE RECORDING OF LUMINESCENCE SPECTRA A) UNDER WHITE LIGHT B) UNDER 15W EXCITATION WITH LIGHT OF 254 NM AT A DISTANCE OF ABOUT 10 CM: 1) CALCITE, 2) CHALCEDONY, 3) MAGNESITE, 4) FLUORITE, 5) PBO REFERENCE GLASS 1, 6) CAB 15, 7) SILICON	122
FIGURE 83: EMISSION SPECTRUM FOR FLUORIT AT EXCITATION WAVELENGTH OF 254 NM A) WITH SECOND ORDER ARTIFACTS, B) WITHOUT SECOND ORDER ARTIFACTS	123
FIGURE 84: TRANSMISSION CURVE OF WG 320	124
FIGURE 85: FLUORESCENCE EMISSION SPECTRUM OF MAGNESITE WITH AND WITHOUT A CUT OFF FILTER	124
FIGURE 86: FLUORITE FLUORESCENCE EMISSION SPECTRA	125
FIGURE 87: FLUORITE PHOSPHORESCENCE EMISSION SPECTRA	126
FIGURE 88: FLUORITE FLUORESCENCE 3D SPECTRA	127
FIGURE 89: FLUORITE PHOSPHORESCENCE 3D SPECTRA	128
FIGURE 90: CALCITE FLUORESCENCE EMISSION SPECTRA	129
FIGURE 91: CALCITE PHOSPHORESCENCE EMISSION SPECTRUM	130
FIGURE 92: CALCITE FLUORESCENCE 3D DATA	131
FIGURE 93: CALCITE PHOSPHORESCENCE 3D SPECTRA	132
FIGURE 94: MAGNESITE FLUORESCENCE EMISSION SPECTRA	133
FIGURE 95: MAGNESITE PHOSPHORESCENCE EMISSION SPECTRA	134
FIGURE 96: MAGNESITE FLUORESCENCE 3D SPECTRA	135
FIGURE 97: MAGNESITE PHOSPHORESCENCE 3D SPECTRA	136
FIGURE 98: CHALCEDONY FLUORESCENCE EMISSION SPECTRA	137
FIGURE 99: CHALCEDONY PHOSPHORESCENCE EMISSION SPECTRA	138
FIGURE 100: CHALCEDONY PHOSPHORESCENCE 3D SPECTRA	139
FIGURE 101: CHALCEDONY PHOSPHORESCENCE 3D SPECTRA	140
FIGURE 102: SI SAMPLE FLUORESCENCE EMISSION SPECTRA	141
FIGURE 103: SI SAMPLE PHOSPHORESCENCE EMISSION SPECTRA	142
FIGURE 104: SI SAMPLE FLUORESCENCE 3 D SPECTRA	143
FIGURE 105: SI SAMPLE PHOSPHORESCENCE 3D SPECTRA	144
FIGURE 106: CAB 15 FLUORESCENCE EMISSION SPECTRA	145
FIGURE 107: CAB 15 PHOSPHORESCENCE EMISSION SPECTRA	146
FIGURE 108: CAB 15 FLUORESCENCE 3D SPECTRA	147
FIGURE 109: CAB 15 PHOSPHORESCENCE 3D SPECTRA	148
FIGURE 110: PB-GLASS 1 FLUORESCENCE EMISSION SPECTRUM	149
FIGURE 111: PB-GLASS 1 PHOSPHORESCENCE EMISSION SPECTRA	150
FIGURE 112: PB-GLASS 1 FLUORESCENCE 3D SPECTRA	151
FIGURE 113: PB-GLASS 1 PHOSPHORESCENCE 3D SPECTRA	152
FIGURE 114: FLUORITE SPECTRA - RAW DATA FOR THE DECAY CURVES	153
FIGURE 115: PEAK HEIGHT AT 424 NM VS. DELAY TIME	154

List of tables

TABLE 1: AVAILABLE DETECTION SYSTEMS, MATERIALS PROPERTY AND APPLICATION ACCORDING TO [6].....	17
TABLE 2: CHARACTERISTICS OF THE 7 CRYSTAL SYSTEMS AND 14 BRAVAIS LATTICES [17].....	19
TABLE 3: COMPARISON OF SCHOENFLIES NOTATION AND HERMANN-MAUGUIN NOTATIONS FOR SYMMETRY OPERATIONS [19, 20]	21
TABLE 4: SIMPLIFIED CLASSIFICATION SYSTEM FOR MINERALS ACCORDING TO STRUNZ [30]	23
TABLE 5: OVERVIEW OVER COMMON SPECTROSCOPIC TECHNIQUES AND THEIR WAVELENGTH RANGE [33].....	25
TABLE 6: THE 32 POINT SYMMETRY GROUPS IN CRYSTALS [44,45].....	29
TABLE 7: GENERAL APPEARANCE OF A CHARACTER TABLE	31
TABLE 8: O _h CHARACTER TABLE (FOR AN OCTAHEDRAL SYSTEM) [51]	32
TABLE 9: ELECTRON CONFIGURATIONS FOR SELECTED TRANSITION METAL IONS [55].....	34
TABLE 10: LETTER CODE VALUES FOR ORBITAL ANGULAR MOMENTA [55]	34
TABLE 11: MINERALS LUMINESCENT UNDER UV LAMP EXCITATION	52
TABLE 12: SCHEMATIC PARTITION OF MINERALS INTO GROUPS WITH VARIOUS LUMINESCENT PROPERTIES DUE TO DIFFERENT TYPES OF CHEMICAL BONDING AND COMPOSITION [79]	54
TABLE 13: OVERVIEW OVER FLUORESCENCE DATABASES FOR CERTAIN MINERALS.....	60
TABLE 14: OVERVIEW OVER REFLECTION SPECTROSCOPIC DATABASES	61
TABLE 15: SUMMARY OF THE FIVE MOST IMPORTANT DATABASES WITH THEIR CORRESPONDING LINK	62
TABLE 16: INFORMATION ON 8 INDUSTRIAL MINERALS IN THE 5 RELEVANT DATABASES	63
TABLE 17: MEASUREMENT PARAMETERS FOR REFLECTION MEASUREMENTS WITH THE L950	65
TABLE 18: PROPOSED SETTING FOR LS 55 FOR LONG LIVED LUMINESCENCE	68
TABLE 19: OVERVIEW OVER EXCITATION POWER P FOR MINERAL FLUORESCENCE FROM SEVERAL REFERENCES....	72
TABLE 20: ILLUMINANCE VALUES FOR SEVERAL SLIT WIDTHS AND WAVELENGTHS	77
TABLE 21: ILLUMINANCE AND SLIT WIDTH AT 550 NM	78
TABLE 22: ILLUMINANCE VALUES FOR THE LS 55 AT REFLECTION POSITION OF THE EXCITATION MONOCHROMATOR	79
TABLE 23: VARIOUS EXCITATION SLIT WIDTHS - TESTO 545 RESULTS IN PHOTOMETRIC AND RADIOMETRIC UNITS.	81
TABLE 24: CONSTANT EMISSION WAVELENGTH - TESTO 545 RESULTS IN PHOTOMETRIC AND RADIOMETRIC UNITS	81
TABLE 25: EXCITATION MONOCHROMATOR IN REFLECTION POSITION – TESTO 545 RESULTS IN PHOTOMETRIC AND RADIOMETRIC UNITS.....	82
TABLE 26: EXPERIMENTAL DATA OF IRRADIANCE FOR VARIOUS DISTANCES TO THE UV-LIGHT SOURCE	84
TABLE 27: ORIGINAL MEASUREMENT DATA FOR THE CHEMICAL ACTINOMETER MEASUREMENTS	87
TABLE 28: CORRECTED MEASUREMENT DATA FOR THE CHEMICAL ACTINOMETER MEASUREMENTS	88
TABLE 29: CORRECTED ABSORBANCE VALUES @ 352 NM AND CALCULATED IRRADIANCE VALUES	91
TABLE 30: DIFFERENT LASERS AND IRRADIANCE VALUES FORM BROICHER’S LIF REPORT [121]	92
TABLE 31: IRRADIANCE VALUES FOR SEVERAL FLUORESCENCE APPLICATIONS	93
TABLE 32: CO ₃ ²⁻ FUNDAMENTALS FOR INTERPRETATION OF THE CARBONATE FEATURE IN NIR [157].....	96
TABLE 33: INSTRUMENT SETTINGS FOR THE MEASUREMENT OF INTENSITY VS. EMISSION SLIT WIDTH	109
TABLE 34: EMISSION SLIT WIDTH AND MEASURED PEAK HEIGHTS FOR FLUORITE.....	110
TABLE 35: RESULTS FOR RELATIVE INTENSITIES FOR SEVERAL GLASS AND MINERAL SAMPLES	111
TABLE 36: QUANTUM YIELD DATA FOR SEVERAL SAMPLES FROM QUANTAURUS MEASUREMENTS.....	112
TABLE 37: INSTRUMENT SETTINGS FOR CALIBRATION MEASUREMENT OF LS 55.....	115
TABLE 38: FILTER SETTINGS AND EXCITATION WAVELENGTHS FOR THE CALIBRATION EXPERIMENT	115

TABLE 39: METHOD PARAMETERS FOR FLUORITE FLUORESCENCE EMISSION SPECTRA	125
TABLE 40: METHOD PARAMETERS FOR FLUORITE PHOSPHORESCENCE EMISSION SPECTRA	126
TABLE 41: METHOD PARAMETERS FOR THE CALCITE FLUORESCENCE EMISSION SPECTRA.....	129
TABLE 42: METHOD PARAMETERS FOR THE CALCITE PHOSPHORESCENCE EMISSION SPECTRA	130
TABLE 43: METHOD PARAMETERS FOR THE MAGNESITE FLUORESCENCE EMISSION SPECTRA	133
TABLE 44: METHOD PARAMETERS FOR THE MAGNESITE PHOSPHORESCENCE EMISSION SPECTRA.....	134
TABLE 45: METHOD PARAMETERS FOR THE CHALCEDONY FLUORESCENCE EMISSION SPECTRA.....	137
TABLE 46: METHOD PARAMETERS FOR THE CHALCEDONY PHOSPHORESCENCE EMISSION SPECTRA	138
TABLE 47: METHOD PARAMETERS FOR THE SI SAMPLE FLUORESCENCE EMISSION SPECTRA.....	141
TABLE 48: METHOD PARAMETERS FOR THE SI SAMPLE PHOSPHORESCENCE EMISSION SPECTRA	142
TABLE 49: METHOD PARAMETERS FOR THE CAB 15 FLUORESCENCE EMISSION SPECTRA	145
TABLE 50: METHOD PARAMETERS FOR THE CAB 15 PHOSPHORESCENCE EMISSION SPECTRA.....	146
TABLE 51: METHOD PARAMETERS FOR THE PB-GLASS 1 FLUORESCENCE EMISSION SPECTRA	149
TABLE 52: METHOD PARAMETERS FOR THE PB-GLASS 1 PHOSPHORESCENCE	150
TABLE 53: DECAY EXPERIMENT – RESULTS AND METHOD PARAMETERS.....	153

List of Symbols and Abbreviations

a.u.	arbitrary units (for fluorescence intensities)
CCD	charge coupled device
cf	crystal field
EM	Electromagnetic radiation
Emfilter	Emission filter
Emslit	Emission slit of the fluorimeter
EPR	Electron Paramagnetic Resonance (Spectroscopy)
EUV	extreme UV part of the EM spectrum with a wavelength of 100 -10 nm
Exslit	Excitation slit of the fluorimeter
FIR	Far infrared part of the electromagnetic spectrum. It is the region of wavelengths between 50 – 1000 μm .
FWHM	full width at half maximum
LIBS	laser induced breakdown spectroscopy
MIR	mid infrared part of the electromagnetic spectrum It is considered as the region between 4000 – 400 cm^{-1} (about a wavelength of 3 – 50 μm) and is often used for structure determination in chemical syntheses.
MUL	Montanuniversität Leoben
NIR	Near infrared part of the electromagnetic spectrum. In the present work wavelengths from 780 nm to 2500 nm are considered as NIR-region, because no experiments with radiation over 2500 nm were carried out.
NMR	Nuclear Magnetic Resonance (Spectroscopy)
REE	rare earth element
TIR	Thermal Infrared Reflection
U	electrical voltage
UV	The ultraviolet part of the electromagnetic spectrum. In the present work wavelengths from 200 nm to 380 nm are considered as UV-region, because no experiments with radiation beneath a wavelength of 200 nm were carried out.
UV-C-FUV	far UV part of the electromagnetic spectrum with wavelengths of 280 – 200 nm

UV-C-VUV	vacuum UV part of the EM spectrum with wavelength of 200 – 100 nm
TS	Tanabe – Sugano (abbreviation used for the term “Tanabe-Sugano – diagrams”)
VIS	the visible part of the electromagnetic spectrum: 380 nm to 780 nm
XRF	X-ray fluorescence
XRT	X-ray transmission

1 Introduction

1.1 Background

The present master thesis is part of a research project initiated by the local company Binder + Co with the aim to develop a flexible optical sensor based sorting system for a wide range of minerals and ores. In the frame of the thesis a representative sample set had to be compiled and optically characterized in terms of reflection- (UV-Vis-NIR) and luminescence spectra (UV-Vis).

The research project has the intern name Minexx UV/Vis/NIR or Minexx Plus, based on the Minexx mineral sorting system, manufactured by Binder + Co.

The whole research project is carried out by the three project partners [14]:

- Binder + Co
- Montanuniversität Leoben (MUL)
- Graz University of Technology (TUG)

Those three organizations provide project-relevant know how and resources in their special field of expertise [85]:

- Binder + Co:
 - Know-how concerning the limits of VIS-sorting for industrial relevant materials.
 - Applications.
 - Employer of the project.
- MUL:
 - Process technological know-how.
 - Knows the shortcomings and problems with actual processes and separation procedures.
 - Provides information where in the process a sensor based sorter can be placed.
 - Contacts to mining industry.
 - Deposit know-how.
 - Higher degree of professionalism by using the correct language e.g. “Tailings”, “Veinstuff”, and so on.
 - Mine run analysis via classical conditioning methods.
- TUG:
 - Know how concerning structural chemistry/lattice structure of the minerals of interest (Solid State Chemistry)
 - Know-how in the area of optical effects and spectroscopic background (Solid State Spectroscopy)
 - Spectroscopic fundamental studies for Binder + Co (2009 until today)
 - Database research concerning spectroscopic data bases.

1.2 Sorting and Beneficiation Technologies

There is a vast variety of beneficiation technologies on the market. The present work deals with fundamental research on optical sorting of minerals, glasses and other secondary raw materials.

Different traditional principles for material sorting are known [1]:

- **Free settling:** Sinking of particles in a volume of fluid which is large with respect to the total volume of particles, hence particle crowding is negligible. The particle density plays an important role in this sorting technology.
- **Hindered settling:** As the proportion of solids in the pulp increases, the effect of particle crowding becomes more apparent and the falling rate of the particles begins to decrease. The system begins to behave as a heavy liquid whose density is that of the pulp rather than that of the carrier liquid. This process is also based on particle density in comparison to the liquid.
- **Hydraulic classification:** The feed stream and additional fresh water are pumped through a cascade of columns. The direction of flow opposes that of the settling particles. The rising currents are graded from a relatively high velocity in the first sorting column, to a relatively low velocity in the last, so that a series of spigot products can be obtained.
- **Hydrocyclones:** Centrifugal force is used to accelerate the settling rate of particles.
- **Gravity concentration:** Specific heavier minerals are sorted from specific lighter ones by a liquid of intermediate density.
- **Froth flotation:** Different surface properties of the minerals and the gangue are used for separation. Three phases are encountered: solids, water and froth. Often the froth as “mineralized froth” contains the valuable content of the feed. Different collectors-agents, from a chemical point of view tensides and soaps are in use to create the desired froth. Furthermore it can be distinguished between activators (increasing the hydrophobicity of mineral surfaces) and depressants (increasing hydrophilicity of certain mineral fractions).
- **Magnetic separation:** Materials are sorted according to their magnetic properties. All materials can be subdivided into *diamagnetics* and *paramagnetics*. Diamagnetics are repelled from magnetic fields. This interaction is, however, rather small and cannot be used for sorting purposes. Paramagnetics (in particular ferromagnetic materials) are attracted by magnetic fields. There are several examples for commercial sorting of paramagnetic minerals. Magnetic separations can be furthermore subdivided into low-intensity and high intensity separating technologies with a threshold of 2 Tesla magnetic flux density.
- **Electrical separation:** This technology takes advantage of the different electric conductivities of minerals and gangue.
- **Electronic sorting principles:** The stream of minerals contaminated with gangue or other minerals is automatically separated using the response of a sensor. Different fundamental interactions of light with matter like reflectance, color in the VIS region of the electromagnetic spectrum, natural γ -radiation, X-Ray luminescence, IR-, Raman- or microwave attenuation are in use.

However, all those classification techniques can be broken down to physical or physico-chemical interactions and fundamentals.

1.3 Mineral and Glass Sorting

This work deals with the possibilities and fundamentals of sensor based sorting of minerals and glasses. As Kieler [2] has shown in her diploma thesis luminescence of lead doped glasses can easily be measured in UV-VIS range and hence can be used in optical sorting machines. An implementation of this basic phenomenon was made in the “CLARITY lead” system of Binder + Co, which has a capacity of up to 14 t/h [3]. A source for fundamental research data at pilot plant scale for sorting of fluorescent minerals is provided by Ören [5].

When either too low concentrations of a luminophor or concentration quenching effects for too high concentrations suppress luminescence signals, another useful tool can be the UV or NIR cut-off of the materials. Fundamental research of this useful topic was provided by Ohnewein [4].

A good technological overview of available sensor systems for optical sorters was provided by Wotruba and Kleine in 2010 and is reproduced in table 1 [6].

Table 1: Available detection systems, materials property and application according to [6]

Sensor	Material Property	Application
Radiometric	Natural Gamma Radiation	Uranium, Precious Metals
XRT	Atomic Density	Base/ Precious Metals, Coals
Energy dispersive XRF	Elemental Composition	Base/ Precious Metals
XRF	Visible Fluorescence under X-Rays	Diamonds
VIS	Reflection/ Absorption of Visible radiation	Metals, Industrial Minerals, Gem Stones
CCD Color	Color, Reflection, Brightness, Transparency	Base/ Precious Metals, Industrial Minerals, Gem Stones
Photometric	Monochromatic Reflection, Absorption	Industrial Minerals, Gem Stones
NIR	Reflection/ Absorption of NIR Radiation	Base Metals, Industrial Minerals
TIR	Microwave Excitation and Thermal Infrared Reflection	Base Metals, Precious Metals
LIBS	Emitted radiation of the plasma generated by a focused pulse laser	Al-alloy sorting, all kinds of homogeneous materials because a the small measurement spot

Direct sorting criteria for minerals are defined as directly linked to the main elemental or mineralogical content. Therefore sensor techniques based on direct sorting criteria are XRT, XRF, NIR-spectroscopy and LIBS. NIR-sorting is based on the measurement at the surface, whereas XRT-sorting works with electromagnetic radiation penetrating the minerals. The attenuation of the radiation is measured in the latter technique. LIBS sensors measure the elemental composition of a small area of about $< 1 \text{ mm}^2$ of the sample. The emission of the plasma generated via a laser is analyzed and used for sorting [7].

1.4 Minerals

1.4.1 Origin and Definitions

Minerals are by definition substances that are naturally occurring parts of the earth or other celestial bodies, and can be represented by a chemical formula. Most of the minerals (with only a few exceptions) are inorganic, solid and crystalline [8]. Exceptions from this rule are for example naturally occurring mercury (Hg), opal ($\text{SiO}_2 \cdot n\text{H}_2\text{O}$) and vitreous silica (SiO_2) [10].

The origin of terrestrial minerals is mostly based on inorganic processes. There are, however minerals whose origin is found in biologic activities of certain organisms. A good example for a mineral of biologic origin is Apatite, which builds up teeth and bones of vertebrates. Minerals build up rocks and stones. Earth's mantle and earth's core as well as the moon and other celestial bodies can be considered to consist of minerals, even though their constitution is not exactly known or purely hypothetical [8].

A rock is defined as a solid aggregate of minerals. While the breakdown of a mineral leads to smaller parts of the same chemical and crystallographic composition, the breakdown of a rock leads to inhomogeneous parts. A common example for a rock is granite, which is a mixture of feldspar, biotite and quartz. There are rocks with one specific mineral (e.g. marble with CaCO_3) and rocks with more than one specific mineral (e.g. granite) [12].

Different classifications of minerals and rocks according to their genesis are known [9]:

- Igneous Rock
- Metamorphic Rock
- Sedimentary Rock

However, some minerals are formed stepwise via a combination of these three processes.

Igneous rocks are formed by solidification of molten fluids, generated in the earth's crust under high pressure and temperature. When these rocks undergo natural breakdown processes like weathering or transportation by streams to form beds of clay, sand and finally deposits of new minerals, they are called sedimentary rocks. When these sedimentary rocks undergo high pressure and temperatures which lead to changes in chemical composition or crystal structure metamorphic rocks are formed [11].

Ores are defined as aggregates of minerals or rocks of ore minerals, which have significant concentrations of metals or nuclear fuels like Uranium or Thorium. Ores can be subdivided as follows into classes with certain elements of interest [13]:

- **Ores of ferrous metals** (iron and elements which are used for steel refining): Fe, Mn, Ni, Co, Cr, V, Ti, Mo, Re, W, Nb, Ta, Zr, Hf, Te
- **Ores of non-ferrous metals** (base metals): Cu, Pb, Zn, Cd, Sn, Hg, As, Sb, Bi, Ga, In, Tl, Si, Ge
- **Ores of light metal**: Al, Mg, Be
- **Ores of precious metals**: Au, Ag, Pt and Pt-metals, Ru, Rh, Pd, Os, Ir
- **Ores of Lanthanides** (rare earth elements)
- **Ores of Actinides** (reactor fuels): Uranium, Thorium, Radium

1.4.2 Chemical Properties, Symmetry and Classification according to Strunz

Minerals usually are crystals. A possible definition of a “crystal” is: Crystals are solid, homogeneous and anisotropic bodies with a three-dimensional periodic arrangement of their chemical components (atoms, ions or molecules). These components build up what is called a crystal lattice. This lattice leads to the anisotropic properties of the crystal, which means that physical properties like the refractive index can vary in different directions [14].

When the lattice is visualized as a regular arrangement of points three lattice vectors can be found with the lengths of a , b and c . The three lattice vectors include the three angles α , β , and γ . This lattice vectors define the so-called unit cell of a crystal. It can be considered as the smallest repeat-unit which upon continuous duplication along the directions of the lattice vectors reproduces the complete crystal lattice. In 1845 Bravais defined 14 Bravais lattices in 7 crystal systems which turned out to be sufficient to describe the structures of all crystalline solids [16]. The 14 Bravais lattices are depicted in figure 1.

Table 2: Characteristics of the 7 crystal systems and 14 Bravais lattices [17]

Crystal Systems			Bravais Lattices
Structure	Axes	Angles between the Axes	
Cubic	$a = b = c$	all angles equal to 90°	simple, face centered, body centered
Tetragonal	$a = b \neq c$	all angles equal to 90°	simple, body centered
Orthorhombic	$a \neq b \neq c$	all angles equal to 90°	simple, body centered, base centered, face centered
Hexagonal	$a = b \neq c$	two angles equal to 90° , one angle equals 120°	hexagonal
Trigonal	$a = b = c$	all angles are equal and none equals 90°	rhombohedral
Monoclinic	$a \neq b \neq c$	one angle (β) not equal to 90°	simple, base centered
Triclinic	$a \neq b \neq c$	all angles are different and none equals 90°	triclinic

After the type of the Bravais lattice is determined the points of the corresponding unit cell have to be filled with atoms or small groups of atoms generating the structure of the unit cell. This is called the basis. The basis builds up the unit cell of the crystal and the unit cell is the smallest repeating unit of the crystal itself. After considering the symmetry of both, the basis and the lattice, the crystal can be sorted into one of 32 point symmetry groups and of 230 possible space groups [18].

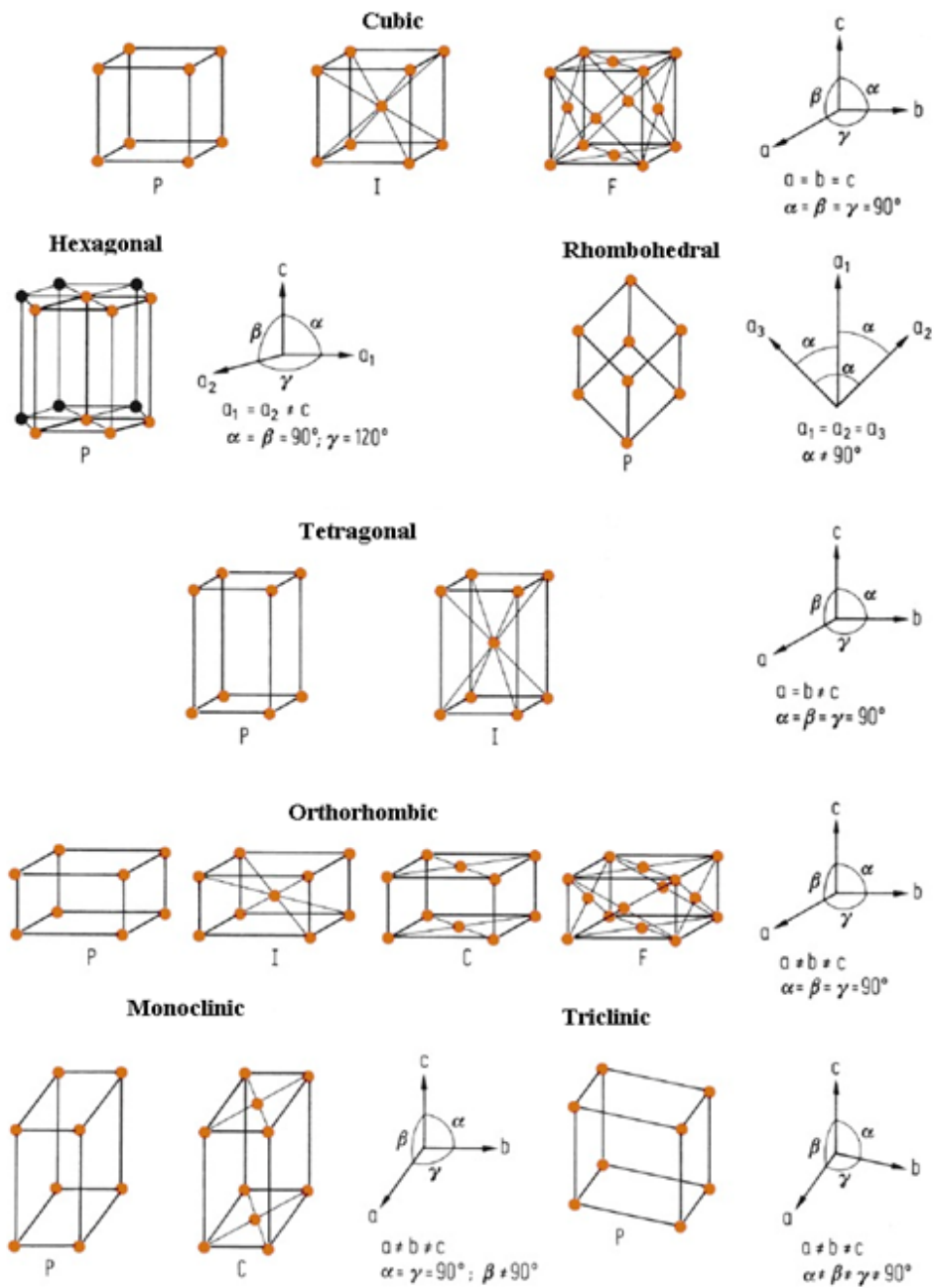


Figure 1: 14 Bravais lattices [126]

To understand crystal morphology of minerals and artificial crystals one has to know about symmetry. Symmetry operations are defined as operations which lead to arrangements of the atoms which are indistinguishable from the starting arrangement. These operations can be purely hypothetical in the sense of physical feasibility [15].

For every molecule or unit cell a list of possible symmetry operations can be found. According to this list a molecule can be assigned to a certain *point group*. Only operations corresponding to symmetry elements that intersect at least in one point of the molecule are taken into consideration – this specific point of a molecule is its center of gravity. Thus the term “point” group is used. For the classification of crystals translational symmetry has to be taken into account. Therefore for crystals the term *space group* is used. Every symmetry operation is linked to a symmetry element, e.g. the point, line or plane with respect to which the symmetry operation is carried out. There are two different notations for symmetry elements known: Schoenflies notation and the Hermann-Mauguin notation (also known as International notation system) which are compared in table 3 [19].

Table 3: Comparison of Schoenflies notation and Hermann-Mauguin notations for symmetry operations [19, 20]

Symmetry operation	Schoenflies	Hermann-Mauguin	Comment
unity	E	1	Necessary for the mathematical description of symmetry. It is a neutral element and equal with doing nothing.
n-fold rotation	C_n with $n = 1,2,3,4,6$	n with $n = 1,2,3,4,6$	Rotation about an axis with an angle $2\pi/n$
reflection	σ	m	Reflection on a mirror plane
inversion	i	$\bar{1}$	Inversion through a center of symmetry
n-fold improper rotation	S_n	with $n = 3,4,6$	Also called “rotary reflection”; or equivalently “rotary inversion”; n-fold rotation followed by a reflection on a plane perpendicular to the n-fold axis.

However, in contrary to molecules in crystals there are three more symmetry elements: *pure translations*³ of the unit cell with the value of the lattice constant, *screw axes*⁴ which rotate a part of the cell around an axis and then translate parallel to the axis and *glide planes*⁵ which reflect a part of the cell through a plane and then translate it parallel to the plane [21].

³ German: Translation (einfache Verschiebung um einen bestimmten Wert)

⁴ German: Schraubenachse

⁵ German: Gleitspiegelebene

Atoms in crystals arrange themselves in a certain way. Helpful tools to understand the arrangement of ions in solids are Pauling's rules [26] for ionic structures (even though there are many exceptions known today):

1. A coordinated polyhedron of anions is formed about each cation, the cation-anion distance is determined by the radius sum and the coordination number of the cation by the radius ratio.
2. In a stable coordination structure the electric charge of each anion tends to compensate the strength of the electrostatic valence bonds from the cations at the centers of the polyhedra of which it forms a corner.
3. The presence of shared edges, and particularly of shared faces, in a coordinated structure decreases its stability; this effect is large for cations with large valence and small coordination number, and is especially large in case the radius ratio approaches the lower limit of stability of the polyhedron.
4. In a crystal containing different cations those with large valence and small coordination number tend not to share polyhedron elements with each other.
5. The number of essentially different kinds of constituents in a crystal tends to be small.

In all packing types of atoms there are small holes between the atoms. Into these holes smaller atoms can be positioned. For example in a FCC (face centered cubic) unit cell there are four octahedral and eight tetrahedral sites for including atoms [24].

Since ideal crystals have a higher free energy than crystals with imperfections there are no perfect crystals in nature. The Gibbs free energy of every crystal encountered is lowered via increase of entropy, which means disturbance of the perfect order [22].

The Gibbs energy ΔG of a crystal is defined as:

$$\Delta G = \Delta H - T \Delta S \quad \text{Equ. 1}$$

with ΔH the enthalpy of formation, T the temperature and ΔS the entropy associated with the large number of positions that a defect can occupy. Since ΔH increases linearly with the defect concentration and $-T \Delta S$ decreases, a minimum of ΔG can be reached with a certain concentration of defects [27].

Point defects are defined as localized disruptions in perfect atomic or ionic arrangements in a crystal structure. Point defects are [23]:

- vacancy
- interstitial atom
- small substitutional atom
- large substitutional atom
- Frenkel defect (a smaller ion is displaced from its original position to an interstitial site, a vacancy defect is created in its original position, while creating an interstitial on its new place)
- Schottky defect (ions of opposite charge leave the crystal and vacancies are left behind, the ratio of anionic and cationic charge stays the same)

A well-established notation for point defects is the Kröger-Vink notation [28]:

In M_S^C M is the species, e.g. atoms, vacancies, holes and electrons are possible, S is an index for the lattice site where the species can be found (the letter i is used to mark an interstitial) and C represents the electronic charge of the species in comparison to the site that it occupies. The symbols for charge are “x” for zero charge, “.” for a single positive charge, “..” for double positive charge and so on and “ ’ ” for one negative charge.

For example: $Cu_i^{..}$ indicates a copper interstitial ion with a double positive charge.

It should be mentioned that there are some other notations for point defects available in literature [29].

Another type of imperfections in crystalline solids are dislocations. Dislocations are line imperfections which are introduced when a crystal is forming from a melt or when a solid body is deformed. The common known dislocations are: [24]

- *Screw dislocations*
- *Edge dislocations*
- *Mixed dislocations* with both edge and screw components

A consistent systematization of minerals has been made by Strunz [30]. Minerals are assigned to 10 classes which are subdivided on chemical-structural principles into divisions, subdivisions and groups of isotypic⁶ or homeotypic⁷ species, or individual minerals of a structure type. The alphanumeric coding scheme works as follows: The first numeric digit represents a class, the first alphabetic character represents a division and the second alphabetic character represents a subdivision. The final two numeric digits represent a group or individual mineral. The classes of the system are presented in table 4.

Table 4: Simplified classification system for minerals according to Strunz [30]

Classes in the Strunz Mineralogical Tables
1. Elements
2. Sulfides and Sulfosalts
3. Halides
4. Oxides
5. Carbonates + Nitrates
6. Borates
7. Sulfates
8. Phosphates, Arsenates, Vanadates
9. Silicates
10. Organic Compounds

⁶ Isotypy: Isotypic substances have the same crystallographic space group and analogous chemical formulae and crystal structures.

⁷ Homeotypy: Homeotypic substances have similar crystal structures, but with different crystallographic space groups and/or chemical compositions.

1.5 Solid State Spectroscopy

1.5.1 General Introduction

1.5.1.1 Quantum mechanical basics and overview on techniques

The wave-length range of the electromagnetic radiation used in this thesis was between 200 and 2500 nm. The introduction will also contain some basic information on the neighboring spectral ranges but will not go into details.

When talking about spectroscopy one should have in mind the spectrum of the electromagnetic radiation. It is depicted in figure 2. The energy of electromagnetic radiation depends on its wavelength or frequency according to Planck's equation:

$$E = h\nu = \frac{hc}{\lambda} = hc\bar{\nu} \quad \text{Equ. 2}$$

In equation 2 E is the energy in Joule, $h = 6,626 \cdot 10^{-34}$ Js is Planck's constant, ν is the frequency in s^{-1} (Hz), $c = 299,8 \cdot 10^6$ m/s is the speed of light, λ the wavelengths in m and $\bar{\nu}$ the wavenumber in m^{-1} [32].

Electronic or vibrational energy levels in matter cover a wide range of the energy scale. Which transitions are observed in an experiment is mostly dependent on the wavelength of the electromagnetic radiation used. The vibration frequencies of atoms in solids are about 10^{12} - 10^{13} Hz. Hence IR-radiation can be used to investigate the vibrational properties of a solid by recording its absorption or reflection by the sample. Information about the vibrating lattice is also obtained from Raman spectroscopy, where the scattering of the more energetic visible laser light (Raman scattering) is used [33].

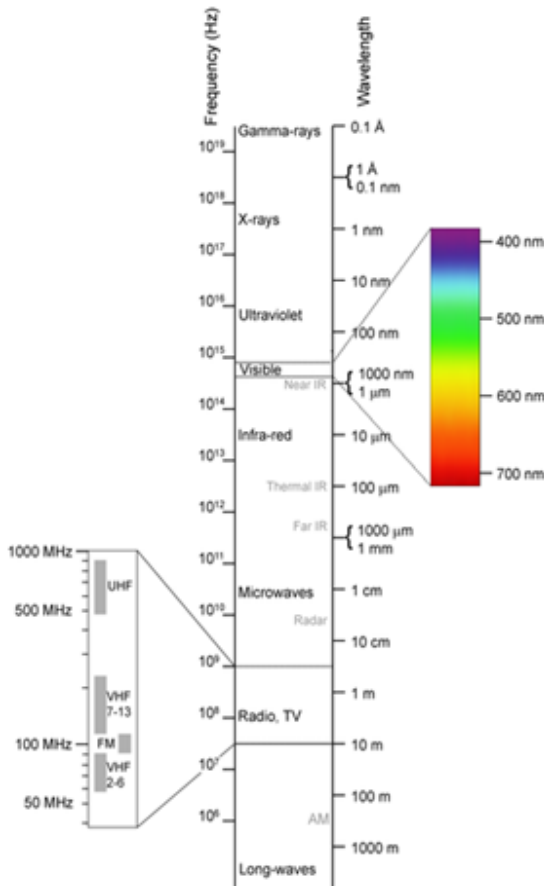


Figure 2: the electromagnetic spectrum [31]

For solid state spectroscopy the rotations which are also excited via IR- and more efficiently via microwave radiation are not important, because in a solid body there are no rotational degrees of freedom left. For investigation of small molecules like CO_2 , H_2O , I_2 and others rotations are of great importance and have to be considered.

An overview from shorter to longer wavelength and corresponding radiation – matter interactions are given in table 5. The subdivision of the IR region into NIR, MIR and FIR was made according to the

recommendations in ISO 20473. The subdivision of the UV-region into UV-A, UV-B, UV-C-FUV, UV-C-VUV and EUV was made according to DIN 5031-7.

Table 5: Overview over common spectroscopic techniques and their wavelength range [33]

Name of method or EM-radiation used	Wavelengths	Interaction between radiation and matter	Comment
NMR	in the scale of meters	transitions between nuclear spin states are induced	NMR transitions are excited at frequencies of about 10^8 Hz
EPR	in the scale of millimeters to centimeters	transitions between electron spin states are induced	EPR transitions occur at frequencies of about 10^{10} Hz
IR	780 nm - 1 mm	vibrational modes and rotational can be excited to higher energy states	
	FIR: 50 - 1000 μ m	intramolecular and intermolecular vibrations [35]	for special applications
	MIR: 3 - 50 μ m	mostly fundamentals and some overtones of vibrations and rotations [34]	standard laboratory technique
	NIR: 0,78 - 3 μ m	overtones and combinations of fundamentals of vibrations and rotation [34] and excitations of valence electrons	today available in combined spectrometers for UV-VIS-NIR measurement
VIS	780 - 380 nm	excitation of valence shell electrons excitations of electrons in unfilled d- or f-shells	
UV	380 - 10 nm	excitation of valence and inner shell electrons	with a standard spectrometer the range of 380 - 200 nm is available
	UV-A: 380 - 315 nm		
	UV-B: 315 - 280 nm		
	UV-C-FUV: 280 - 200 nm		
	UV-C-VUV: 200 - 100 nm		Can only be handled under inert gas or vacuum.
	EUV: 100 - 10 nm		Can only be handled under vacuum.
X-ray	10 - 0,01 nm	ionization and inter-shell transitions	X-ray excitation is used to get absorption (XRT) and emission spectra (XRF)
γ-ray	$\leq 0,01$ nm	transitions inside atomic nuclei	used in Mössbauer spectroscopy (information on oxidation state, CN, bond character and radioactive ions in solids)

Since about 100 years it is known that for the discussion of molecular and atomic energy levels the concepts of classical mechanics are not suitable. In 1926 Erwin Schrödinger postulated his famous equation for the description of a particle with a mass of m and energy of E , that moves along x in some potential V [41]:

$$-\frac{\hbar^2}{2m} \frac{d^2\psi}{dx^2} + V(x)\psi = E\psi \quad \text{Equ. 3}$$

In equation 3 ψ is the wave function.

To make the transition from the world of classical mechanics to quantum mechanics quantities like the kinetic or potential energy have to be replaced by operators. These operators are applied to the wave functions of a system [39]. The operator which contains all possible contributions to the energy of a system is called “Hamiltonian Operator” \hat{H} . For the simple system of a particle moving in x-direction the Hamiltonian has two contributions:

$$\hat{H} = \hat{T} + \hat{V} \quad \text{Equ. 4}$$

In equation 4 \hat{T} is the operator for the kinetic energy and \hat{V} is the operator for the potential energy.

The kinetic energy is a function of x, the distance:

$$\hat{T} = -\frac{\hbar}{2m}\nabla^2 \quad \text{Equ. 5}$$

where m is the mass of the particle and ∇^2 is the gradient operator with

$$\nabla^2 = \frac{d^2}{dx^2} + \frac{d^2}{dy^2} + \frac{d^2}{dz^2} \quad \text{Equ. 6}$$

and \hbar is defined as [40]:

$$\hbar = \frac{h}{2\pi} = 1,05457 \cdot 10^{-34} \text{Js} \quad \text{Equ. 7}$$

So Schrödinger’s equation can be written for the simple cases as [41]:

$$\hat{H}\psi = E\psi \quad \text{Equ. 8}$$

Even in these simple cases not a single energy is obtained from the solution of this equation, but a series of solutions differing in energy. These different energies correspond to the possible states of the system and are discriminated by a set of numbers – the quantum numbers.

Spectroscopic experiments show the transitions between these different energy states. In vibrational spectroscopy (IR, Raman) transition between different vibrational energy levels are observed.

1.5.1.2 Vibrational Spectroscopy and Symmetry Considerations

The energy levels of a simplified system consisting of two atoms can be depicted as in figure 3.

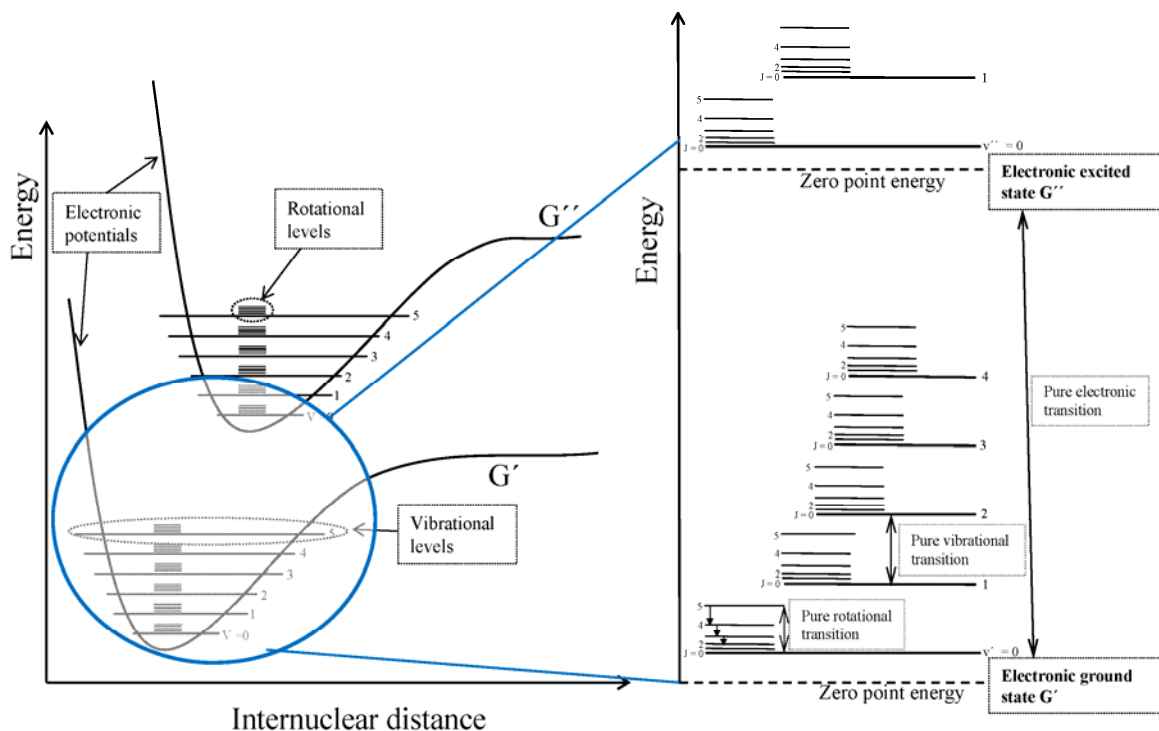


Figure 3: Energy levels of a diatomic molecule [37, 74]

Figure 3 shows the three most important transitions of a molecule: rotational transitions, vibrational transitions and electronic transitions.

The zero point energy of a system is the energy of its lowest permitted state. This zero point energy represents the difference between the minimum of the molecular potential curve and the vibrational state with quantum number $v = 0$. The zero point energy is based on the boundary conditions the wave functions of a system have to satisfy [38].

Several types of vibrations can be classified [36]:

- Symmetric vibrations or totally symmetric vibrations: symmetry properties of the molecule is preserved
- Nonsymmetric vibrations: symmetry properties like a C_2 -axis or a σ -plane get lost during vibration

How can spectroscopic features be predicted? What is necessary to understand whether or not a molecule is active in the IR or Raman experiment? The key to these questions are the changes in symmetry when molecules undergo vibrations and deformations and the selection rules that are caused.

Vibrational excitation is modulated by diverse selection rules. These rules make it possible to predict whether a specific excitation will show up in the spectra. These predictions are based on quantum mechanical integrals related to the intensity of transitions. If these integrals are zero, the corresponding transitions are not observed and are called “forbidden”. Again symmetry plays an important role.

The most important selection rule for each normal vibration is as follows: A vibration is **active in the IR** spectrum if the **dipole moment** of the molecule **is changed** during the vibration. This is the reason why homonuclear diatomic molecules (e.g. O₂, N₂, etc.) do not have IR spectra. In contrast, the Raman process is based on inelastic scattering which has nothing to do with dipole moments but requires an anisotropic polarizability. The polarizability of the electron cloud of a molecule is a measure for its ability to deform upon the action of external electric fields (like the strong electric field that go along with a laser beam). A vibration, is **active in the Raman** spectrum **if the polarizability** of the molecule **is changed** during the vibration. The polarizability of a molecule can be visualized as an ellipsoid containing the electron cloud of the molecule and therefore a vibration is Raman active if the ellipsoid changes in size, shape or orientation during the vibration. In a polyatomic molecule with a center of symmetry, the vibrations symmetric with respect to the center of symmetry are Raman active and are called “g” vibrations and are not IR active. “g” stands for the German word “gerade”(even).The vibrations antisymmetric to the center of symmetry are IR active and are called “u” vibrations, furthermore they are not Raman active. “u” stands for the German word “ungerade” (odd). This is called the “mutual exclusion rule” and it should be mentioned that there are several exceptions to this rule, especially when there are several symmetry elements in addition to the center of symmetry [36].

Group theory can be used to apply symmetry considerations to spectroscopically active centers. The symmetry properties of the active center (e.g. a transition metal or rare-earth ion in a solid) are also the symmetry properties of the Hamiltonian. These symmetry considerations can be used to solve problems such as [42]:

- Determining the number of energy levels of a particular active center
- Labelling these electronic energy levels with irreducible representations and determining their degeneracy
- Predicting the energy level splitting caused by the symmetry of the electric field surrounding the active center
- Establishing selection rules for optical transitions and determining their polarization character
- Determining the symmetry properties of the active centers eigenfunctions
- Analyzing the vibrations of a complex center

As mentioned in the previous chapter 32 point symmetry groups are known, which are listed in table 6. The order of the point group gives the number of possible symmetry operations and the number of classes⁸ indicates the number of sets of conjugate elements in the group [42, 43].

Again the symmetry point groups can be denoted either in the Schoenflies or the Hermann-Mauguin system. In Hermann-Mauguin notation n denotes an n-fold axis of rotation and m a mirror plane. A forward dash “/” means that the mirror plane is perpendicular to the axis of rotation. A bar over a number shows that this element is combined with an inversion. It is also important to distinguish symmetry

⁸ The term „class“ comes from the definitions of group algebra. A good discussion of this topic is given in [43], but would go too far in the present work.

elements of the same sort but of a different class. E.g. 4/mmm denotes a symmetry group with 3 different classes of mirror elements σ_v , σ_h and σ_d [45].

Table 6: The 32 Point symmetry groups in crystals [44,45]

Schoenflies Symbol	Hermann-Mauguin Symbol	Group order	Number of classes	Crystal System
C_1	1	1	1	Triclinic
C_i	$\bar{1}$	2	2	Triclinic
C_s	m	2	2	Monoclinic
C_2	2	2	2	Monoclinic
C_{2h}	2/m	4	4	Monoclinic
C_{2v}	2mm	4	4	Orthorhombic
D_2	222	4	4	Orthorhombic
D_{2h}	mmm	8	8	Orthorhombic
C_4	4	4	4	Tetragonal
S_4	$\bar{4}$	4	4	Tetragonal
C_{4h}	4/m	8	5	Tetragonal
C_{4v}	4mm	8	5	Tetragonal
D_{2d}	$\bar{4}2m$	8	5	Tetragonal
D_4	422	8	5	Tetragonal
D_{4h}	4/mmm	16	10	Tetragonal
C_3	3	3	3	Trigonal
S_6	$\bar{3}$	6	6	Trigonal
C_{3v}	3m	6	3	Trigonal
D_3	32	6	3	Trigonal
D_{3d}	$\bar{3}m$	12	6	Trigonal
C_{3h}	$\bar{6}$	6	6	Hexagonal
C_6	6	6	6	Hexagonal
C_{6h}	6/m	12	12	Hexagonal
D_{3h}	$\bar{6}2m$	12	6	Trigonal
C_{6v}	6mm	12	6	Hexagonal
D_6	622	12	6	Hexagonal
D_{6h}	6/mmm	24	12	Hexagonal
T	23	12	4	Cubic
T_h	m3	24	8	Cubic
T_d	$\bar{4}2m$	24	5	Cubic
O	432	24	5	Cubic
O_h	m3m	48	10	Cubic

If the point group a molecule or a unit cell is not known, it can be found by successively working off the flow chart for point group determination [46].

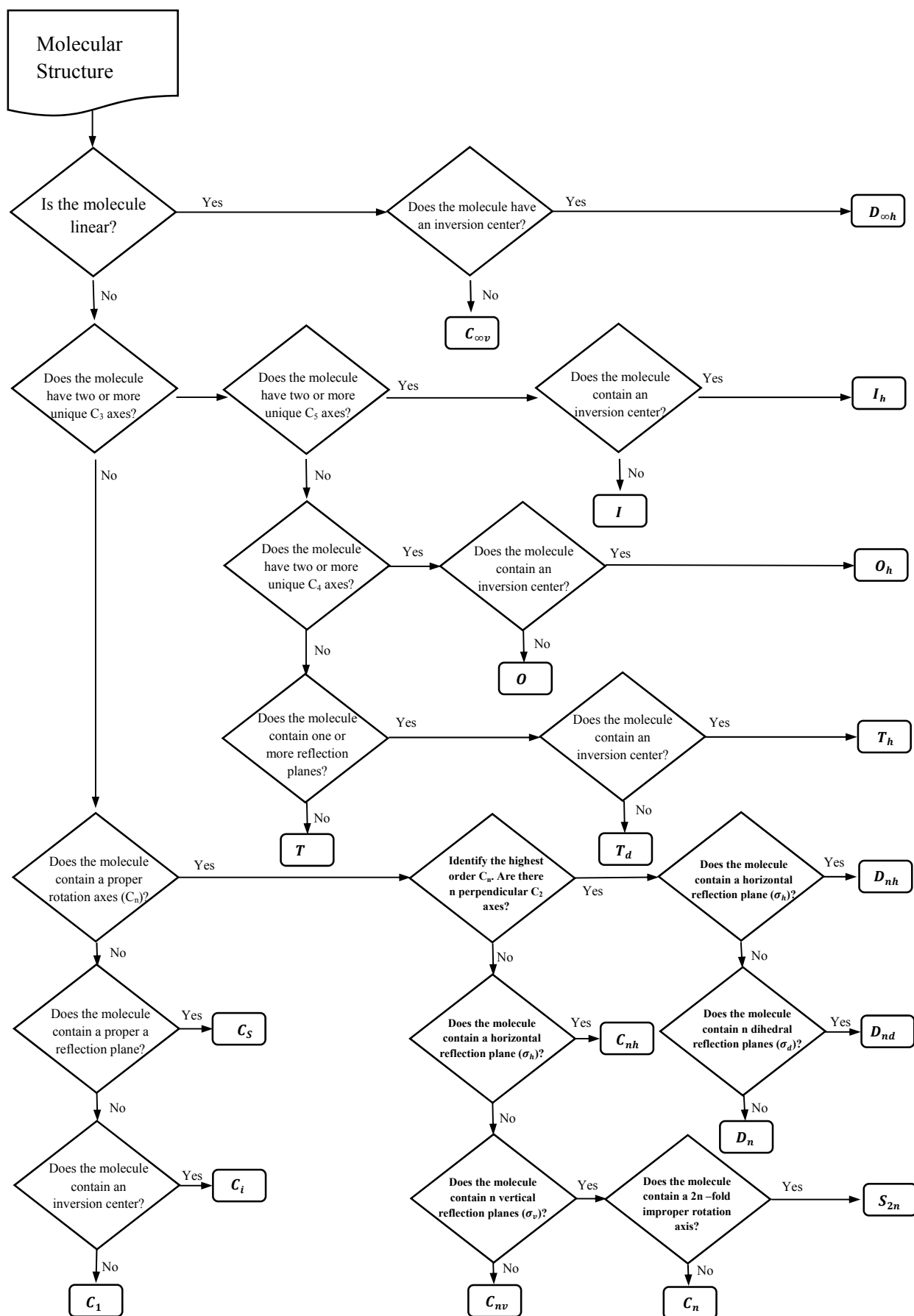


Figure 4: Flow chart to find the proper point group for a molecular structure [46,47]

Mathematically every symmetry operation that can be performed on a spectroscopically active center can be considered as an operator. Performing the operation, in the mathematical picture, means to let this operator act on some basis. In the simplest case the basis could be a row vector holding the labels of all atoms of a molecule. By the action of the operator the basis is transformed, but can always be expressed by the original basis multiplied by a matrix. This matrix is quadratic and serves as a representation of the operator in the chosen basis. Other useful bases sets are the Cartesian coordinates or the p- and d- atomic orbitals. For example all 48 symmetry operations of the O_h group can be represented by sets of 48 matrices, whose dimensions depend on the chosen basis. Most of these sets of matrices are called “reducible representations” of the group O_h . The traces (i.e. sum over diagonal elements) of these matrices are known as “characters” in group theory. The character of a representation is independent of the chosen basis and contains a lot of useful information. The reducible representations can be broken down to smaller irreducible representations via a reduction algorithm. It turns out that the number of irreducible representations of a group equals the number of classes. The characters of the irreducible representations are contained in so-called character tables and are also used to perform the reductions of larger representations. The full information for a given group is contained in its character table. A character table is a quadratic array, its rows correspond to the irreducible representations (e.g. 10 for the O_h group), its columns to its classes and it contains the characters, and the set of basis functions [48].

Three main facts on character tables are important [48]:

- The number of classes is equal to the number of irreducible representations
- The set of characters of a representation is unique
- The dimension (that is the dimension of the matrices) of each irreducible representations is given by the character corresponding to the class E^9 .

Table 7: General appearance of a character table

Group Symbol	Symmetry Classes	
Irreducible Representations in Mulliken Notation	Characters	Basis functions

In the Mulliken notation representations A and B are one-dimensional, E representations are two-dimensional and T representation are three-dimensional. Higher irreducible representations are G, four-dimensional and H, five-dimensional [48]. The A’s and the B’s are distinguished by the fact, that A’s have numbers of +1 for the rotation of about the axis of highest symmetry whilst B’s have numbers of -1 [50].

As an example for a character table, the O_h character table is given in table 8.

⁹ The dimension of the representation matrices, can always be seen from the character of the (n,n) matrix representing the identity operation E.

Table 8: O_h character table (for an octahedral system) [51]

O_h ($m3m$)	E	$8C_3$	$6C_2$	$6C_4$	$3C_2$ ($= C_4^2$)	i	$6S_4$	$8S_6$	$3\sigma_h$	$6\sigma_d$	$h = 48$	Basis sets
A_{1g}	1	1	1	1	1	1	1	1	1	1		$x^2 + y^2 + z^2$
A_{2g}	1	1	-1	-1	1	1	-1	1	1	-1		
E_g	2	-1	0	0	2	2	0	-1	2	0		$(2z^2 - x^2 - y^2, x^2 - y^2)$
T_{1g}	3	0	-1	1	-1	3	1	0	-1	-1	(R_x, R_y, R_z)	
T_{2g}	3	0	1	-1	-1	3	-1	0	-1	1		(xz, yz, xy)
A_{1u}	1	1	1	1	1	-1	-1	-1	-1	-1		
A_{2u}	1	1	-1	-1	1	-1	1	-1	-1	1		
E_u	2	-1	0	0	2	-2	0	1	-2	0		
T_{1u}	3	0	-1	1	-1	-3	-1	0	1	1	(x, y, z)	
T_{2u}	3	0	1	-1	-1	-3	1	0	1	-1		

1.5.1.3 Crystal field spectroscopy

The dimension of a representation corresponds to the degeneracy of its associated energy level [48].

For example the degeneracy of the set of the five d-orbitals in a free ion is 5 and all five d-orbitals have the same energy. When the free ion is placed into an octahedral crystal field – it could for example occupy a lattice site in a solid which is octahedrally surrounded by six ligands - the degenerate electron energy levels split. This is immediately seen by looking at the O_h character table: It does not have any five-fold degenerate irreducible representations. The set of 5 d-orbitals is split into two sets: e_g (two-dimensional = doubly degenerate) and three t_{2g} (three-dimensional = threefold degenerate) [49]. This example is illustrated in figure 5. In figure 5 the t_{2g} -orbitals are d_{xy} , d_{yz} and d_{zx} , the e_g orbitals are d_{z^2} and $d_{x^2-y^2}$.

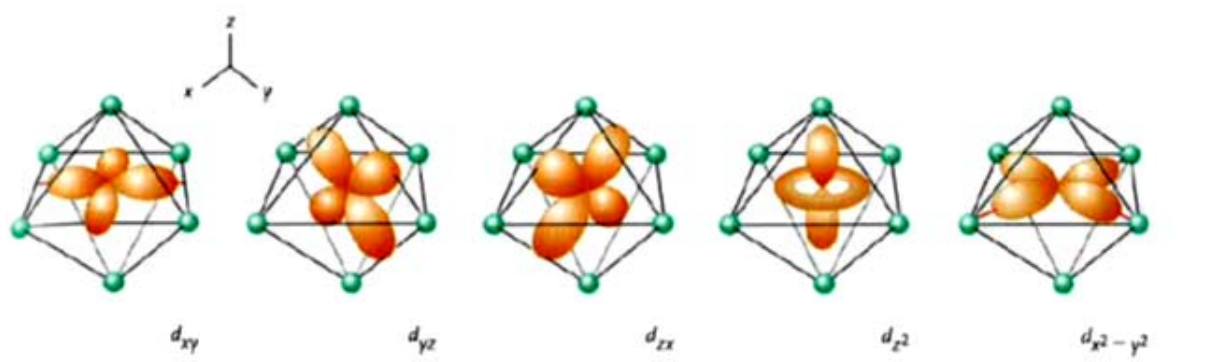


Figure 5: d-orbitals in an octahedral crystal field [49]

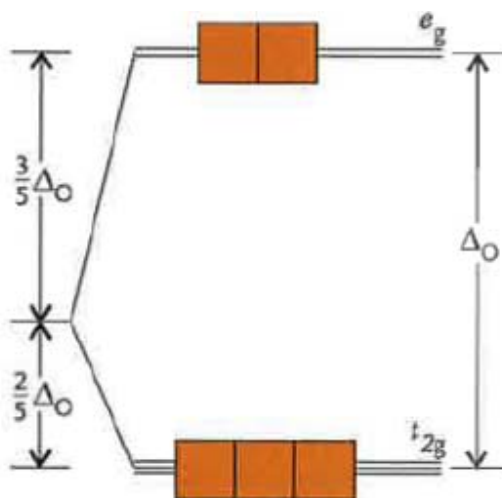


Figure 6: Energy level splitting of the five degenerate states of a d-electron in an octahedral crystal field [49]

The energetic situation for the single electron d-orbitals in an octahedral electric field is easy to understand and can even be predicted by just looking at their shapes (the e_g orbitals have lobes pointing directly towards negatively charged ligands, and will therefore be energetically less favorable than the t_{2g} orbitals with their lobes pointing in between the ligands). The energetic situation for atoms having more than one electron in the d-shell is more complicated, but can nonetheless be calculated and predicted along the same symmetry and group theoretical lines outlined for the one-electron case. The results are usually presented in terms of so-called Tanabe-Sugano (TS) - diagrams. On the left-hand side of such diagrams the energies of the free ion Russell-Saunders terms are given. The TS - diagram shows how the energies of the terms of an ion change as the strength of a crystal field increases. The ordinate is energy and the abscissa shows the strength of the crystal field. A special feature of TS-diagrams is, that the state of lowest energy (= the ground state) is always taken as the zero point of energy. The energies of the free ion energy levels are usually given in terms of the Racah parameters B and C. These parameters represent radial integrals which arise from electron-electron repulsion in the unfilled d-shell and are difficult to evaluate. Normally they are obtained from experimental gas phase atomic spectra of the respective d-element. It turns out that the values of B and C are in a constant ratio for a given d-element. It is convenient to normalize the axes of the TS-diagram to the Racah parameter B. Δ is the ligand field strength. Terms of the same symmetry follow the “non-crossing rule”, which means that they mustn’t cross each other and bend away, when Δ is increased. TS – diagrams for different symmetries of the crystal field and different ions are available in the literature [52]. An example of a TS-diagram is given in figure 9.

The ground state of an ion may change, as the crystal field is increased. In this case the diagram shows a sudden increase of other energy levels at the point of the change.

The crystal field energy states in the TS-diagrams are labeled with the irreducible representations of the corresponding symmetry group. Figure 9 shows for example that the 5D Russell-Saunders ground state of the free Fe^{3+} iron with the d^6 configuration is split into a $^5T_{2g}$ (lower energy = crystal field ground state) and a 5E_g crystal field level (this is in perfect analogy with the splitting of the 5 d-orbitals into t_{2g} and e_g states). At higher crystal field strengths the $^1A_{1g}$ crystal field level which arises from the splitting of the 1I

term becomes even lower in energy and is the new ground state from there onward. The notation of the free ion states is briefly reviewed [53, 54, 55]:

The electron configurations of several transition metal ions from the first period are given in table 9. Only the unfilled d-shell is indicated, in addition all ions have a closed argon core [Ar]:

Table 9: Electron configurations for selected transition metal ions [55]

	Ti ³⁺	Ti ²⁺	Cr ³⁺	Cr ²⁺	Fe ³⁺	Fe ²⁺				
Sc ³⁺	V ⁴⁺	V ³⁺	Mn ⁴⁺	Mn ³⁺	Mn ²⁺	Co ³⁺	Co ²⁺	Ni ²⁺	Cu ²⁺	Zn ²⁺
3d⁰	3d¹	3d²	3d³	3d⁴	d⁵	3d⁶	3d⁷	3d⁸	3d⁹	3d¹⁰

As usual the letter code for the orbital angular momenta l (for one-electron systems) and L (for multi-electron systems) is:

Table 10: Letter code values for orbital angular momenta [55]

$l = L =$	0	1	2	3	4	5
letter	s	p	d	f	g	h
	S	P	D	F	G	H

According to the vector model for atoms, an orbital angular momentum of value l has several possibilities for its spatial arrangement, indicated by its z-component m_l :

$$m_l = l, l - 1, l - 2, \dots, -l \quad \text{Equ. 9}$$

Therefore $(2l + 1)$ values for m_l are possible. For a d-electron, with $l = 2$ the values of m_l are $m_l = 2, 1, 0, -1, -2$. Thus there are five d-orbitals.

In multi-electron transition metal free ions the electrons can occupy any of the degenerate d-orbitals. If as the only physical constraint the Pauli principle is taken (only two electrons per orbital and spin-pairing) then there are for example 45 possible arrangements of the two d-electrons of V^{3+} . These 45 arrangements however are no longer degenerate because of electron-electron repulsion. Some arrangements (with less possibility of repulsion) will be lower in energy than others. Hence the degeneracy of the 45 arrangements is lifted and discrete free ion energy levels occur, which are called the Russell-Saunders terms represented by a term symbol:

$$^{2S+1}L_J$$

In a term symbol the letter L is S, P, D, F, etc. and corresponds to the **orbital angular momentum quantum number L** (0, 1, 2, 3, etc.). The multiplicity of the term is $2S + 1$, where **S is the total spin quantum number** and **J is the total angular momentum quantum number** which is a consequence of spin-orbit coupling which is not considered as an important effect for the first period transition elements. Therefore their Russell-Saunders terms were denoted by just ^{2S+1}L . Each of these terms has a degeneracy of $(2L+1) \cdot (2S+1)$ which can be lifted by external electric fields (like the crystal field in a solid).

For example the 45 degenerate d^2 configuration is split into (degeneracy is indicated underneath):

$$d^2 \rightarrow {}^3F, {}^3P; {}^1G, {}^1D, {}^1S$$

$$(45) \quad (21) \quad (9) \quad (9) \quad (5) \quad (1)$$

Spin-orbit coupling is a major effect in ions with unfilled f-shells (lanthanides, rare-earth elements) and must be taken into account there. So the free ion RS terms of Rare earth ions ${}^{2S+1}L$ consist of $2J+1$ states, which are usually degenerate in the absence of an external electric magnetic field and are split in their presence [53].

The J-values can be calculated from the L and S values [54]:

$$J = L + S, L + S - 1, \dots, |L - S| \quad \text{Equ. 10}$$

What was said about term symbols can be summarized [53]:

$$\text{multiplicity} \rightarrow 2S+1 \quad L_{J \leftarrow \text{level}} \leftarrow \text{orbital angular momentum}$$

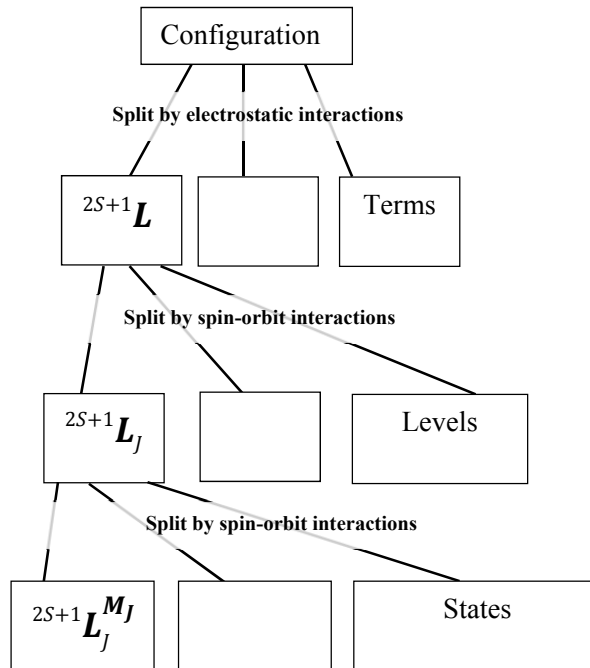


Figure 7: Notation and origin of the splittings of energy levels in atoms and ions [53]

The correct term symbol of an electronic ground state can be found via the formalism of the orbital graph [55]. An orbital graph is a pictorial scheme of the d-shell, where the orbitals are represented by boxes. There are five rows with two boxes each, the rows are labeled with m_l and the columns with m_s . These boxes may be filled with electrons. By summing the individual m_l and m_s values of the electrons M_l and M_s values are obtained:

$$M_L = \sum m_l \quad \text{Equ. 11}$$

$$M_S = \sum m_s \quad \text{Equ. 12}$$

From: $M_L = L, L-1, L-2, \dots, -L$; and $M_S = S, S-1, S-2, \dots, -S$ it is clear that $M_{L,\max} = L$ and $M_{S,\max} = S$.

By filling the boxes in such a way that the maximal value for M_L and at the same time the maximal value for M_S is results, one makes sure that the electronic ground state according to Hund's rules is obtained. This is always the case when the orbital graph is filled with electrons starting from top left.

This procedure is in accordance with Hund's rules [54]:

1. The term with maximum multiplicity lies lowest in energy.
2. For a given multiplicity, the term with the highest value of L lies lowest in energy.
3. For atoms with less than half-filled shells, the level with the lowest value of J lies lowest in energy.

For transition metal ions Hund's first and second rule have to be considered only. For rare earth ions, Hund's third rule has to be taken into consideration because of the spin-orbit coupling, which plays an important role for rare earths [55].

As an example Fe^{2+} and Fe^{3+} ground states will be determined. A neutral iron atom has the electron configuration $1s^2 2s^2 2p^6 3s^2 3p^6 3d^6 4s^2$ or simpler $[\text{Ar}]3d^6 4s^2$. When the neutral Fe loses 2 electrons and becomes Fe^{2+} the electronic configuration is $[\text{Ar}]3d^6$. This leads to a Russell-Saunders term symbol for the ground state of 5D . When the Fe^{2+} ion loses another electron $[\text{Ar}]3d^5$ to become Fe^{3+} the corresponding Russell-Saunders term symbol is 6S (see figure 9).

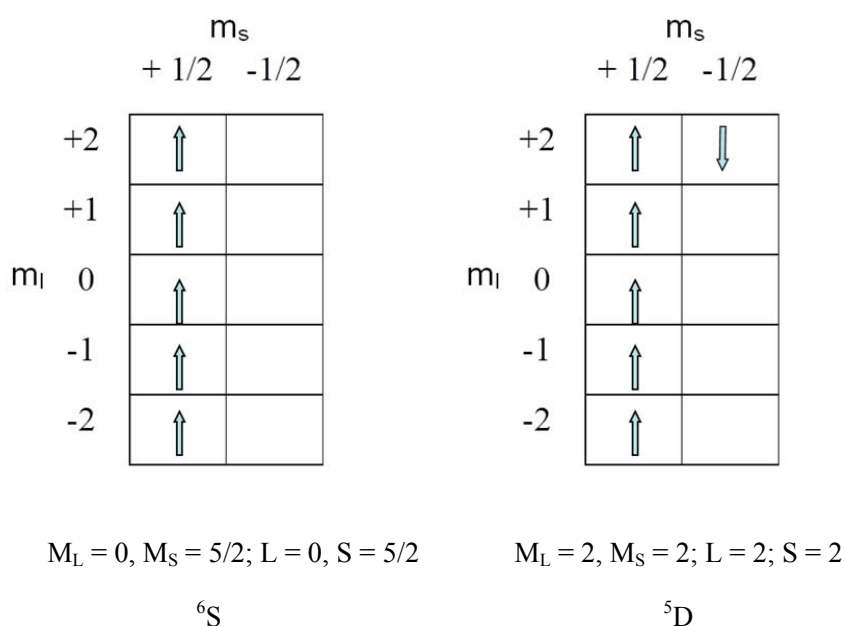


Figure 8: Orbital graphs for the d^5 and d^6 configuration of Fe^{3+} and Fe^{2+} , respectively

The higher energy states of an ion can be found by application of the Gray-Wills [57] or the Shudeman [56] method. Figure 9 shows the TS-diagram for these ions in O_h symmetry.

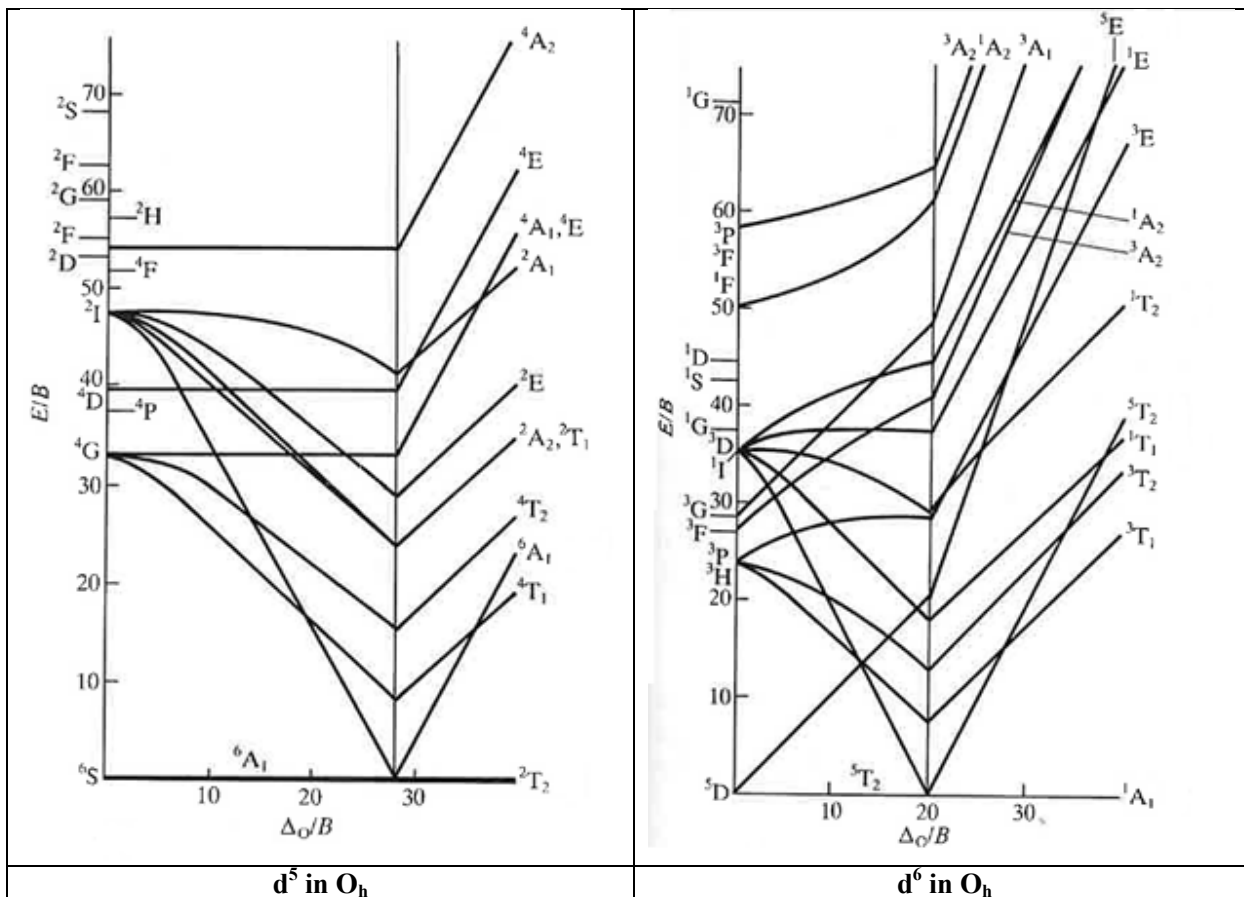


Figure 9: Tanabe Sugano diagrams for two d -electron systems in octahedral symmetry (for convenience the “g” index is not written – all states arising from d -systems are g)

1.5.1.4 Anharmonic Oscillator and IR-spectra

The short wave to long wave side of transmission or reflection spectra from 200 to approximately 900 nm can be understood with the concepts presented in the previous chapters. For the NIR to MIR region of the spectra the oscillator model gives a good explanation.

A molecule can be considered as a system of several masses, tied together by springs. Every possible oscillation of such a system can be visualized as an idealized harmonic oscillator or, more realistically, as an anharmonic oscillator. The anharmonic oscillator model includes the zero point energy, the energy of the state with quantum number $v = 0$ (which is not zero) and the dissociation limit of a molecule. The transition from $v = 0$ to $v = 1$ is called the fundamental. The transition $v = 0$ to $v = 2$ is called the first overtone and so forth. The energy of a vibration E_{VIB} can be calculated as follows: [58]

$$E_{VIB} = h\nu_{osc} \left(v + \frac{1}{2} \right) = \frac{h}{2\pi} \sqrt{\frac{k}{\mu}} \left(v + \frac{1}{2} \right) \quad \text{Equ. 13}$$

In equation 13 h is Planck's constant, ν_{osc} the oscillation frequency, v the quantum number of the oscillation, k the force constant and μ the reduced mass.

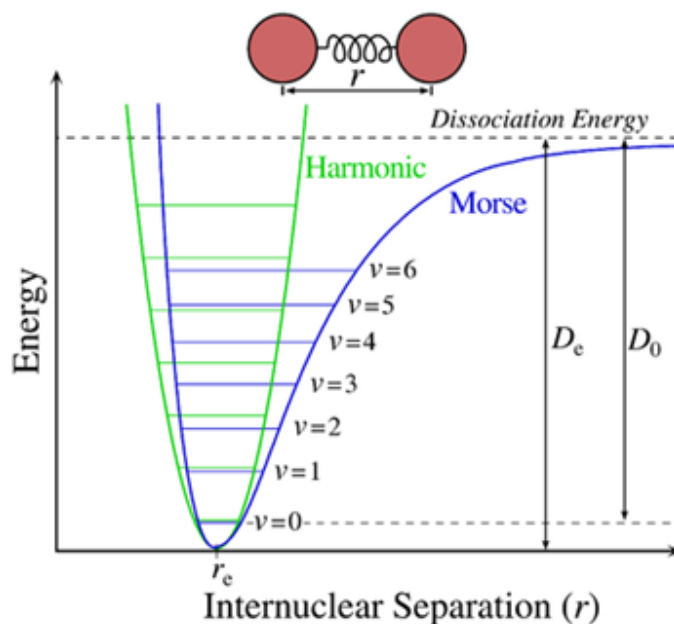


Figure 10: Potential curve for a harmonic (green) and an anharmonic (blue) oscillator [59]

For anharmonic systems the potential curve is well represented by the “Morse”-potential.

Overtone can be approximated within the harmonic oscillator model with the following equations [62]:

$$n = 0: E_0 = \frac{1}{2} h\nu_{osc}$$

$$n = 1: E_1 = \frac{3}{2} h\nu_{osc}$$

$$n = 2: E_2 = \frac{5}{2} h\nu_{osc}$$

$$n = 3: E_3 = \frac{7}{2} h\nu_{osc}$$

etc.

Combination vibrations of the system can be calculated as follows [60, 61]:

$$\nu_{comb} = a \cdot \nu_1 \pm b \cdot \nu_2 \pm c \cdot \nu_3 \pm \dots \quad \text{Equ. 14}$$

In equation 14 ν_{comb} is the wavenumber of the combination vibration, ν_n is the n-th fundamental (with $n = 1, 2, 3, \dots$) and a, b and c non-negative integral numbers.

However, the number of observable combinations and overtones of molecules is reduced by symmetry constraints. Furthermore the observed wavenumbers for combinations and overtones are lower than the calculated ones from the harmonic oscillator model due to the anharmonicity of the system [60, 61].

1.5.2 Reflection Spectroscopy with the L950 on Minerals

Since the theory of absorption of light was discussed in detail in previous parts of the work, this chapter will deal with some practical aspects of reflection measurements of solids.

The state of the art spectrometer type in laboratories is the double beam spectrometer. A schematic drawing of the optical system of the dispersive Lambda 950 transmission/reflection spectrometer is given in figure 11.

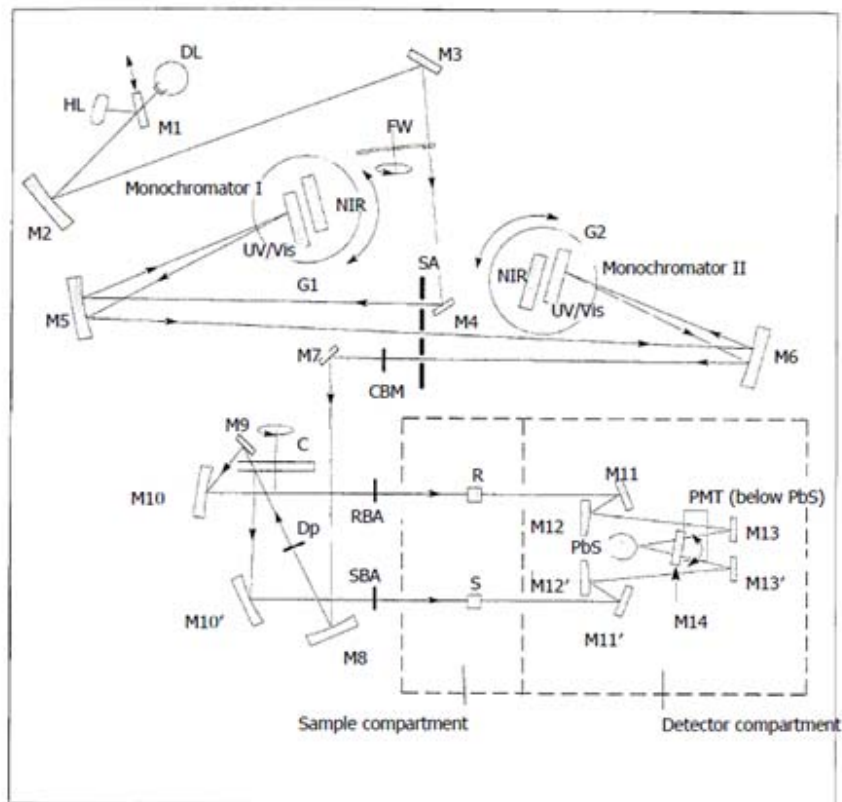


Figure 11: The optical system of the L950 spectrometer [63]

In figure 11 DL is the deuterium lamp, HL the halogen lamp, Mx the mirror number x, SA the slit assembly, G the grating, C the chopper assembly, CBM the common beam mask, FW the filter wheel assembly, C the chopper, Dp the depolarizer, R the reference and S the sample [64]. Figure 12 shows the L950 spectrometer, which was used to record all reflection and transmission spectra in this work.

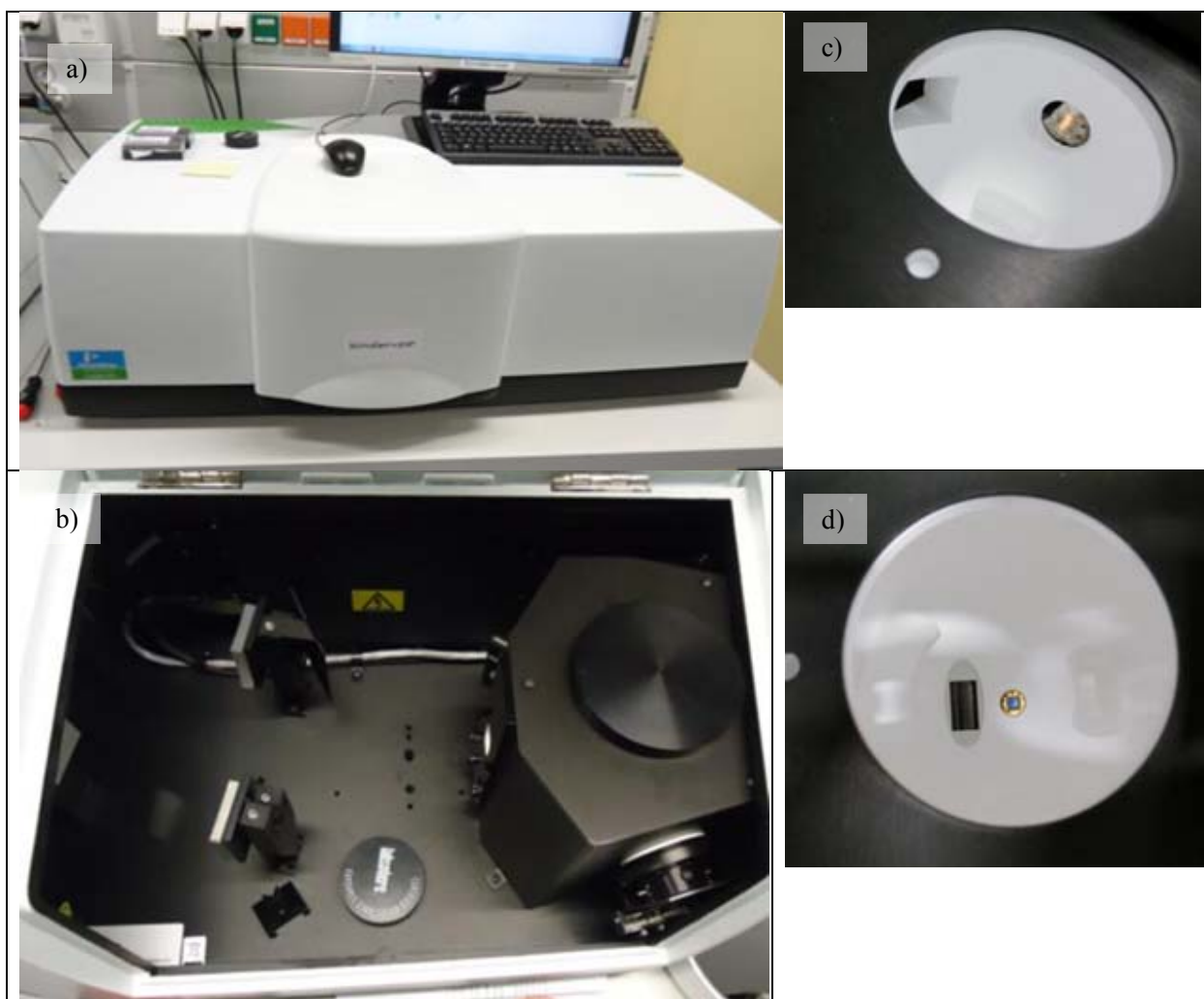


Figure 12: a) the L950 spectrometer, b) the integrating sphere detector module, c) a Bauxite sample at the diffuse reflection port of the integrating sphere, d) the PMT-detector for UV-VIS-detection (left) and the InGaAs-detector for NIR-detection (right)

The most important law for all day laboratory work is the Beer-Lambert law:

$$I = I_0 \cdot \exp(-\epsilon cd) \quad \text{Equ. 15}$$

or in the more common form:

$$\log\left(\frac{I_0}{I}\right) = A = \epsilon cd \quad \text{Equ. 16}$$

In equations 15 and 16 I_0 is the intensity of the reference beam, I the intensity of the beam which passed the sample, A the Absorbance, ϵ the molar absorption coefficient, d the length of the cuvette and A the absorbance [65].

When light hits matter four phenomena can be encountered: reflection (R), scattering (S), transmission (T) and absorption (A).

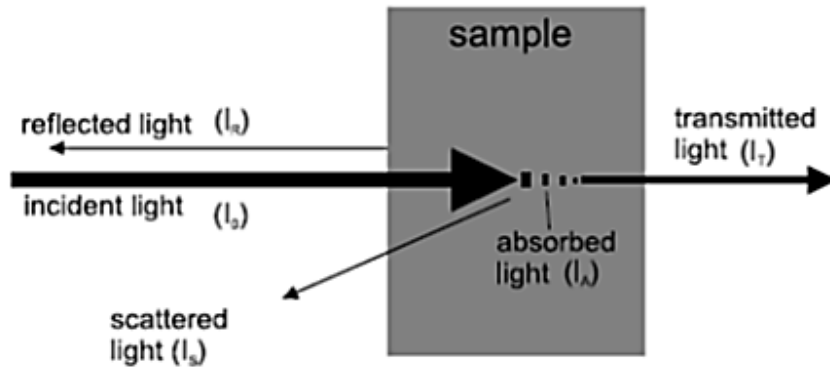


Figure 13: Interaction of light with a sample [66]

In figure 13 I_R is the intensity of the reflected light, I_0 the intensity of the incident light, I_S the intensity of the scattered light, I_A the intensity of absorbed light and I_T the intensity of transmitted light.

The measurements in this work fall in the category of diffuse reflection measurement. The surface of the sample, which could be a powder, a rough surface of a mineral or a microcrystalline sample is optically scattering. The incident light may be partly reflected regularly (i.e, the angle of incidence is the same as the emergent angle), partly scattered diffusively and partly enter the substrate. The part that enters the substrate can undergo absorption within particles, undergo diffraction at grain boundaries, re-emerge at the sample surface and mix with reflected parts. Measured reflection values are therefore a sum of all these contributions. Reflectivity values can be transformed to absorbance values via mathematical models. One of these models is the Kubelka-Munk theory, which can be found in the literature [127]. For practical use the reflectivity will be defined as follows:

$$R_{\lambda} [\%] = \frac{I_{R,\lambda}}{I_0} \quad \text{Equ. 17}$$

In equation 17 R_{λ} is the reflectivity at a certain wavelength λ , $I_{R,\lambda}$ is the intensity of reflected light at a certain wavelength and I_0 is the intensity of the incident beam.

The L950 spectrometer uses an integrating sphere with two possible measurement ports: a) the diffuse transmission port and b) the diffuse reflection port, where the sample is twisted 8° to the incident beam. The diffuse transmission port can be used for transmission measurements of opaque samples, since the scattered part of the transmitted light is gathered by the integrating sphere and reflected to the detector system. The slight twist of the sample at the diffuse reflection port is necessary to ensure that no reflected light goes back to the light source and is therefore lost for detection. It is also possible to exclude all the regular reflection from detection, by opening the integrating sphere at one side opposite to the sample.

The integrating sphere of the L950 system is coated with so called ‘‘Spectralon’’ which is pure Teflon (Poly(1,1,2,2-tetrafluorethylene)). Teflon has a rather high reflectivity in the interesting region from 200 nm to 2500 nm. But it should be noted, that even this highly reflecting material is not a 100% reflector over all wavelengths. A reflection spectrum of spectralon is depicted in figure 14.

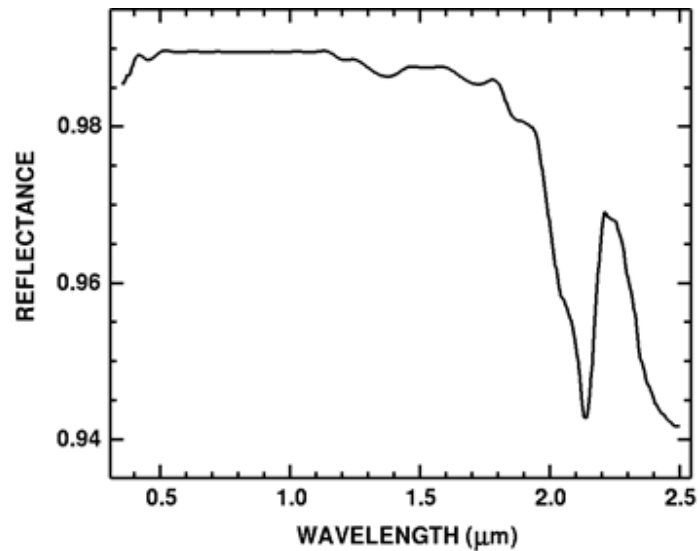


Figure 14: Spectralon reflection spectrum [128]

Since no two integrating spheres do have the same optical properties, even if they have the same coating material, correction of the reflection spectrum is necessary if reflection spectra are to be compared in detail as proposed by Clark et al. [128].

After cutting and polishing the mineral samples can be easily positioned at the reflection port of the integrating sphere and fixed by tape, the positioning mechanism at the outside of the sphere or plasticine. For samples smaller than the reflection port diameter of about 2,5 cm , a Teflon aperture was constructed, which has a hole diameter of 8 mm. If the Teflon aperture is used, it has to be positioned properly using the align-mode of the spectrometer.

The positioning of the samples is shown in figure 15.

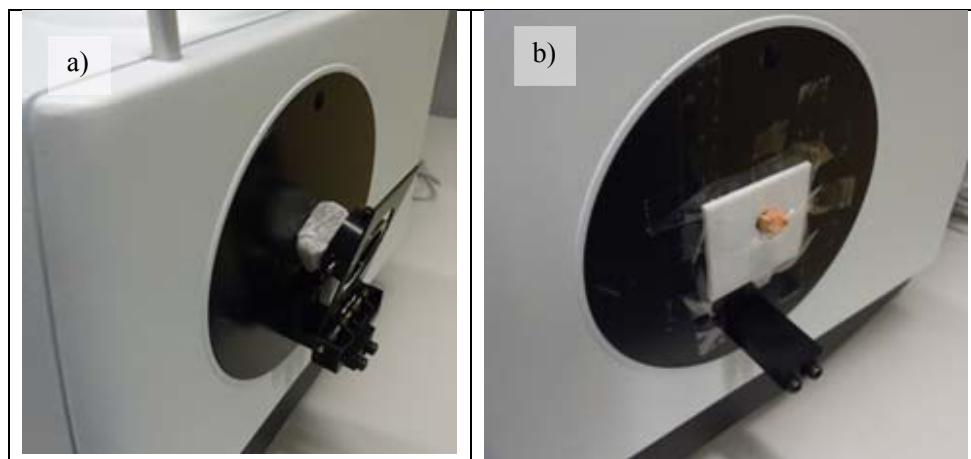


Figure 15: Sample positioning at the L950 integrating sphere reflection port a) with the original holder, b) with tape using a Teflon aperture with 8 mm hole diameter

It should be avoided that samples fall into the integrating sphere, since the PMT-detector and the InGaAs-detector are positioned at the bottom side of the detector module. If the reflection coating is contaminated with dust from the laboratory, it can be cleaned with a N₂-gas stream.

The integrating sphere of the L950 system has a diameter of about 150 mm. Therefore the light (especially in the NIR region) reflected from the sample is attenuated and has to be intensified via the so called “InGaAs gain”. It turned out, that a value of 16 yields good results. Figure 16 shows the schematic diagram of the control software UV-Winlab.

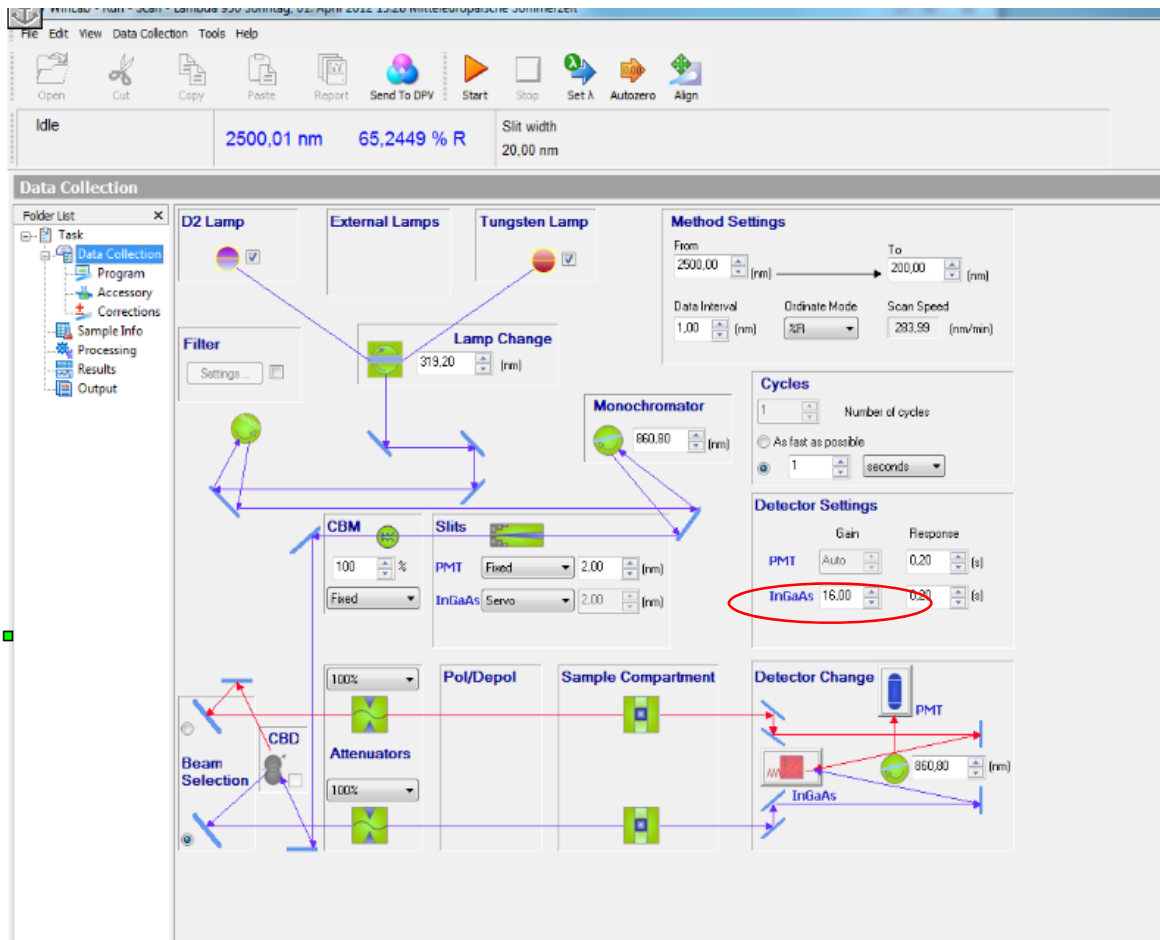


Figure 16: Schematic diagram of the control window of UV-Winlab

A comparison of two spectra of the same Holmium oxide reflection standard is given in figure 17.

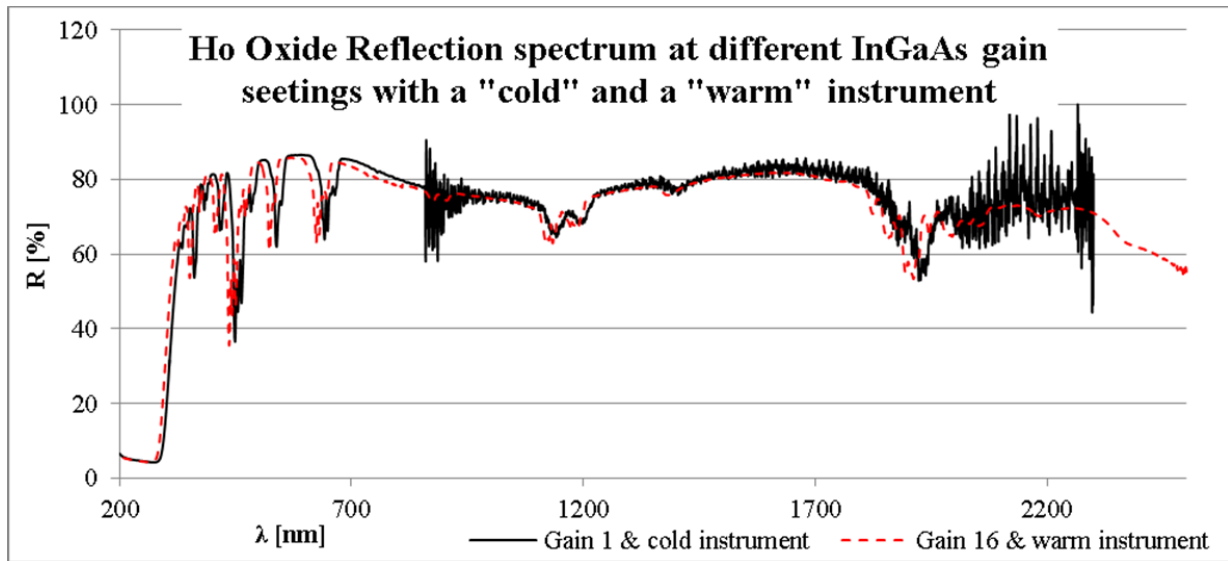


Figure 17: Ho-oxide reflection spectrum with and without proper warm up time and gain settings

It is seen, that the proper gain setting greatly increases the signal to noise ratio and also that for a good wavelength accuracy the instrument has to be switched on for about 30 minutes to warm up the system.

1.5.3 Raman Spectroscopy of Minerals

Raman spectroscopy is based on the inelastic scattering of light by matter. It can be used to classify minerals and inclusions in minerals via comparison of the sharp Stokes peaks in Raman-spectra of minerals with database entries. A good overview over the basics of the technology and applications for minerals with some data on Raman bands is given by Frezotti et al. [129]. The authors give also some examples for the identification of mineral phases with Raman-spectroscopy. An energy level scheme, example spectrum and basic setup of a Raman spectrometer are depicted in figure 18.

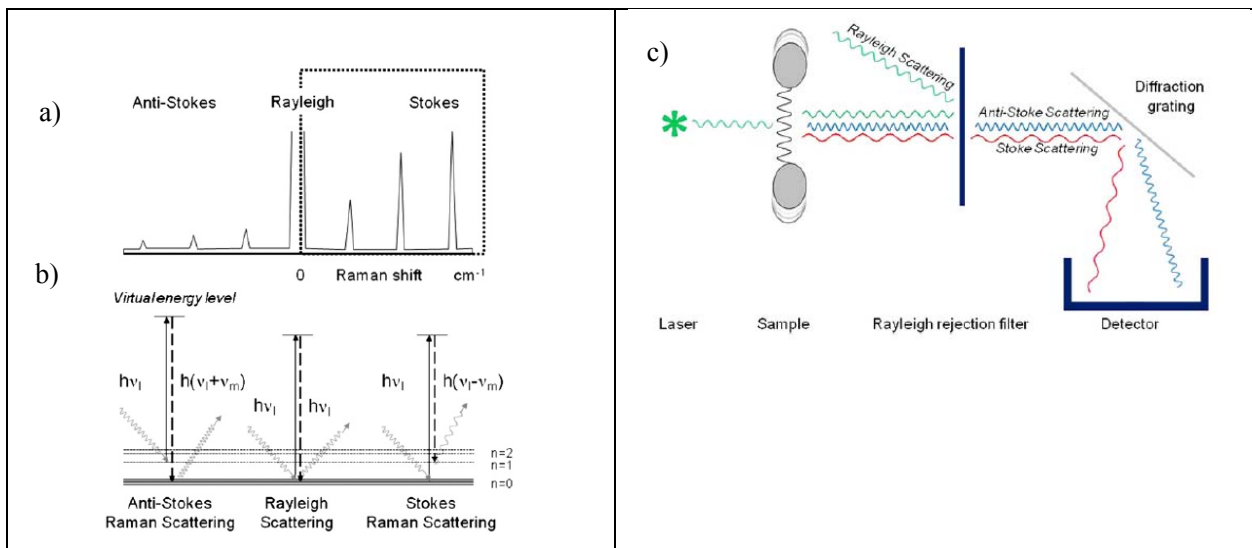


Figure 18: a) Example Raman spectrum, b) Energy level scheme for elastic Rayleigh scattering and inelastic Anti-Stokes and Stokes Raman scattering, c) basic setup of a Raman spectrometer [129]

Raman scattering can be explained as an interaction of light with matter in a quantum mechanical model: A molecule has different vibrational energy levels, the ground state $v = 0$ and the excited states $v = 1$, $v = 2$, $v = 3$, etc. are separated by a quantum energy $\Delta E = h\nu_m$. h is Planck's constant and ν_m the frequency of the molecular vibration. The incident light induces transitions to virtual energy levels of the molecule. This virtual energy levels are generated when light interacts with the molecule and the energy is risen. Because virtual energy levels are unstable the energy is released as scattered light immediately. Light of the frequencies ν_i (excitation frequency), $\nu_i - \nu_m$ (Stokes) and $\nu_i + \nu_m$ (Anti-Stokes) is emitted, where ν_m is the fundamental rotational, vibrational or lattice frequency of the molecule. The Raman effect is a very weak optical phenomenon and since anti-Stokes lines are much weaker than Stokes lines, only Stokes lines are plotted in a Raman spectrum. The Rayleigh peak has the same frequency as the excitation source (usually a VIS laser) and is defined as the zero point in a Raman spectrum. The Stokes lines in Raman spectra represent vibrational energies (stretching and bending) of the analyzed molecules. When a vibration is observed in the Raman spectrum it changed the polarizability of the molecules [129].

The project partner Montanuniversität Leoben has a lab scale Raman spectrometer for identification of mineral phases in use.

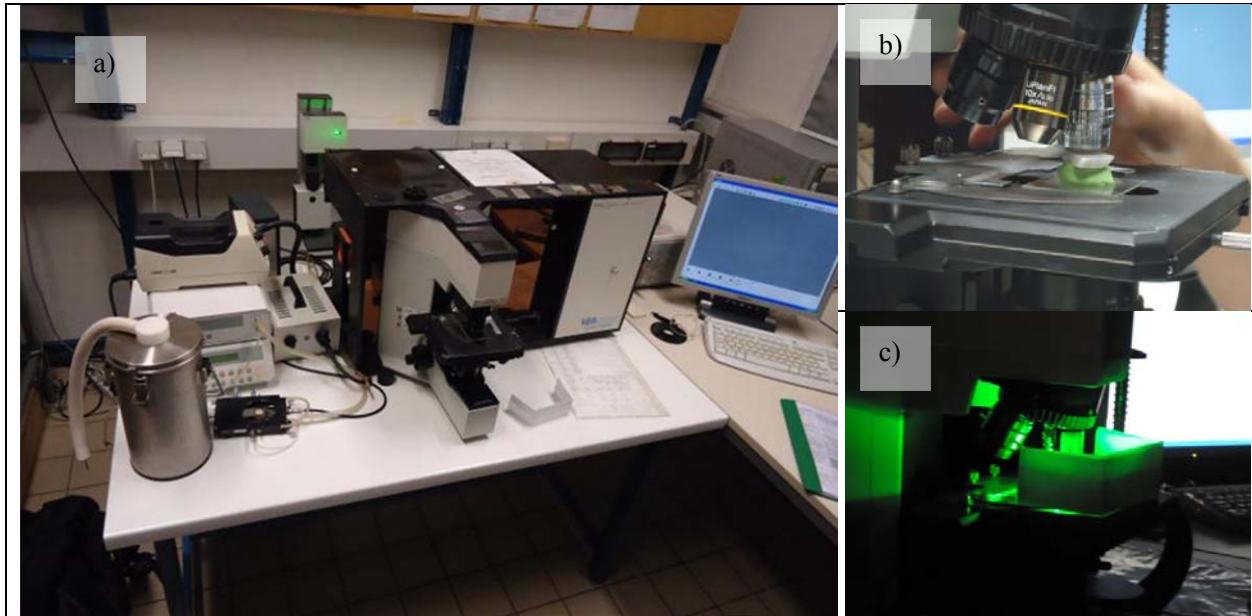


Figure 19: Raman spectrometer at the MUL: a) Raman workplace, b) sample positioned in the apparatus, c) Raman spectrometer at work with the green laser light source.

For lack of space no Raman spectra are presented in the present work. However, it should be mentioned, that Raman spectrometers focus only on a small spot of the sample. Therefore the method is prone to errors originating from sample inhomogeneities.

1.5.4 Fluorescence Spectroscopy and Sorting of Minerals

1.5.4.1 From Molecular Fluorescence to Solid State Fluorescence

Molecular fluorescence is often explained with the configuration coordinate- or, alternatively, the Jablonski diagram, which are depicted in figure 20. A molecule can be excited from its electronic ground state to an excited or “activated state”. This activated state can relax without emission of radiation for example by molecule-molecule or molecule-wall collisions in a liquid system or via phonons in a solid system. The energy is converted into rotational, vibrational and translational energy. This process is also known as “thermal dissipation”.

Fluorescence is considered as a rather fast phenomenon (nanoseconds), while phosphorescence is an emission that can last longer (microseconds to several hours). Usually the emitted light has a longer wavelength, corresponding to a lower energy, as the excitation light. This is known as the Stokes-shift of the system. Fluorescence can be summarized as follows:

1. Absorption of light
2. Excitation of the system from its ground state (singlet, S_0) to a higher electronic state (singlet, S_1)
3. Radiative and non radiative deactivation of the system

In Phosphorescence there is another step called intersystem crossing. Intersystem crossing is a spin forbidden transition, but enabled by spin-orbit coupling. Spin orbit coupling is usually high, when a molecule contains heavy elements like sulfur.

It is a transition from an excited singlet state to a triplet state. The triplet state serves as a slow radiative reservoir, because to return to the ground state is also spin forbidden. Therefore phosphorescence can be summarized as follows [131]:

1. Absorption of light
2. Excitation of the system from its ground state (singlet, S_0) to a higher electronic state (singlet, S_1)
3. Intersystem crossing: transition from S_1 to T_1
4. Radiative deactivation of the system

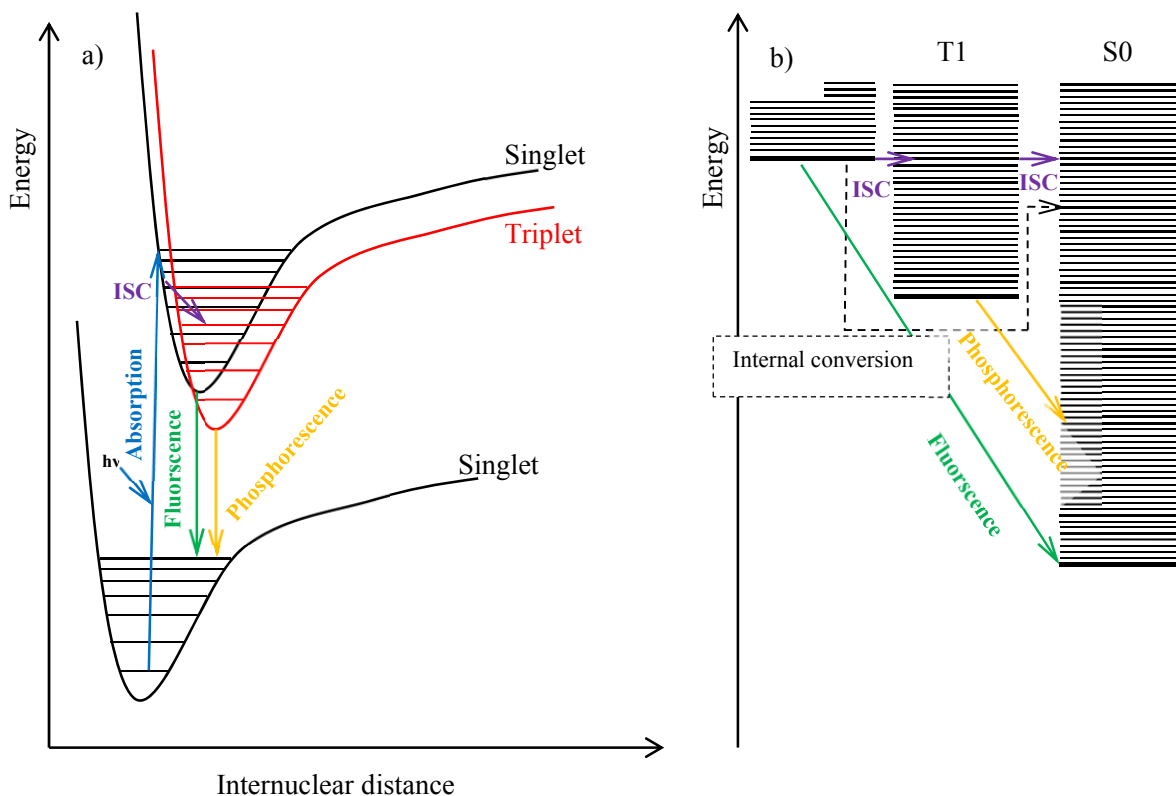


Figure 20: a) Mechanism of phosphorescence and fluorescence. The crucial feature for phosphorescence is the intersystem crossing (ISC) as a change from singlet to triplet state, which is possible because of the spin orbit coupling. b) Jablonski diagram [130]

For solids a very similar model can be applied. For example if a Cr^{3+} -ion is considered in an octahedral crystal field, like it is the situation in ruby ($\text{Al}_2\text{O}_3:\text{Cr}^{3+}$). Several vibrational modes can be found. An octahedron can be considered as a molecule with 7 atoms. The $3N-6$ rule states, there must be $3 \cdot 7 - 6 = 15$ normal modes. The totally symmetric breathing mode can be described like a diatomic oscillator with one parameter Q which describes the in-phase vibration of the ligands towards the central Cr^{3+} .

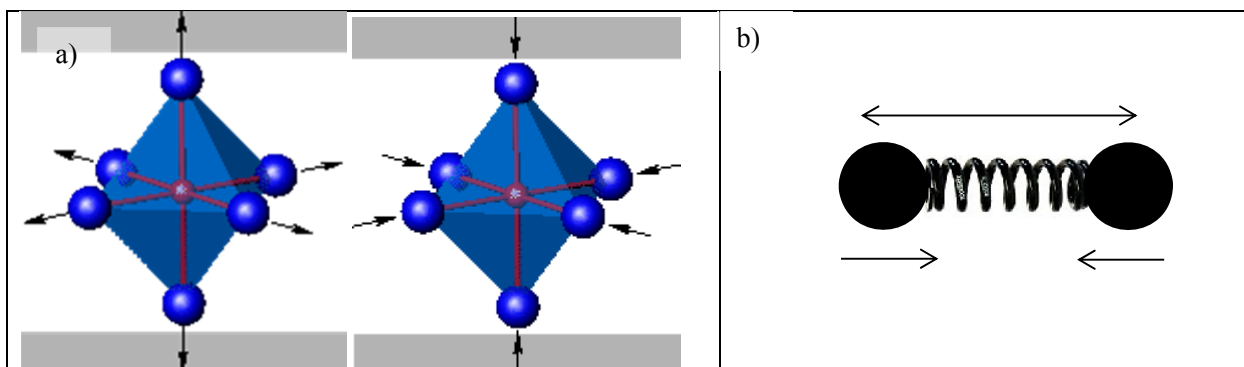


Figure 21: a) Breathing mode of an octahedron [133], b) a diatomic oscillator

A combination of the Tanabe-Sugano diagram and configuration coordinate diagrams can serve to predict emission spectra of solids. A combined diagram for the Cr^{3+} system in octahedral crystal field is presented

in figure 22. This diagram is the key to understand the emission spectrum of ruby, which was the first laser material.

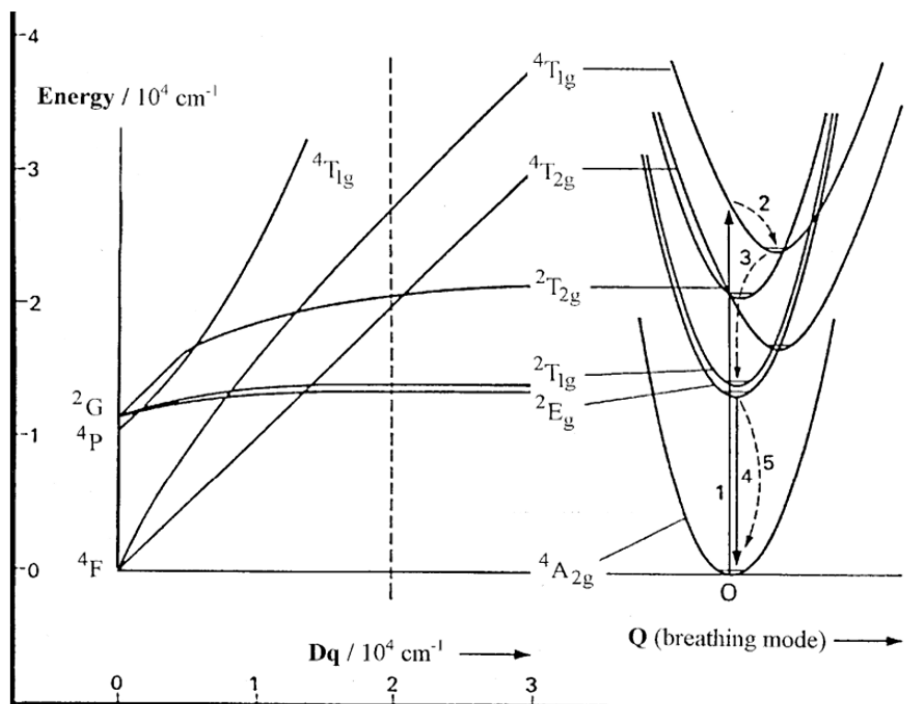


Figure 22: Combined diagram for the system Cr^{3+} in octahedral crystal field [132]

The numbered steps in figure 22 can be described as follows:

1. ${}^4A_{2g} \rightarrow {}^4T_{1g}$: Excitation of electrons into the blue absorption band of the system populates excited vibrational levels of the ${}^4T_{1g}$ state.
2. Radiationless relaxation to the vibrational ground state of ${}^4T_{1g}$
3. ${}^4T_{1g} \rightarrow {}^2T_{1g}$: non radiative transition to ${}^2T_{1g}$ (this corresponds to ISC in the molecular model)
 ${}^2T_{1g} \rightarrow {}^2E_g$: vibronic transition
4. ${}^2E_g \rightarrow {}^4A_{2g}$: emission of photons (694 nm)
5. Possible non radiative transition in concurrence to 4

Thus the absorption and emission transitions can be predicted and are plotted in figure 23.

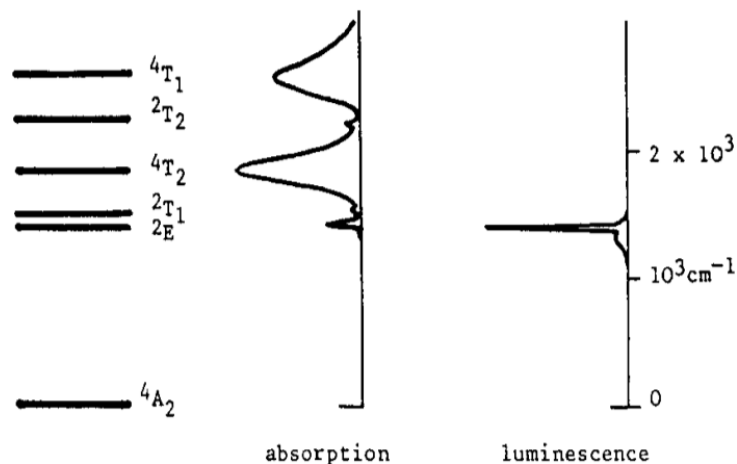


Figure 23: Absorption and emission spectrum of ruby (Cr³⁺ in Al₂O₃) [132]

In general relative fluorescence intensities are measured. Intensity data recorded with the same instrument, using the same set of instrumental parameters (slit width, gain, etc.) can be compared easily. Comparing fluorescence intensities obtained with different instrumental parameters is more difficult (see chapter 3.2.1). If datasets from different instruments are compared, differences can occur because of the different optical properties of the instruments. Measurement of absolute intensities is also possible, but requires particular instruments.

Therefore the determination of absolute fluorescence intensity requires a much bigger experimental effort [86]. There is a commercial device provided by Hamamatsu: The “Absolute PL Quantum Yield Measurement System” consists of an excitation source and an integrating sphere. Details on this method can be found on the Hamamatsu homepage [87].

1.5.4.2 Mineral Fluorescence

Fluorescence of minerals of natural origin could be a promising field for sorting applications in industry. The existing data on mineral fluorescence, combined with available sensor-technologies can be used for sorting of industrially relevant minerals and ores [75].

The book “**Luminescence Spectroscopy of Minerals and Materials**” by Gaft et al gives a good overview on minerals fluorescing upon UV-light excitation [76]. The introduction chapter contains a table with 62 common fluorescing minerals which is reproduced below (see table 11).

Table 11: Minerals luminescent under UV lamp excitation

Native	Diamond
Oxides	Brucite $Mg(OH)_2$, Corundum Al_2O_3 , Ruby Al_2O_3 , Sapphire Al_2O_3
Halogenides	Fluorite CaF_2 , Halite $NaCl$, Calomel $HgCl$
Silica	Agate SiO_2 , Opal SiO_2 , Quartz SiO_2
Phyllosilicates	Pyrophyllite $AlSi_2O_5OH$, Talc $Mg_3Si_4O_{10}(OH)_2$, Serpentine $(Mg,Fe)_3Si_2O_5(OH)_4$
Feldspar	Albite $NaAlSi_3O_8$, Microcline $KAlSi_3O_8$
Pyroxenes	Diopside $CaMgSi_2O_6$, Spodumene $LiAlSi_2O_6$
Amphiboles	Anthophyllite $(Mg, Fe)_7Si_8O_{22}(OH)_2$, Tremolite $Ca_2Mg_5Si_8O_{22}(OH)_2$
Zeolites	Natrolite $Na_2Al_2Si_3O_{10} \times 2H_2O$, Laumontite $CaAl_2Si_4O_{12} \times 4H_2O$, Analcite $NaAlSi_2O_6 \times H_2O$
Feldspathoids	Sodalite $Na_4Al_3(SiO_4)_3Cl$
Other silicates	Zircon $ZrSiO_4$, Datolite $CaBSiO_4(OH)$, Danburite $CaB_2Si_2O_8$, Eucryptite $LiAlSiO_4$, Willemite Zn_2SiO_4 , Wollastonite $CaSiO_3$, Sphene $CaTiSiO_5$, Scapolite $Na_4(Al, Si)_{12}O_{24}$, Axinite $Ca_2(Mn, Fe, Mg)Al_2(BO_3OH)(SiO_3)_4$, Benitoite $BaTiSi_3O_9$, Thorite $(Th,U)SiO_4$
Carbonates	Aragonite $CaCO_3$, Calcite $CaCO_3$, Cerussite $PbCO_3$, Magnesite $MgCO_3$, Strontianite $SrCO_3$, Witherite $BaCO_3$
Sulfides	Sphalerite $(Zn,Fe)S$, Wutzite $(Zn,Fe)S$
Sulfates	Barrite $BaSO_4$, Celestine $SrSO_4$, Gypsum $CaSO_4 \times 2H_2O$, Anhydrite $CaSO_4$, Alunite $KAl_3(SO_4)_2(OH)_6$, Zippeite $K_4(UO_2)_6(SO_4)_3OH_{10} \times 4 H_2O$, Ettringite $Ca_6Al_2(SO_4)_3(OH)_{12} \times 26 H_2O$, Hanksite $Na_{22}K(SO_4)_9(CO_3)_2Cl$
Phosphates	Apatite $Ca_5(PO_4)_3(OH,F,Cl)$, Wavellite $Al_3(PO_4)_2(OH)_3 \times 5 H_2O$, Amblygonite $(Li,Na)AlPO_4(F,OH)$, Pyromorphite $Pb_5(PO_4)_3Cl$, Monazite $(Ce,La,Th,Nd,Y)PO_4$, Autunite $Ca(UO_2)_2(PO_4)_2 \times 10 H_2O$, Xenotime YPO_4
Tungstates	Scheelite $CaWO_4$
Molybdates	Powellite $CaMoO_4$, Wulfenite $PbMoO_4$
Borates	Colemanite $CaB_3O_4(OH)_3 \cdot H_2O$
Organics	Amber $C_{10}H_{16}O$

The book also provides a short but good overview of the theory of mineral fluorescence and a collection of time resolved luminescence spectra. As minerals are by definition natural crystalline solids they can contain more than one luminescence center. For example two luminescence centers in the same mineral can show emission in the same spectral range with different decay and life times of the excited state. So

Gaft et al refer to the terms “delay time” abbreviated D and “gate time” abbreviated G in their book to describe this behavior in the quoted spectra. The spectra contained in the book are sorted by luminescent minerals bearing cations of interest such as Ca^{2+} , Pb^{2+} , Sn^{4+} , Ba^{2+} , Sr^{2+} , Ti^{4+} , Zn^{2+} , Zr^{4+} , Si^{4+} , Al^{3+} , Na^+ , Ag^+ , Mn^{2+} , U^{6+} , Mg^{2+} , rare earths and carbon.

A standard reference book with the title “**Luminescent spectra of minerals**” has been published by Gorobets and Rogojine in 2001. It summarizes the main achievements in that field up to the year 2000 [77]. It provides a systematization of luminescent minerals with a hierarchical order in three levels:

- **1st level:** Luminescent minerals are divided into dielectrics (insulators), semiconductors and metals together with intermetallic compounds. This means *classification by the energy bandgap* E_g . Metals are minerals with $E_g = 0$. Low-bandgap semiconductors have values of E_g such as $0 \leq E_g \leq 1$ eV. Metals and semiconductors are opaque to optical photons (so they are incapable of luminescence in principle). Insulators with $4 < E_g < 10$ eV and large-bandgap semiconductors with $1 < E_g < 4$ eV are to some extent transparent to UV and visible light. Under certain circumstances this materials can transform external energy (photons or electrons) into luminescence photons.
- **2nd level:** Luminescent minerals are *subdivided by the type of chemical compounds* like homo-atomic compounds, sulfides, halides and oxygen bearing compounds. The knowledge of the chemical composition gives hints to the mechanisms of the luminescence phenomenon.
- **3rd level:** Luminescent Minerals are partitioned by their *mineral formulae*. The associations of the donor-acceptor centers for examples with vacancies or interstitials determine whether a luminescence center is formed or not.

One further step in the system of Gorobets and Rogojine is to predict which luminescent metal impurities (luminescent cations) are to be expected for a given mineral according to the host cation in the mineral [78]. A compact overview over 25 possible classes of fluorescing minerals was provided by Gorobets et al and is reproduced in table 12. Furthermore it is stated that a luminescing mineral should satisfy the following three conditions [79]:

1. A suitable type of crystal lattice favorable for emission centers is formed.
2. The content of photoluminescent centers is high enough (usually $> 0,01\%$)
3. The amount of iron or other quenchers is small enough (around 0,5 – 1 %). Iron is a principal quenching element in nature.

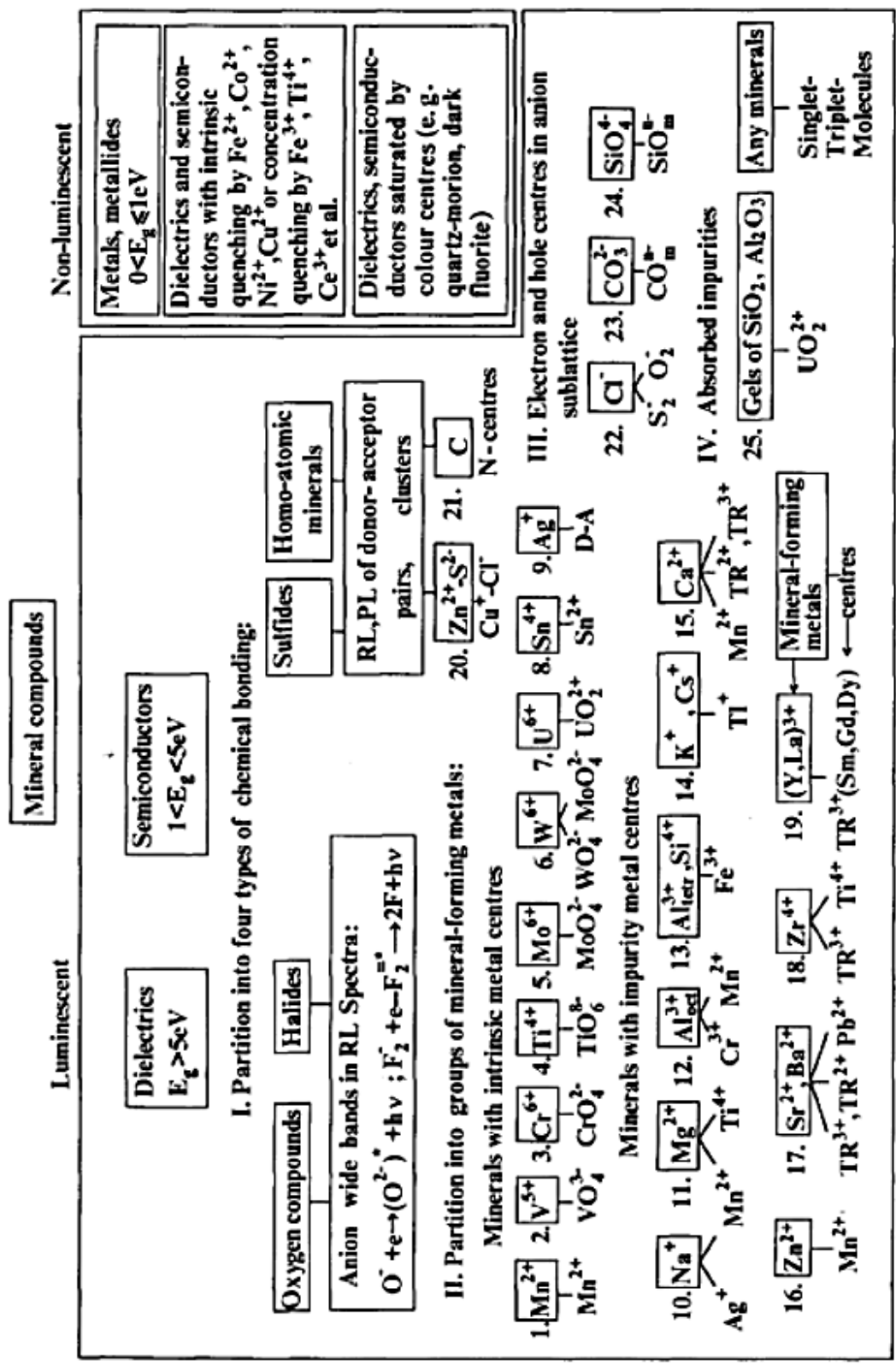


Table 12: Schematic partition of minerals into groups with various luminescent properties due to different types of chemical bonding and composition [79]

Examples for the 25 classes of luminescing minerals in table 12 are given with their chemical formulas and the corresponding crystal systems which were looked up in [80]:

1. **Mn²⁺**: *Rhodonite*: Mn₃[Si₅O₁₅], triclinic
2. **V⁵⁺**: *Vanadinite*: Pb₅[Cl|(VO₄)₃], hexagonal
3. **Cr⁶⁺**: *Crocoite*: Pb[CrO₄], monoclinic
4. **Ti⁴⁺**: *Ramsayite*¹⁰: Na₂Ti₂[O₃|Si₂O₆], orthorhombic
5. **Mo⁶⁺**: *Powellite*: Ca[MoO₄], tetragonal
6. **W⁶⁺**: *Scheelite*: Ca[WO₄], tetragonal
7. **U⁶⁺**: *Otunite*¹¹: Ca[UO₂|PO₄]·10H₂O, tetragonal
8. **Sn⁴⁺**: *Cassiterite*: SnO₂, tetragonal
9. **Ag⁺**: *Chlorargyrite*: AgCl, cubic
10. **Na⁺**: *Halite*: NaCl, cubic
11. **Mg²⁺**: *Forsterite*: Mg₂[SiO₄], orthorhombic
12. **Al³⁺_{oct}**: *Spinel*: MgAl₂O₄, cubic
13. **Al³⁺_{tetr}, Si⁴⁺**: *Feldspars*: (Ba, Ca, Na, K, NH₄)(Al, B, Si)₄O₈, family of minerals in different crystal systems and of different chemical compositions
14. **K⁺, Cs⁺**: *Microline*: K[AlSi₃O₈], triclinic; *Pollucite*: (Cs_{0.7}H₂O_{0.3})Na_{0.3}[AlSi₂O₆], cubic
15. **Ca²⁺**: *Calcite*: Ca[CO₃], trigonal; *Apatite*: Ca₅(F, Cl, OH)|(PO₄)₃, family of minerals in different crystal systems and of different chemical compositions; *Fluorite*: CaF₂, cubic
16. **Zn²⁺**: *Willemite*: Zn₂[SiO₄], trigonal
17. **Sr²⁺, Ba²⁺**: *Strontianite*: SrCO₃, orthorhombic; *Baryte*: Ba[SO₄], orthorhombic
18. **Zr⁴⁺**: *Zircon*: Zr[SiO₄], tetragonal
19. **(Y, La)³⁺**: *Gagarinite*: NaCaYF₆, hexagonal
20. **Zn²⁺-S²⁻**: *Sphalerite*: ZnS, cubic
21. **C**: *Diamond*: C, cubic; *Moissanite*: SiC, family of minerals in different crystal systems and of different chemical compositions
22. **Cl⁻**: *Sodalite*: Na₈[Cl₂|(AlSiO₄)₆], cubic; *Pyromorphite*: Pb₅[Cl|(PO₄)₃], hexagonal
23. **CO₃²⁻**: *Calcite*: Ca[CO₃], trigonal; *Dolomite*: CaMg[CO₃], trigonal; *Hydrozincite*: Zn₅[(OH)₆(CO₃)₂], monoclinic
24. **SiO₄⁴⁻**: *Forsterite*: Mg₂[SiO₄], orthorhombic
25. **Gels of SiO₂, Al₂O₃**: *Chalcedony*¹²: SiO₂, different crystal structures are known (trigonal, hexagonal, orthorhombic, hexagonal, tetragonal, cubic); *Opal*: SiO₂·nH₂O, three crystal structures of opal are known (A: amorphous, CT: cristobalite & tridymite, T: tridymite); *Allophane*: Al₂O₃·SiO₂·H₂O to 2 Al₂O₃·SiO₂·H₂O, amorphous and semi-crystalline

Since luminescence in minerals is often caused by rare earth elements the Dieke diagram is a useful tool in interpretation of unknown spectra. The Dieke diagram describes all ^{2S+1}L_J multiplets for the REs (rare earth elements).

¹⁰ Also known under the name Lorenzenite.

¹¹ Also known as Autunite.

¹² Chalcedony is often referred to as cryptocrystalline quartz. Cryptocrystalline means that the texture cannot be resolved in a conventional light microscope.

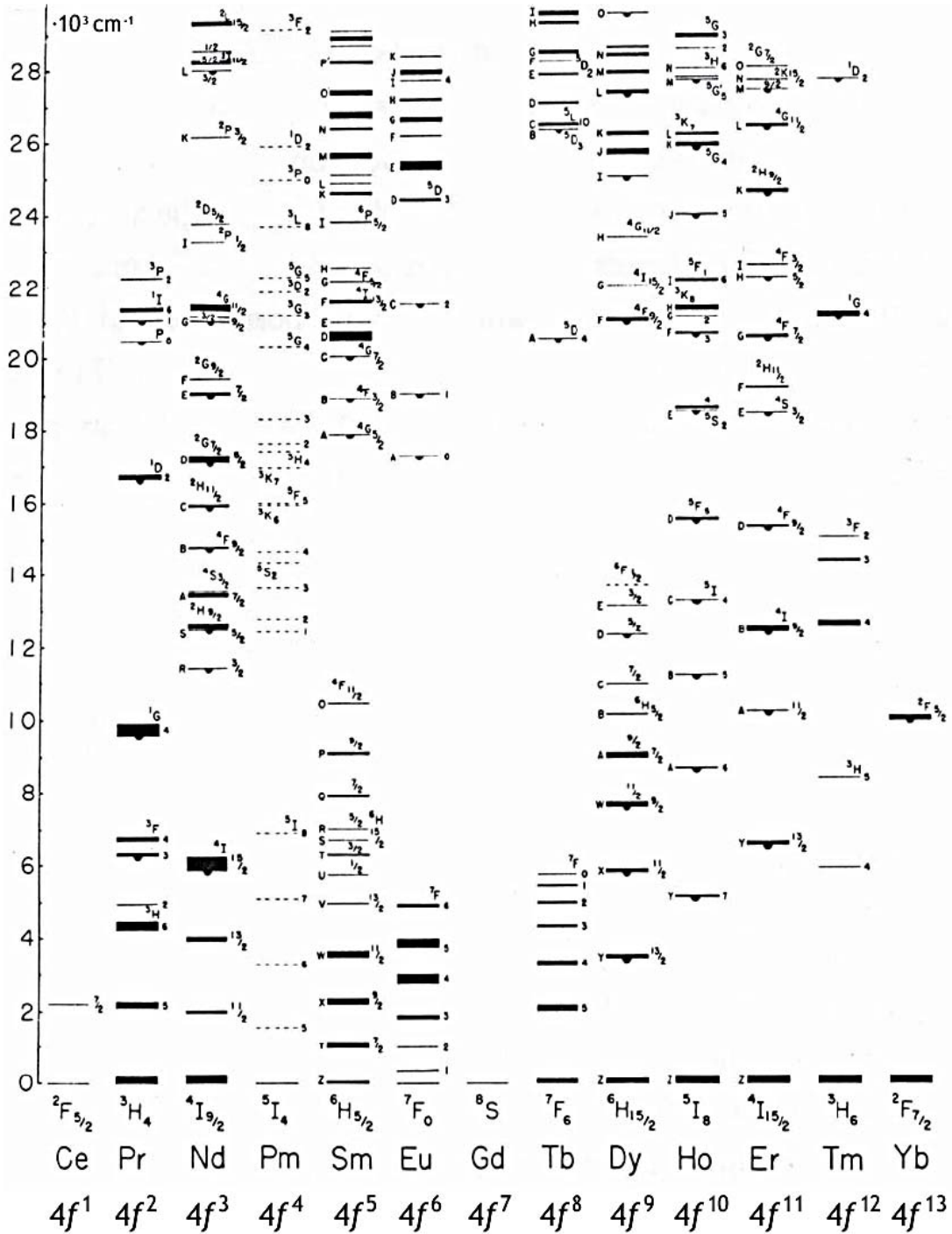


Figure 24: Dieke diagram for rare earth ions in crystals [134]

1.5.5 The LS 55 – a lab scale spectrofluorimeter

The LS 55 is a spectrofluorimeter from Perkin Elmer. It uses a pulsed Xe-flashlamp as light source. A solid sample holder was mounted in the measurement chamber. The solid sample holder should provide a good signal free from stray light. Prior to a measurement the solid sample holder has to be adjusted via the positioning screws at the bottom of the holder to its optimal position. This is done by operating the device in read mode while exciting a known sample (e.g. a Fluorite sample) with a wavelength of a good quantum efficiency for the emission (e.g. for the Fluorite with 366 nm) and observation at a known emission wavelength (e.g. 424 nm for Fluorite) while changing the positioning of the holder.

The LS 55 is depicted in figure 25.

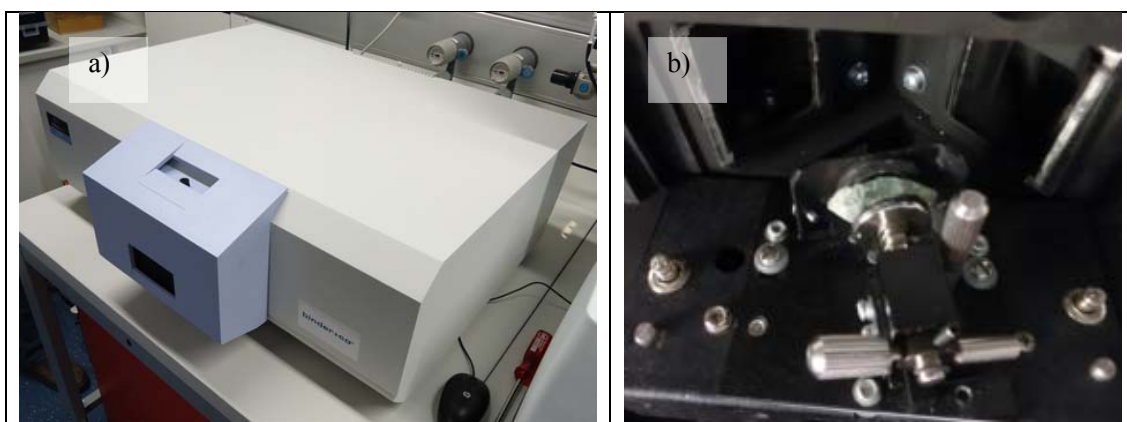


Figure 25: a) the LS 55, b) solid sample holder of the LS 55 with a fluorite sample mounted

As can be seen in figure 25 b an additional ring was inserted between the sample and the front side of the solid sample holder. This was done because it turned out that the holder could be adjusted to a more intense signal that way. The guiding slots from the original positioning system seemed to be too short. The ring was made of steel and painted with black stove enamel. Figure 26 shows the light path in the instrument.

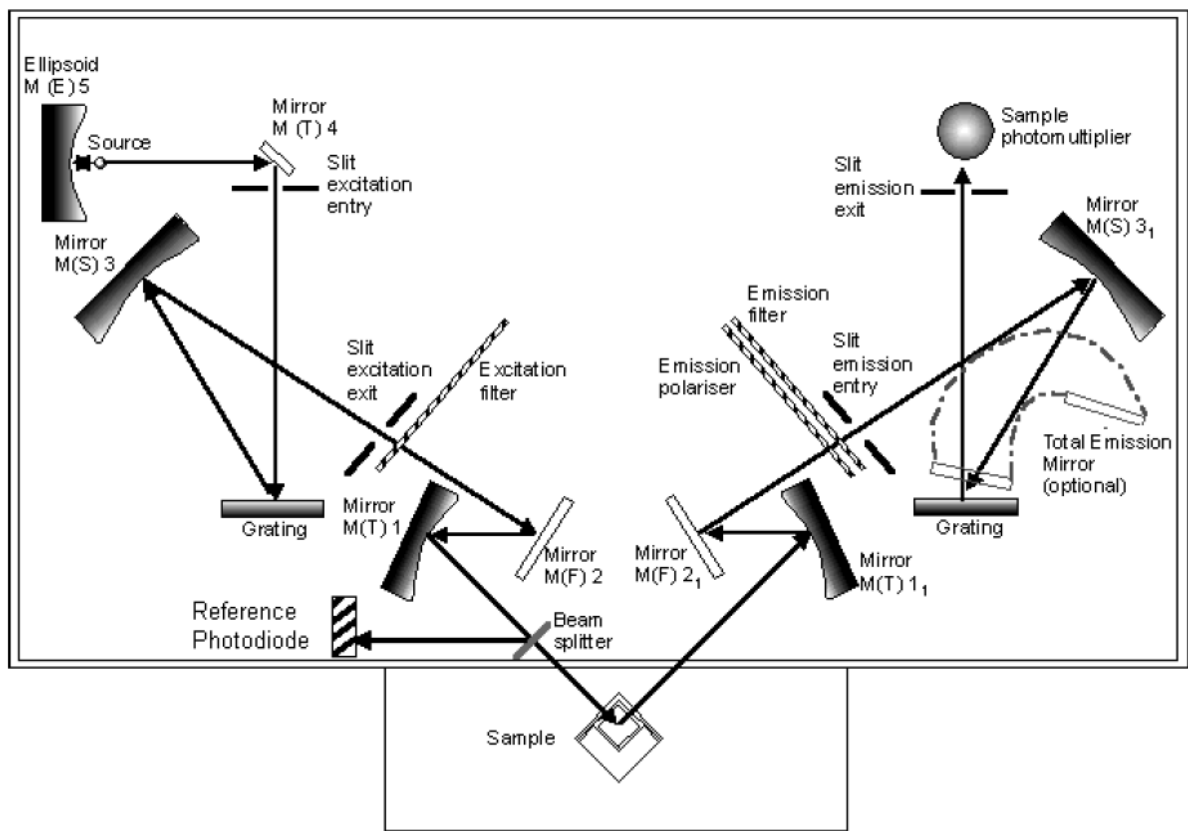


Figure 26: Optical layout of the LS 55 [135]

1.6 Spectral Databases

According to the diploma thesis contract with Binder + Co this thesis should contain an overview over the current situation concerning available spectral data of minerals in the literature, with the main focus on industrially relevant minerals. This chapter should reach the goal of working package 3b, mentioned in the contract [81]. An overview over free and commercially available spectral databases is given.

The spectral behavior of minerals, especially luminescence in general and fluorescence in particular are reported by many authors with hobby-mineralogical background [82, 83, 84]. In those publications fluorescent minerals are photographically documented under UV-light. Many authors distinguish between illumination with LW- (Long Wave) and SW- (Short Wave) – UV-light. These notations mean:

- LW: excitation at 366 nm wavelength
- SW: excitation at 254 nm wavelength

These wavelengths are available with many UV-mercury-lamps for laboratory or field use.

It should be noted, that some fluorescence databases on minerals in the internet are provided by semi-professional hobby-collectors. In this chapter not only fluorescence databases of minerals are covered, but also databases containing information on transmission and reflection data of minerals. Some minerals show transparency which can be compared with the transparency of glass. An example for that is Quartz. Most of the project relevant materials are not transparent. For reflectance spectroscopy wide applications can be found in astronomy, industry and the military sciences.

Though this chapter gives a good overview over possible sources of information, the spectral features of minerals are often deposit-dependent. Thus data from data bases can only give hints were to look for interesting peaks in a spectrum. Therefore no database can substitute a careful experimental study in the spectroscopic laboratory for the particular case of mineral.

To the best of the author's knowledge 4 reference books on fluorescence spectroscopy of minerals have been printed in the last 30 years and are essential for understanding:

- Gorobets, B. S., *Luminescent Spectra of Minerals – Reference Book, Luminescent Spectra of Minerals*; RPC VIMS; Moscow; 2002: **a spectral atlas with a good theoretical introduction**
- Gaft, M., Reisfeld, R., Panczer, G.; *Modern Luminescence Spectroscopy of Minerals and Materials*; Springer; Berlin, Heidelberg; 2010: **a spectral atlas, most of the spectral data are available in the free *fluomin.org* database**
- Marfunin, A.S.; *Spectroscopy, Luminescence and Radiation Centers in Minerals*; Springer; Berlin, Heidelberg; 1979: **The first published textbook which explicitly mentions fluorescence in minerals. Provides a good theoretical and practical overview, not of interest for practical application.**
- Marfunin, A.S.; *Physics of Minerals and Inorganic Materials*; Springer; Berlin, Heidelberg; 1979: **Introduction to solid state chemistry, solid state spectroscopy, quantum mechanics and group theory with focus on minerals.**

1.6.1 Fluorescence databases

After exhaustive search in the internet a collection of the following fluorescence databases were obtained:

Table 13: Overview over fluorescence databases for certain minerals

Name of the database	Link	Comment
Fluomin	http://www.fluomin.org/uk/accueil.php	free database; contains spectroscopic data as a gallery; spectra reproduced but no spectral data files (ASCII or .csv) available; 970 data sets available; information on certain luminescence centers "activators"
Mindat	http://www.mindat.org/min-3560.html	free database; provides a good overview over crystallographic data and fluorescence; no spectral data files provided; very elaborate data on minerals; information on certain luminescence centers "activators" and tailings
The Fluorescent Mineral Society	http://uvminerals.org/fms/join-fms	Commercial with fee; database for collectors and hobby mineralogists; Account for Binder + Co ordered.
Fact-Index	http://www.fact-index.com/ http://www.fact-index.com/s/se/serpentine.html	free database; rough overview over certain minerals (also fluorescence behavior); not too detailed information, comparable to Wikipedia;
Athena	http://athena.unige.ch/athena/mineral/search.html#	free database; database was not operable at the time of the search; not relevant because database didn't work properly
Jm-derochette	http://jm-derochette.be/spectrometer.htm	free database; small database providing information on a few minerals; Spectral data under microscope; not relevant for the project

1.6.2 Reflectance spectroscopy databases

Table 14 gives an overview on the databases in the internet which provide reflectance spectra and further information on minerals.

Table 14: Overview over reflection spectroscopic databases

Name of the database	Link	Comment
United States Geological Survey	usgs.gov http://speclab.cr.usgs.gov/spectral.lib06/ds231/datatable.html	Part of the ASTER database; free; overview over statistical data to minerals; the second link leads to the spectral database
ASTER Spectral Library	http://speclib.jpl.nasa.gov/	Summarizes data from smaller databases; free; all data are available as .csv files
GHOOST	http://ghosst.obs.ujf-grenoble.fr/	French database project; data should be available with July 2012; because of this, no sample data available presently
Bio Rad	http://www.bio-rad.com/ http://www.knowitall.com/literature/default.asp?gclid=CNrIo6eR864CFQJj3wod6hXWJg#Databases	Commercial database; contains about 420 spectra to minerals and clays
JPL	http://speclib.jpl.nasa.gov/documents/jpl_desc	Part of the ASTER database, no explicit sample data provided in the report (for sample data see chapter for ASTER database); free
Caltech-Datenbank/RRUFF-Projekt	http://rruff.info/chem=Al/display=default/R050610	Summarizes various databases; XRD, Raman and IR data available; free; links to primary literature are provided; original data cannot be downloaded
NIST-database	http://webbook.nist.gov/chemistry/#Search	Provides spectra for many chemicals; free; focus on photoelectron spectroscopy; because of that no reference data provided
Spectral Library of Arizona State University	http://speclib.asu.edu/	Database for minerals and rocks; focus on data for astronomy and astronautics
Laboratory of Photoinduced Effects Vibrational and X-Ray Spectroscopie	http://www.fis.unipr.it/phevix/ramandb.php	Free database from the University of Parma (Italy); focus on Raman data; because of this the database is not relevant for the project
Thermo Scientific	http://www.thermoscientific.com/ecommerce/servlet/productsdetail?productId=13281397&groupType=PRODUCT&searchType=0&storeId=11152&form=search	Commercial database; no access available at the date of writing; presumably more data on samples from organic chemistry than from mineralogy
FDM Reference Spectra Database	http://www.fdmspectra.com/index.html	Commercial database on ATR-IR-spectra; no access available at the date of writing; possibility of 14 day free trial; focus on samples from organic chemistry

1.6.3 Assessment of the Databases

The database and literature search showed that for the same mineral from different deposits different fluorescence behavior is to be expected depending on the content of luminescence centers (rare earths and others).

For powder reflection spectra (see dataset for Scheelite in ASTER) it can be said that the intensity of the peaks depends on the particle size of the powder. For Scheelite the intensity increases with increasing particle size.

Commercial databases for NIR data of minerals are not so extensive in comparison with free databases (for example ASTER). ASTER provides about 1400 spectra of minerals whereas Bio Rad has only 400 spectra in their database. Based on these facts it is recommended to stay with the free databases.

The Henkel Glossary, however, may be an interesting source of information. It contains a collection of fluorescence data covering about 570 mineral species. The price of the glossary is 18,50 \$. But after 3 months of e-mail correspondence and waiting for an answer the glossary must be considered as not available any more.

The whole database search can be broken down to two sections with five relevant and recommendable databases. For clarity each of these databases is indicated by a number to refer to it:

Reflection spectroscopic databases on minerals:

- **ASTER (1)**
- **USGS (2)**
- **Speclib (3)**

Fluorescence spectroscopic databases on minerals:

- **Fluomin (4)**
- **Mindat (5)** (also very good to get general and further information on the interesting mineral)

These five databases are listed with their link in the table 15.

Table 15: Summary of the five most important databases with their corresponding link

Database	Number	Link
ASTER	1	http://speclib.jpl.nasa.gov/
USGS	2	http://speclab.cr.usgs.gov/spectral.lib06/ds231/datatable.html
Speclib	3	http://speclib.asu.edu/
Fluomin	4	http://www.fluomin.org
Mindat	5	http://www.mindat.org

During the research for this report it became obvious that there is a lot of data for NIR-reflection spectroscopy on minerals available, but only little data for the UV-VIS reflection and fluorescence

behavior of minerals. The books of Gorebets & Rogojine and Gaft et al could be considered as the only source books for mineral fluorescence spectra available on the market.

Since the fluorescence and reflection behavior of minerals is highly dependent on the deposit there is no way to avoid careful studies in the lab or pilot installation. For each application concrete measurements have to be carried out because there is no database that covers all deposits of industrial mineral in all interesting spectral ranges. This justifies the investment in certain lab-instruments in the context of the ongoing research project.

Finally the five remaining databases were searched to get information on 8 minerals of interest, defined in the introduction. The results are summarized in table 16.

Table 16: Information on 8 industrial minerals in the 5 relevant databases

Mineral of interest	Tailings	Fluorescence of the mineral (spectra)	Reflection properties of the mineral (spectra)	Further information
Bauxite	5			5
Chromite	5	4	1, 2	5
Feldspar	5	4	1	5
Calcite	5	4	1,2,3	5
Scheelite	5	4	1	5
Talc	5	4	1,2,3	5
Fluorite	5	4	1,3	5
Magnesite	5	4	1,3	5

2 Materials and Methods

2.1 Sample Preparation

The mineral samples were cut with a flagstone cutting machine mounted with a diamond cutting disc. The cut face was then polished with abrasive papers of different roughness. The samples presented in this work were prepared with TU-Graz preparation devices, the other project relevant samples were prepared by Georg Weingrill with the machines at the MUL.

Both preparation places are depicted in figure 27.

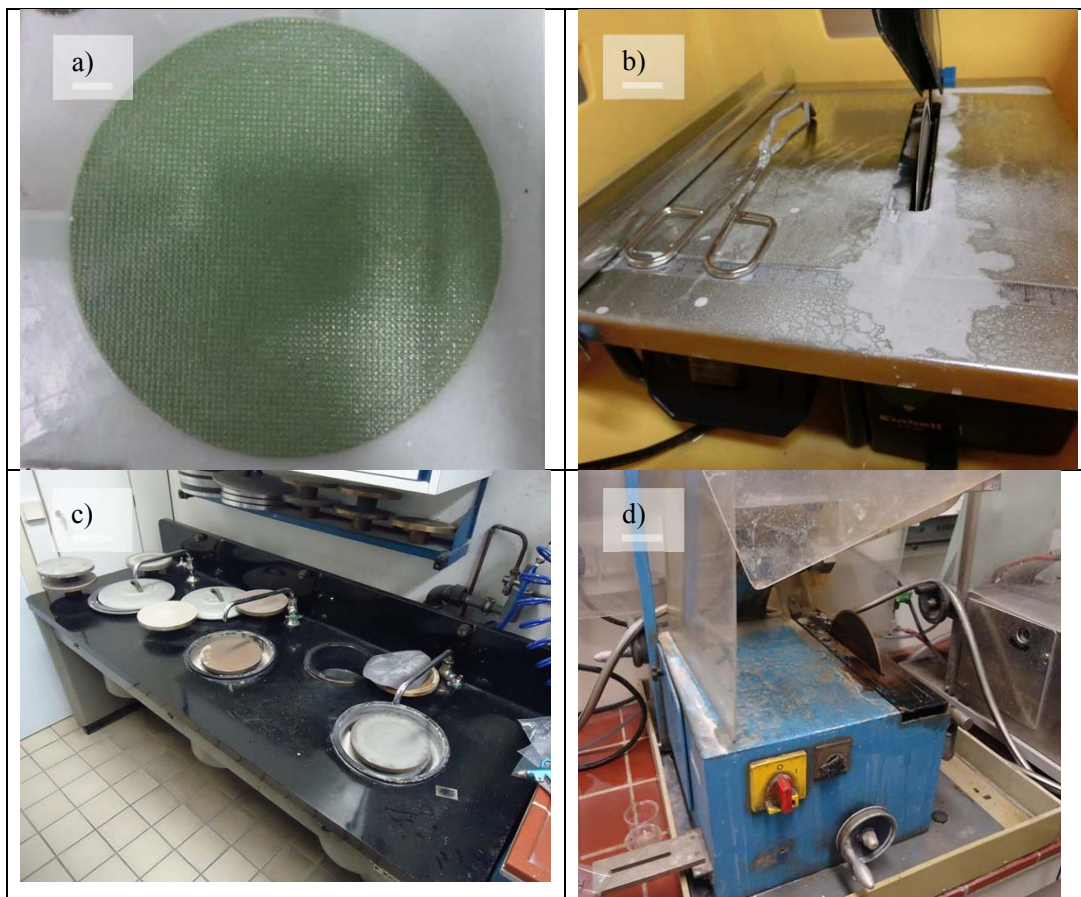


Figure 27: a) polishing device TUG, b) cutting machine TUG, c) polishing place MUL and d) cutting machine MUL

It turned out that cutting and polishing of the monolithic mineral samples is a sufficient preparation for further analysis in the L950 the LS 55 or the Raman-spectrometer.

2.2 Reflection Measurement of Minerals

2.2.1 Measurement Procedure

The L950 spectrometer was allowed to warm up for about 30 minutes. After that the measurement parameters were set in the control window. The most important measurement parameters are given in table 17.

Table 17: Measurement parameters for reflection measurements with the L950

D ₂ - lamp	on
Tungsten-lamp	on
Scan from [nm]	2500
Scan to [nm]	200
Data interval [nm]	5
Ordinate mode	%R
Lamp Change [nm]	319,2
Gain - InGaAs	16,00
PMT - response [s]	0,20
InGaAs - response [s]	0,20
PMT -slit [nm]	2,00
InGaAs - slit	auto
CBM [%]	100,00
CBD	off
detector change [nm]	860,80

However, it should be mentioned that the measurement settings can vary according to the measurement task. For example the data interval can be minimized up to 0,01 nm, at the cost of scan speed. For mechanical reasons the scan should always start from maximal wavelength to the smallest wavelength of a spectrum.

After setting the parameters, the instrument was blanked with a certified spectralon standard¹³ from labsphere® using the autozero function. The sample was fixed at the reflection port with adhesive tape or modeling material. Then the measurement chamber was sealed lightproof with the sealing cap. When a 8 mm teflon aperture was used, e. g. for measurement of small samples, the blanking was done with the aperture already in position, to avoid disturbing signals from the aperture.

¹³ USRS- 99-020
AS-01159-060
Serial Number: 7A 33D-7000

2.3 Fluorescence Measurements of Minerals

2.3.1 Method Development and Measurement Procedure

All samples can be placed into the measurement chamber of the LS 55 after proper cutting and polishing. The luminescence measurement, which seemed an easy task at the beginning, is rather difficult for minerals, because they seem to have rather long living excited states. The LS 55 which is usually designed for life sciences applications can be disturbed by life time effects of the sample.

The LS 55 works in certain measurement cycles. Data are obtained from the photomultiplier, integrated, converted, digitally filtered and rationed before the PC receives the data. The path of the signal is described in the Perkin Elmer User Manual for the LS 55 [136].

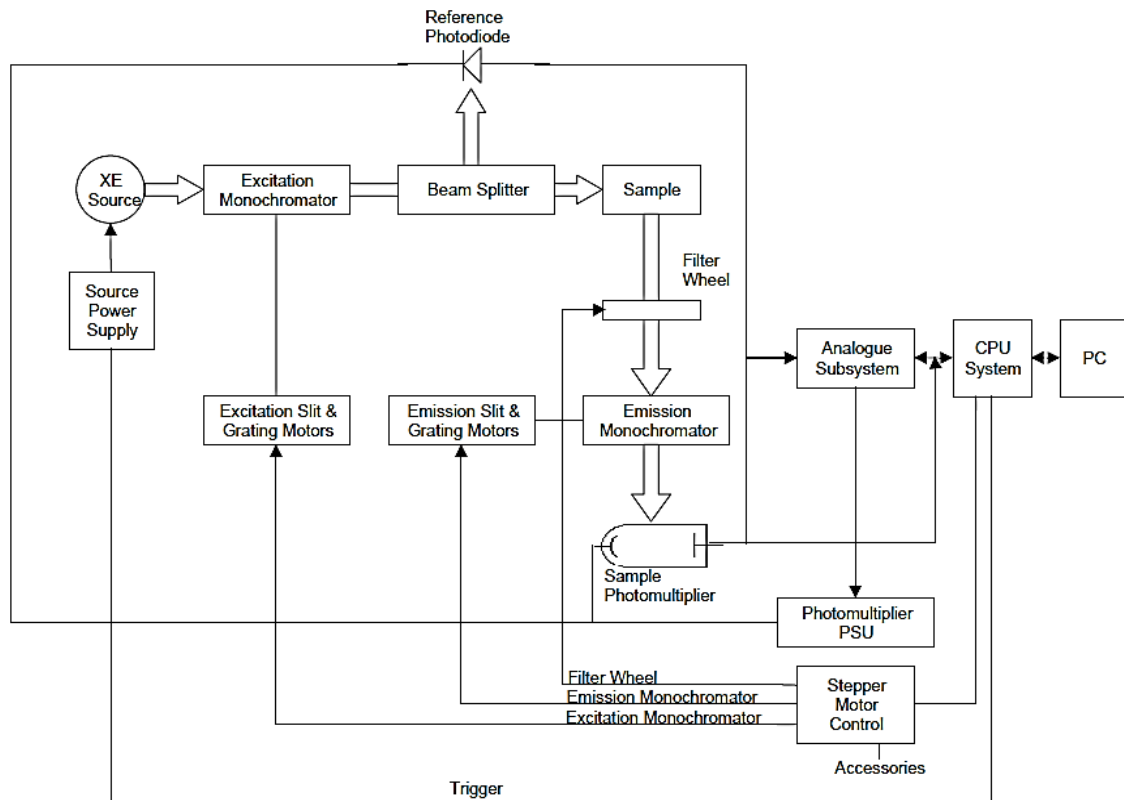


Figure 28: Electronics diagram for the LS 55 [136]

According to the manual the instrument can operate in two possible measurement modes:

- Fluorescence
- Phosphorescence

In fluorescence mode four integrations are performed for every data collection cycle. Two integrations are taken from the emission channel and two from the excitation channel. These integrations are performed at fixed times with respect to the last source flash. Emission from the light source has a width at half peak height of less than 10 microseconds, the integrators are opened for 80 microseconds to collect all the signal. The effect of dark current (signal produced when no light is falling on the photomultiplier) is eliminated by gating open both channels a second time just before the next flash and integrating the signal. The dark current signals are then subtracted from the main fluorescence signals to give a dark current corrected signal [137].

In phosphorescence mode the integration time is not fixed, but can be selected by the operator. The integration can be started between 0 s and 9000 ms after the start of the flash. This is the delay time. The time period over which the integration is performed, the gate time, can be varied from 0,01 ms to 500 ms. If the sum of the delay and gate times exceeds 13,0 ms the cycle time must be increased to allow a longer data collection period. The source can be pulsed between 1 and 10 times, to optimize the sample excitation and data collection. The exciting pulses occur on consecutive mains cycles (50 Hz for AC supply in Austria) at the start of the data collection cycle. The gate and delay times are measured from the beginning of the last pulse in the excitation pulse train. On initiating a phosphorescence measurement the dark current is measured and the value stored and subtracted from all sample signals [178].

The further details of signal handling will not be discussed, but can be looked up in figure 29.

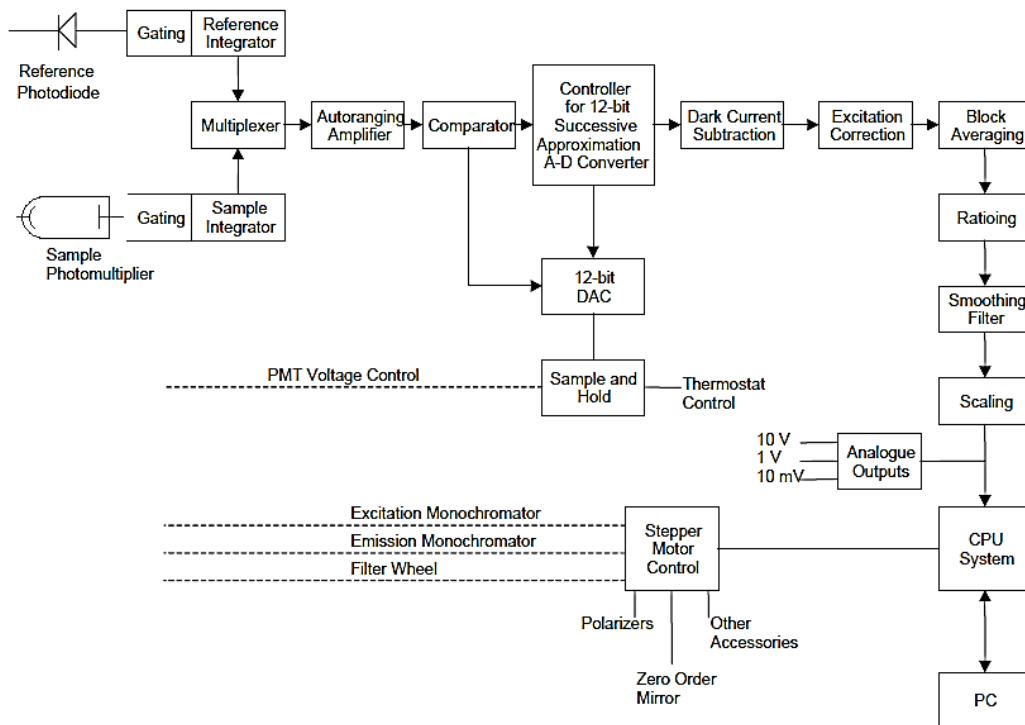


Figure 29: Data handling diagram

The measurement procedure can be broken down to a simple diagram:

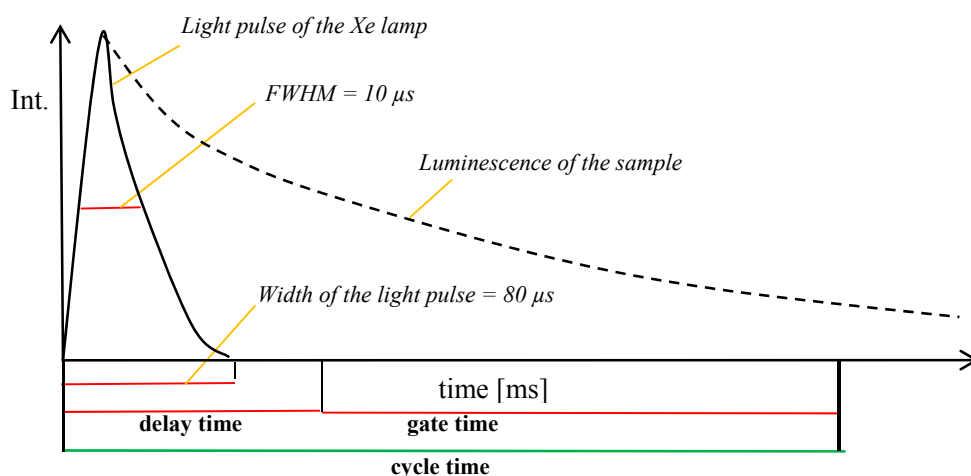


Figure 30: Measurement scheme of the LS 55 (not to scale)

Now in fluorescence mode any long lived luminescence can be rejected due to dark current subtraction, whereas in phosphorescence mode short lived luminescence can not be measured because of the time gating.

Based on these facts method details for the luminescence measurement in solids, which can show either fluorescence or phosphorescence, were proposed by Dr. Stuart Huckins, a former product developer of Perkin Elmer [138].

Table 18: Proposed setting for LS 55 for long lived luminescence

Cycle time [ms]	20
Flash Count	1
Delay time [ms]	0,1
Gate time [ms]	3

Only using these proposed settings sensible spectra, which agree with the visual color impression for several luminescent minerals were obtained. Based on this experience an optimal measurement routine for fluorescing minerals should be as follows:

1. Take a photograph of the sample under UV-light (e.g. 254 nm or 366 nm)
2. Measure the sample in fluorescence mode
 - 2.1. If no signal can be obtained increase sensitivity via the slit width or the detector voltage
3. Measure the sample in phosphorescence mode
 - 3.1. If no signal can be obtained increase sensitivity via the slit width or the detector voltage
4. Compare the photograph (visual color impression) with the fluorescence and/or phosphorescence data and make sure they match in principle.
5. Compare the spectra with spectra of the same mineral in databases.
6. If possible cross reference with data from other spectrofluorimeters

2.4 Illumination situation in the LS 55

2.4.1 Fundamentals

An important question is how the illumination situation in the measurement chamber and the detector performance can be compared with the illumination conditions in industrial sorting systems.

Several approaches have been made to find this out:

- Investigation in the manuals of the manufacturer and references therein.
- Information search in the data sheets for the Xe-flash lamp and the used detection system.
- Summary of the signal processing in the LS 55 instrument.
- Measurement of irradiance in the VIS (400 – 700 nm) with the Testo 545 luxmeter with various slit width.
- Measurement of the irradiance in the UV C with the UVM CP radiometer in the reflection position of the monochromator.
- Measurement of the irradiance at 254 nm with various slit width with a chemical actinometer.
- Comparison of the irradiance of several fluorescence excitation systems.

First a few definitions from the field of “Photonics” [67, 88] :

It can be distinguished between the radiometric and the photometric approach. The radiometric approach is based on straight forward physical reasoning. The photometric approach takes into account the brightness sensitivity¹⁴ of the standard observer. This brightness sensitivity is defined as a function in the DIN 5031 in 10 nm steps.

Some definitions:

The **radiant energy**¹⁵ Q is the amount of energy transferred via electromagnetic radiation in J ($J = W \cdot s$).

The **radiant power**¹⁶ Φ is defined as

$$\Phi = \frac{dQ}{dt} \quad \text{Equ. 18}$$

and is given in W ($1 \text{ W} = 1 \text{ Js}^{-1}$).

The **irradiance**¹⁷ E is defined as

$$E = \frac{d\Phi}{dA} \quad \text{Equ. 19}$$

Where A is the *irradiated area* and is given in W/m^2 .

¹⁴ German: Hellempfindlichkeitsgrad

¹⁵ German: Strahlungsenergie

¹⁶ German: Strahlungsleistung

¹⁷ German: Bestrahlungsstärke

The **irradiation**¹⁸ H is defined as the time integral of the *irradiance*:

$$H = \int E dt \quad \text{Equ. 20}$$

These are the main equations we have to keep in mind, when talking about irradiation measurement in radiometric terms.

All these quantities have their counterpart in photometric terms, where the sensitivity of the human eye for certain wavelengths is taken into account.

Figure 31 shows the brightness sensitivity of a standard observer for daylight (photopic range) [89] defined by the CIE (Commission International de l'Éclairage) and documented the German DIN 5031 as a function of the wavelength λ in nm.

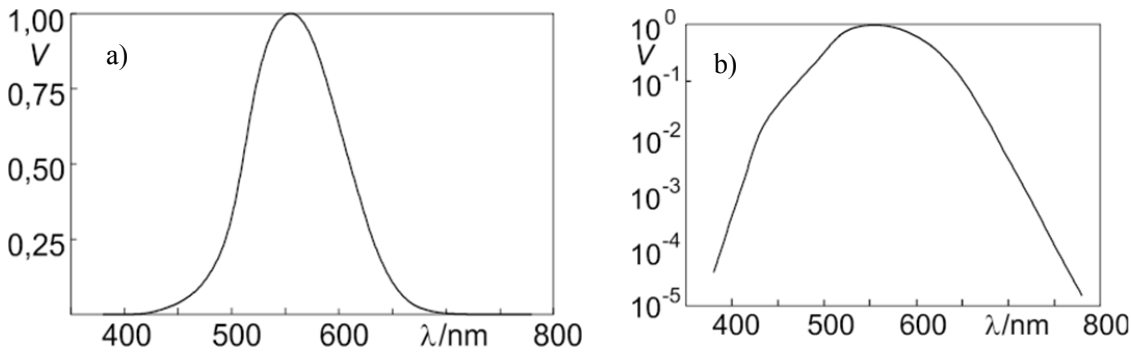


Figure 31: Spectral brightness sensitivity $V(\lambda)$ as a function of the wavelength in nm; a) linear presentation b) logarithmic presentation [1]

The **luminous flux**¹⁹ Φ is measured in Lumen (lm). This leads to the unity for the **quantity of light**²⁰ in $\text{lm}\cdot\text{s}$ (“lumensecond”). This leads to the **luminance intensity**²¹ in lm/m^2 which is defined as one **lux** (lx):

$$1 \text{ lx} = 1 \frac{\text{lm}}{\text{m}^2} \quad \text{Equ. 21}$$

For the conversion of photometric units X_p to radiometric X_r units and vice versa in the case of monochromatic radiation the following equation can be used

$$X_p = K_m V(\lambda) X_r \quad \text{Equ. 22}$$

where $K_m = 683 \text{ lm}/\text{W}$ is the maximum value of the *photometric radiation equivalent*²², whose value comes from the definition of the measurement unit **candela**.

¹⁸ German: Bestrahlung

¹⁹ German: Lichtstrom

²⁰ German: Lichtmenge

²¹ German: Beleuchtungsstärke

²² German: Photometrisches Strahlungsequivalent

For polychromatic radiation the spectral entities $X_{r,\lambda} = dX_p/d\lambda$ have to be integrated in the limits of the visible radiation [67]:

$$X_p = K_m \int_{380 \text{ nm}}^{780 \text{ nm}} V(\lambda) X_{e,\lambda} d\lambda \quad \text{Equ. 23}$$

The definition of the unit candela was a consequence from the practical properties resulting of the handling of a real black body at higher temperatures to get a standard source for radiation in the VIS-range to measure the optical radiation power. It is defined as [90]:

The **candela** is the luminous intensity, in a given direction, of a source that emits monochromatic radiation of frequency $540 \cdot 10^{12}$ hertz (i.e. a wavelength of 555 nm) and that has a radiant intensity in that direction of 1/683 watt per steradian.

From the author's point of view the most useful quantity for a comparison of the illumination situation in the LS55 and in industrial sorting machines is the irradiance in W/m^2 or W/cm^2 .

To get the energy of one photon we can apply the known equation [91]:

$$E_{ph} = h\nu = \frac{hc_0}{\lambda} \quad \text{Equ. 24}$$

where E_{ph} is the energy of the photon in [J], h is Planck's constant $h = 6,626 \cdot 10^{-34}$ [Js], ν is the frequency of the photon in [s^{-1}], c_0 is the vacuum-velocity of light $c_0 = 299 \cdot 10^6$ [m s^{-1}] and λ is the wavelength in [m].

Table 19 gives an overview over radiometric and photometric quantities.

Table 19: Radiometric and photometric quantities [92, 93, 94, 95]

Radiometry			Photometry		
Quantity	symbol	units	Quantity	symbol	units
Radiant Energy	Q	J	Luminous energy	Q	lm s
Radiant Flux	Φ	W	Luminous flux	Φ	lm
Irradiance	E	W/m^2	Illuminance	E	$\text{lm}/\text{m}^2 = \text{lx}$
Radiant Intensity	I	W/sr	Luminous Intensity	I	lm/sr
Radiance	L	$\text{W}/(\text{m}^2\text{sr})$	Luminance	L	$\text{lm}/(\text{m}^2\text{sr})$

2.4.2 Manuals and Quotes

According to the quote for the LS 55 fluorescence spectrometer the device is equipped with a pulsed Xenon light source. Neither information on the power of this source nor on the energy of one pulse was provided. The spectrometer can be used to measure fluorescence, phosphorescence and bio- or chemiluminescence. The dark current of the detector is automatically corrected (which is known in the literature as “excitation correction”) and the dark current of the detection system is automatically compensated. Available filters, polarizers and attenuators are [96]:

- 290 nm cut off filter (emission side)
- 350 nm cut off (emission side)
- 390 nm cut off(emission side)
- 430 nm cut off (emission side)
- 515 nm cut off (emission side)
- 1 % attenuator (emission side)
- shutter (emission side)
- horizontal and vertical polarizers (on excitation and emission side)

From the technical specifications for the LS 55 we know that the Xe flash lamp is pulsed at line frequency (50 or 60 Hz) with a pulse width at half peak height < 10 μs and a power equivalent to 20 kW at continuous operation. The excitation slit can be varied in the interval 2,5 – 15 nm and the emission slit in the interval 2,5 – 20 nm [97].

In general authors provide information on the pulse energy of their lasers in millijoule and the deliver pulse duration in Nanoseconds. The power can be easily calculated with the known equation

$$P[W] = \frac{E[J]}{t[s]} \quad \text{Equ. 25}$$

The following table gives a short overview of the Xe-flash lamp power in comparison to some examples for Laser Induced Fluorescence (LIF) from the literature.

Table 19: Overview over excitation power P for mineral fluorescence from several references

E [mJ]	[ns]	P [W]	Reference	Comment
	*	$20 \cdot 10^3$	[97]	Power for the whole emission spectrum
80	10	$8 \cdot 10^6$	[99]	pulse energy maintained between 10 - 80 mJ
80	10	$8 \cdot 10^6$	[100]	pulse energy maintained between 10 - 80 mJ
80	10	$8 \cdot 10^6$	[101]	pulse energy maintained between 10 - 80 mJ
2	3 according to [103]	$6,7 \cdot 10^5$	[102]	laser energy between 1 - 2 mJ per Pulse @ 20 Hz

*The emission from the source has a width at half peak height of less than 10 μs [98]

However the pulse duration to pause ratio was not mentioned in the literature references [99], [100] and [101].

Concerning the rather high excitation power of the laser sources the question remains how these laser intensities can be compared to irradiation intensities in common UV-C lamps.

For example the UV-C tube in Binder + Co sorting systems has a irradiance of 20 mW/cm² at the closest possible measurement point to the lamp and a irradiance of about 1,6 mW/cm² at the position of the material that should be sorted [104].

From the data in table 20 it becomes obvious why many authors use lasers as excitation source. Lasers emit their whole energy within one sharp coherent emission line whereas Xe-flashlamps have a continuum emission spectrum.

Since Nd-YAG-Lasers have an emission wavelength of about 1060 nm a frequency doubling or even tripling is necessary to get into the visible range of electromagnetic radiation [105]. For frequency doubling from 1,08 to 0,54 μm up to 85 % conversion efficiency are reported [106]. In everyday laboratory work conversion efficiencies of 60 % are realistic [107].

2.4.3 Xe-flash lamp and the detector

2.4.3.1 The lamp

Though the emission in the UV is not too high for a Xe-flash lamp it is used in the LS 55. A Mercury-Lamp would only have several sharp maxima which make the recording of excitation spectra almost impossible. The excitation spectrum would be biased by the strong emission lines [108].

There are several types of excitation sources known from the literature [110]:

- Arc and incandescent Xe lamps
- Pulsed Xe lamps
- High pressure Hg lamps
- Xe-Hg arc lamps
- Quartz-Tungsten Halogen (QTH) lamps
- Low pressure Hg and Hg-Ar lamps
- LED light sources
- Laser Diodes

The emission spectrum of a Xe-flash lamp in comparison to a continuous arc lamp is shown in figure 32.

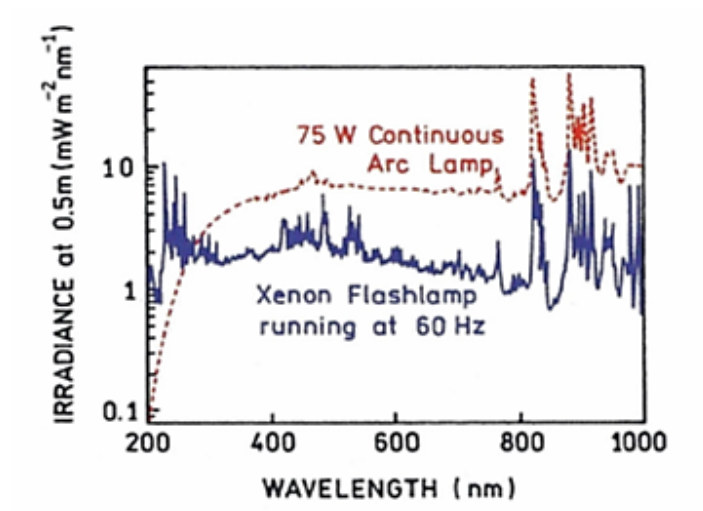


Figure 32: Spectral output of a continuous Xe arc lamp and Xe flash lamp [109]

For comparison the emission spectra²³ of the commercially available UV-lamp NU-4 KL were recorded with the LS 55 and are shown in figure 33:

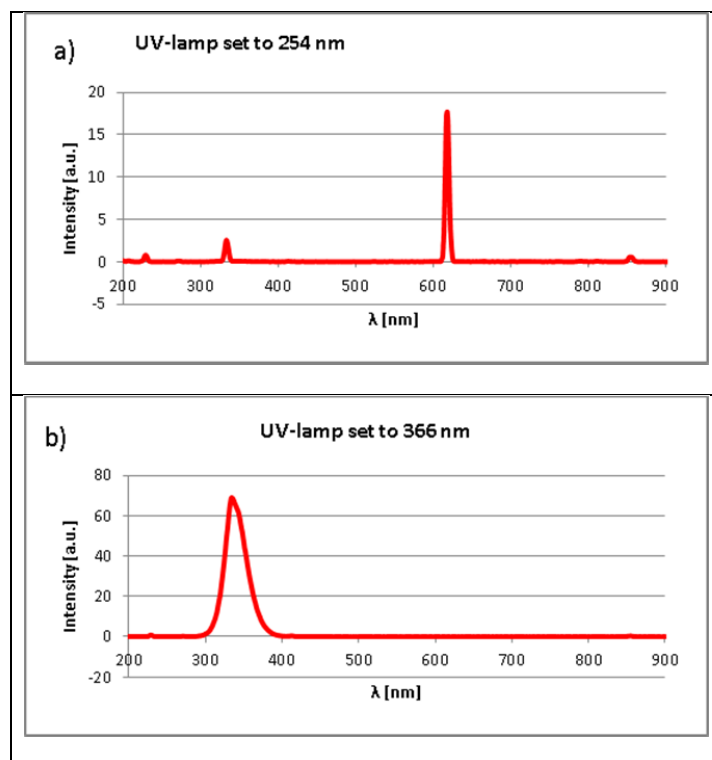


Figure 33: Emission spectra for the UV-lamp NU-4 KL for setting of lamp to a) 254 nm and b) 366 nm

Figure 34 shows the emission spectrum of a low pressure Hg-Ar-lamp:

²³ These spectra were emission corrected with the emred.corr function provided by Perkin Elmer

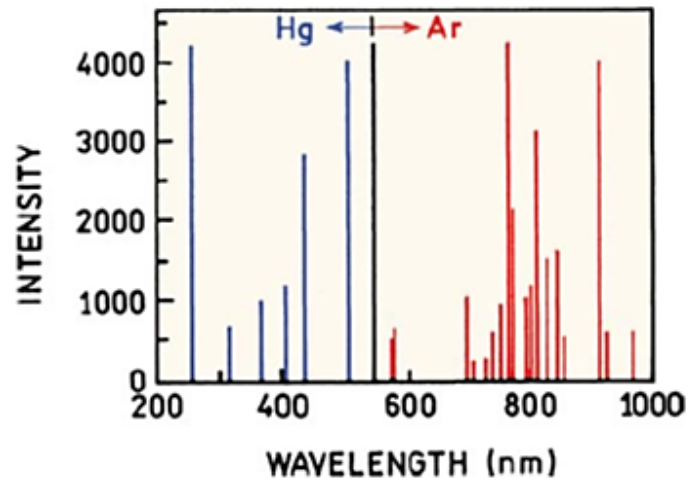


Figure 34: Emission spectrum of a low pressure Hg-Ar-lamp [111]

However, the Xe flash lamp in the LS 55 seems to be a good compromise between versatility and intensity.

2.4.3.2 R955 detector

To elevate the performance of the LS 55 a more sensitive photomultiplier tube was used as a detector. The original detector was a R8630 PMT from Hamamatsu. The R928 and the R955 are more sensitive than the R8630 which is a standard detector for biochemical applications. The R928 and R955 are also more sensitive towards the red region of the visible electromagnetic spectrum [112]. Figure 35 shows the spectral response for both, the R928 and the R955.

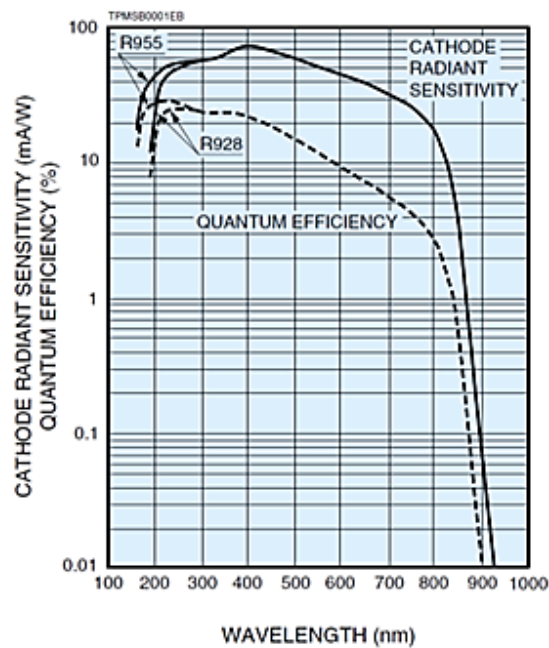


Figure 35: Typical spectral response for R928- and R955-PMT [112]

2.4.4 Testo 545 measurements: VIS

The Illuminance E was measured with the Testo 545 Luxmeter. The measuring chamber was opened and the measurement carried out at different wavelengths and slit widths. The laboratory was kept dark to avoid a bias from the light sources in the lab. Figure 36 shows the positioning of the measurement surface of the Testo 545 in the measurement spot. The instrument was held at a position where it gave maximal signal. The area of the measurement surface is 33,36 mm².

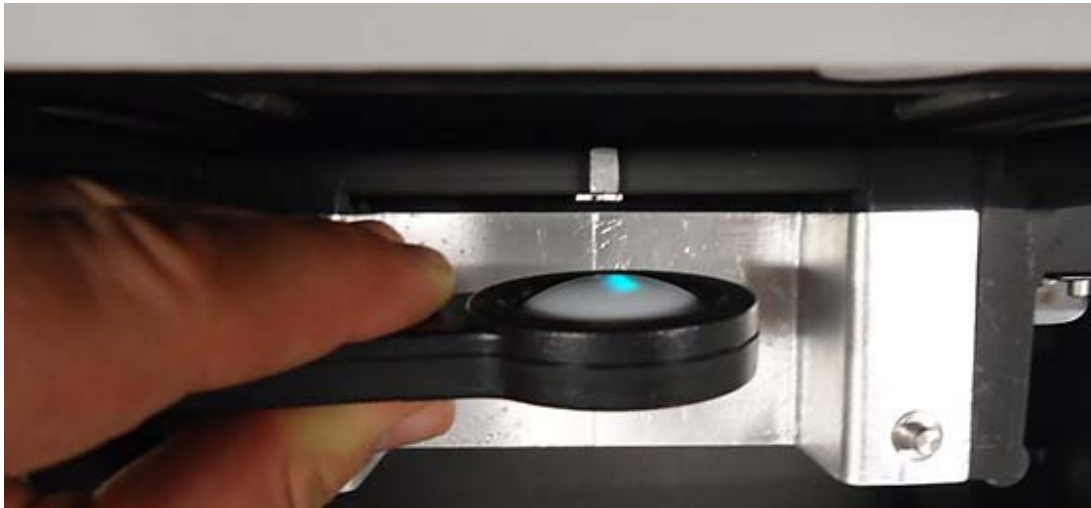


Figure 36: Measurement surface of Testo 545 in the LS 55

The results of the measurements are presented in tables 20 and 21 and figures 37 and 38.

Table 20: Illuminance values for several slit widths and wavelengths

slit width [nm]											
2,5		5		7,5		10		12,5		15	
λ [nm]	E [Lux]	λ [nm]	E [Lux]	λ [nm]	E [Lux]	λ [nm]	E [Lux]	λ [nm]	E [Lux]	λ [nm]	E [Lux]
200	0	200	0	200	0	200	0	200	0	200	0
254	0	254	0	254	0	254	0	254	0	254	0
300	0	300	0	300	0	300	0	300	0	300	0
366	0	366	0	366	0	366	0	366	0	366	0
400	0	400	0	400	0	400	1	400	1	400	1
450	0	450	1	450	2	450	2	450	3	450	5
500	1	500	10	500	20	500	40	500	55	500	78
550	6	550	53	550	70	550	253	550	308	550	459
600	3	600	18	600	44	600	68	600	107	600	115
650	1	650	1	650	3	650	3	650	3	650	7
700	0	700	0	700	1	700	1	700	1	700	1

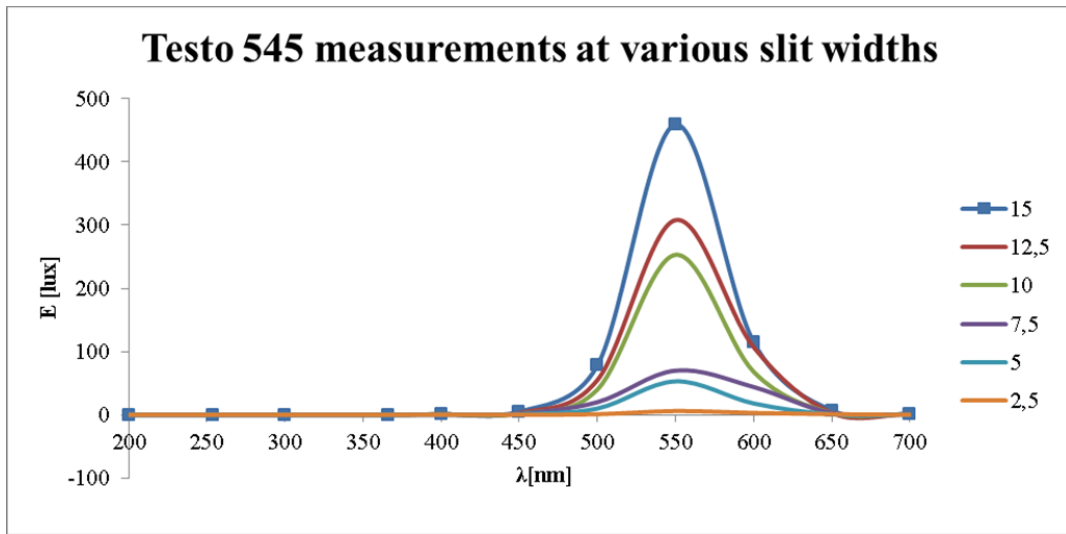


Figure 37: Illuminance values for several slit widths (in nm) and wavelengths at the measurement spot of LS 55

Table 21: Illuminance and slit width at 550 nm

slit width [nm]	illuminance [lux]
2,5	6
5	53
7,5	70
10	253
12,5	308
15	459

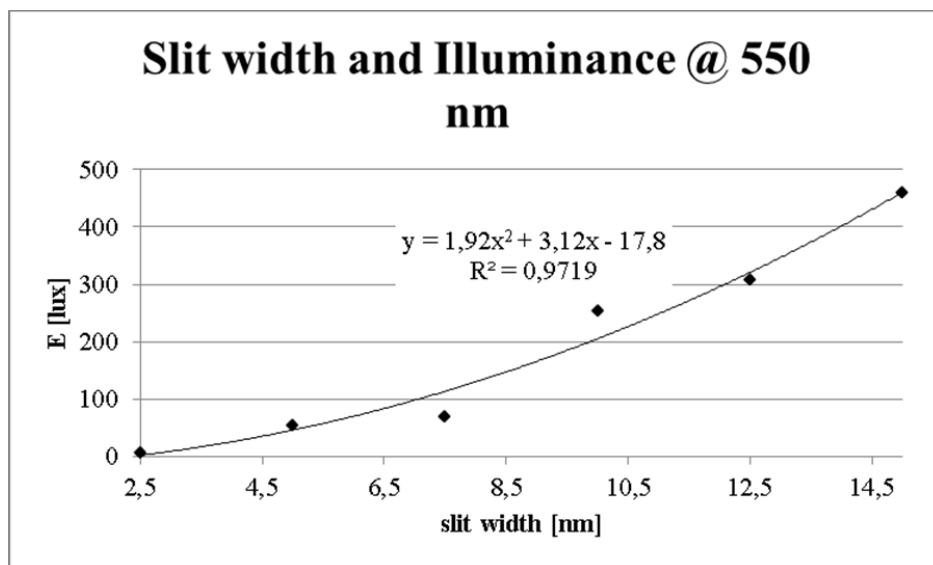


Figure 38: Illuminance values for several slit widths at 550 nm

After the experiments at several excitation wavelengths, the excitation monochromator was set to the reflection position. So the whole emission spectrum of the Xe-flash lamp was directed to the Testo 545 instrument. First positioning of the measurement area was tried by free hand. To get higher accuracy the measurement device was fixed to the cuvette holder with tape. Results of these measurements are presented in table 22 and figure 39.

Table 22: Illuminance values for the LS 55 at reflection position of the excitation monochromator

Positioning by hand		fixing to the cuvette holder	
slit width [nm]	E [lux]	slit width [nm]	E [lux]
15	2580	15	880
14	2500	14	855
13	2470	13	820
12	2390	12	790
11	2308	11	740
10	2280	10	690
9	2050	9	630
8	1980	8	566
7	1590	7	486
6	1005	6	408
5	663	5	313
4	605	4	218
3	362	3	124
2,5	293	2,5	73

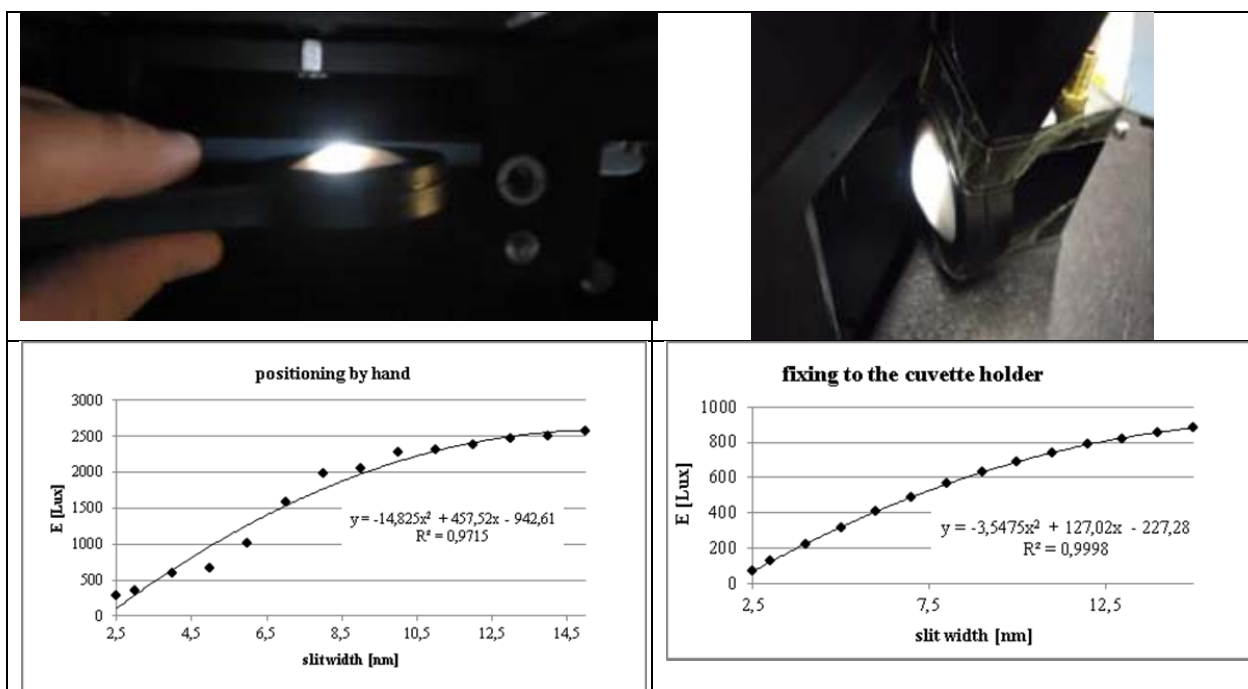


Figure 39: Illuminance values for the LS 55 at reflection position of the excitation monochromator

The photometric values for illuminance can be converted to radiometric values for Irradiance using equation 26 [115]:

$$E_{irrad} = \frac{E_{illum}}{K_m \cdot V(\lambda)} \quad \text{Equ. 26}$$

In equation 26 E_{irrad} is the irradiance in W/m^2 , E_{illum} is the Illuminance in lm/m^2 , K_m the luminous efficacy of radiation²⁴ in lm/W and $V(\lambda)$ the spectral luminous efficiency²⁵ defined in DIN 5031. All E_{irrad} values were multiplied with $10^{-4} [m^2/cm^2]$ to get the irradiance in units of W/cm^2 . $K_m = 683 \text{ lm/W}$ and $V(550 \text{ nm}) = 1$ [115]. The results of the unit conversion are presented in tables 23, 24 and 25 as well as in figure 40.

²⁴ luminous efficacy of radiation: Ger.: photometrisches Strahlungsäquivalent

²⁵ spectral luminous efficiency: Ger.: spektraler Hellempfindlichkeitsgrad

Table 23: Various excitation slit widths - Testo 545 results in photometric and radiometric units

Slit width [nm]								
2,5			5			7,5		
WL [nm]	Ill.[Lux]	Irr. [W/cm ²]	WL [nm]	Ill. [Lux]	Irr. [W/cm ²]	WL [nm]	Ill. [Lux]	Irr. [W/cm ²]
200	0	0,00E+00	200	0	0,00E+00	200	0	0,00E+00
254	0	0,00E+00	254	0	0,00E+00	254	0	0,00E+00
300	0	0,00E+00	300	0	0,00E+00	300	0	0,00E+00
366	0	0,00E+00	366	0	0,00E+00	366	0	0,00E+00
400	0	0,00E+00	400	0	0,00E+00	400	0	0,00E+00
450	0	0,00E+00	450	1	1,46E-07	450	2	2,93E-07
500	1	1,46E-07	500	10	1,46E-06	500	20	2,93E-06
550	6	8,78E-07	550	53	7,76E-06	550	70	1,02E-05
600	3	4,39E-07	600	18	2,64E-06	600	44	6,44E-06
650	1	1,46E-07	650	1	1,46E-07	650	3	4,39E-07
700	0	0,00E+00	700	0	0,00E+00	700	1	1,46E-07
Slit width [nm]								
10			12,5			15		
WL [nm]	Ill. [Lux]	Irr. [W/cm ²]	WL [nm]	Ill. [Lux]	Irr. [W/cm ²]	WL [nm]	Ill. [Lux]	Irr. [W/cm ²]
200	0	0,00E+00	200	0	0,00E+00	200	0	0,00E+00
254	0	0,00E+00	254	0	0,00E+00	254	0	0,00E+00
300	0	0,00E+00	300	0	0,00E+00	300	0	0,00E+00
366	0	0,00E+00	366	0	0,00E+00	366	0	0,00E+00
400	1	1,46E-07	400	1	1,46E-07	400	1	1,46E-07
450	2	2,93E-07	450	3	4,39E-07	450	5	7,32E-07
500	40	5,86E-06	500	55	8,05E-06	500	78	1,14E-05
550	253	3,70E-05	550	308	4,51E-05	550	459	6,72E-05
600	68	9,96E-06	600	107	1,57E-05	600	115	1,68E-05
650	3	4,39E-07	650	3	4,39E-07	650	7	1,02E-06
700	1	1,46E-07	700	1	1,46E-07	700	1	1,46E-07

Table 24: Constant emission wavelength - Testo 545 results in photometric and radiometric units

slit width [nm]	Illum. @ 550 nm [Lux]	Irrad. @ 550 nm [W/cm ²]
2,5	6	8,78477E-07
5	53	7,75988E-06
7,5	70	1,02489E-05
10	253	3,70425E-05
12,5	308	4,50952E-05
15	459	6,72035E-05

Table 25: excitation monochromator in reflection position – Testo 545 results in photometric and radiometric units

Positioning by hand			Fixing to the cuvette holder		
slit width [nm]	Illum. [Lux]	Irrad. [W/cm ²]	slit width [nm]	Illum. [Lux]	Irrad. [W/cm ²]
15	2580	3,78E-04	15	880	1,29E-04
14	2500	3,66E-04	14	855	1,25E-04
13	2470	3,62E-04	13	820	1,20E-04
12	2390	3,50E-04	12	790	1,16E-04
11	2308	3,38E-04	11	740	1,08E-04
10	2280	3,34E-04	10	690	1,01E-04
9	2050	3,00E-04	9	630	9,22E-05
8	1980	2,90E-04	8	566	8,29E-05
7	1590	2,33E-04	7	486	7,12E-05
6	1005	1,47E-04	6	408	5,97E-05
5	663	9,71E-05	5	313	4,58E-05
4	605	8,86E-05	4	218	3,19E-05
3	362	5,30E-05	3	124	1,82E-05
2,5	293	4,29E-05	2,5	73	1,07E-05

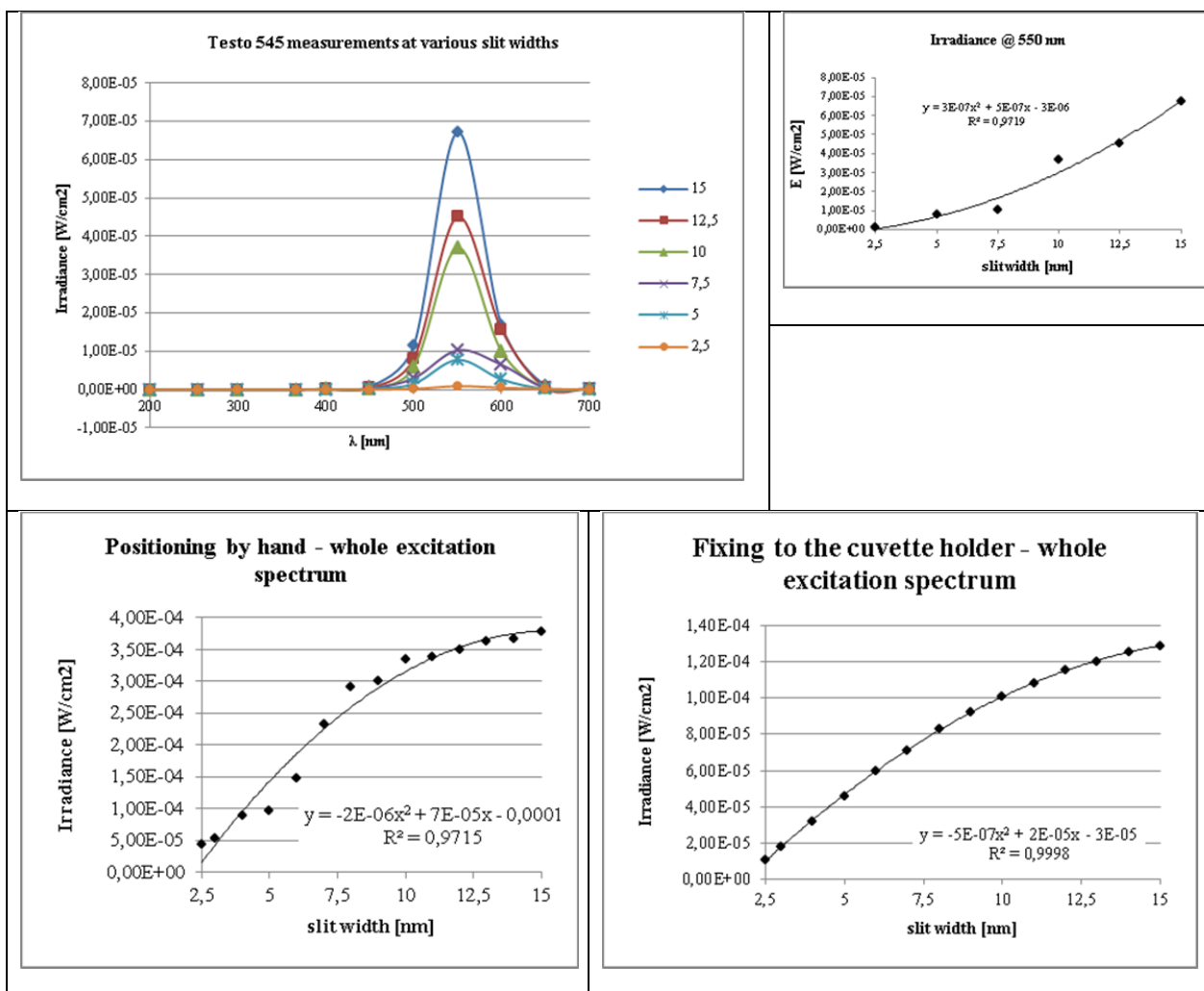


Figure 40: Testo 545 results in irradiance

2.4.5 UVC intensity measurements

All measurements with the UVM-CP radiometer in the LS 55 showed a value of zero W/cm^2 . Therefore it could be assumed, that the used instrument is not sensitive enough. The functionality of the device was tested with a 4W UV-lamp.

Several measurements have been carried out with the UVM-CP instrument on the NU-4 KL UV-lamp at various distances of measurement device to lamp.



Figure 41: a) The UV-Lamp NU-4 KL, b) UVM CP radiometer, c) experimental setup

Table 26: Experimental data of irradiance for various distances to the UV-light source

wavelength			
254 nm		366 nm	
distance [cm]	Irradiance [W/cm^2]	distance [cm]	Irradiance [W/cm^2]
0	3,12	0	0,03
5	0,71	5	0
10	0,25	15	0
15	0,12	20	0
20	0,06	20	0
25	0,02	25	0
30	0,01	30	0
35	0	35	0
40	0	40	0
45	0	45	0
50	0	50	0
55	0	55	0
60	0	60	0
65	0	65	0

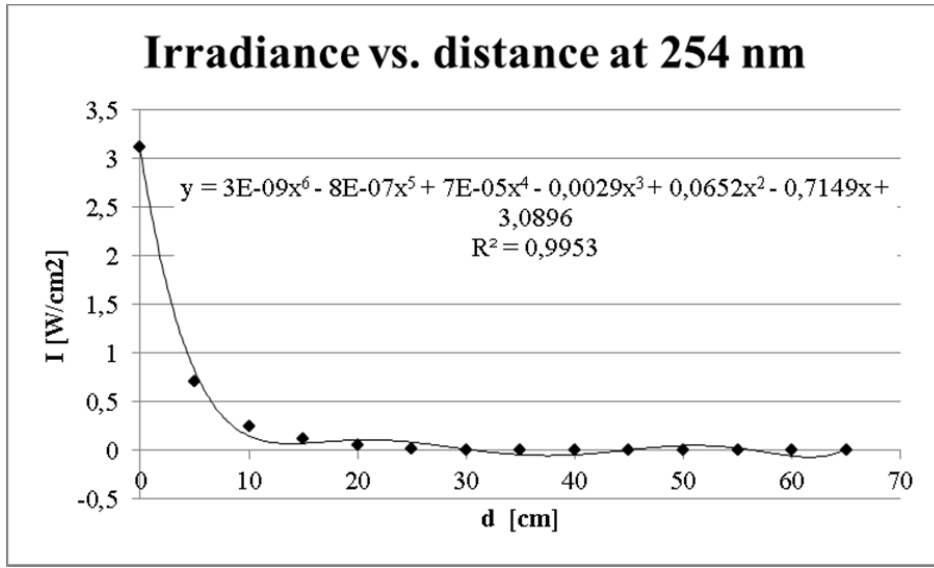


Figure 42: irradiance vs. distance to a 4 W UV-lamp set at 254 nm emission wavelength

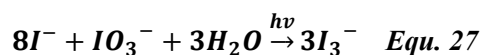
2.4.6 Actinometer measurements

Measurements with a chemical actinometer for the UV-region reported by Rahn [116] were used to determine the irradiation intensity (in W/m^2) in the Luminescence Spectrometer LS 55. A solution of 0,6 M iodide and 0,1 M iodate in 0,01 M borate buffer at a pH of 9,25 was illuminated in the LS 55 at various slit widths.

The Borate-buffer contained 2,0127 g of water free $\text{Na}_2\text{B}_4\text{O}_7$ dissolved in 1000 mL H_2O to yield a concentration of 0,01 mol/L. The pH-value of the buffer was tested with a pH-meter²⁶ which was calibrated with standard buffer solutions²⁷ at 7,00 and 11,01 before the measurement (pH = 9,23).

For the actual measurement 9,9606 g KI and 2,1400 g KIO_3 were dissolved in 100 ml Borate-buffer solution.

The illumination wavelength was kept at 254 nm. According to the publication of Rahn [115] the overall reaction equation is:



After illumination at maximum slit width dark smears can be seen in the cuvette indicating the production of I_3^- a species, which absorbs in the short wavelength part of the visible range with a maximum at 352 nm. Before the measurement of the transmission spectra of the illuminated samples the cuvette was shaken to ensure good homogenization.

Transmission spectra of the irradiated solutions were measured in the L950 spectrometer, using the detector for transmission measurements. An empty cuvette of the same manufacturer was used as a reference in the reference beam slot. Before illumination of the sample a baseline was collected using both cuvettes (empty sample and reference cuvette).

Figure 43 compares the spectrum of the original and the illuminated solution.

²⁶ WTW – Vario with pH-Electrode SenTix 41

²⁷ Buffer solutions: Hanna Instruments buffers HI 70007 and HI 70010

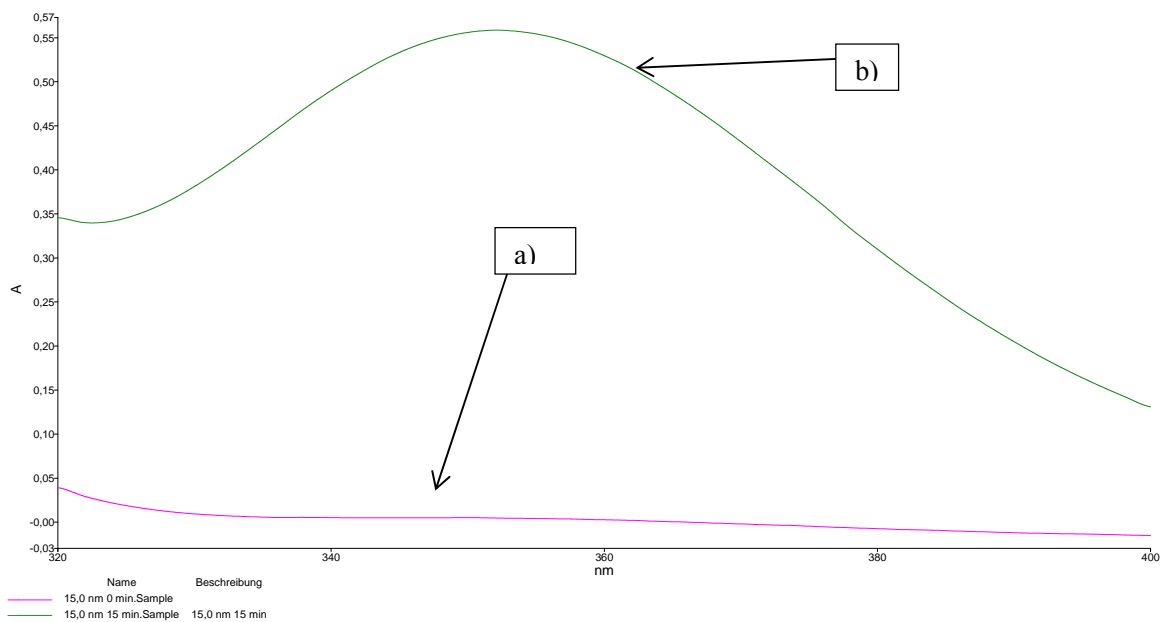


Figure 43: Absorbance of a) the original and b) the illuminated actinometer solution

Six cuvettes with actinometer solutions were prepared, one cuvette for every slit adjustment. The cuvette for the actual adjustment was measured in the instrument after illumination periods of 0, 5, 10 and 15 minutes, respectively. The slit width was varied starting from 2,5 nm to 15,0 nm in steps of 2,5 nm.

Table 27: Original measurement data for the chemical actinometer measurements

slit width [nm]/ illumination time [min]	Absorbance values @ 352 nm				date experiment was carried out
	0	5	10	15	
15,0	0,0077095	0,17248	0,36558	0,55866	03.07.2012
12,5	0,0093607	0,18122	0,34908	0,51255	03.07.2012
10,0	0,00956	0,11215	0,20117	0,3155	03.07.2012
7,5	0,010037	0,071831	0,13242	0,19653	03.07.2012
5,0	0,054061	0,079556	0,10468	0,12754	04.07.2012
2,5	0,10048	0,1034	0,10459	0,10687	05.07.2012

The experiment was carried out in 3 days. This explains the slight increase of the absorbance of the non-irradiated solutions (see table 27), which is caused by ambient UV light, cosmic radiation and/or radioactivity. The sensitivity of the actinometer can even be used for dosimetry of ionizing radiation as reported from Rahn et al [117].

For the evaluation the zero value of each experiment at the fixed slit width was subtracted. These values are noted in table 28.

Table 28: Corrected measurement data for the chemical actinometer measurements

slit width [nm]/ illumination time [min]	Absorbance values @ 352 nm			
	0	5	10	15
15,0	0	0,1647705	0,3578705	0,5509505
12,5	0	0,1718593	0,3397193	0,5031893
10,0	0	0,10259	0,19161	0,30594
7,5	0	0,061794	0,122383	0,186493
5,0	0	0,025495	0,050619	0,073479
2,5	0	0,00292	0,00411	0,00639

These data can be plotted. It becomes evident that the absorbance increases with the length of the illumination period as well as the slit width and hence the chemical actinometer is a useful tool to assess the irradiation of the sample.

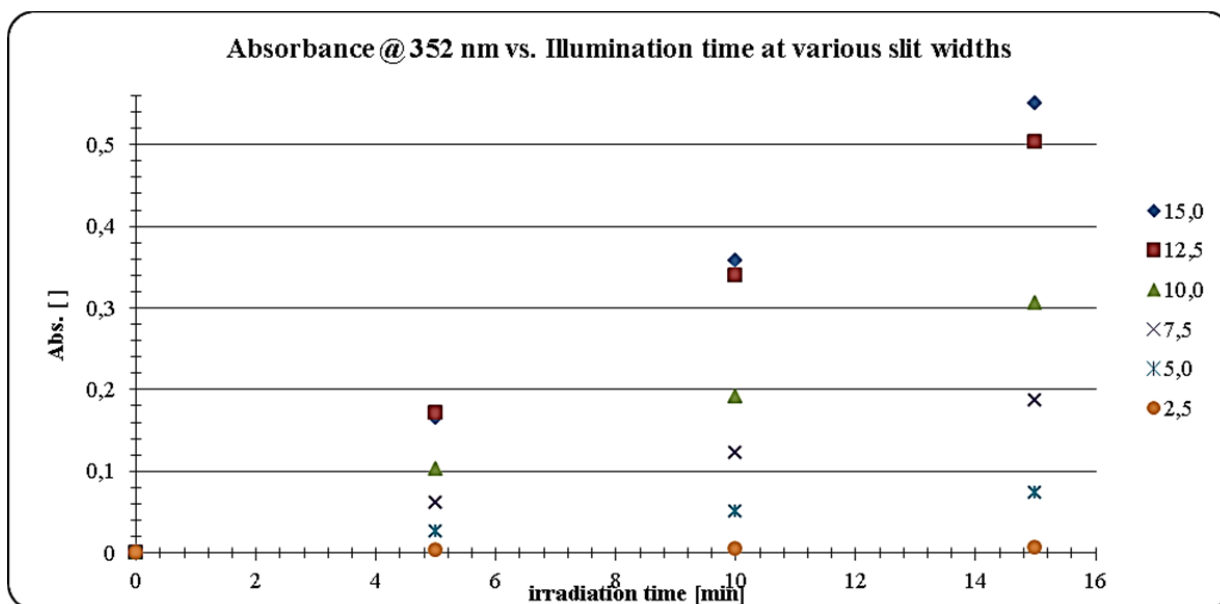


Figure 44: Absorbance values after correction for the actinometer experiment

The chemical actinometer was successfully used at the assessment of a corona reactor in a diploma thesis [118] at the TU-Graz. The following calculation of the irradiation intensity was taken from this work and the original papers from Rahn [116,119].

The absorption values of the actinometer solution can be used to calculate the irradiation intensity as follows:

$$c(I_3^-) = \frac{A_{352} \cdot S}{\varepsilon_{352} \cdot d} \quad \text{Equ. 28}$$

Where $c(I_3^-)$ is the concentration of the iodate ion in mol/L, A is the value of the (corrected) absorbance in dimensionless unit of the actinometer solution, ε_{352} is the extinction coefficient for the iodate ion at 352 [nm] with the known value of $\varepsilon_{352}(I_3^-) = 27.600 \left[\frac{1}{M \cdot cm} \right]$ and d is the thickness of the cuvette. (d = 1 [cm] for standard cuvettes). S is a dilution factor, which is S = 1 here, because the irradiated solutions were measured without further dilution.

The number of incident photons N_{ph} in [mol] can be calculated as follows:

$$N_{ph} = \frac{\Delta c(I_3^-) \cdot V_{cuv}}{QE_\lambda} \quad \text{Equ. 29}$$

Where $\Delta c(I_3^-)$ is the change in the concentration of the iodate ion in [mol/l], V_{cuv} is the volume of the cuvette in [m³] and QE_λ is the quantum yield of the actinometer-reaction in dimensionless units [] from 0 to 1. To keep the value for V_{cuv} constant, the cuvette was filled with the actinometer solution using a volumetric pipette²⁸ with nominal volume of 3 mL or $3 \cdot 10^{-6}$ m³.

The photon flux in [mol photons/s] can be calculated according to:

$$\Phi_P = \frac{N_{ph}}{\Delta t} \quad \text{Equ. 30}$$

Where N_{ph} is the number of incident photons in [mol] and Δt is the time of irradiation in [s].

The desired irradiance P_λ in W without respect of the irradiated area follows the equation

$$P_\lambda = \Phi_P \cdot \frac{h \cdot c}{\lambda} \cdot N_A \quad \text{Equ. 31}$$

Where Φ_P is the photon flux in [mol photons/s], h is Planck's constant with $h = 6,626 \cdot 10^{-34}$ [Js], c is the velocity of light with $c = 299 \cdot 10^6$ [m/s], λ the wavelength of the used radiation in m and N_A Avogadro's constant with $N_A = 6,022 \cdot 10^{23}$ [1/mol].

The quantum yield QE_{254} of the actinometer reaction follows the empiric equation:

$$QE_{254} = 0,75[1 + 0,02 \cdot (T - 20,7)][1 + 0,23 \cdot (c - 0,577)] \quad \text{Equ. 32}$$

²⁸ German: Vollpipette

Where T is the temperature in [°C]²⁹ and c is the concentration of KI in [mol/L]. The temperature in the laboratory was kept constant at 23[°C] via air condition and the actinometer solution was allowed to come to the room temperature. The concentration of KI is 0,6 [mol/L]. This gives a value of $PE_{254} = 0,789$

The illuminated area in the instrument was determined with a piece of millimeter paper an illumination of a spot of this paper at an excitation slit width of 15 nm, which is the maximum setting for the LS 55, at a wavelength of 550 nm. The illuminated area was 10·3 mm, which yields an illuminated area of 30 mm² or $3 \cdot 10^{-5} \text{ m}^2$.

It was assumed that the illuminated area does not change with the variation of the slit width.

The combination of equations 28-32 and division of P_λ with the irradiated area in cm² yields the irradiation intensity $P_{\lambda,A}$ in [W/cm²]:

$$P_{\lambda,A} = \frac{A_{352} \cdot S \cdot V_{cuv} \cdot h \cdot c \cdot N_A}{QE_{254} \cdot \epsilon_{352} \cdot d \cdot \Delta t \cdot \lambda \cdot A \cdot K} \quad \text{Equ. 33}$$

Explanation of the terms in equation 33 is given above. K is the conversion factor from an area in m² to cm². Using equation 33 the corrected absorbance values from table 29 can be used to calculate the irradiation intensity:

Table 30: Parameters for calculation of irradiance with Equ. 33

term	explanation	unit	value	
$P_{\lambda,A}$	irradiance	[W/cm ²]	x	numerator
A_{352}	absorbance @ 352 nm	[]	y	
S	dilution factor	[]	1	
V_K	cuvette volume	[m ³]	3,00E-06	
h	Planck's constant	[J s]	6,626E-34	
c	velocity of light	[m/s]	2,99E+08	
N_A	Avogadro's constant	[1/mol]	6,022E+23	
ϵ_{352}	extinction coefficient	[1/((mol/l)m)]	2,76E+03	denominator
d	thickness of the cuvette	[m]	1,00E-02	
Δt	irradiation time	[s]	z	
λ	wavelength	[m]	2,54E-07	
A	irradiated area	[m ²]	3,00E-05	
QE_{254}	quantum yield of reaction	[]	0,789	
K	conversion factor	[cm ² /m ²]	1E04	

²⁹ It is important to use the temperature in degree Celsius for the calculation.

Table 29: Corrected absorbance values @ 352 nm and calculated irradiance values

		corrected absorbance values @ 352 nm				
illumination time [sec]	0	300	600	900		
slit width [nm]	-	-	-	-		
15	0	0,1647705	0,3578705	0,5509505		
12,5	0	0,1718593	0,3397193	0,5031893		
10	0	0,10259	0,19161	0,30594		
7,5	0	0,061794	0,122383	0,186493		
5	0	0,025495	0,050619	0,073479		
2,5	0	0,00292	0,00411	0,00639		
slit width [nm]		irradiance [W/cm ²]			mean [W/m ²]	stdev. [W/m ²]
15	0	0,00E+00	1,18E-04	2,57E-04	2,57E-04	1,39E-04
12,5	0	0,00E+00	1,24E-04	2,44E-04	2,43E-04	1,19E-04
10	0	0,00E+00	7,38E-05	1,38E-04	1,44E-04	7,33E-05
7,5	0	0,00E+00	4,44E-05	8,80E-05	8,88E-05	4,48E-05
5	0	0,00E+00	1,83E-05	3,64E-05	3,59E-05	1,73E-05
2,5	0	0,00E+00	2,10E-06	2,96E-06	3,22E-06	1,27E-06

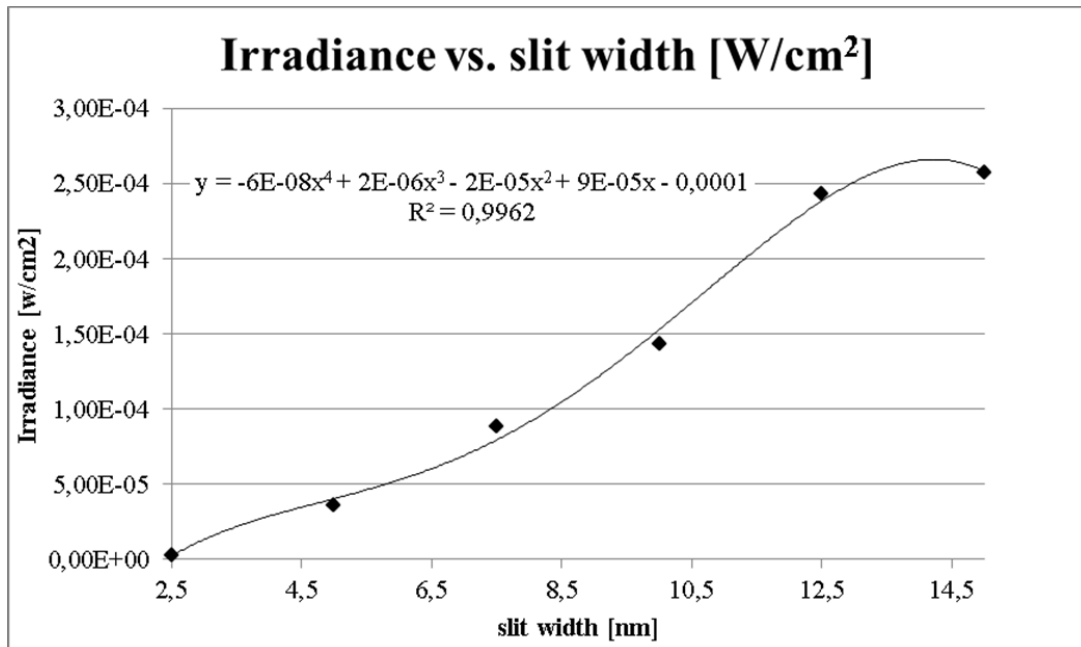


Figure 45: Irradiance vs. slit width

2.4.7 Comparison to other illumination techniques

To summarize it could be said, that the irradiance of the measurement spot in the LS 55 is in the scale of about 10^{-4} – to 10^{-5} W/cm². In comparison the lead glass sorting systems of Binder + Co uses an irradiance of about $1,6 \cdot 10^{-3}$ W/cm². Typical pulse characteristics of a Nd-YAG laser used by Gaft et al for laser excitation of minerals are pulse durations $t = 6 - 10$ ns and pulse energies between $P = 0,1 - 1$ J [120]. This³⁰ and the assumption of an irradiated area of about 1 mm² yields irradiance values of about 10^9 W/cm² to about 10^{11} W/cm².

For a comparison to possible LIF-laser sources the lasers which are listed by Broicher are shown in table 30 [121]. For the following table only conditions of highest possible irradiance³¹ were chosen (e.g. maximum power and smallest pulse duration). If no beam width was indicated about 1 mm was assumed to calculate the irradiance.

Table 30: Different lasers and irradiance values form Broicher's LIF report [121]

Laser Type	Name	Model	WL [nm]	Beamwidth [mm]	Pulse energy [J]	Power [W]	Pulse duration [s]	durability	Irradiance [W/cm ²]
real cw lasers	Laser-Star	DUV LS266 xxxS	266	0,8	-	1,00E-01	-	3000 h	1,99E-03
	Klasstec h	VERVE	266	1,0	-	1,00E-01	-	12 months guaranteed	1,27E-03
	Coherent	MDB266	266	1	-	2,00E-01	-	?	2,55E-03
	Coherent	Azure TM CW 266	266	1,05	-	2,30E-01	-	> 6250 h	2,66E-03
	Coherent	Genesis CX 355	355	1,0	-	1,00E-01	-	?	1,27E-03
	CryLas	DL 375-100/200	375	1,0	-	2,00E-01	-	?	2,55E-03
quasi cq lasers	Teem Phot.	PNU-M1510	266	1	?	1,7E-02	3,50E-10	?	2,17E-04
	CryLas	FQCW 266-100	266	0,55	?	1,00E-01	?	?	4,21E-03
	EKSPL A	NL20#	266	0,7	7,0E-04	1,00E+05	7,00E-09	?	2,60E+03
	Spectra-Ph	Hippo Prime 266-2 DPSS	266	1	?	2,00E+00	?	?	2,55E-02
	Coherent	AVIA 266-3	266	2	?	3,00E+00	?	2 years	9,55E-03
	EdgeWave	Innoslab BxxxIV	266	3	1	6,00E+00	9,00E-09	?	8,49E-03
	Spectra-Ph	Hippo 355-5 DPS	355	1	?	5,00E+00	?	?	6,37E-02
	Coherent	AVIA 355-5	355	2	?	5,00E+00	?	> 12.000 h	1,59E-02
	Coherent	MATRIX 355-1-60 BE	355	2,2	-	1,00E+00	?	very long	2,63E-03
	EKSPL A	NL20#	355	0,7	1,50E-03	2,15E+05	7,00E-09	?	5,59E+03
pulsed laser	CryLas	FQSS 266-Q DPSS	266	1	?	3,00E+02	?	?	3,82E+00
	Quantel	Centurion DPSS	266	2,6	2,00E-03	2,50E+02	?	about 10 ⁹ pulses	4,71E-01
	Spectra-Ph	Explorer 349 DPSS	349	0,18	?	2,40E+04	?	?	9,44E+03
	CryLas	FTSS 355 - 300	355	0,8	?	2,00E+05	?	?	3,98E+03
	Quantel	Centurion DPSS	355	2,6	6	7,50E+05	?	> 10 ⁹ pulses	1,41E+03

³⁰ $P_{\text{lowest}} = 10^7$ J, $P_{\text{highest}} = 1/6 \cdot 10^9$ J

³¹ The laser spot was assumed spherical therefore $A = \frac{\pi \cdot d^2}{4} = 0,785 \cdot d^2$

The relevant facts can be summarized in table 31.

Table 31: Irradiance values for several fluorescence applications

Application	Irradiance values for measuring spots [W/cm²]
LS 55 – measuring chamber	$10^{-5} - 10^{-4}$
Binder + Co lead glass sorting system	$10 \cdot 10^{-3} - 1,6 \cdot 10^{-3}$
Lasers for LIF recommended from Broicher	$2,17 \cdot 10^{-3} - 5,59 \cdot 10^{-3}$
LIF – labscale system after Gaft et al	$10^9 - 10^{11}$

The comparison of different types of light sources shows, that the present LS 55 system has the lowest irradiance and is about one to two orders of magnitude lower than the excitation system in the Binder + Co lead glass sorting systems. The lasers reported from Broicher show a very broad band of irradiance values of about six orders of magnitude. The outstanding highest irradiance values occur for the LIF- labscale system reported from Gaft et al. It should be mentioned that many of the calculated values are based on assumptions. However, this survey shows how wide the irradiation span for actual luminescence excitation systems is.

3 Results and Discussion

3.1 Reflection Spectra and Interpretation

From the vast amount of available samples of the Binder + Co R&D department seven minerals have been chosen for further discussion:

- Bauxite
- Magnesite
- Talc
- Fluorite
- Calcite
- Chalcedony
- Baryt

This sample set represents some minerals and mixtures of minerals, which are of interest in the ongoing research project Minexx Plus. Some of the minerals are fluorescent minerals and will be discussed again in following chapters.

Minerals which are fluorescent under UV-light usually show high absorbance in the UV- region. The UV-light is “converted” to light of higher wavelength, which means lower energy. Therefore, when the reflection spectra of such samples are recorded in the UV, sometimes reflectance values over 100 % are encountered. This does not mean violation of the conservation of energy. It simply means, that the sample shows fluorescence when excited in the UV. In order to get rid of this additional intensity (which is of a different wavelength) a second dispersive element like a prism or a diffraction grid between sample and integrating sphere would be required. With respect to the wavelength dependence of features of spectrometer components, e. g. the quantum efficiency of a photomultiplier tube or the absorption of the reflective coating of the integrating sphere, reflectance values over 100 % can only be encountered if the sample emits photons caused by luminescence.

3.1.1 Bauxite

Bauxite is the most important source of Alumina and used for manufacturing of artificial corundum. It is a mixture of several Alumina- and Iron-Hydroxides: Gibbsite: $\gamma\text{-Al(OH)}_3$, Boehmite: $\gamma\text{-AlOOH}$, Diaspore: $\alpha\text{-AlOOH}$, Hematite: Fe_2O_3 , Goethite: $\alpha\text{-FeO(OH)}$ [122,123]. Gibbsite forms crystals with monoclinic, unit cells. In Gibbsite, edge-sharing Al(OH)_6 octahedra form sheets with only 2/3 of the octahedral sites occupied, creating a sheet consisting of a network of 6-membered rings; the sheets are linked by hydrogen bonds [140]. Boehmite forms crystals with orthorhombic unit cells. In Boehmite Al(O,OH)_6 octahedra share six of their 12 edges to form double sheets; the sheets are linked by hydrogen bonds [141]. Diaspore forms crystals with unit cells of orthorhombic symmetry. Edge sharing Al(O,OH)_6 octahedra form double chains; the chains are linked by sharing corners of the octahedra, and by strong H-bonding [142]. Hematite crystallizes with trigonal [143] and Goethite like Diaspore with orthorhombic unit cells [142].

The analyzed Bauxite sample is depicted in figure 46.



Figure 46: Bauxite sample

Interpretations of the Bauxite reflection spectrum was made according to literature [156].

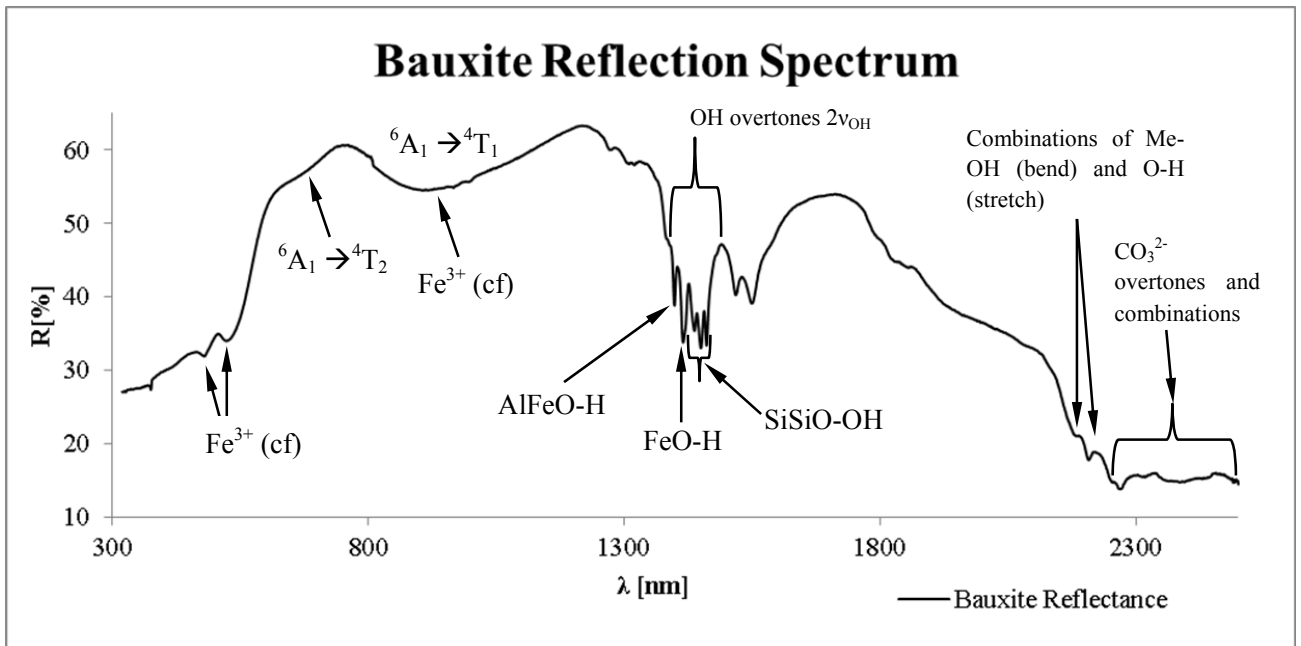
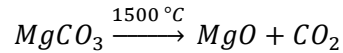


Figure 47: Bauxite reflection spectrum

3.1.2 Magnesite

Magnesite has the chemical formula $MgCO_3$, it crystallizes with trigonal $\bar{3}$ unit cells and forms crystals of rhombohedral habit, the structure is isotypic to the Calcite structure. Magnesite is an important resource for fire resistant coating stones. These coatings are especially used for the reactors of the LD – process and electric furnaces for steel production. Raw Magnesite is sintered to the fireproof sintered magnesia under temperatures of 1500 °C [114, 144].



The analyzed Magnesite sample is depicted in figure 48.



Figure 48: Magnesite sample

In figure 49, the characteristic band for CO_3^{2-} at 2318 nm or 6882 cm^{-1} can be identified as a combination of 3 Carbonate fundamentals. These fundamentals are listed in the table 32.

Table 32: CO_3^{2-} fundamentals for interpretation of the Carbonate feature in NIR [157]

Fundamental	$\bar{\lambda} [\text{cm}^{-1}]^{32}$
ν_1	1373
ν_2	1069
ν_5	1482

The combination of the three fundamentals was calculated in equation 34.

$$2 \cdot (\nu_5 + \nu_1) + \nu_2 = 6779\text{ cm}^{-1} \quad \text{Equ. 34}$$

The deviation of about 3 cm^{-1} is expected and due to the anharmonicity of the vibrations.

³² The wavenumber of fundamentals is given in units of cm^{-1} . The conversion is: $\frac{1}{\lambda[\text{nm}]} \cdot 10^7 = \bar{\lambda}[\text{cm}^{-1}]$

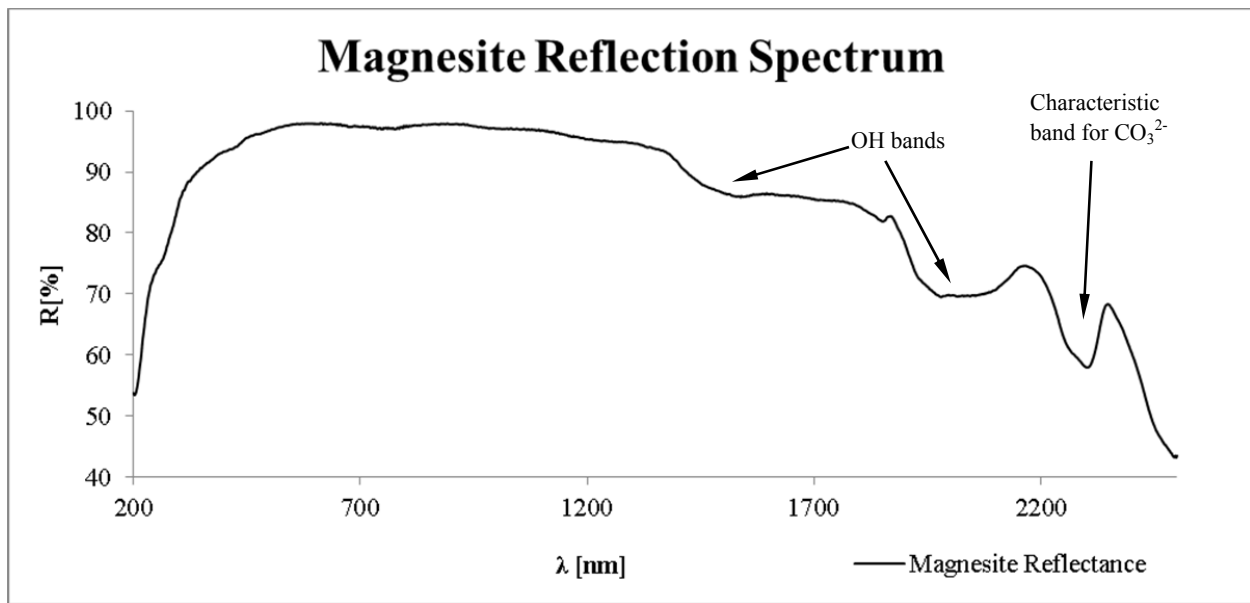


Figure 49: Magnesite reflection spectrum

3.1.3 Talc

Talc is a sheet silicate mineral, $[\text{SiO}_4]$ -tetrahedrons are linked together in an infinite tetrahedron sheet. Each $[\text{SiO}_4]$ tetrahedron has 3 bridging oxygen atoms to neighboring tetrahedrons. Talc has the chemical formula $\text{Mg}_3[(\text{OH})_2/\text{Si}_4\text{O}_{10}]$. Ions like OH^- , F^- , K^+ , Na^+ , Ca^{2+} , etc. can be intercalated between the sheets [139]. Talc is trioctahedral, with three divalent cations occupying occupying all the octahedral sites. These sheets are linked by van der Waals forces [147]. Two different forms of Talc are known: Talc-1A crystallizing in triclinic cells and Talc-2M₁ forming monoclinic unit cells, both of the same chemical formula [145].

Talc forms crystals in the crystal class 2/m, but can also form triclinic or rhombohedral polytopes. Talc has technological value because of its hydrophobic properties and good ability to absorb organic compounds. Powdered talc is known as talcum powder and used in glass-, paper- and dye industry, as lubricant, binder for drugs and cosmetics and extender for plastic [146]. The analyzed talc sample is depicted in figure 50.



Figure 50: Talc sample

The talc reflection spectrum shows several very sharp peaks around 1300 nm, which are presumable combinations and overtones of the OH-group. These sharp features indicate that the OH-groups sit at very defined places in the crystal structure, probably in the surrounding of metal-cations. Talc shows several features which were just encountered in the bauxite spectrum. The complex structure over 1800 nm supposedly consists of OH and Si-O overtones and is hard to interpret. The presence of the broad feature around 900 nm is an indication of Fe³⁺ in the mineral. The presence of Fe³⁺ is also supported by a strong vibrational overtone at around 1400 nm.

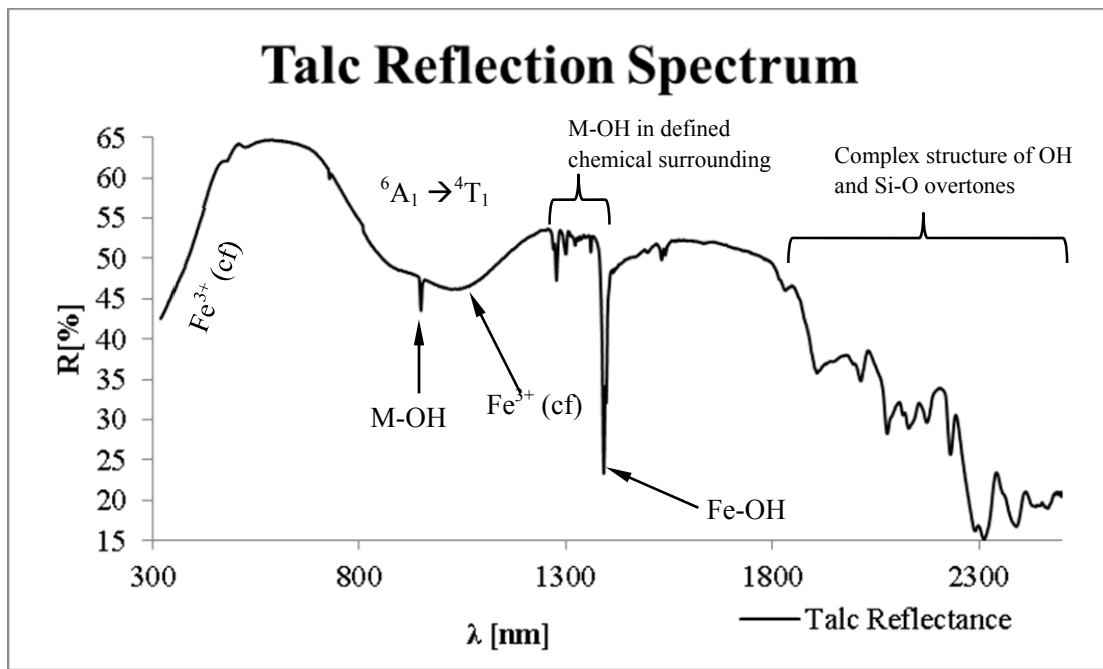


Figure 51: Talc reflection spectrum

3.1.4 Fluorite

Fluorite has the chemical formula CaF₂ and crystallizes with cubic $\bar{3}$ unit cells. It forms a framework of edge-sharing MF₈ cubes. This structure is known as the CaF₂-type [147]. Fluorite occurs in nearly all colors like green, violet, yellow, colorless or black-violet. The color is caused by trace elements, disturbances in the crystal structure, or radioactive irradiation. Many Fluorite show fluorescence under UV-light because they carry rare earth elements instead of Ca²⁺ ions. Dark fluorites bear colloidal elemental Ca, which is reduced Ca²⁺, reduced by nuclear radiation. This metallic Ca works as a dark pigment in the usually colorless host. Fluorite is of technological value as flux melting agent in metallurgy, a raw material for the synthesis of hydrofluoric acid and fluorine containing chemicals. Very pure synthetic Fluorite can be used for optical instruments e.g. as lens. It shows high transmittances in the UV-region [148]. The analyzed fluorite sample is depicted in figure 52.



Figure 52: Fluorite sample

The fluorite reflection spectrum shows broad OH-features in the NIR region at around 1400 and 1900 nm. This indicates that the OH are not so defined in the crystal structure. Maybe these bands come from adsorbed or included water in the mineral.

The features at around 550 and 600 nm come from Eu^{2+} and were reported in the literature. The whole region around 200 – 700 nm can be affected by Eu^{2+} or color centers which are built in presence of Eu^{2+} [158]. The sharp features under and around 400 nm can also origin from intercalated transition metal ions.

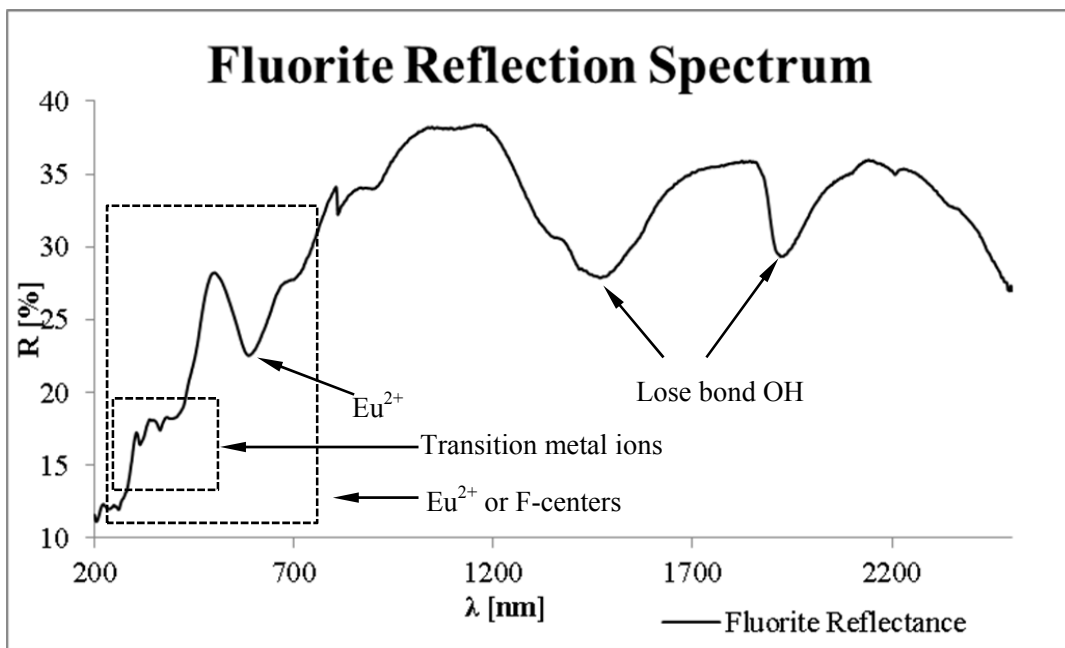


Figure 53: Fluorite reflection spectrum

3.1.5 Calcite

Calcite shows the chemical composition CaF_2 , it forms crystals with trigonal unit cells $\bar{3}$ and is therefore structurally equivalent to Magnesite. Sheets of planar CO_3 groups and sheets of corner sharing Ca-octahedra are formed. Each O of a CO_3 -group connects a Ca atom of the underlying sheet to a Ca atom of the overlying sheet, forming a 3-dimensional framework. This structure is known as the Calcite-structure [149]. Different calcites in varying habit are known. Calcite is easily soluble in cold diluted acids under gas formation (CO_2). Calcite is an important material for the building industry as building stones and decoration stone. Calcites of high quality are known as commercial marble. Furthermore it is a raw material for lime mortar, Portland cement and as a flux material in metallurgical industry. Calcite finds also application as a white pigment in paper [150]. The examined calcite sample is depicted in figure 54.



Figure 54: Calcite sample

The calcite reflection spectrum shows typical features for OH-combinations and overtones around 1400 and 1900 nm, but also the typical CO_3^{2-} feature around 2300 nm encountered in the Magnesite reflection spectrum. The band around 1100 nm can indicate Fe^{2+} and was reported in the literature [159]. The small features around 500 nm and 360 nm indicate small amounts of Mn^{2+} , this feature was reported by several authors. [160, 161, 162]. However, slight differences from the reported wavelength values in the literature can occur, due to the differences in crystal field.

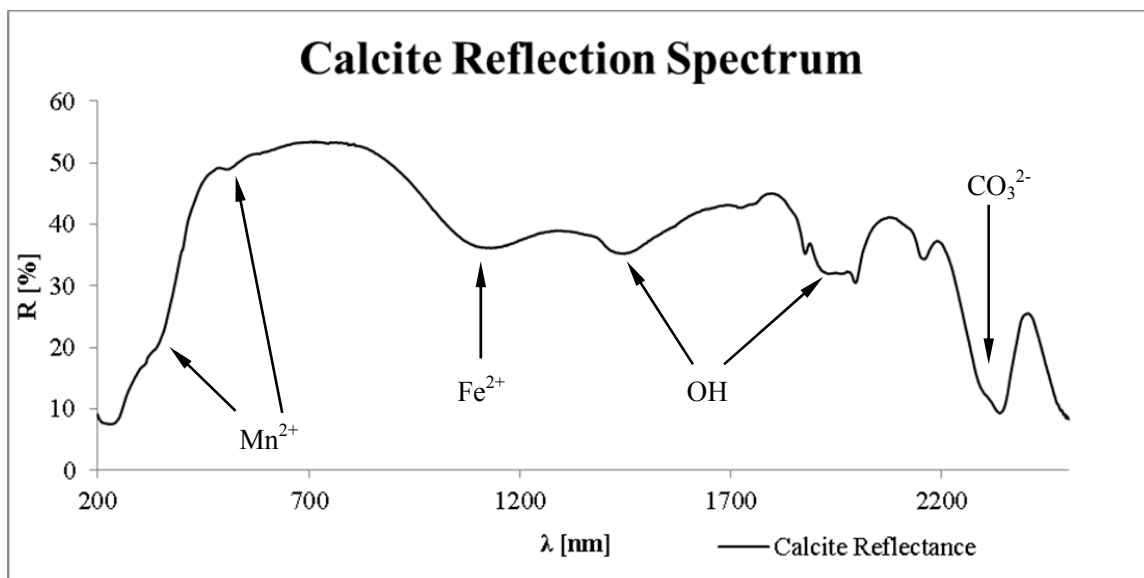


Figure 55: Calcite reflection spectrum

3.1.6 Chalcedony

Chalcedony is cryptocrystalline quartz and has the chemical formula SiO_2 . Cryptocrystalline means, that the crystals, which build up the mineral are very small and only visible under the microscope. 6 Modifications of modifications of Quartz with unit cells of different point groups are known. Several minerals are build up by Quartz: rock crystal, amethyst, citrine, ametrine, tiger-eye, chalcedony, agate, carnelian, chrysoprase, heliotrope, onyx, flint (firestone), chert, jasper, etc. Which form of quartz is build up is determined by the temperature T. Temperature range and point group of the unit cell of the 6 forms of quartz are as follows [151]:

- Quartz/ $T < 573 \text{ }^\circ\text{C}$ / Trigonal
- β -Quartz/ $T > 573 \text{ }^\circ\text{C}$ / Hexagonal
- Tridymite/ $T: 180 - 350 \text{ }^\circ\text{C}$ / Orthorhombic
- β -Tridymite/ $T: 465 - 1470 \text{ }^\circ\text{C}$ / Hexagonal
- Cristobalite/ $T < 268 \text{ }^\circ\text{C}$ / Tetragonal
- β -Cristobalite/ $1470 - 1728 \text{ }^\circ\text{C}$ / Cubic

Chalcedony is a collective term for all micro- and cryptocrystalline parallel-fibrous structured Quartz-varieties. Because of submicroscopic pores and H_2O -contents of 0,5 – 2 % the density is relative low with 2,59 – 2,61 g/cm^3 . Chalcedony is often of bluish color and has shell-shaped break planes [152]. The analyzed sample of chalcedony is depicted in figure 56.

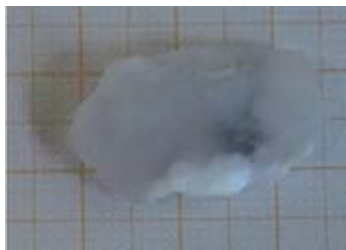


Figure 56: Chalcedony sample

The reflection spectrum of chalcedony shows the typical OH bands around 1400 and 1900. The bands at 988 nm, 1182 nm and 1213 nm are of unknown origin. These unknown bands can indicate a transition element or be unknown features of the UO_2 present in the sample. The slight band around 698 nm comes from a trace amount of UO_2 and was reported in the literature [163].

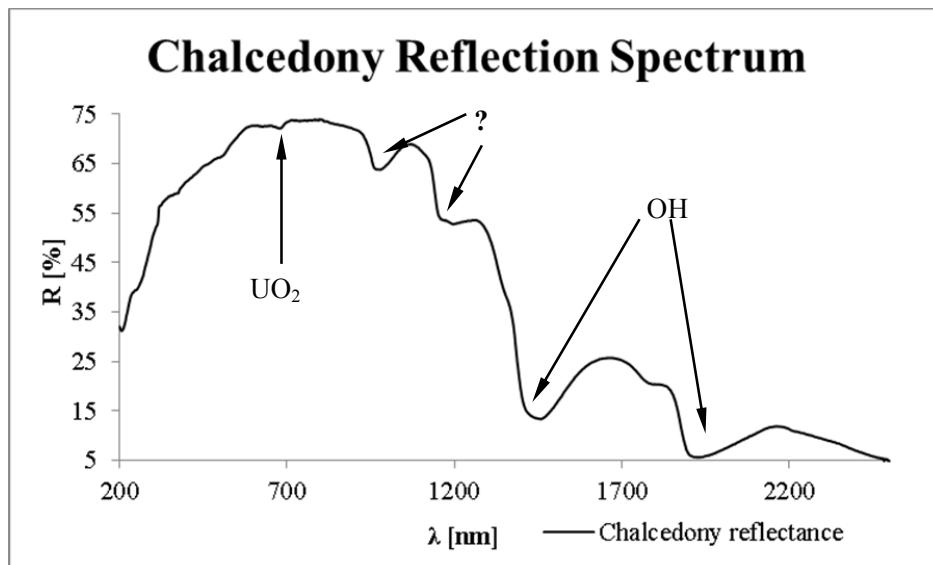


Figure 57: Chalcedony reflection spectrum

3.1.7 Barite

Barite has the chemical formula $BaSO_4$, and forms Orthorhombic unit cells. Ba is in a mirror symmetric coordination and shares three edges and four corners with SO_4 -tetrahedra; six short Ba-O bond lengths and strong binding forces in sheets are responsible for the perfect cleavage of $BaSO_4$. Other minerals in the Barite (often referred to as “Baryte”) group like Celestine, Anglesite, Olscherite and Kerstenite are isostructural [153].

Barite is an important raw material for white dyes. Barite is also used as radiation protection in X-Ray technology and nuclear power plants. It is a component of heavy concrete and used for the preparation of Barium bearing chemicals in chemical industry [168].

The examined barite sample is depicted in figure 58.



Figure 58: Barite sample

The reflection spectrum of barite does not show any significant features except the known OH-peaks at around 1400 nm and 1900 nm. $BaSO_4$ was an alternative to Teflon as a white standard and therefore used

for coatings of integrating spheres or reflection reference material. The OH-peaks indicate adsorbed or included H₂O in the sample.

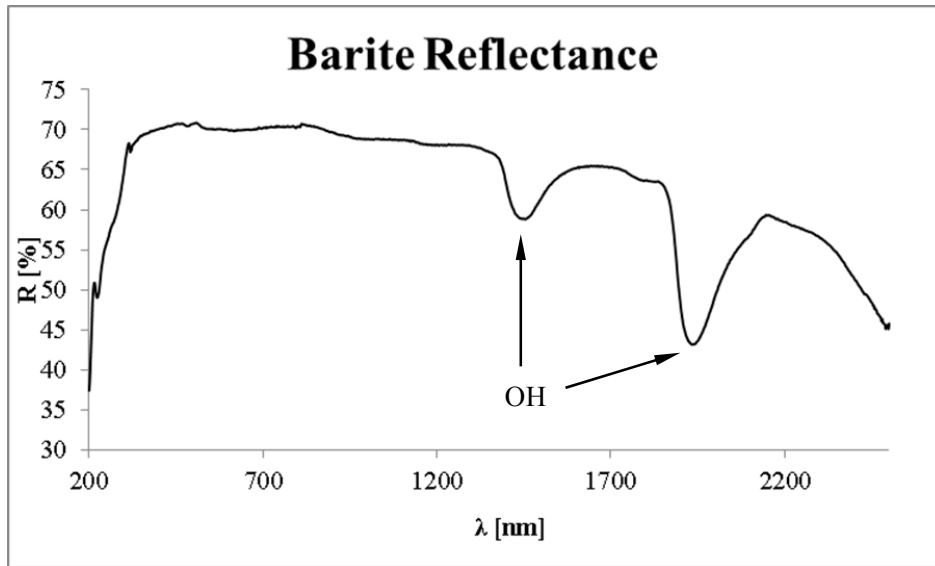


Figure 59: Baryt reflection spectrum

3.1.8 Discrimination of minerals via the reflection spectrum

An easy to use method to distinguish different minerals is the simple comparison of their UV-VIS-NIR reflection spectra.

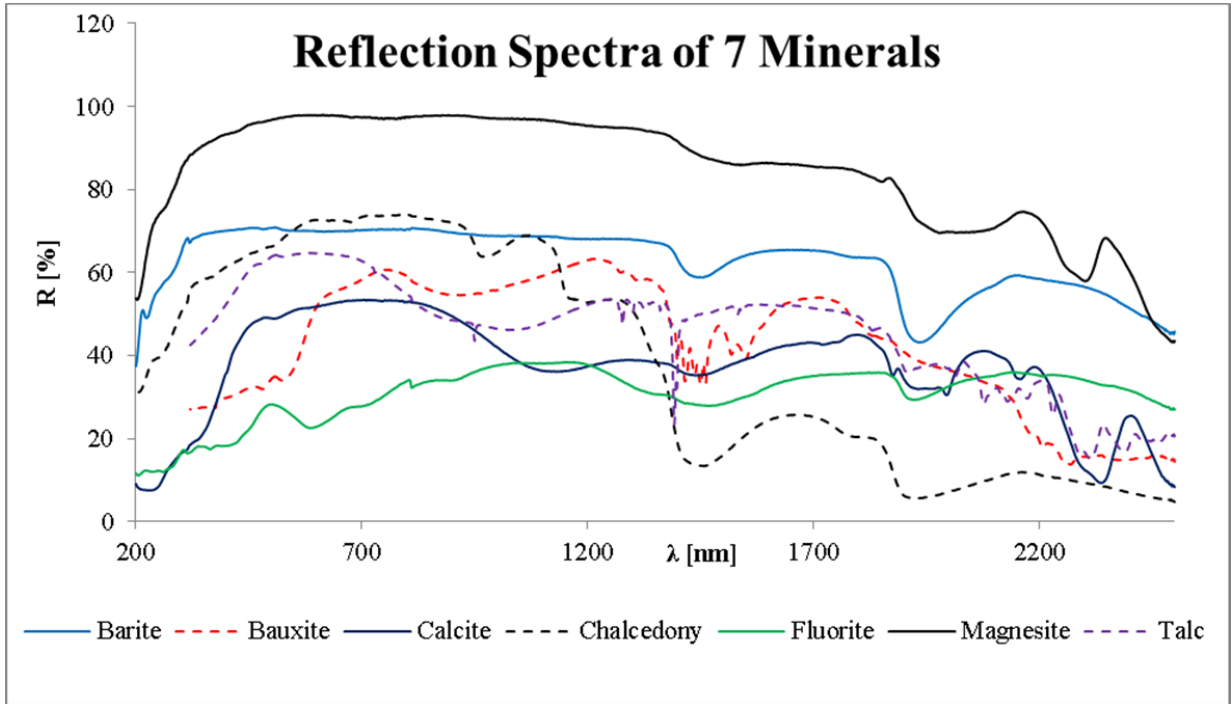


Figure 60: Reflection spectra of 7 minerals

If no evident discriminating spectral feature can be found in the spectra, comparison of the first or second derivation can be useful. The plots for the first and second derivative of the reflection data are presented in the figures 61 and 62. The UV-VIS region is plotted separately in figures 63, 64 and 65 while the NIR data are shown in detail in the plots 66, 67 and 68.

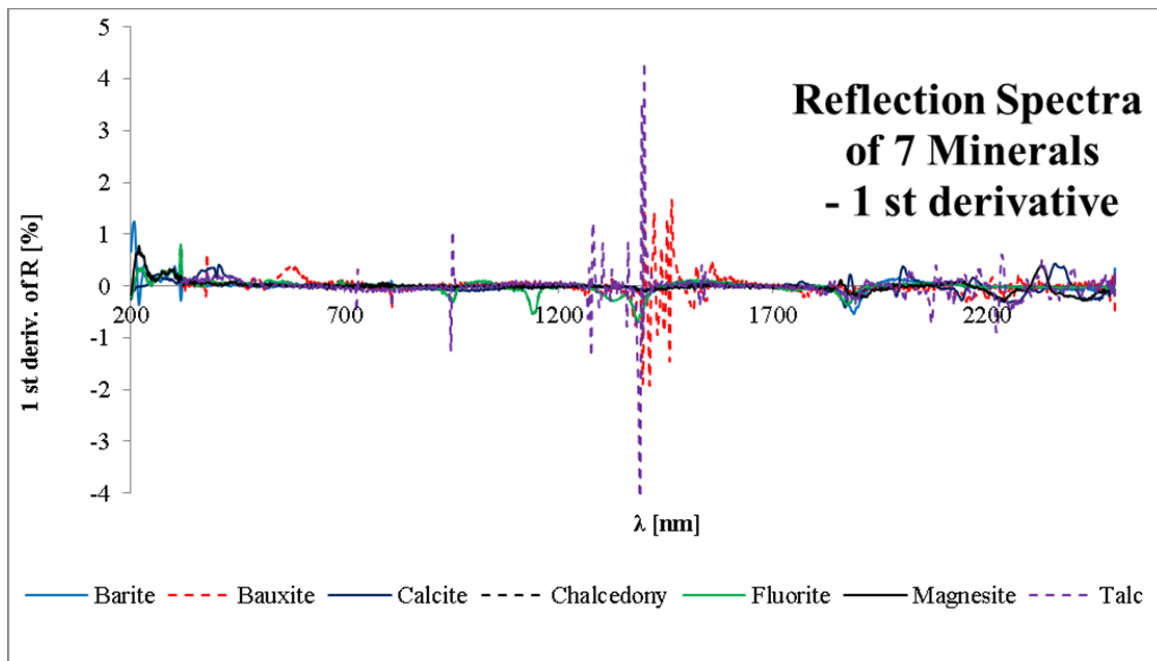


Figure 61: Reflection Spectra of 7 Minerals – 1 st derivative

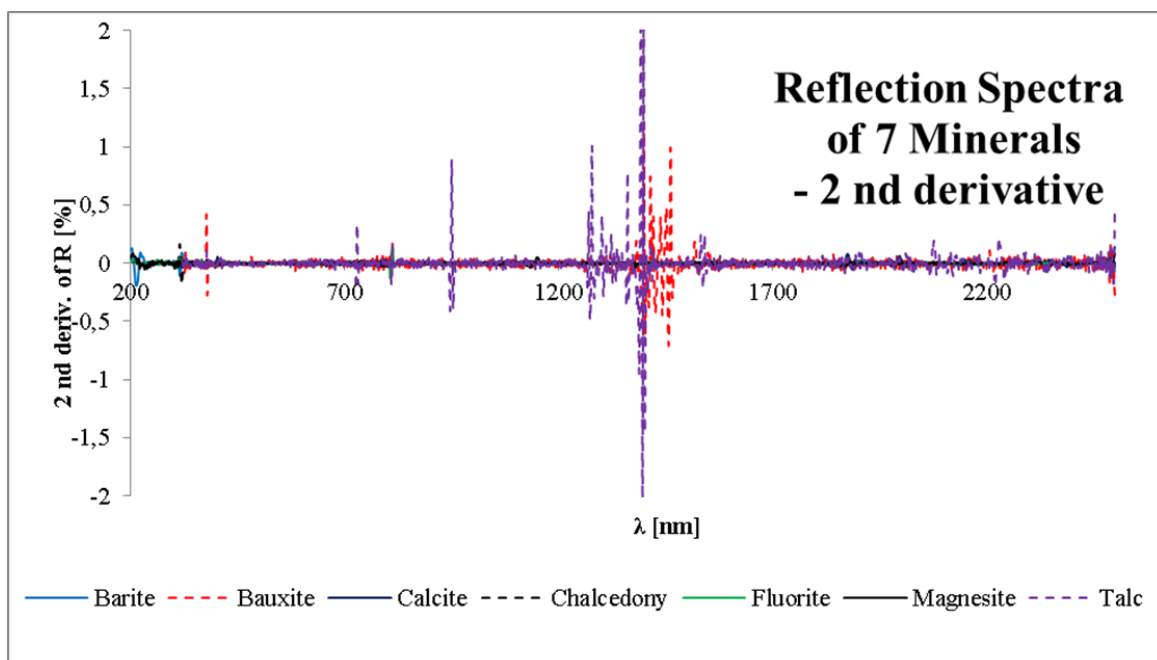


Figure 62: Reflection Spectra of 7 Minerals – 2 nd derivative

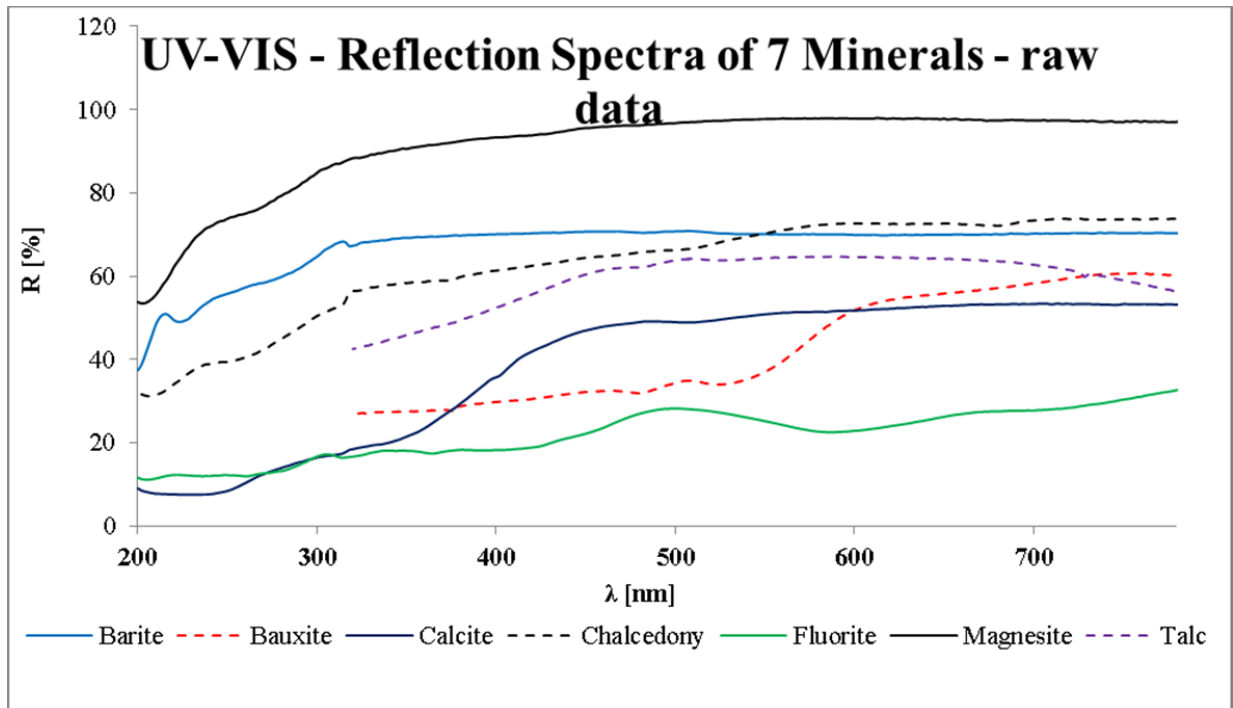


Figure 63: UV-VIS – reflection spectra of 7 minerals – raw data

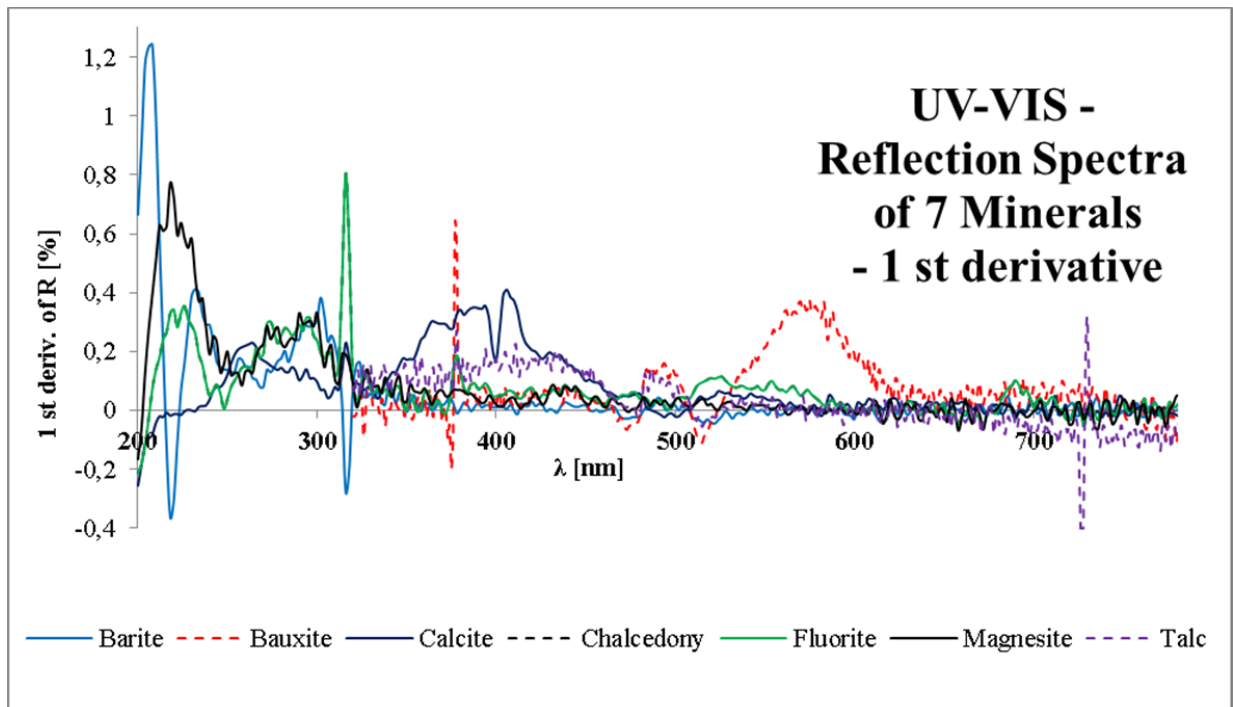


Figure 64: UV-VIS reflection spectra of 7 minerals

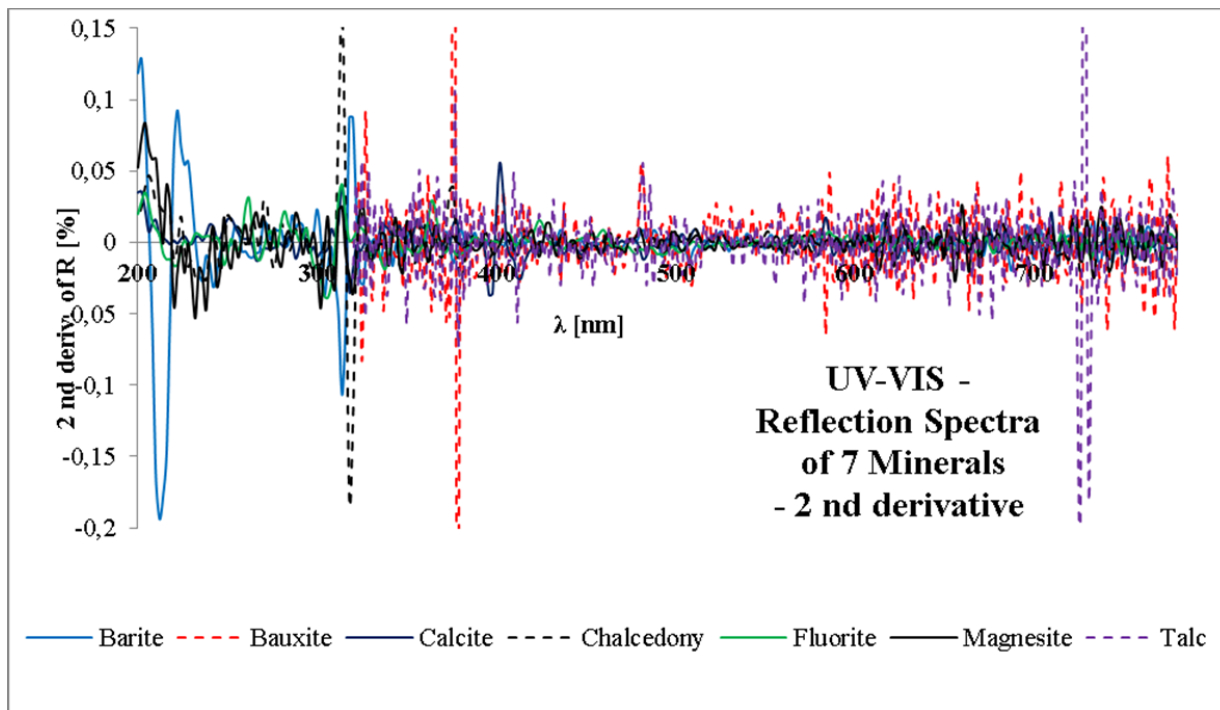


Figure 65: UV-VIS reflection spectra of 7 minerals – 2nd derivative

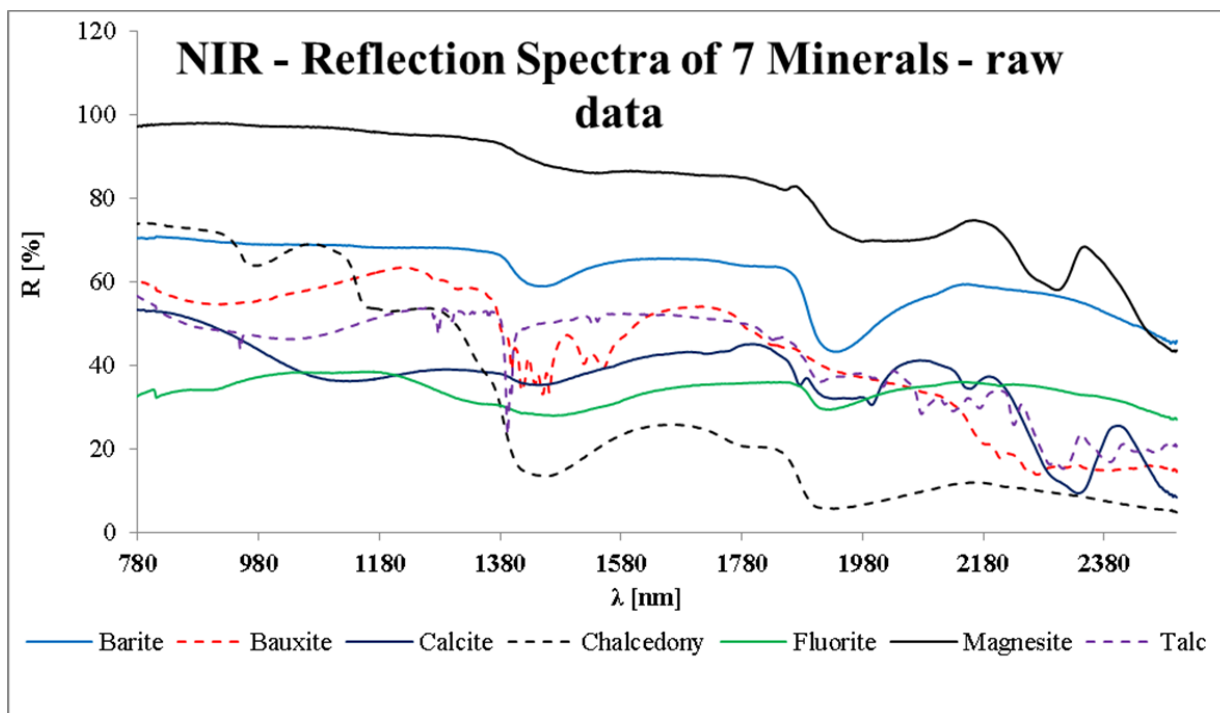


Figure 66: NIR reflection spectra of 7 minerals – raw data

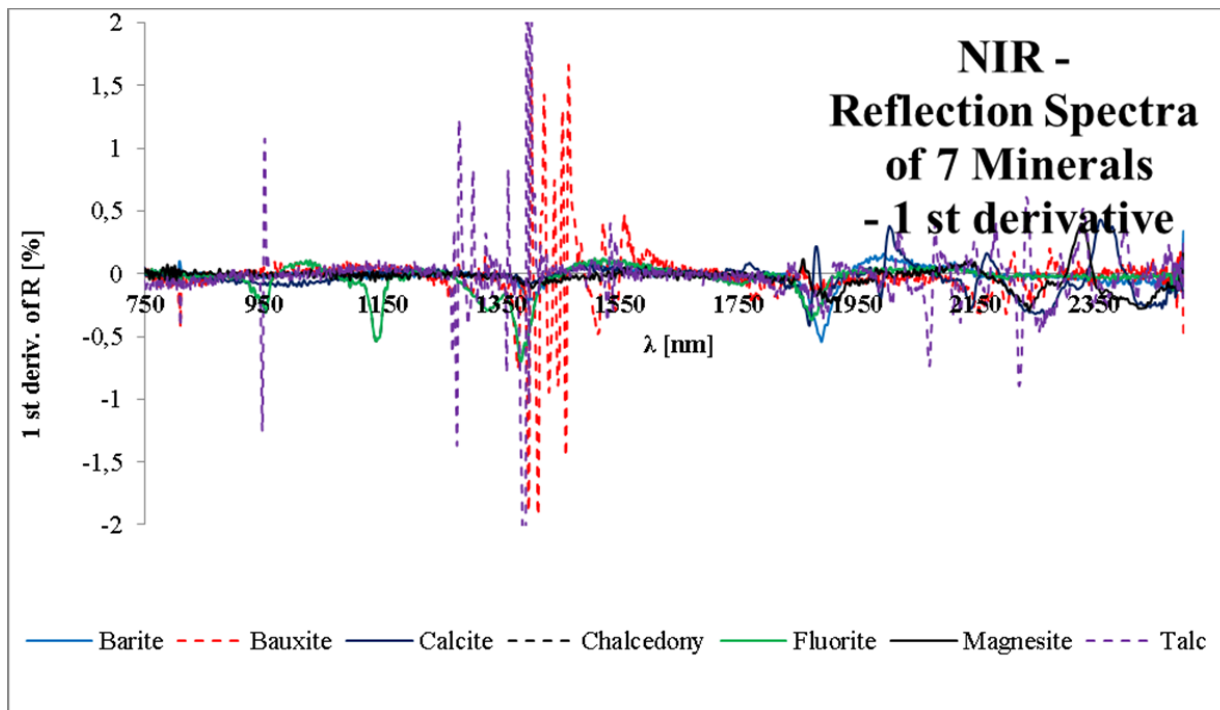


Figure 67: NIR reflection spectra of 7 minerals – 1 st derivative

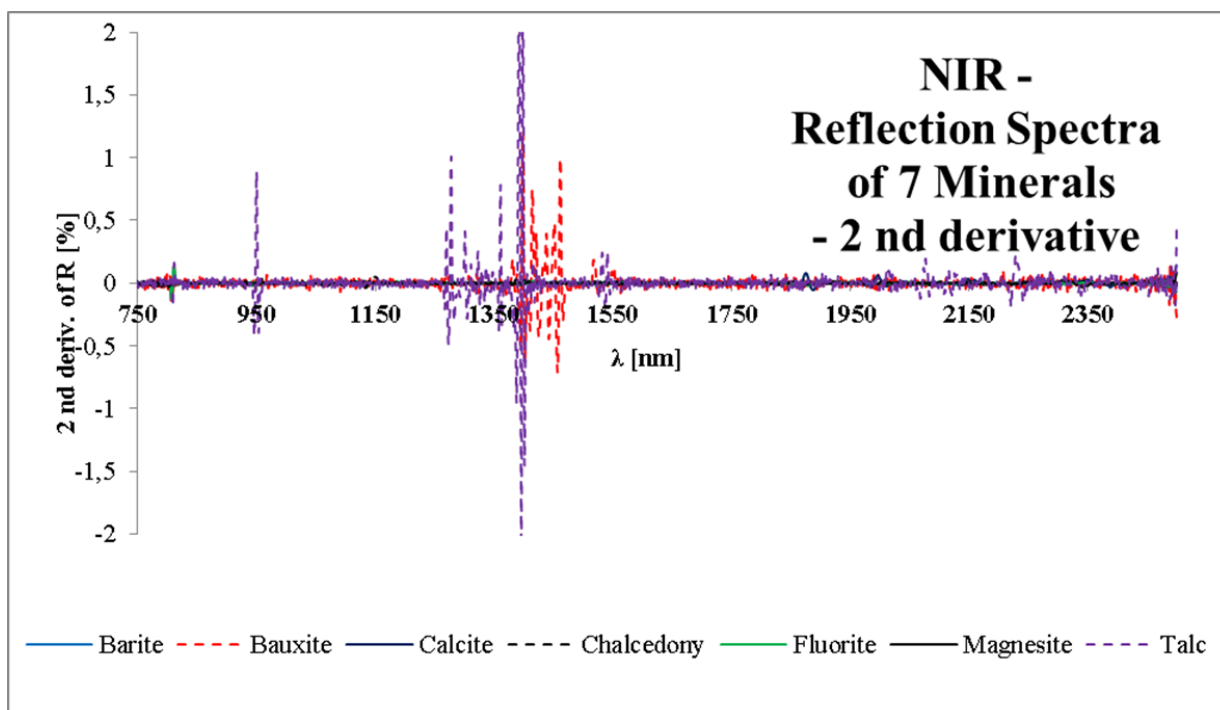


Figure 68: NIR reflection spectra of 7 minerals – 2 nd derivative

3.2 Fluorescence Measurements

3.2.1 Parameter Dependence of Intensities

The measurement of absolute fluorescence intensities is a rather difficult task. Several attempts are described in the literature to determine absolute quantum yield, but none of them is easy to apply [69]. One commercially available system for determination of absolute quantum yields is the Hamamatsu Quantaurus system [70]. However, such a system was not available at the time of the project and it seemed appropriate to work with relative intensities.

Clearly, the measured luminescence intensity of samples excited with a suitable wavelength depends on a number of instrumental settings – in particular on the gain of the photomultiplier and on the emission slit width. Samples showing only weak luminescence require either more gain on the detector or a larger emission slit width in order to be recorded properly. Hence a major problem arises, when relative intensities are to be compared.

To assess the intensity dependence of emission slit width while all other instrument parameters are kept constant an emission experiment with fluorite was performed. The instrument settings are given in table 33.

Table 33: Instrument settings for the measurement of intensity vs. emission slit width

Scan type	Emission
Scan range [nm]	400 - 900
Ex. Wl [nm]	355
Scan Speed [nm/min]	1200
Gain Voltage [V]	775
Measurement mode	Fluorescence
Excitation Correction	on
Delay [ms]	-
Gate [ms]	-
Cycle [ms]	-
Flash count	-
Excitation Slit [nm]	10
Emission Slit [nm]	x
Emission cut off filter [nm]	390

The sample was excited at 355 nm. The characteristic emission peak of fluorite can be found with a maximum at 428 nm. The emission spectra for the four possible emission slit settings are depicted in figure 69. Greater slit widths led to signal overflow. As a measure of the fluorescence intensity the peak height was taken. A fit of the relation between slit width and intensity is given in figure 70.

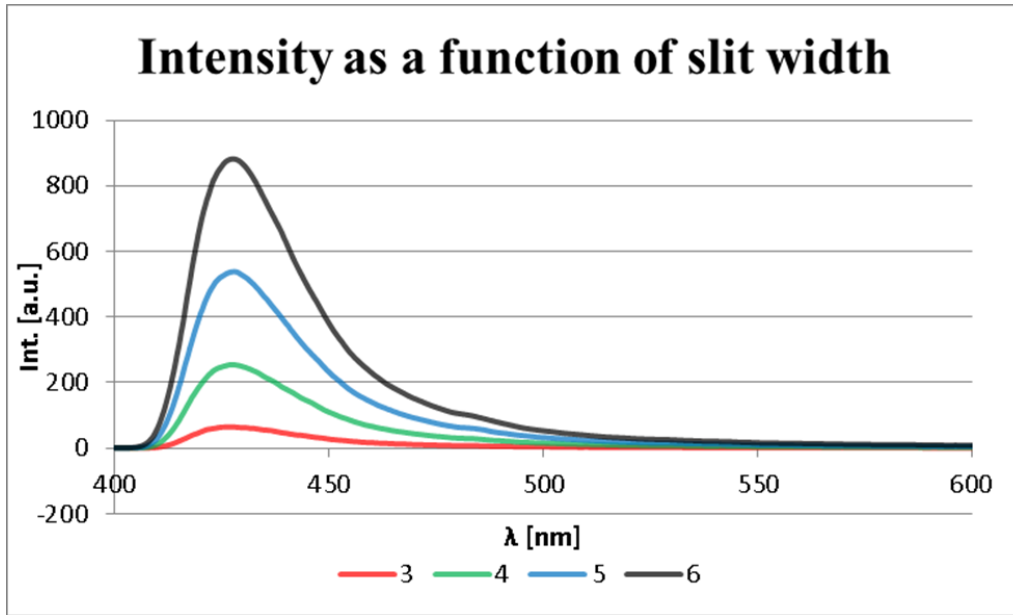


Figure 69: Emission spectra for fluorite at different emission slit settings (in nm)

Table 34: Emission slit width and measured peak heights for fluorite

Em. Slit width [nm]	Peak height
3	65,0
4	253,8
5	539,0
6	882,0

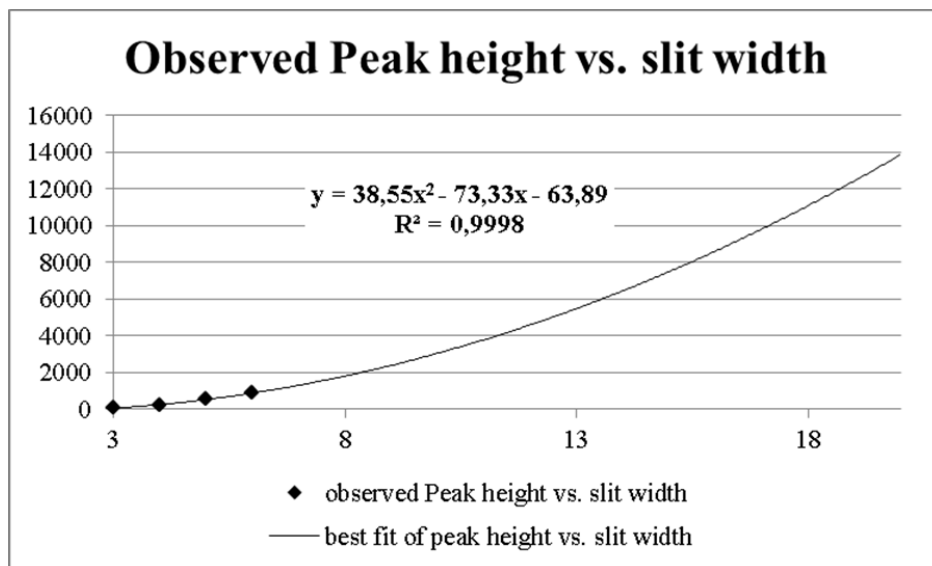


Figure 70: Observed and fitted peak height vs. emission slit width relation

From the best fit to the experimental data points (see figure 70), an empirical equation for the emission slit width dependence of the measured intensity can be obtained:

$$I(sw) = 38,55 sw^2 - 73,33 sw - 63,89 \quad \text{Equ. 35}$$

In equation 35 $I(sw)$ is the intensity and sw the slit width in nm.

For the relative intensity scale the PbO-reference glass no. 1 is set at 100 % because it shows the brightest glow under UV light and furthermore is one of the specimens which can already be sorted with the machines of Binder + Co. The relative intensity of any sample can be calculated according to equations 36 and 37:

$$I_{rel.} = \frac{I_{max}(PbO,no.1)}{I_{max}(sample)} \cdot C \quad \text{Equ. 36}$$

$$C = \frac{(38,55 sw(PbO,no.1))^2 - 73,33 sw(PbO,no.1) - 63,89}{(38,55 sw(sample))^2 - 73,33 sw(sample) - 63,89} \quad \text{Equ. 37}$$

The scale of relative intensities for several minerals is evaluated for the fluorescing samples, which are described in more detail in the next chapters. In fact, when the phosphorescence mode is applied, a considerable bias value for measured intensity can be found. For measurements marked with “phosphorescence” the bias value was subtracted from the maximum intensity.

The results for the calculation of the relative intensities according to equations 36 and 37 are denoted in table 35.

Table 35: Results for relative intensities for several glass and mineral samples

Sample	Rel. Int(calc.) [%]	Excitation WL [nm]	Emission slit width	WL of most intense peak [nm]	Height of most intense peak	Mesurement mode
Fluorite	7,17	366	6	427	714,4	fluorescence
Calcite	0,31	254	20	619	81,3	phosphorescence
Magnesite	0,41	254	20	478	42,5	phosphorescence
Chalcedony	2,84	254	8	525	250	phosphorescence
CAB 15	31,02	266	4	336	367,5	fluorescence
PbO-reference glass 1	100,00	254	3	429	271,3	fluorescence
Si sample	0,00	254	20	0	0	phosphorescence

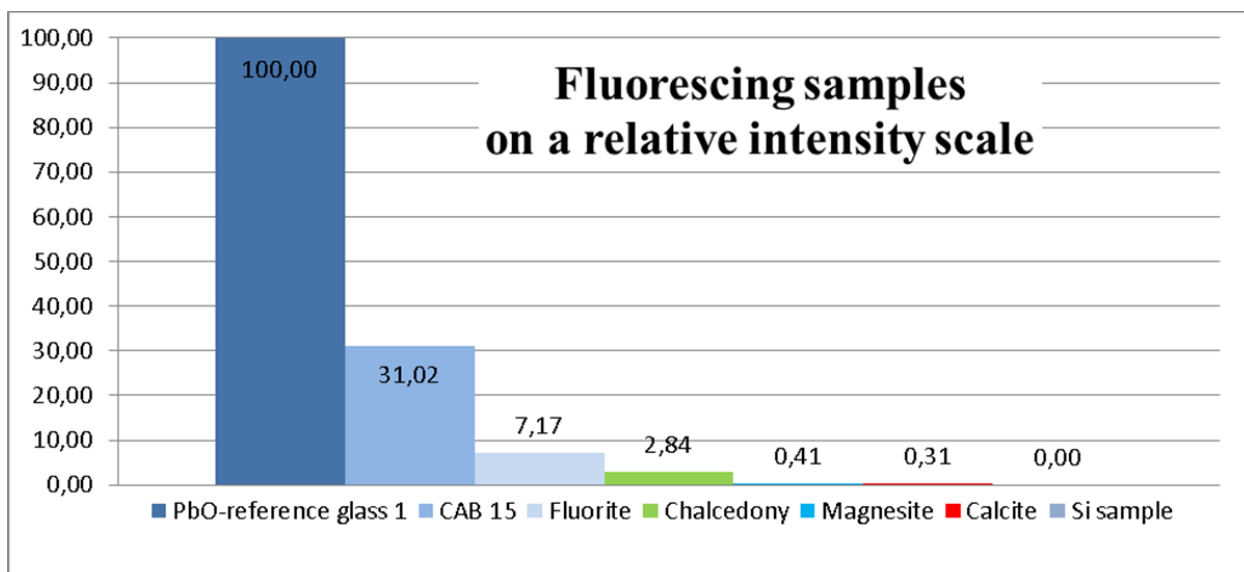


Figure 71: Relative fluorescence intensity scale with some examples

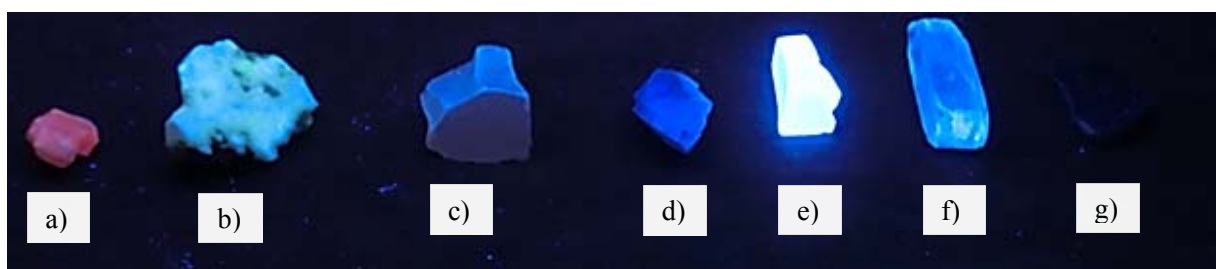


Figure 72: Samples for the comparison of luminescence intensities under 254 nm excitation: a) Calcite, b) Chalcedony, c) Magnesite, d) Fluorite, e) PbO reference glass 1, f) CAB 15, g) Silicon

The proposed scale of relative intensities (see figure 71) is just a very simple approach to get an idea of the order of magnitude of differences in fluorescence intensity. It is an easy to use tool for every day testing practice in the lab. However, the scale is only valid, when only the emission slit width is different in the measurement and the method described in table 33 is applied. PbO ref. glass – 1 and 2, Fluorite and a Scheelite sample were sent to Hamamatsu Germany to analyze absolute quantum yields at their Quantaaurus system. The result from this analysis is presented in table 36.

Table 36: Quantum Yield data for several samples from Quantaaurus measurements

Quantum Yield Data with Quantaaurus system		
Sample	Em. WL [nm]	QY [%]
PbO ref glass - 1	280	16,6
PbO ref glass - 2	280	21,1
Fluorite sample	300	1,4
Scheelite Mittersill	250	8,7

3.2.2 Emission Correction Functions

Fluorescence emission spectra have to be corrected in two ways: a) the excitation correction and b) the emission correction. Excitation correction is realized via a fluorescence cell with a known fluorophor (e.g. Rhodamin B) and a detector in the excitation channel. Excitation correction compensates time dependent alterations of the light source of the spectrofluorometer. The emission correction compensates the wavelength dependent bias of the emission channel. This bias comes from the quantum efficiency of the photomultiplier tube and the wavelength dependent characteristics of the optical parts in the emission channel [71].

One possibility for emission correction is the recording of emission spectra of the certified reference dyes provided from Federal Institute for Materials Research and Testing (BAM).

The measured spectra are compared to the known certified spectra of the dyes. The samples were prepared according to the SOP (Standard Operation Procedure) provided with the standard kit from Fluka. The kit is used for the determination of the spectral responsivity $s(\lambda)$ of the instrument. The inverse spectral responsivity $1/s(\lambda)$ is termed as emission correction curve [72].

The experiments were carried out according to the SOP [72]. The experimental procedure is the depicted in figure 73.

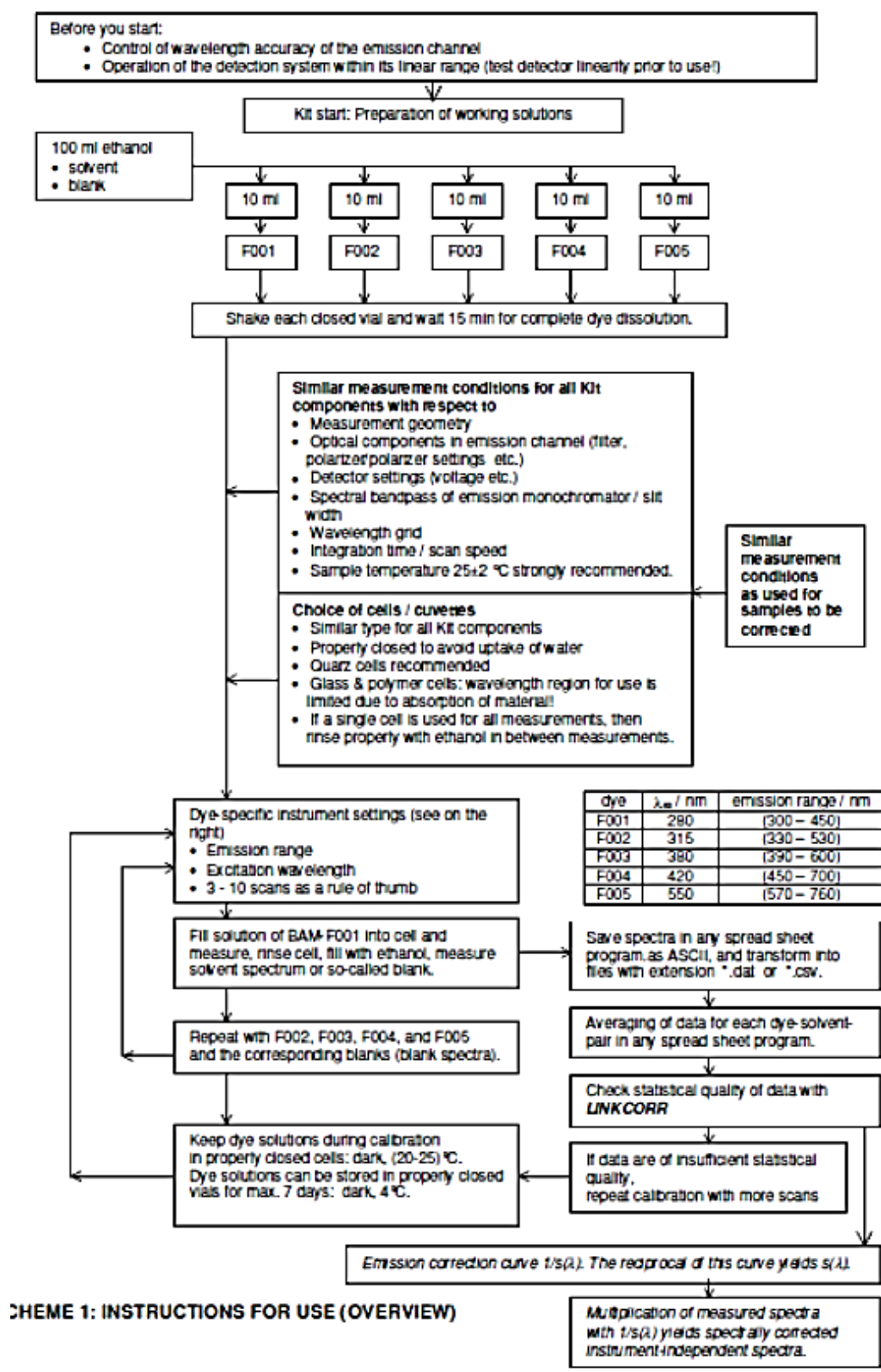


Figure 73: Overview of the experimental procedure according to BAM [72]

Two different instrument settings were chosen. The BAM certificate provides reference spectra for emission bandwidth of 1 nm, 4 nm and 8 nm. The one nm emission bandwidth cannot be set in the LS 55 (range of emission bandwidth is 2,5 – 20 nm). The settings are described in table 37.

Table 37: Instrument settings for calibration measurement of LS 55

Parameter/Setting	a)	b)
excitation bandwidth [nm]	4	2,5
emission bandwidth [nm]	4	8
PMT-voltage [V]	775	690
scan speed [nm/min]	100	100

For every measurement an emission cut-off filter was chosen to avoid second order radiation interference from the excitation source. Table 38 lists the used cut off filters for the measurements.

Table 38: Filter settings and excitation wavelengths for the calibration experiment

Standards	Excitation WL [nm]	Emission cut off WL [nm]
BAM-F001	280	290
BAM-F002	315	350
BAM-F003	380	390
BAM-F004	420	430
BAM-F005	550	-

It was noticed that the noise in the lower excitation wavelength region was less when the cuvette was twisted for a few degrees. For the higher excitation wavelengths the noise disappeared. But all experiments have been carried out with twisted cuvettes for the measurement geometry has to be kept the same all the time.

Figure 74 gives a comparison of technical³³ spectra of BAM-F001 first in a non-twisted and then in a twisted cuvette, recorded under the measurement settings b).

³³ technical spectra means that for the spectrum no emission correction was carried out

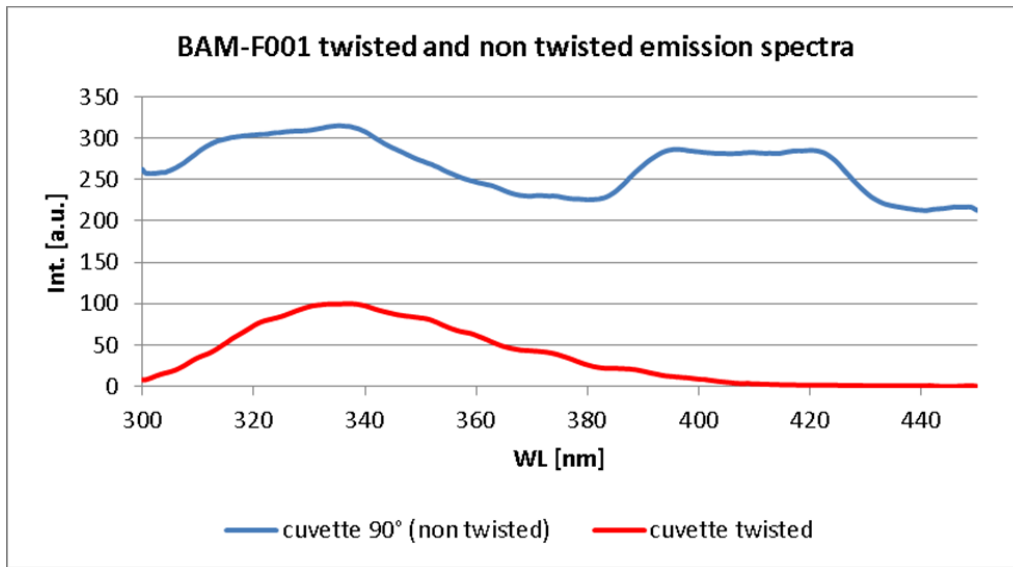


Figure 74: BAM-F001 twisted and non-twisted emission spectra

The experimental setup with the twisted cuvette is depicted in figure 75.

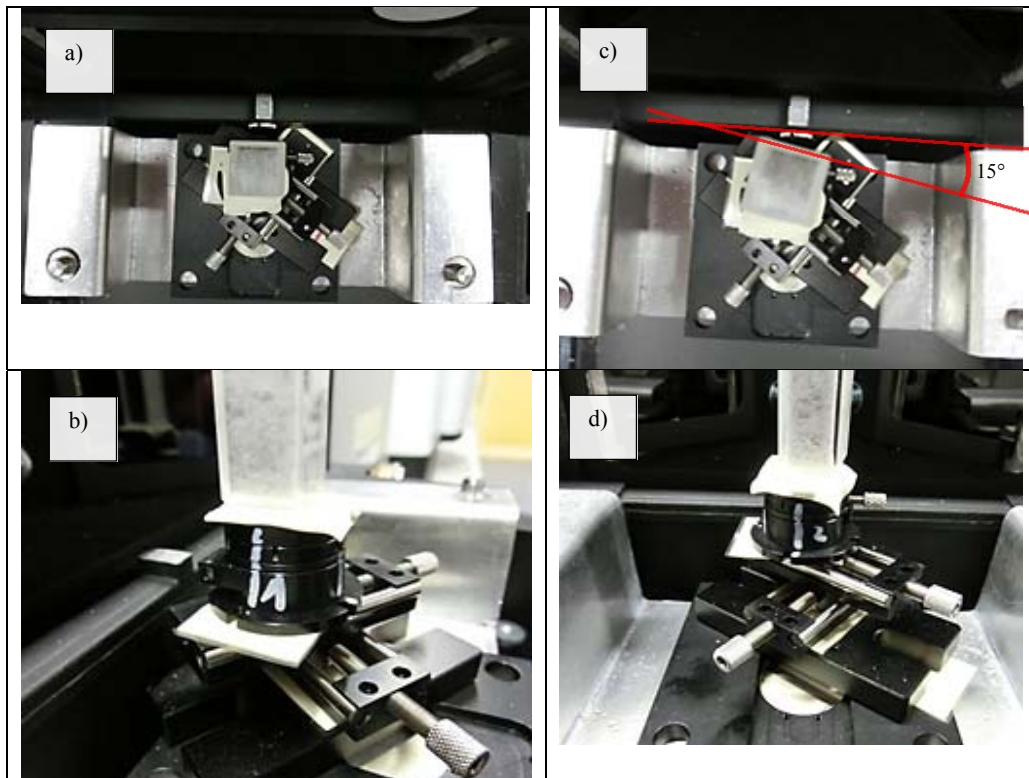


Figure 75: : a) zero degree position – top view; b) zero degree position – side view; c) twisted position – top view; d) twisted position – side view

The twisting angle of the cuvette is approximately 15°. Every emission measurement for the standard and the blank solution was repeated 5 times. The spectral grade ethanol provided with the test kit was used for the blank measurements.



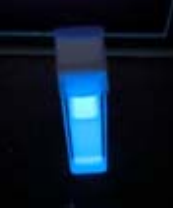




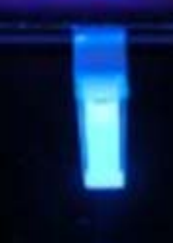


BAM Nr.	F001	F002	F003	F004	F005
excitation@ 254 nm					
excitation@ 366 nm					

Figure 76: BAM standards under UV lamp NU-4 KL

The data were processed with the software provided with the standard test kit. The mean value of 5 measurements for the standards solutions and the blank were averaged³⁴. For the following plot the mean of the blank was subtracted from the mean of the standards. The technical averaged spectra for both settings are depicted in the figures 77 and 78.

For proper data processing of the data files all commas “,” have to be replaced with points “.”. Unfortunately the LinkCorr-Software is not compatible with Windows 7 64 bit-versions. Furthermore the original CD has to be in the CD-drive for proper functioning of the program. Data evaluation has been done on a WinXP(SP2)-PC.

As a result from the LinkCorr-Calculation the relative spectral responsivity $1/s(\lambda)$ was obtained. This factor is used to standardize a technical emission spectrum via multiplication [72].

³⁴ arithmetic mean

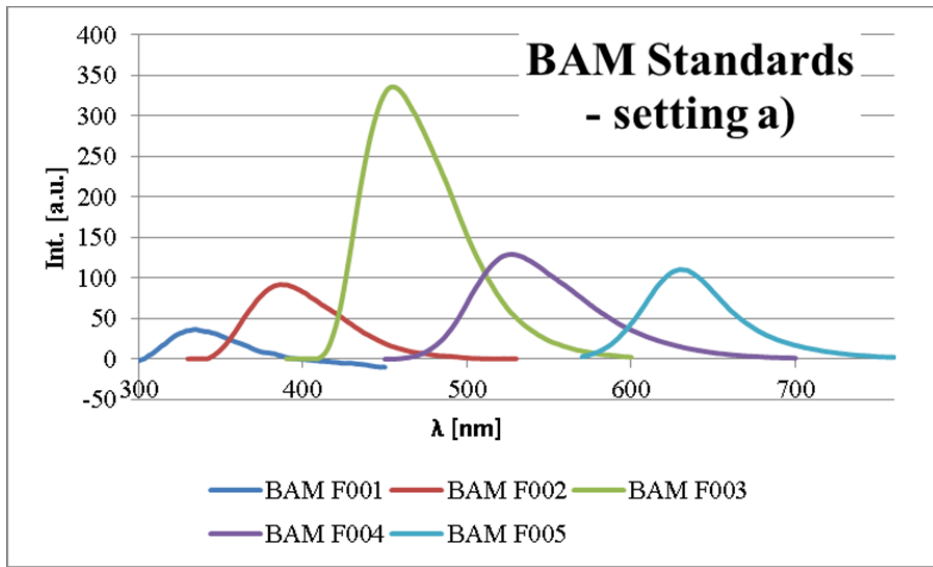


Figure 77: Technical emission spectra for the BAM standards in setting a)

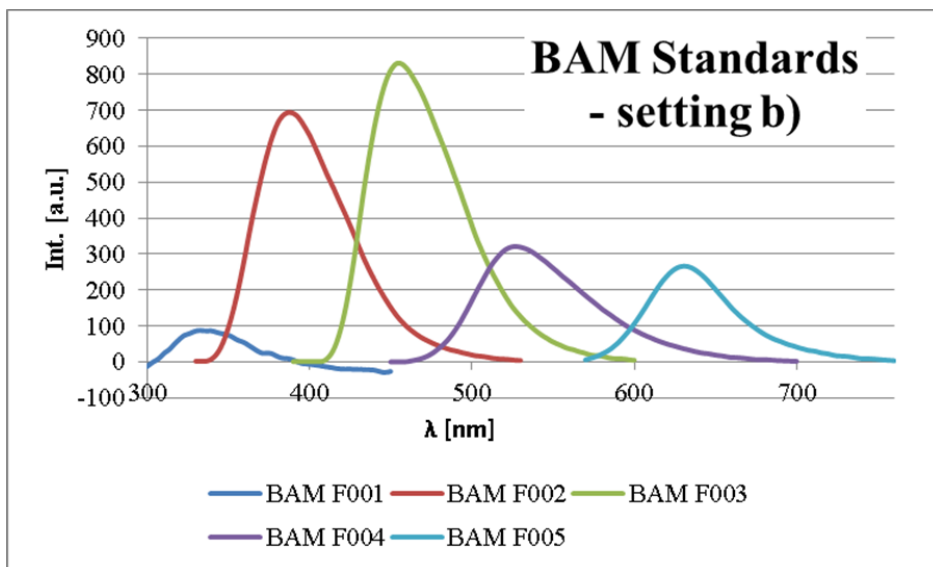


Figure 78: Technical emission spectra for the BAM standards in setting b)

The observed intensity is sensitive to changes in emission or excitation bandwidth. Therefore normalization of the correction function is required for applicability of the correction function to different instrument settings. The reciprocal of $1/s(\lambda)$ was calculated to get $s(\lambda)$. This value was then normalized to the highest value in the series to obtain $s_{\text{norm}}(\lambda)$. Now the new correction spectrum can be used to correct spectra of different spectral bandwidth for correction via simple division.

The correction data are presented in the figure 79 in comparison with the old correction function EMRED.corr from Perkin Elmer.

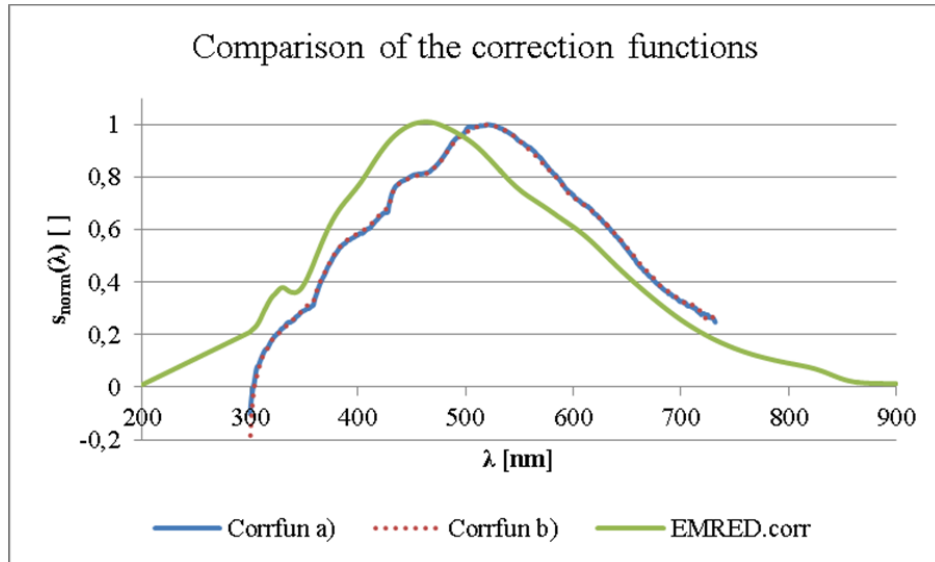


Figure 79: Comparison of available detection functions from the calibration experiment

The comparison of the Perkin Elmer spectrum EMRED.corr with the data from the measurements shows that there are several deviations (see figure 79). Therefore the calibration measurements of the certified BAM standards were an important step in the ongoing research project.

The $s_{\text{norm}}(\lambda)$ -values for the two different settings are nearly equal. Thus the change of the spectral band width between 4 – 8 nm can be seen as not critical.

Unfortunately the data evaluation of the measurements of the BAM-standard kit yielded a correction spectrum which only ranges to 730 nm.

For corrections from 730 to 900 nm the measurement of a calibrated light source could be useful. Correction procedures with standard lamps are described in the literature [73].

The breaking down to zero of the $s_{\text{norm}}(\lambda)$ -function between 300 – 310 nm can be considered as a result of an oscillation of the data evaluation algorithm. Obviously the signal to noise ratio for the measurements of the BAM-F001 was not good enough.

For correction of measurements below 310 nm further calibrations with standard lamps seem to be indicated. Since the resources for such calibration experiments were not available at the time of the work and the values for Corrfun a) and Corrfun b) do not differ too much, the values for Corrfun a) were simply extrapolated between 200 – 300 nm and 720 – 900 nm with a straight line. The result for this correction is depicted in figure 80.

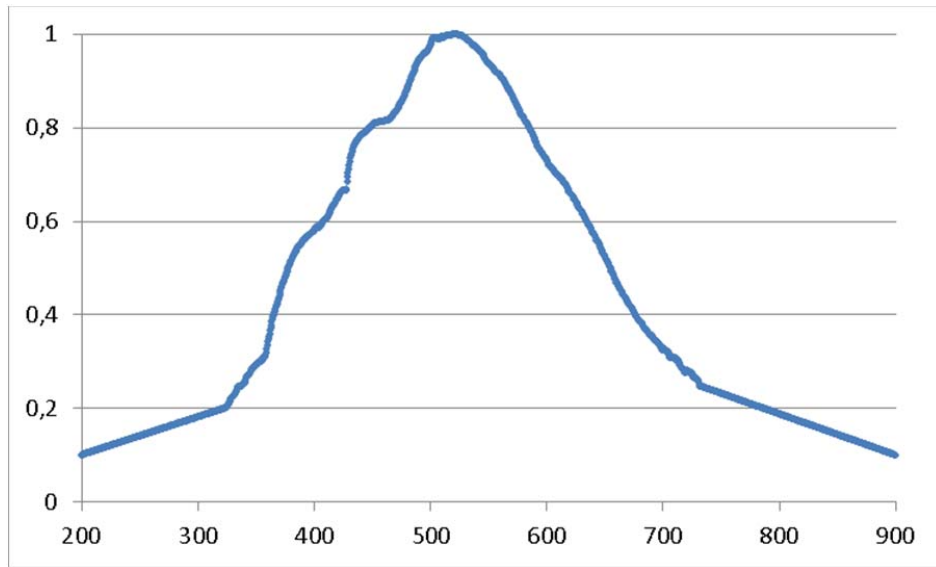


Figure 80: Resulting correction function of calibration experiments

The values for this correction function are tabulated in the Appendix.

3.2.3 Spectra of Minerals and Glasses with Interpretation

Six fluorescing and one not fluorescing samples have been chosen to demonstrate the possibilities for the measurements of luminescence spectra on the LS 55:

- Fluorite (blue fluorescence)
- Calcite (red fluorescence)
- Magnesite (pale blue fluorescence)
- Chalcedony (green fluorescence)
- CAB 15 (blue fluorescence)
- PbO-reference glass no. 1
- Si sample

The Fluorite, Calcite, Magnesite and Chalcedony samples were taken from the same deposit in Turkey. Optical sorting of these samples was a research topic of the R&D department of Binder + Co at the time of the project.

CAB 15³⁵ was one of the most intense fluorescing glasses of Kieler's sample set, prepared in 2009 during her diploma thesis [2]. It contains about 1,47 w% of PbO [2]. It was found, that industrial PbO-containing glasses normally show more intense fluorescence than the CAB-glasses. This can be explained with the different composition and preparation conditions of the glasses. Usually the preparation temperature for industrial glasses is much higher than for the CAB glasses. CAB glasses were chosen as a test system because of the relative ease of preparation and because they still show the typical lead emission band [68].

PbO-reference glass no. 1 was cut out of a commercially available drinking glass of lead crystal. The PbO content of about 24,80 w% of PbO-reference glass no. 1 was determined with XRF (Thermo Scientific; Niton XL3t, see figure 81).



Figure 81: XRF analyzer calibrated with lead crystal of known PbO-content

³⁵ CAB stands for Calcium Aluminum Borate

The Si sample was high-purity silicon from a manufacturer of the semiconductor industry. It was considered that it should not show any fluorescence signal because of high purity. Therefore it was used as a blank sample.

An overview of the samples under white light and under UV-light is presented in figure 82.



Figure 82: Samples for the recording of luminescence spectra a) under white light b) under 15W excitation with light of 254 nm at a distance of about 10 cm: 1) Calcite, 2) Chalcedony, 3) Magnesite, 4) Fluorite, 5) PbO reference glass 1, 6) CAB 15, 7) Silicon

To avoid overflow of the detection system, the emission slit was adjusted in a way that the maximum peak was as large as possible without generation of overflow. The relative intensity scale of the detection system ranges from 0 to 1000. Intensities over 1000 are not in the linear range of the detection system.

It should be mentioned that in the following sections only data without second order artifacts of the emission grating of the LS 55 are presented. An example is presented in figure 83. Second-order transmission artifacts are a device characteristic of fluorimeters with a grating as dispersive element.

The interference maxima of a diffraction grating can be described via the following equation:

$$g \cdot \sin\theta = m \cdot \lambda \quad \text{Equ. 38}$$

$$m = 0, 1, 2, \dots$$

In equation 38 g is the grating constant that describes the distance between the grating lines, θ is the angle between interference maxima, m the reflection order and λ the wavelength [124].

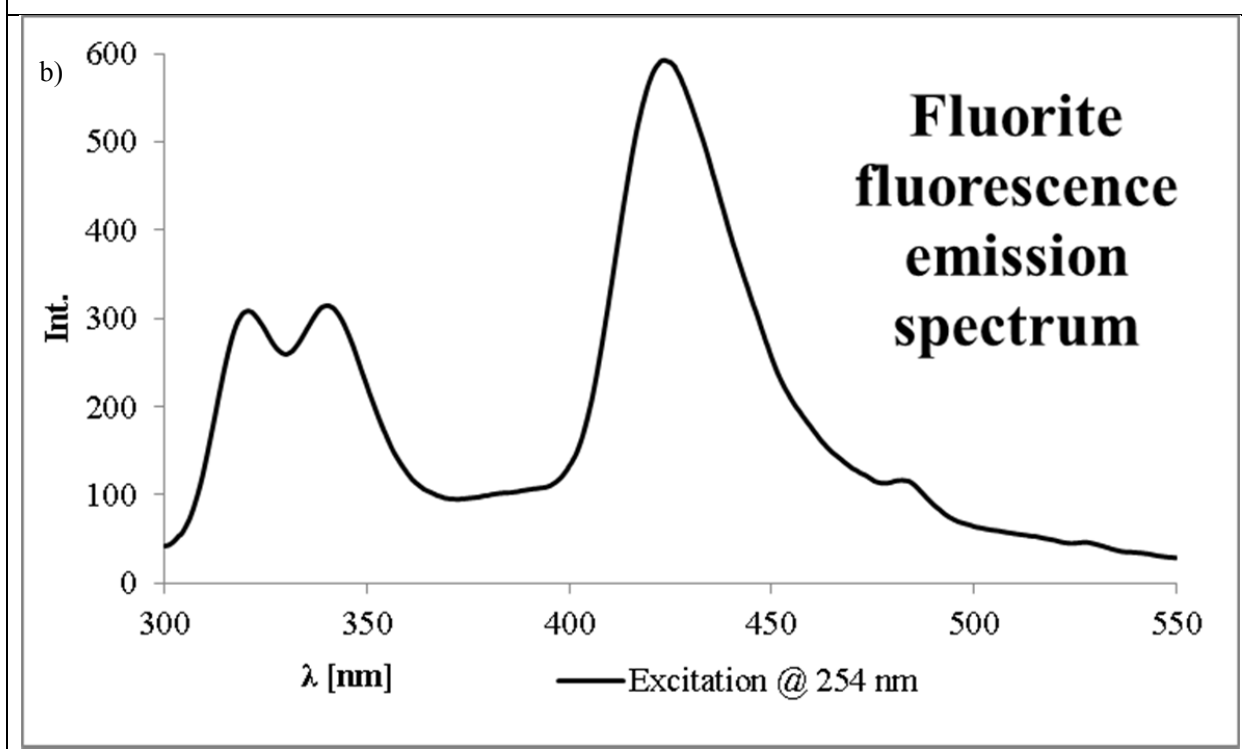
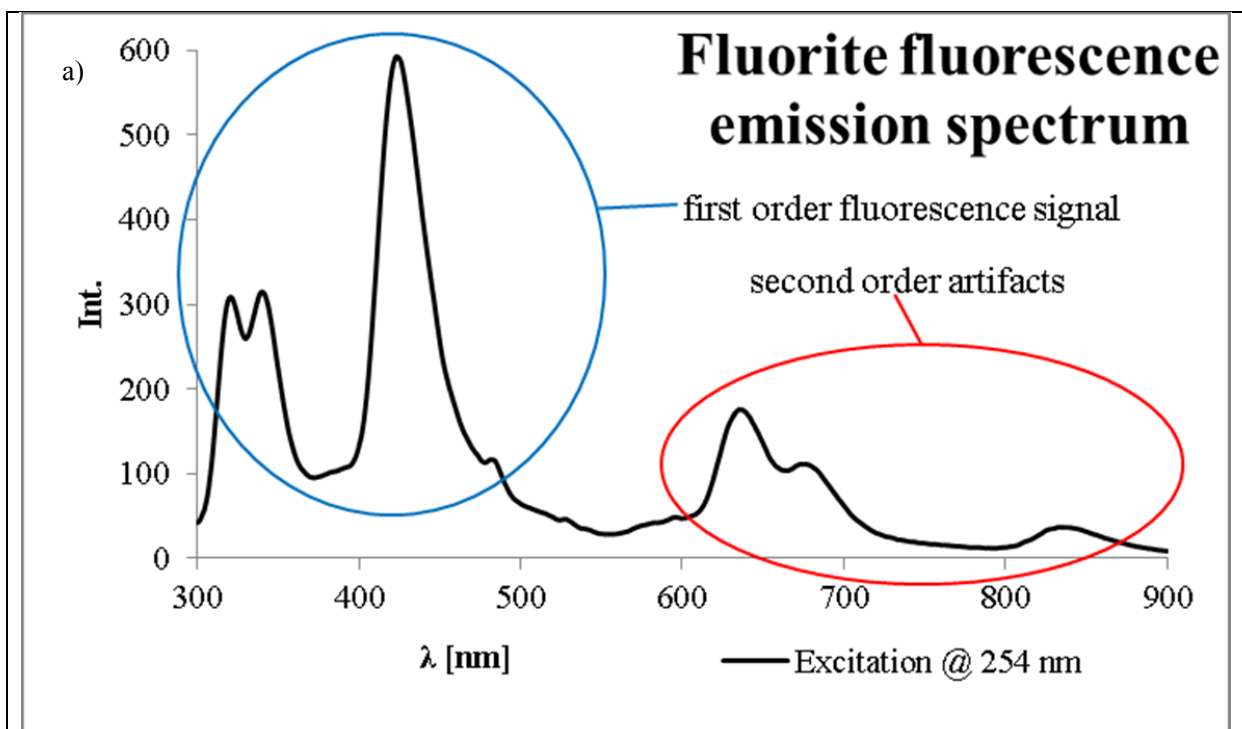


Figure 83: Emission spectrum for Fluorite at excitation wavelength of 254 nm a) with second order artifacts, b) without second order artifacts

For the fluorescence emission measurements at an excitation wavelength of 266 nm an additional cut off-filter was brought into the emission channel of the fluorimeter. The filter WG 320 should cut off the excitation light, which passed the implemented 290 nm cut-off filter. The cut off edge of WG 320 starts at 300 nm and ends at a transmission of 80 % at 330 nm. The transmission spectrum of WG 320 is shown in figure 84.

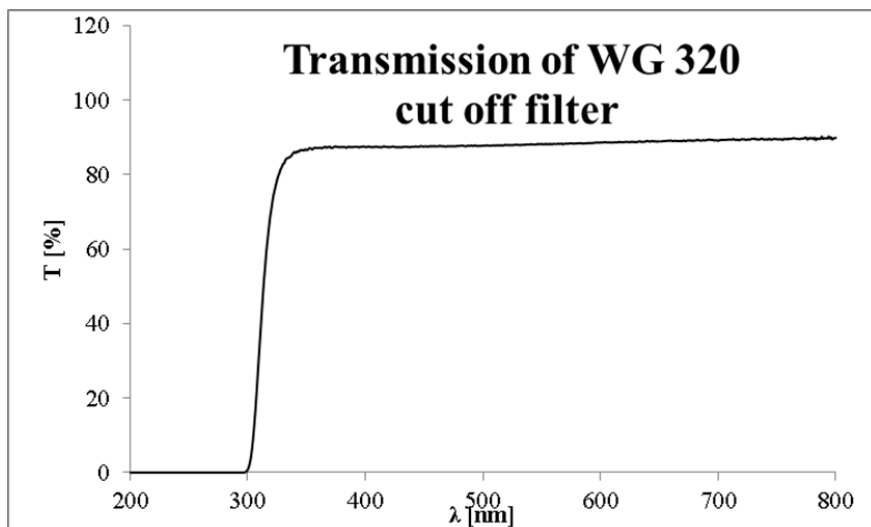


Figure 84: Transmission curve of WG 320

As depicted in figure 83 the excitation light of the source can be found as second order artifact in the spectrum. E.g. the 266 nm excitation wavelength can be found as a huge peak at 532 nm (see figure 85).

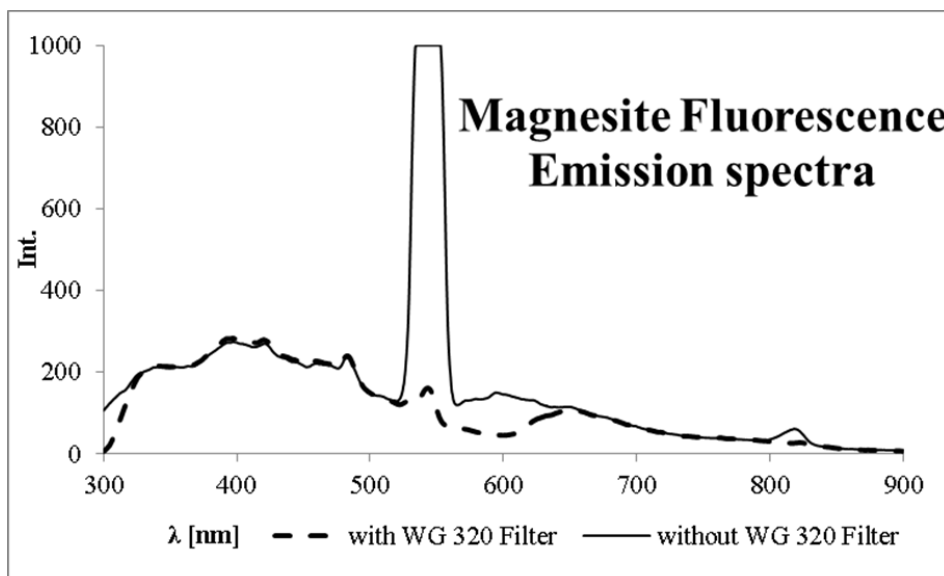


Figure 85: Fluorescence Emission Spectrum of Magnesite with and without a cut off filter

3.2.3.1 Fluorite - Luminescence Spectra

The fluorite fluorescence emission spectrum is in good accordance with the reported spectrum in literature. The peak around 420 nm is related to Eu^{2+} , the two peaks between 300 – 400 nm are of unknown origin. An emission of Gd^{3+} in Fluorite around 310 nm is reported [164].

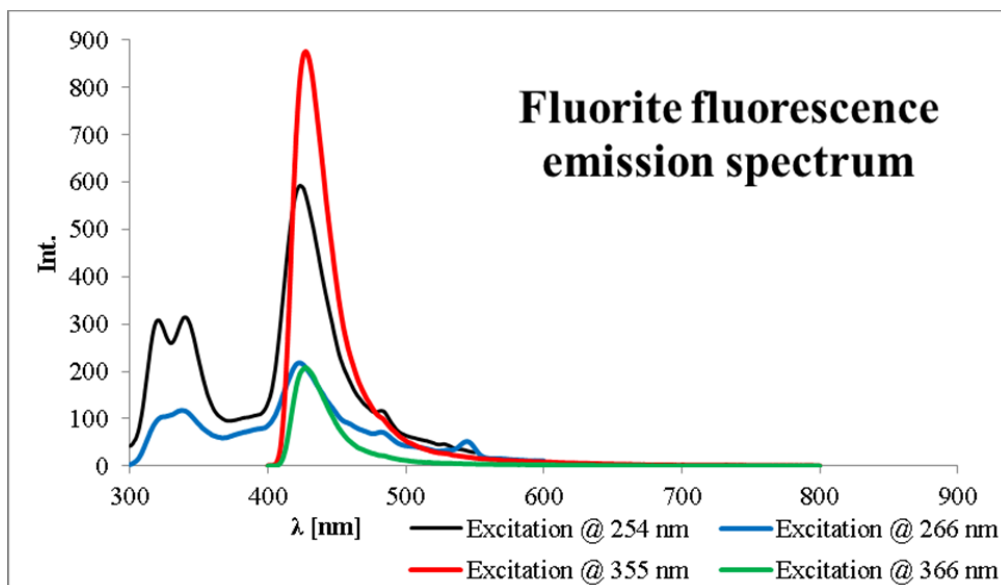


Figure 86: Fluorite fluorescence emission spectra

Table 39: Method parameters for Fluorite fluorescence emission spectra

	Fluorite 2D - Fluorescence Mode			
	Exc. @ 254 nm	Exc. @ 266 nm	Exc. @ 355 nm	Exc. @ 366 nm
Emslit [nm]	8	8	6	4
Exslit [nm]	10	10	10	10
U(PMT) [V]	775	775	775	775
Emfilter [nm]	290	290	390	390
Delay [ms]	-	-	-	-
Gate [ms]	-	-	-	-
Cycle time [ms]	-	-	-	-
Flash count	-	-	-	-
Additional Emfilter	-	WG 320	-	-

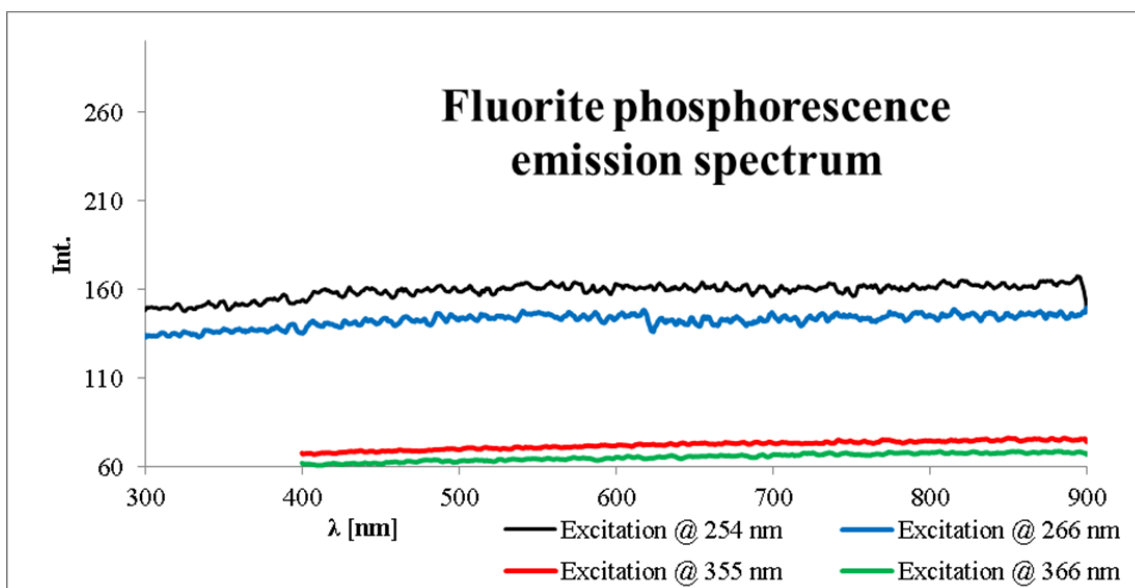


Figure 87: Fluorite phosphorescence emission spectra

Table 40: Method parameters for Fluorite phosphorescence emission spectra

	Fluorite 2D - Phosphorescence Mode			
	Exc. @ 254 nm	Exc. @ 266 nm	Exc. @ 355 nm	Exc. @ 366 nm
Emslit [nm]	8	8	8	8
Exslit [nm]	10	10	10	10
U(PMT) [V]	775	775	775	775
Emfilter [nm]	290	290	390	390
Delay [ms]	0,10	0,10	0,10	0,10
Gate [ms]	3,00	3,00	3,00	3,00
Cycle time [ms]	20	20	20	20
Flash count	1	1	1	1
Additional Emfilter	-	-	-	-

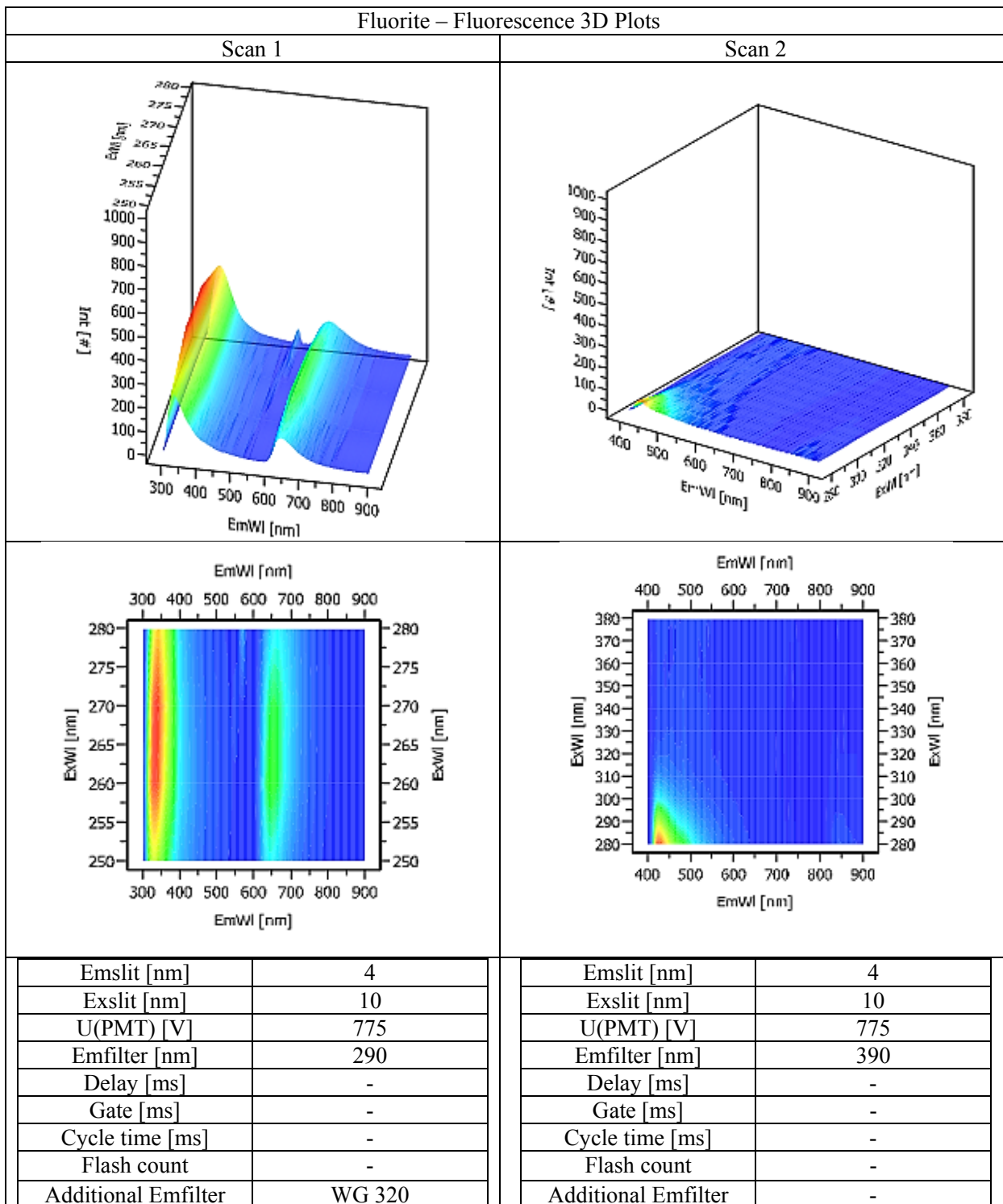


Figure 88: Fluorite fluorescence 3D spectra

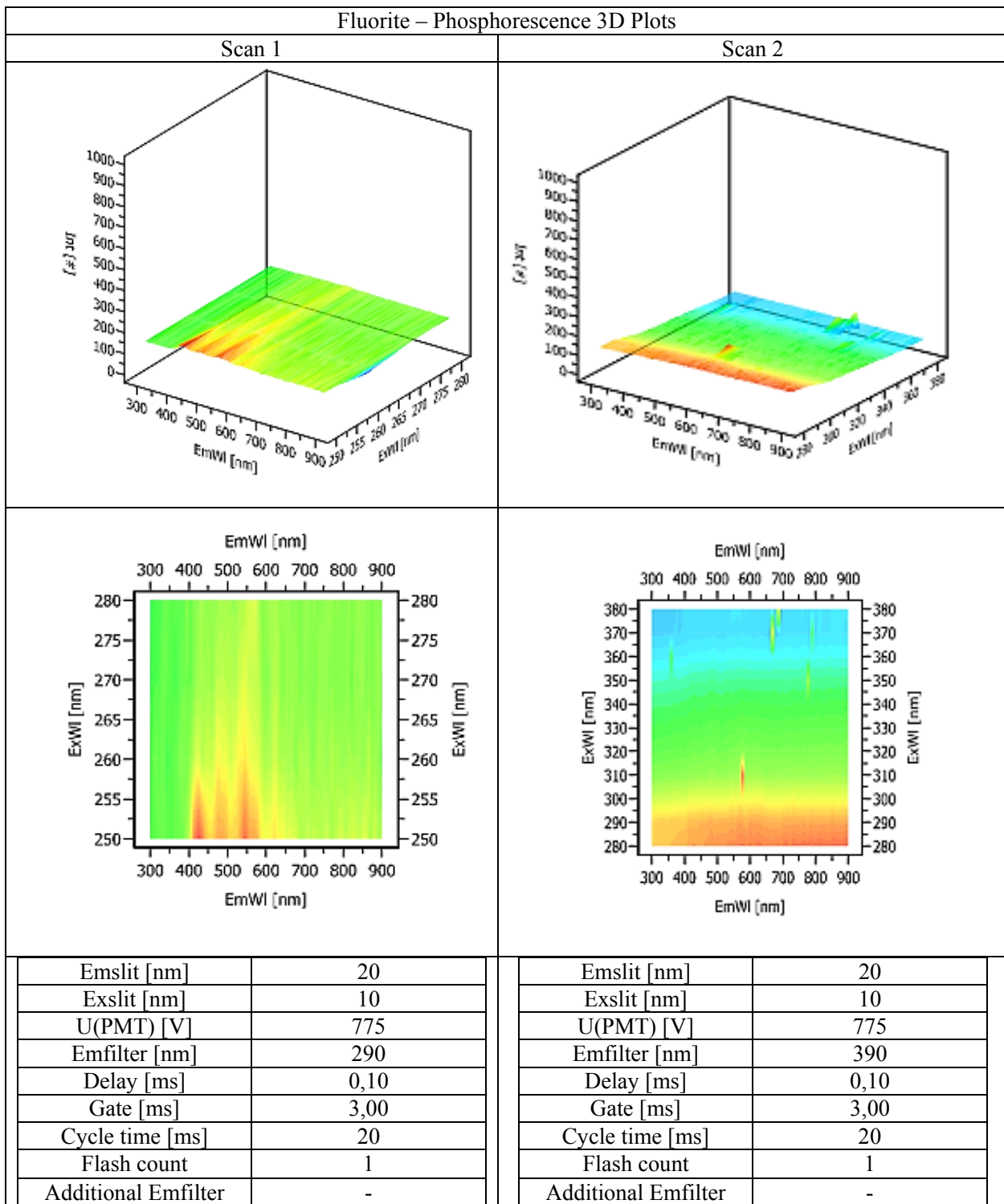


Figure 89: Fluorite phosphorescence 3D spectra

3.2.3.2 Calcite - Luminescence Spectra

The calcite phosphorescence emission spectrum shows an emission feature at 620 nm which is linked to Mn^{2+} [165]. The fluorescence spectra do not show any useful results.

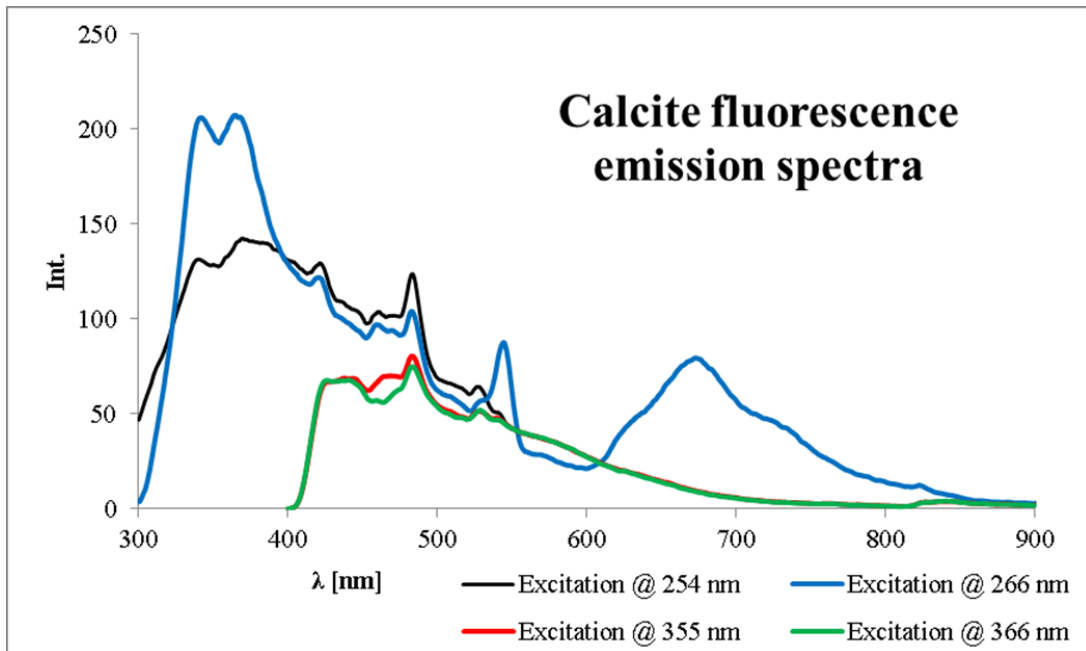


Figure 90: Calcite fluorescence emission spectra

Table 41: Method parameters for the Calcite fluorescence emission spectra

	Calcite 2D - Fluorescence Mode			
	Exc. @ 254 nm	Exc. @ 266 nm	Exc. @ 355 nm	Exc. @ 366 nm
Emslit [nm]	8	8	8	8
Exslit [nm]	10	10	10	10
U(PMT) [V]	775	775	775	775
Emfilter [nm]	290	290	390	390
Delay [ms]	-	-	-	-
Gate [ms]	-	-	-	-
Cycle time [ms]	-	-	-	-
Flash count	-	-	-	-
Additional Emfilter	-	WG 320	-	-

The fluorescence data of Calcite are not plausible in comparison to the image of the mineral under UV-light.

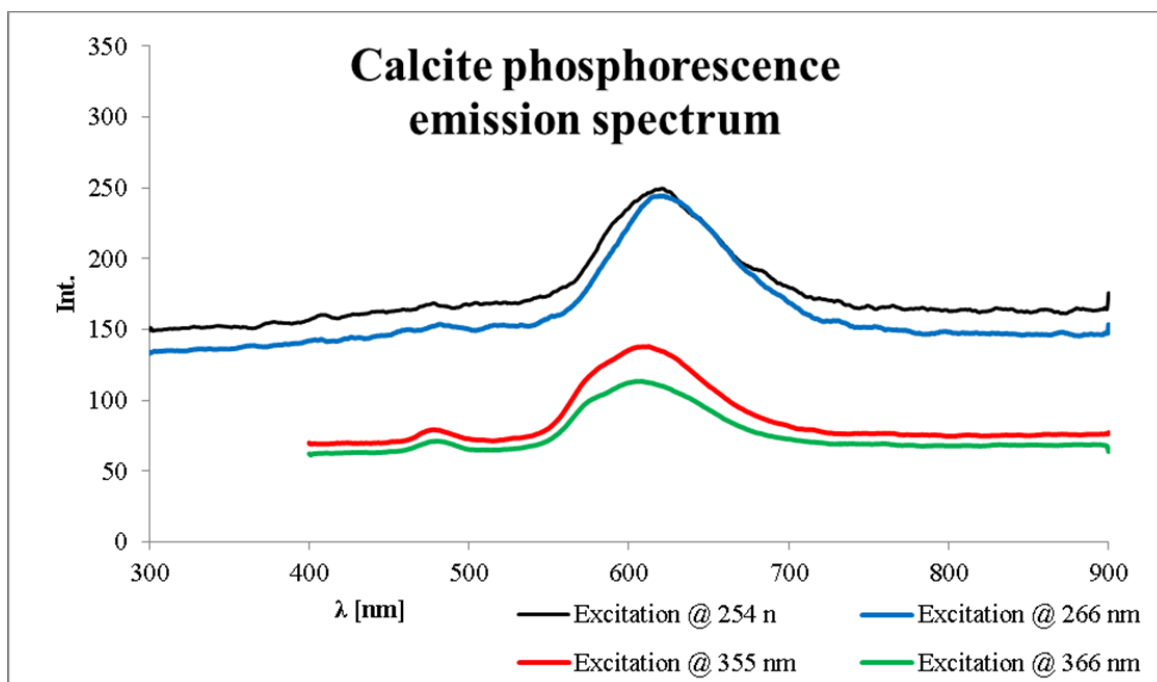


Figure 91: Calcite phosphorescence emission spectrum

Table 42: Method parameters for the Calcite phosphorescence emission spectra

	Calcite 2D - Phosphorescence Mode			
	Exc. @ 254 nm	Exc. @ 266 nm	Exc. @ 355 nm	Exc. @ 366 nm
Emslit [nm]	20	20	20	20
Exslit [nm]	10	10	10	10
U(PMT) [V]	775	775	775	775
Emfilter [nm]	290	290	390	390
Delay [ms]	0,10	0,10	0,10	0,10
Gate [ms]	3,00	3,00	3,00	3,00
Cycle time [ms]	20	20	20	20
Flash count	1	1	1	1
Additional Emfilter	-	-	-	-

It should be mentioned, that the red emission of the Calcite sample could only be measured properly, when the emission slit was opened at its maximum.

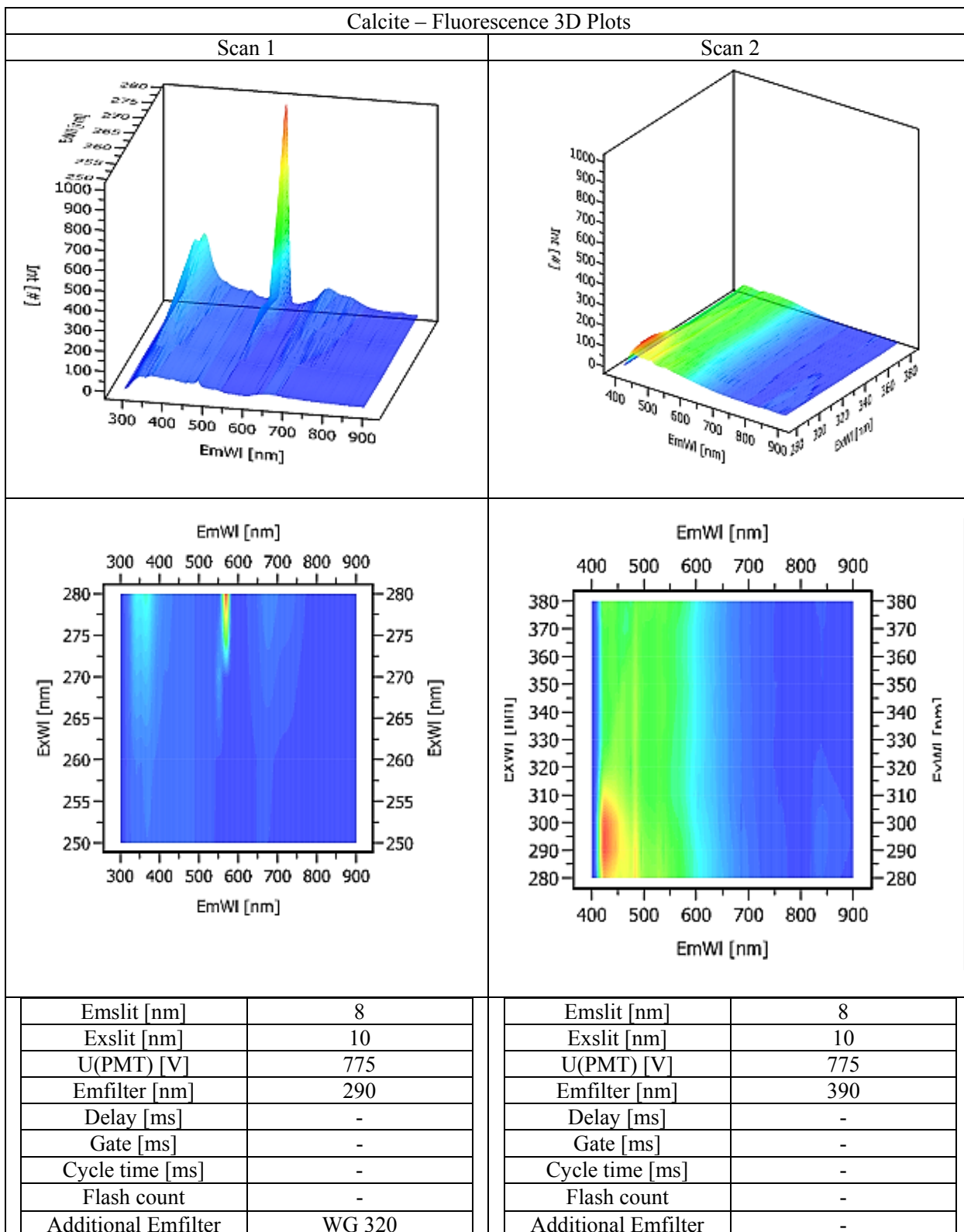


Figure 92: Calcite fluorescence 3D data

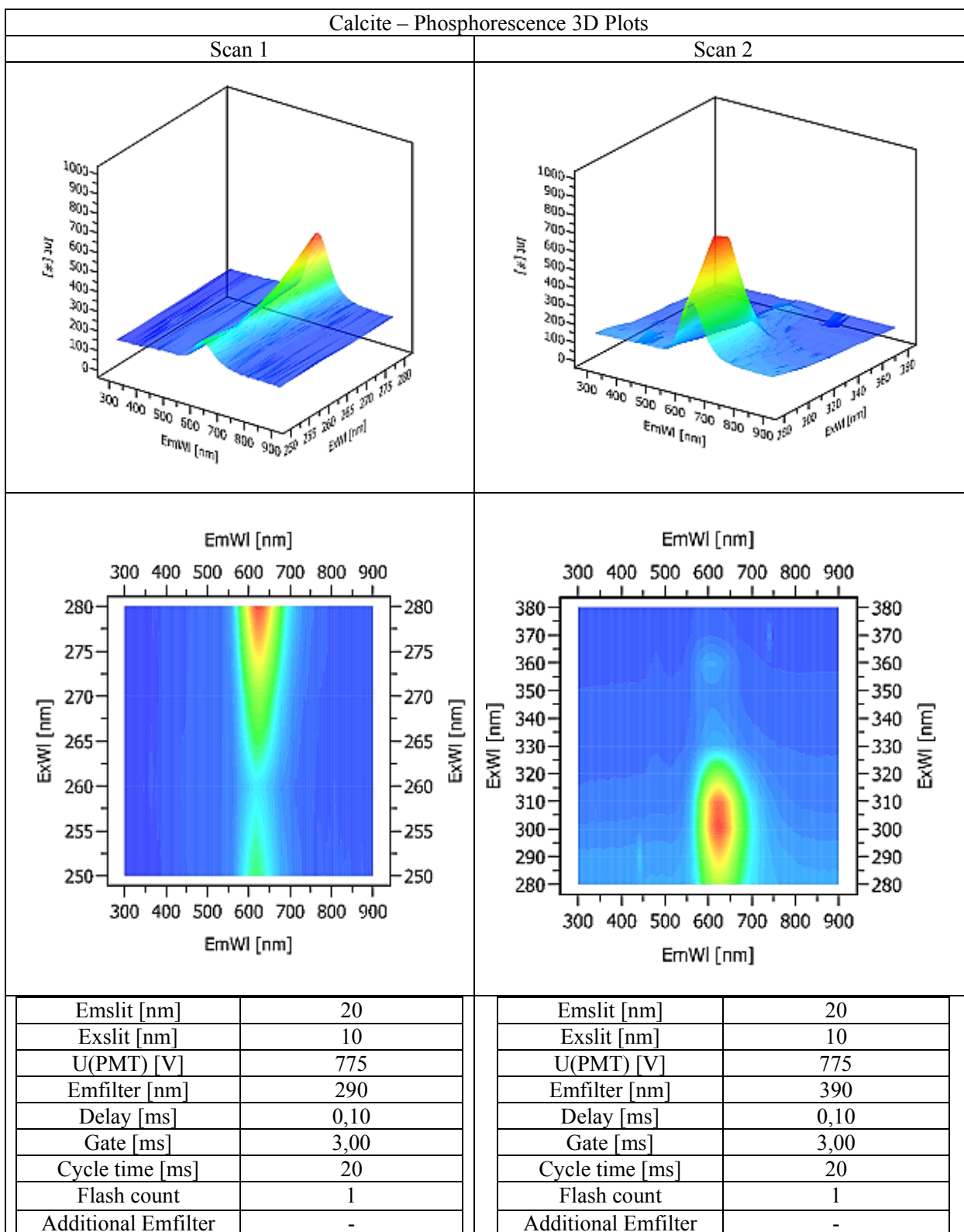


Figure 93: Calcite phosphorescence 3D spectra

3.2.3.3 Magnesite - Luminescence Spectra

The Magnesite phosphorescence spectra show a bluish emission peak around 450 nm, which is not clearly defined in the literature [166]. The Magnesite fluorescence spectrum is plausible concerning the maximum in the blue region, but resembles the emission spectrum of Calcite, Chalcedony and even the Si-sample.

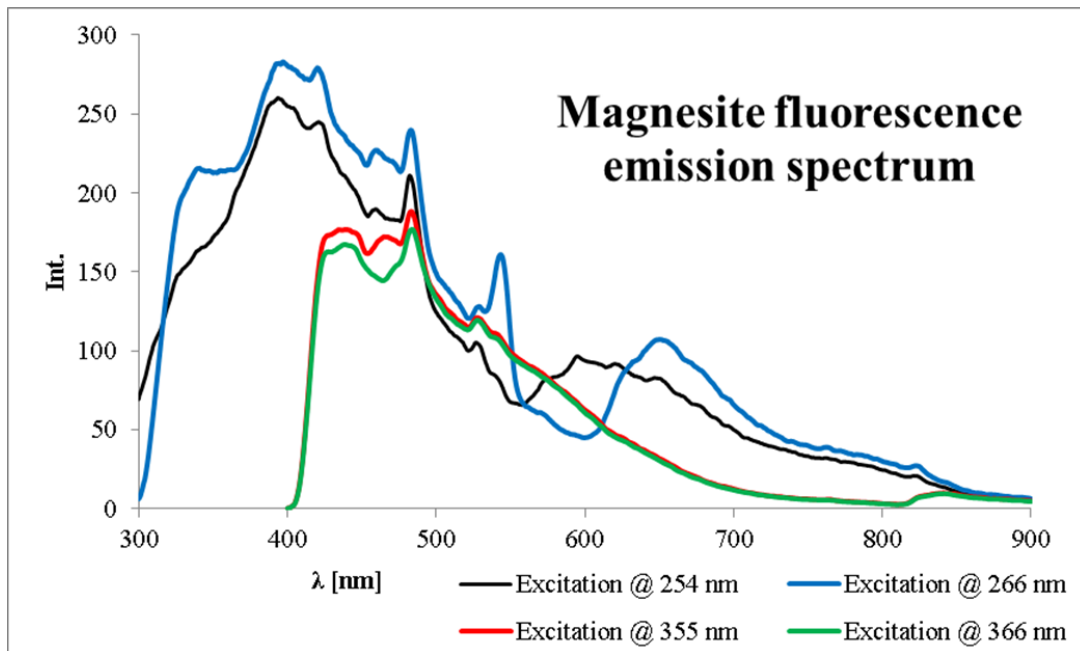


Figure 94: Magnesite fluorescence emission spectra

Table 43: Method parameters for the Magnesite fluorescence emission spectra

	Magnesite 2D - Fluorescence Mode			
	Exc. @ 254 nm	Exc. @ 266 nm	Exc. @ 355 nm	Exc. @ 366 nm
Emslit [nm]	8	8	8	8
Exslit [nm]	10	10	10	10
U(PMT) [V]	775	775	775	775
Emfilter [nm]	290	290	390	390
Delay [ms]	-	-	-	-
Gate [ms]	-	-	-	-
Cycle time [ms]	-	-	-	-
Flash count	-	-	-	-
Additional Emfilter	-	WG 320	-	-

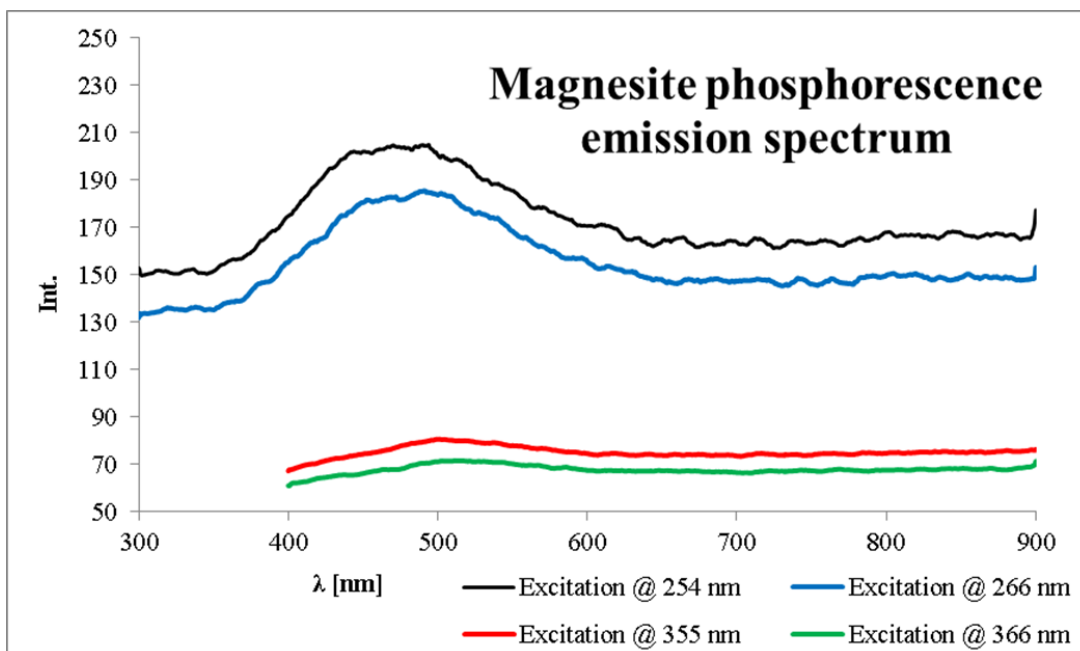


Figure 95: Magnesite phosphorescence emission spectra

Table 44: Method parameters for the Magnesite phosphorescence emission spectra

	Magnesite 2D - Phosphorescence Mode			
	Exc. @ 254 nm	Exc. @ 266 nm	Exc. @ 355 nm	Exc. @ 366 nm
Emslit [nm]	20	20	20	20
Exslit [nm]	10	10	10	10
U(PMT) [V]	775	775	775	775
Emfilter [nm]	290	290	390	390
Delay [ms]	0,10	0,10	0,10	0,10
Gate [ms]	3,00	3,00	3,00	3,00
Cycle time [ms]	20	20	20	20
Flash count	1	1	1	1
Additional Emfilter	-	-	-	-

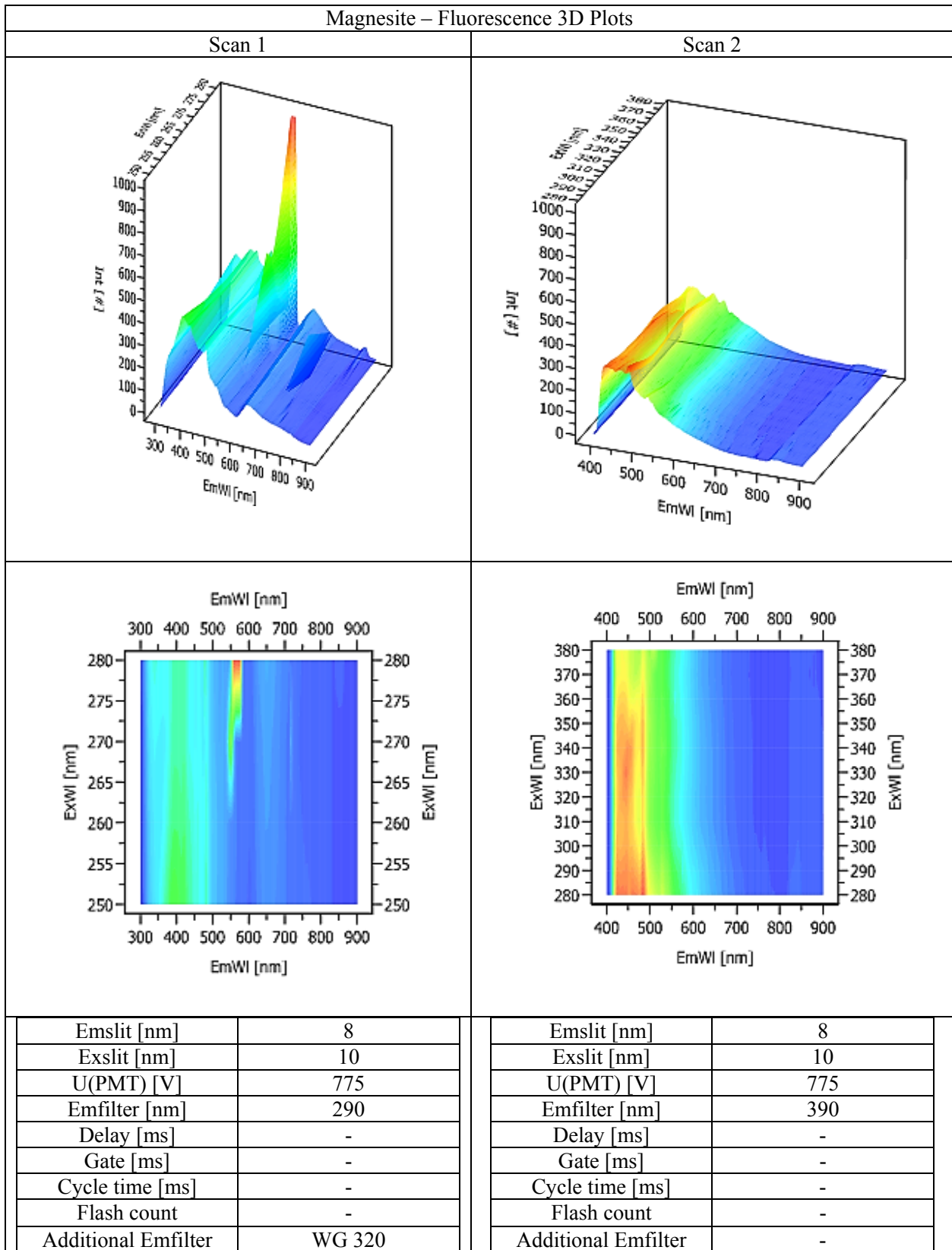


Figure 96: Magnesite fluorescence 3D spectra

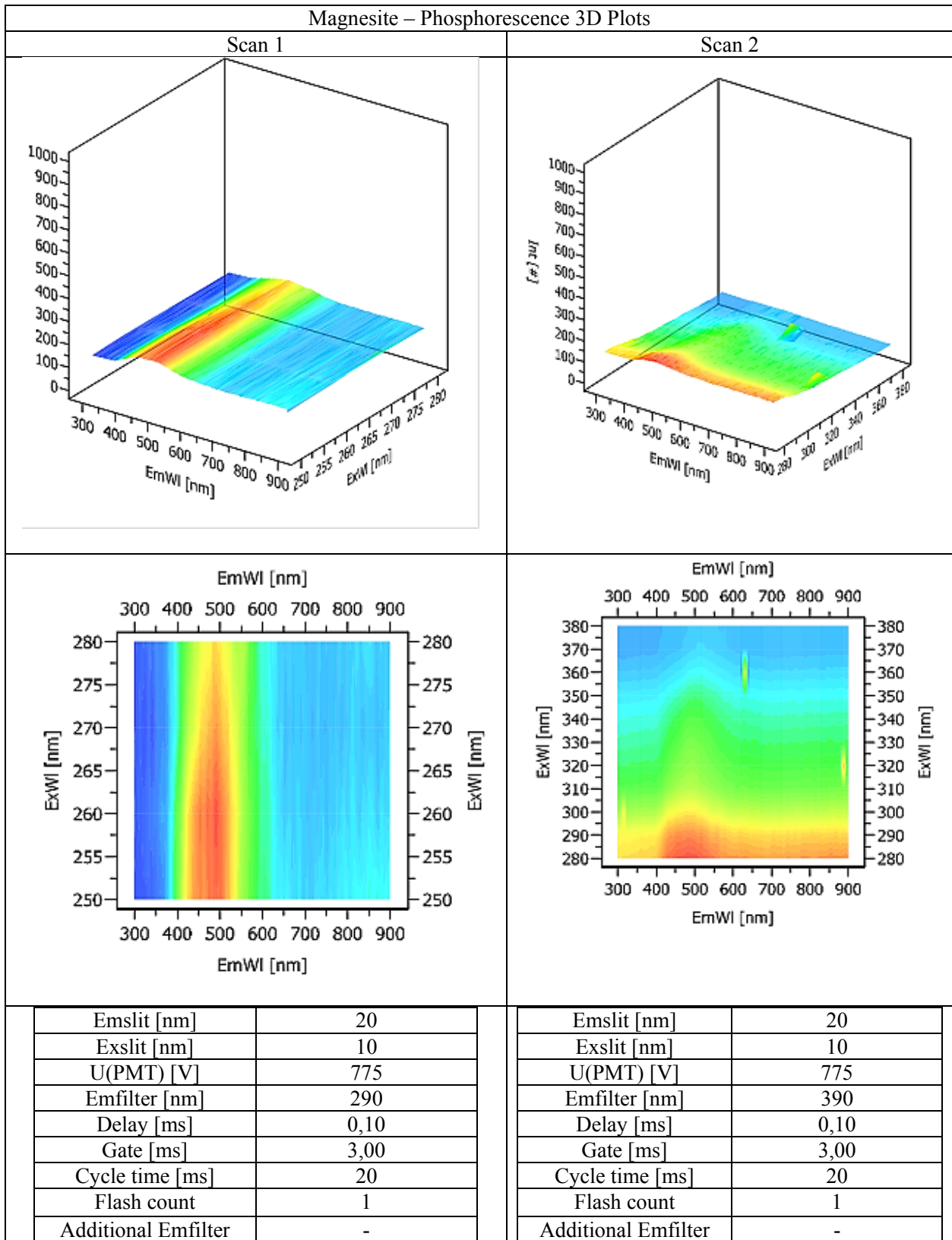


Figure 97: Magnesite phosphorescence 3D spectra

3.2.3.4 Chalcedony – Luminescence Spectra

The phosphorescence spectrum of Chalcedony shows the characteristic triple peak of $(\text{UO}_2)^{2+}$ at 502 nm, 521 nm and 544 nm, reported in the literature [167]. The fluorescence spectra are similar to Calcite, Fluorite, Silicon and Magnesite.

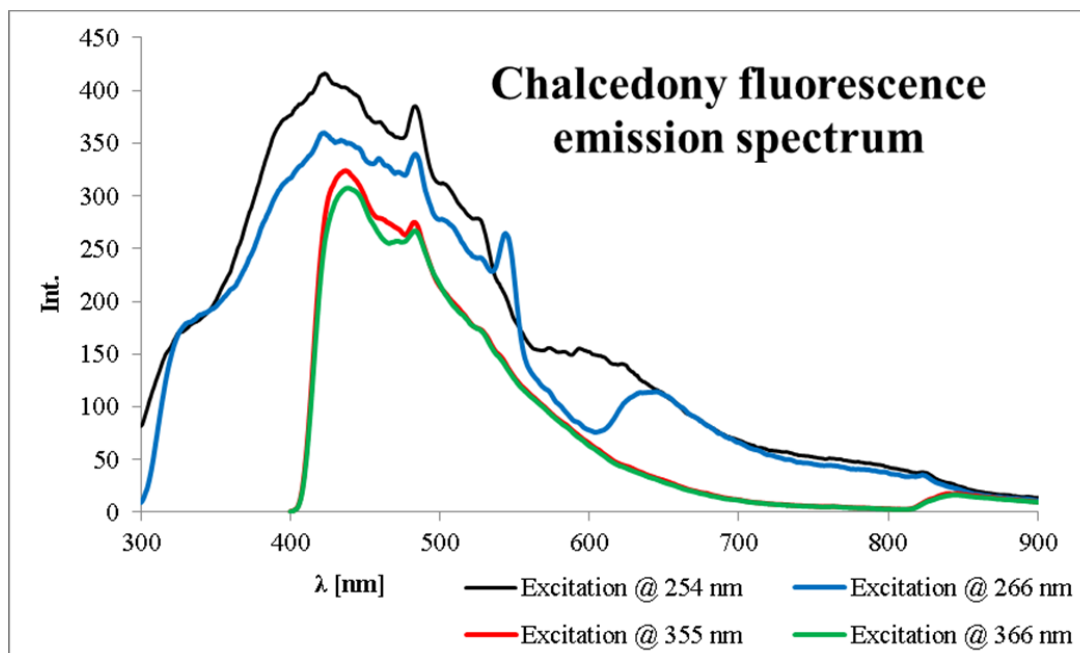


Figure 98: Chalcedony fluorescence emission spectra

Table 45: Method parameters for the Chalcedony fluorescence emission spectra

	Chalcedony 2D - Fluorescence Mode			
	Exc. @ 254 nm	Exc. @ 266 nm	Exc. @ 355 nm	Exc. @ 366 nm
Emslit [nm]	8	8	8	8
Exslit [nm]	10	10	10	10
U(PMT) [V]	775	775	775	775
Emfilter [nm]	290	290	390	390
Delay [ms]	-	-	-	-
Gate [ms]	-	-	-	-
Cycle time [ms]	-	-	-	-
Flash count	-	-	-	-
Additional Emfilter	-	WG 320	-	-

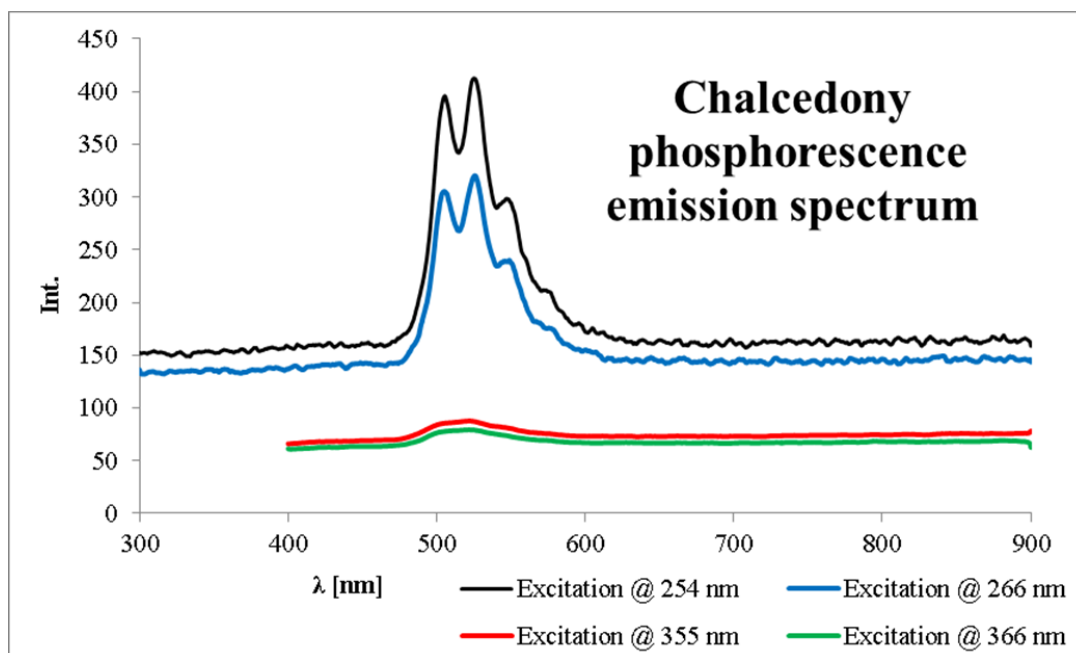


Figure 99: Chalcedony phosphorescence emission spectra

Table 46: Method parameters for the Chalcedony phosphorescence emission spectra

	Chalcedony 2D - Phosphorescence Mode			
	Exc. @ 254 nm	Exc. @ 266 nm	Exc. @ 355 nm	Exc. @ 366 nm
Emslit [nm]	8	8	20	20
Exslit [nm]	10	10	10	10
U(PMT) [V]	775	775	775	775
Emfilter [nm]	290	290	390	390
Delay [ms]	0,10	0,10	0,10	0,10
Gate [ms]	3,00	3,00	3,00	3,00
Cycle time [ms]	20	20	20	20
Flash count	1	1	1	1
Additional Emfilter	-	-	-	-

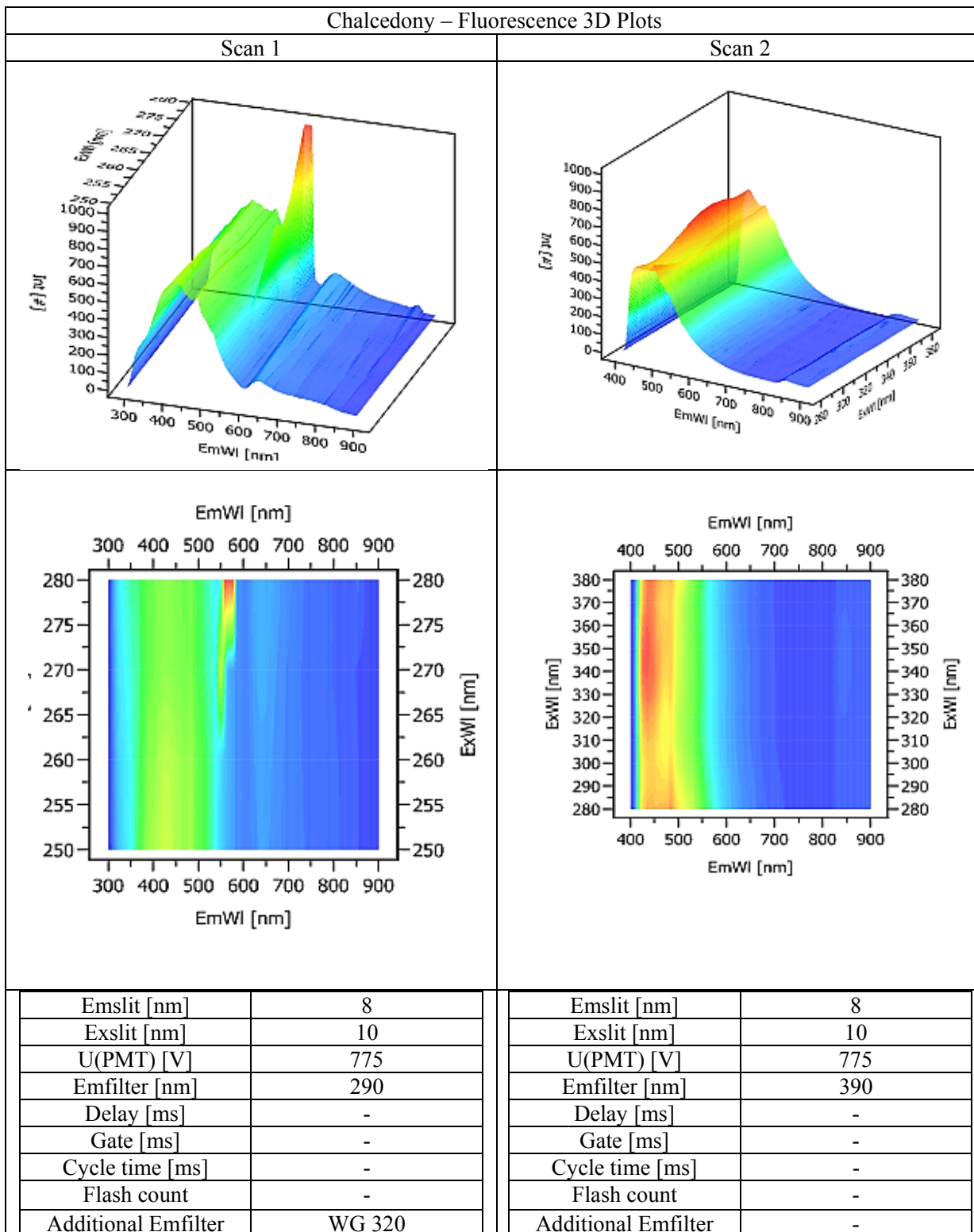


Figure 100: Chalcedony phosphorescence 3D spectra

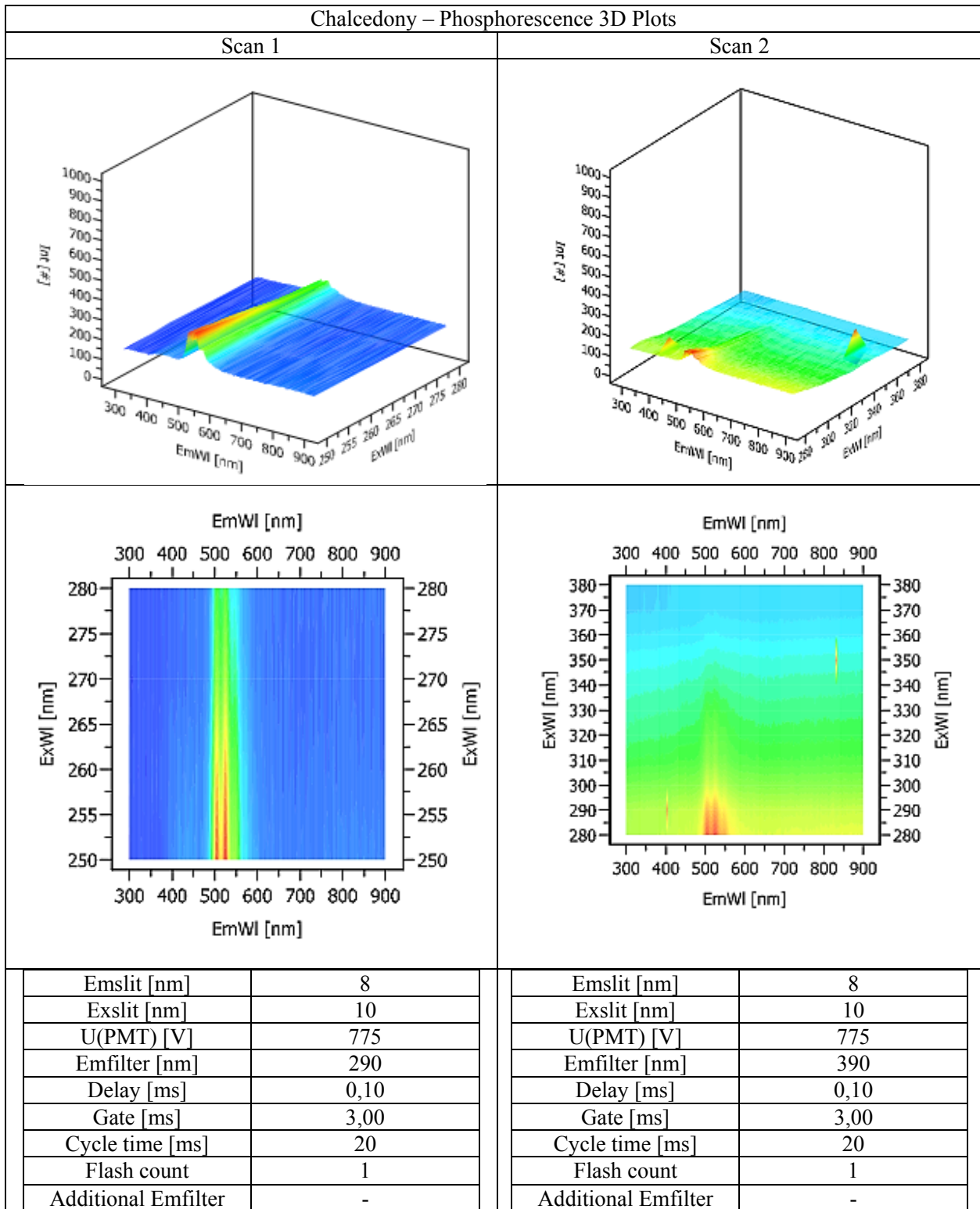


Figure 101: Chalcedony phosphorescence 3D spectra

3.2.3.5 Silicon - Luminescence Spectra

Silicon was used as a blank for fluorescence and phosphorescence measurement. Since the fluorescence measurement (see fig. 102) shows very intensive peaks, which are not plausible if the Si sample is seen under UV light, the fluorescence mode of the LS 55 has to be considered as not reliable for non- or very weak fluorescing minerals. Very similar fluorescence spectra were obtained with Chalcedony, Magnesite and Calcite. However, a nearly straight baseline, as expected for Si was observed in the phosphorescence mode.

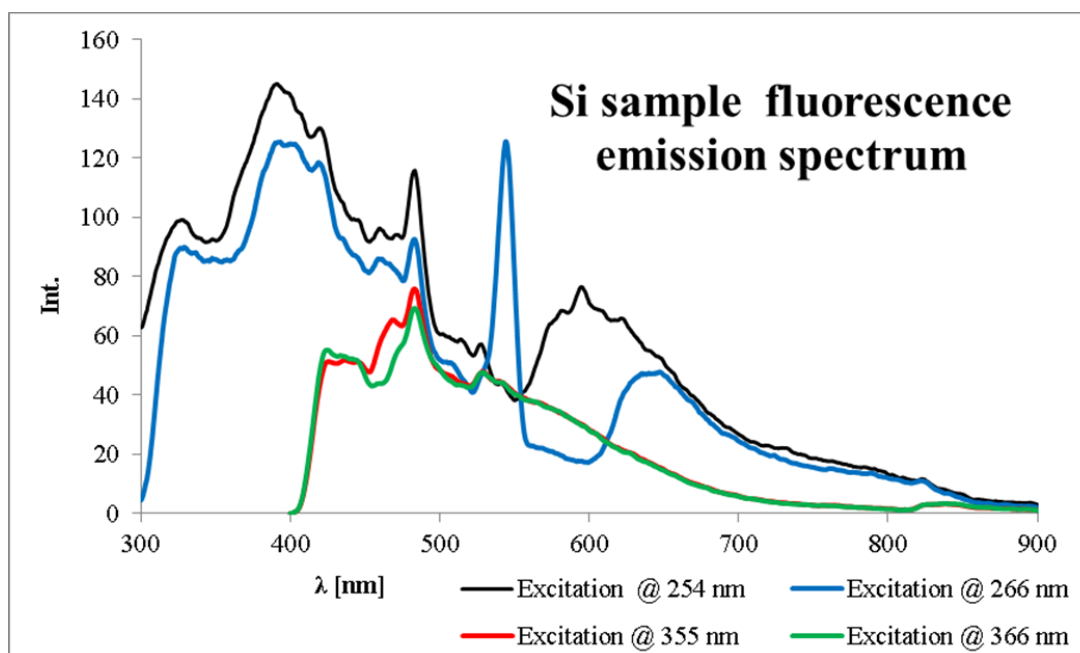


Figure 102: Si sample fluorescence emission spectra

Table 47: Method parameters for the Si sample fluorescence emission spectra

	Si sample 2D - Fluorescence Mode			
	Exc. @ 254 nm	Exc. @ 266 nm	Exc. @ 355 nm	Exc. @ 366 nm
Emslit [nm]	8	8	8	8
Exslit [nm]	10	10	10	10
U(PMT) [V]	775	775	775	775
Emfilter [nm]	290	290	390	390
Delay [ms]	-	-	-	-
Gate [ms]	-	-	-	-
Cycle time [ms]	-	-	-	-
Flash count	-	-	-	-
Additional Emfilter	-	WG 320	-	-

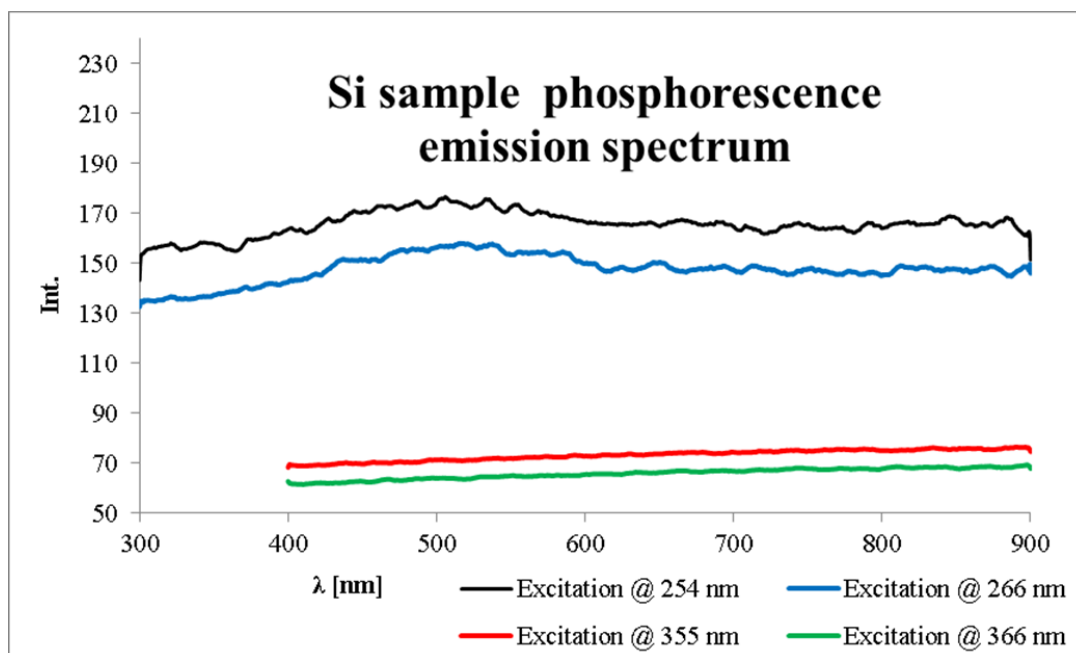


Figure 103: Si sample phosphorescence emission spectra

Table 48: Method parameters for the Si sample phosphorescence emission spectra

	Si sample 2D - Phosphorescence Mode			
	Exc. @ 254 nm	Exc. @ 266 nm	Exc. @ 355 nm	Exc. @ 366 nm
Emslit [nm]	20	20	20	20
Exslit [nm]	10	10	10	10
U(PMT) [V]	775	775	775	775
Emfilter [nm]	290	290	390	390
Delay [ms]	0,10	0,10	0,10	0,10
Gate [ms]	3,00	3,00	3,00	3,00
Cycle time [ms]	20	20	20	20
Flash count	1	1	1	1
Additional Emfilter	-	-	-	-

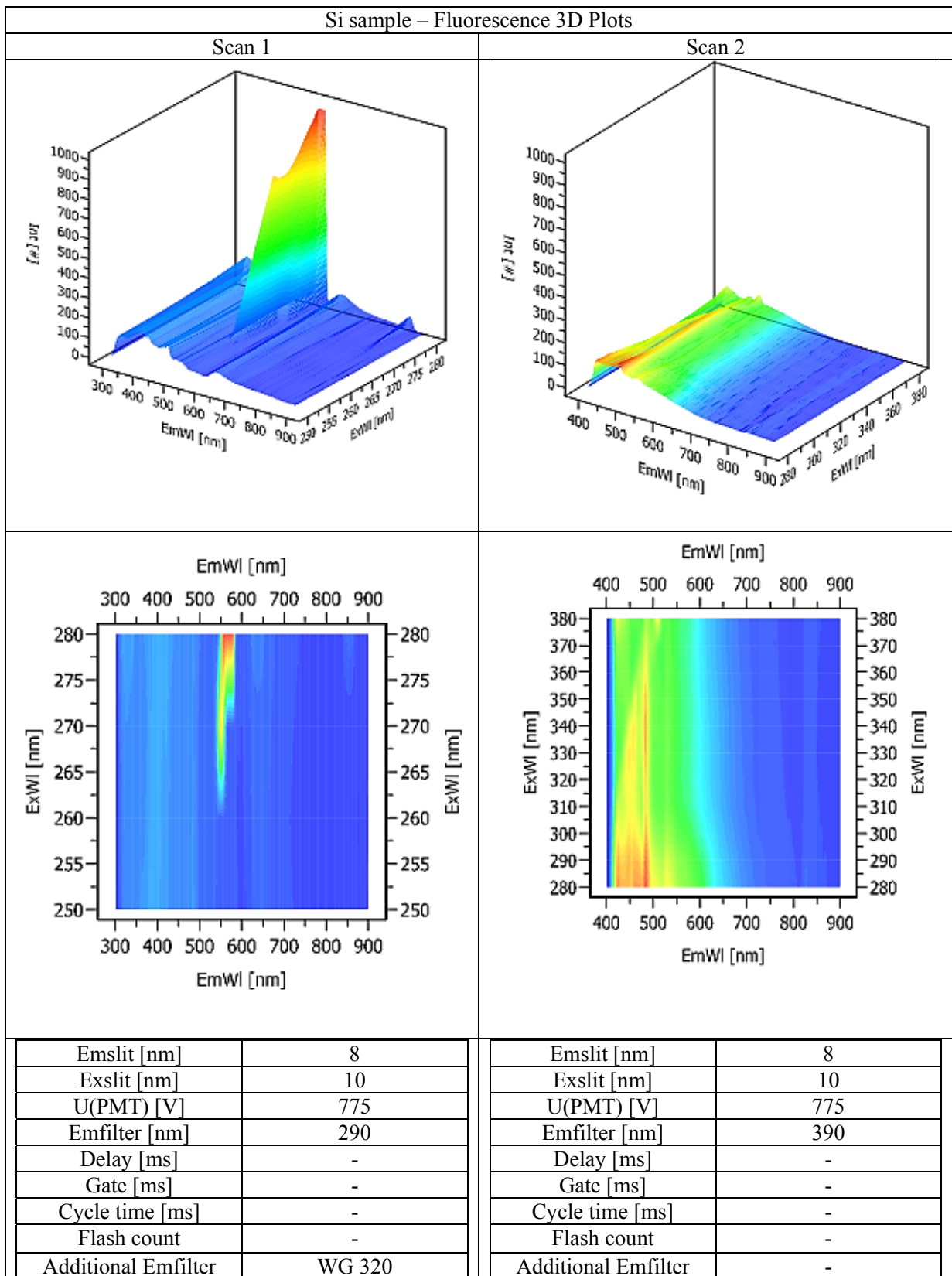


Figure 104: Si sample fluorescence 3 D spectra

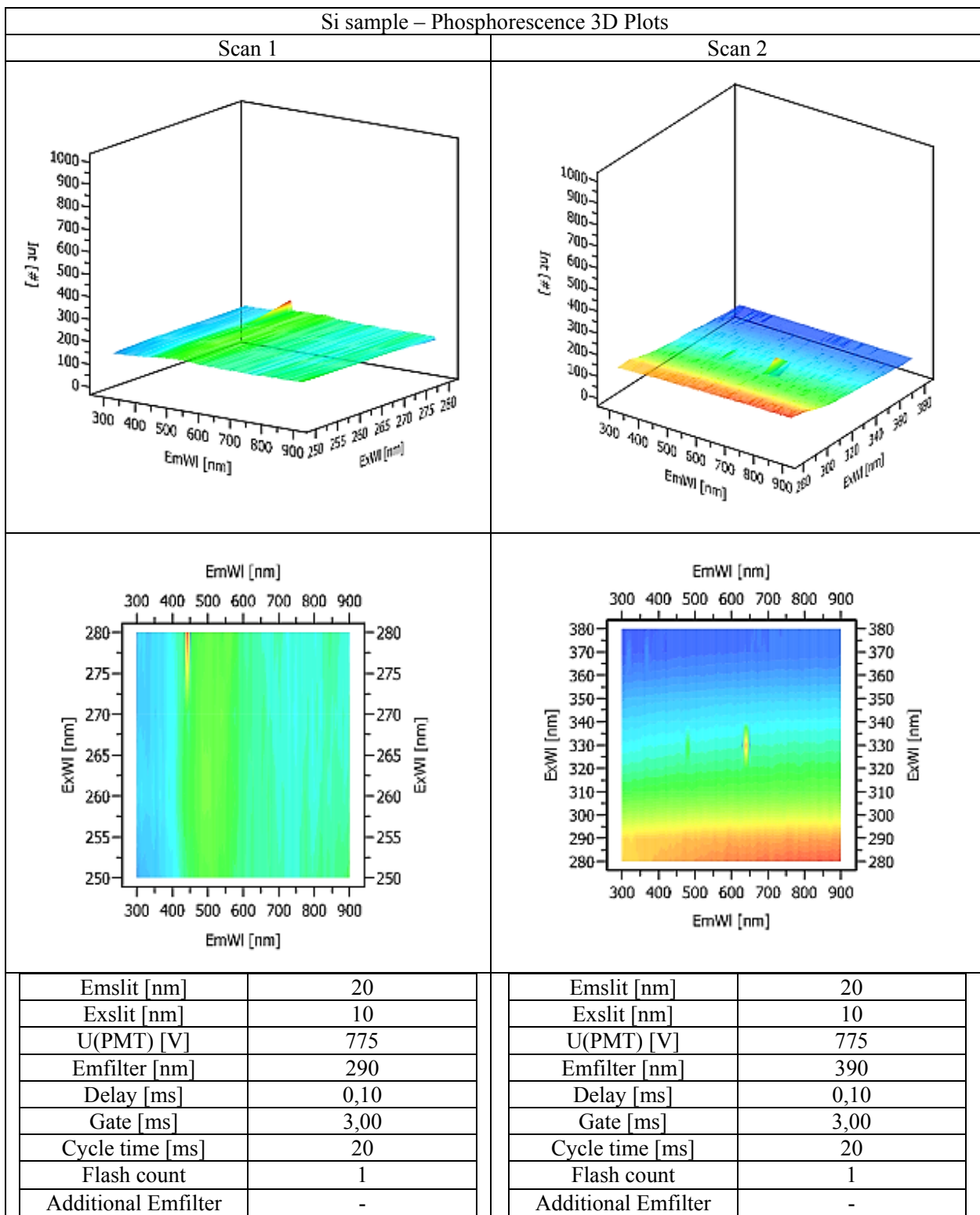


Figure 105: Si sample phosphorescence 3D spectra

3.2.3.6 CAB 15 - Luminescence Spectra

The CAB 15 sample showed an intense peak around 350 nm in the fluorescence spectrum. This peak is assigned to the $s^2 \rightarrow sp$ transition, which was reported from Kieler in her master thesis [2]. The phosphorescence spectra show a baseline, which indicates fast decay of the PbO-activator.

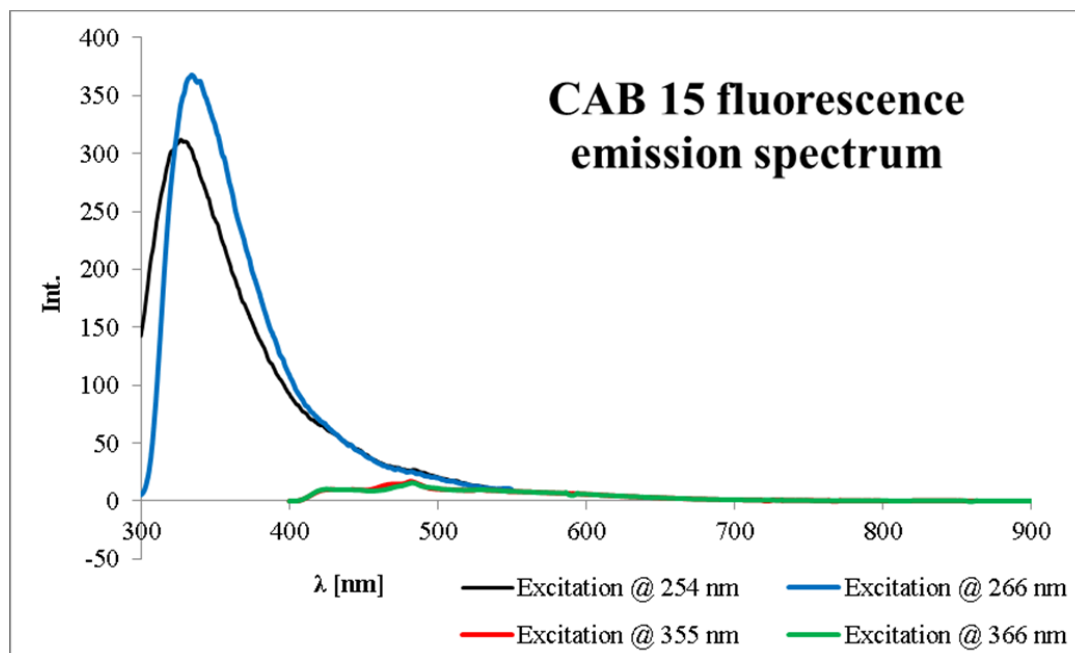


Figure 106: CAB 15 fluorescence emission spectra

Table 49: Method parameters for the CAB 15 fluorescence emission spectra

	CAB 15 2D - Fluorescence Mode			
	Exc. @ 254 nm	Exc. @ 266 nm	Exc. @ 355 nm	Exc. @ 366 nm
Emslit [nm]	4	4	8	8
Exslit [nm]	10	10	10	10
U(PMT) [V]	775	775	775	775
Emfilter [nm]	290	290	390	390
Delay [ms]	-	-	-	-
Gate [ms]	-	-	-	-
Cycle time [ms]	-	-	-	-
Flash count	-	-	-	-
Additional Emfilter	-	-	-	-

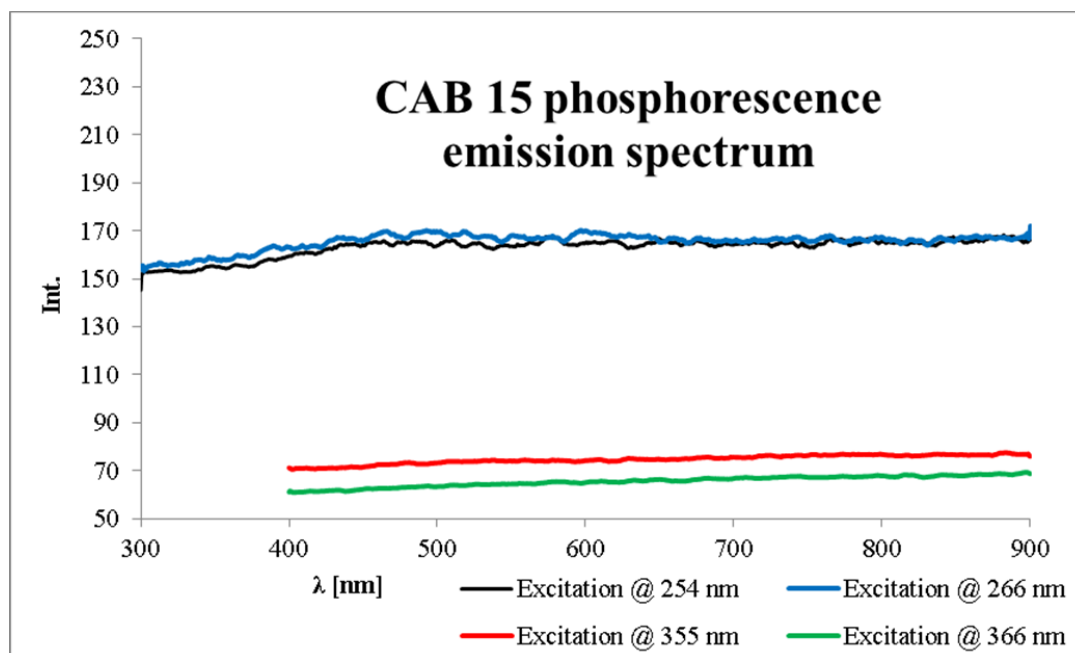


Figure 107: CAB 15 phosphorescence emission spectra

Table 50: Method parameters for the CAB 15 phosphorescence emission spectra

	CAB 15 2D - Phosphorescence Mode			
	Exc. @ 254 nm	Exc. @ 266 nm	Exc. @ 355 nm	Exc. @ 366 nm
Emslit [nm]	20	20	20	20
Exslit [nm]	10	10	10	10
U(PMT) [V]	775	775	775	775
Emfilter [nm]	290	290	390	390
Delay [ms]	0,10	0,10	0,10	0,10
Gate [ms]	3,00	3,00	3,00	3,00
Cycle time [ms]	20	20	20	20
Flash count	1	1	1	1
Additional Emfilter	-	-	-	-

CAB 15 – Fluorescence 3D Plots

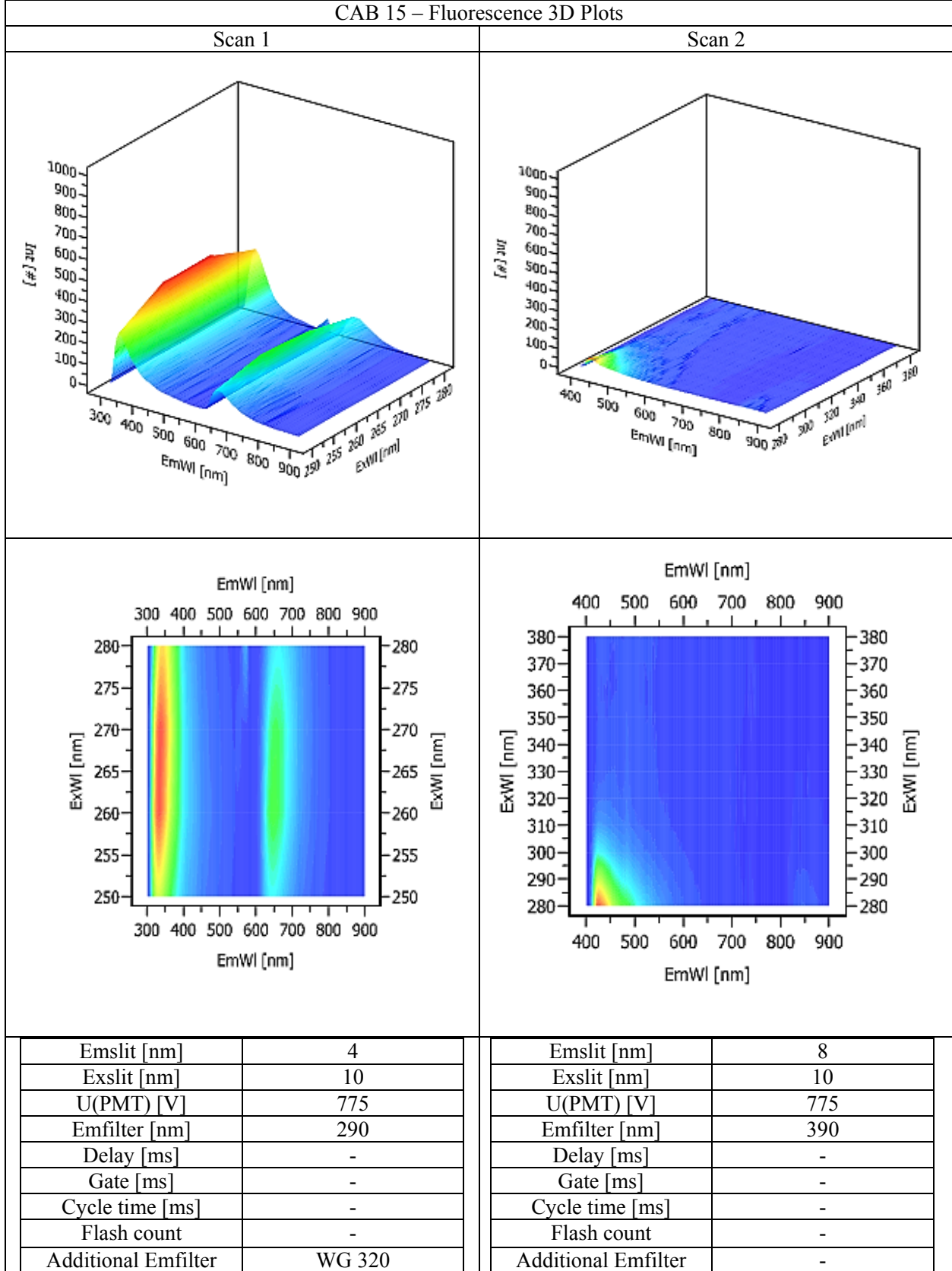


Figure 108: CAB 15 fluorescence 3D spectra

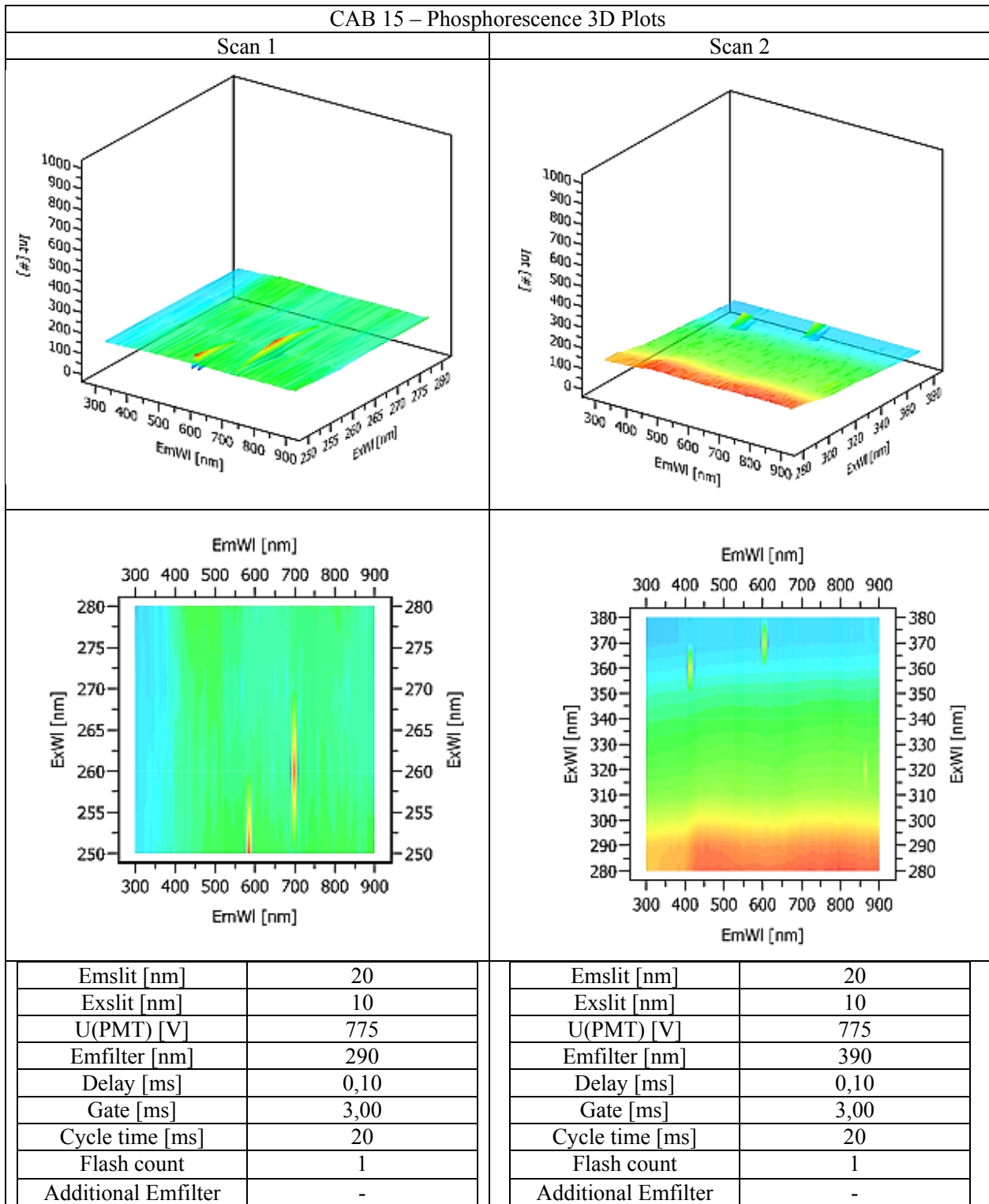


Figure 109: CAB 15 phosphorescence 3D spectra

3.2.3.7 PbO reference glass 1 - Luminescence Spectra

The Pb reference glass 1 shows much higher fluorescence intensity, than it is observed for CAB 15. This peak is assigned to the $s^2 \rightarrow sp$ transition of Pb^{2+} [2]. Like for CAB 15 no peak can be measured under phosphorescence settings.

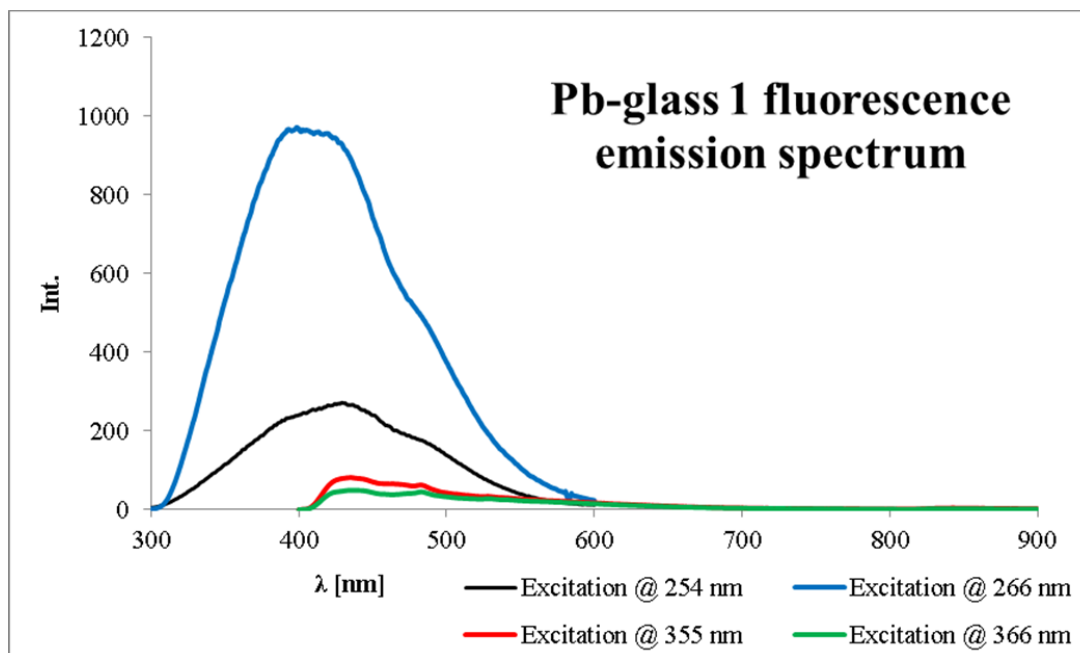


Figure 110: Pb-glass 1 fluorescence emission spectrum

Table 51: Method parameters for the Pb-glass 1 fluorescence emission spectra

	Pb-Glas_1 2D - Fluorescence Mode			
	Exc. @ 254 nm	Exc. @ 266 nm	Exc. @ 355 nm	Exc. @ 366 nm
Emslit [nm]	3	4	8	8
Exslit [nm]	10	10	10	10
U(PMT) [V]	775	775	775	775
Emfilter [nm]	290	290	390	390
Delay [ms]	-	-	-	-
Gate [ms]	-	-	-	-
Cycle time [ms]	-	-	-	-
Flash count	-	-	-	-
Additional Emfilter	-	-	-	-

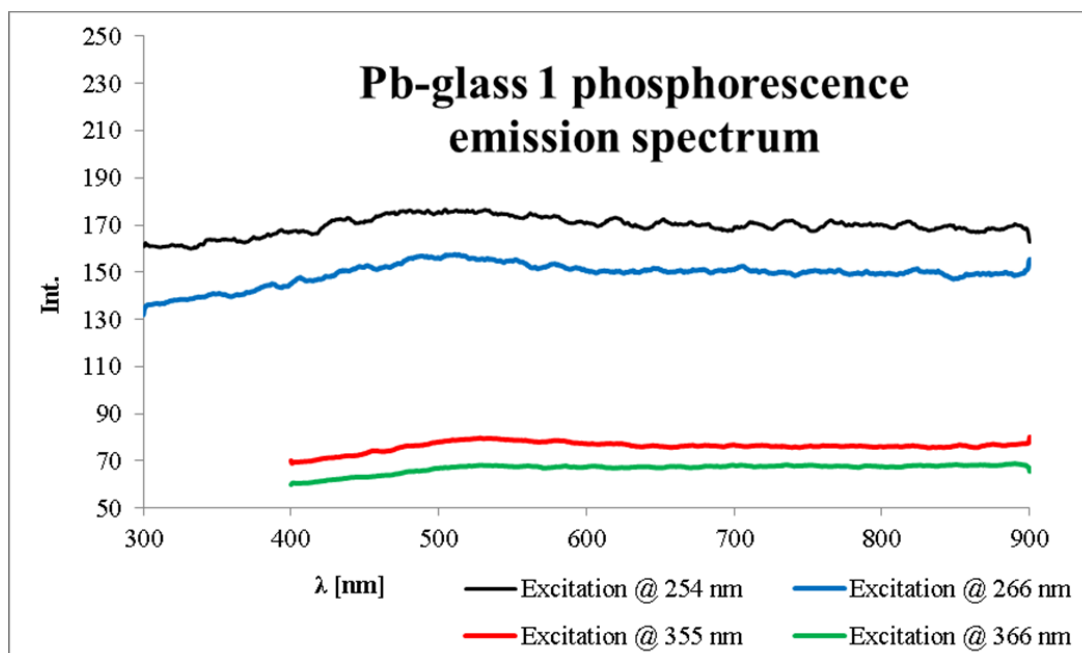


Figure 111: Pb-glass 1 phosphorescence emission spectra

Table 52: Method parameters for the Pb-glass 1 phosphorescence

	Pb-Glas_1 2D - Phosphorescence Mode			
	Exc. @ 254 nm	Exc. @ 266 nm	Exc. @ 355 nm	Exc. @ 366 nm
Emslit [nm]	20	20	20	20
Exslit [nm]	10	10	10	10
U(PMT) [V]	775	775	775	775
Emfilter [nm]	290	290	390	390
Delay [ms]	0,10	0,10	0,10	0,10
Gate [ms]	3,00	3,00	3,00	3,00
Cycle time [ms]	20	20	20	20
Flash count	1	1	1	1
Additional Emfilter	-	-	-	-

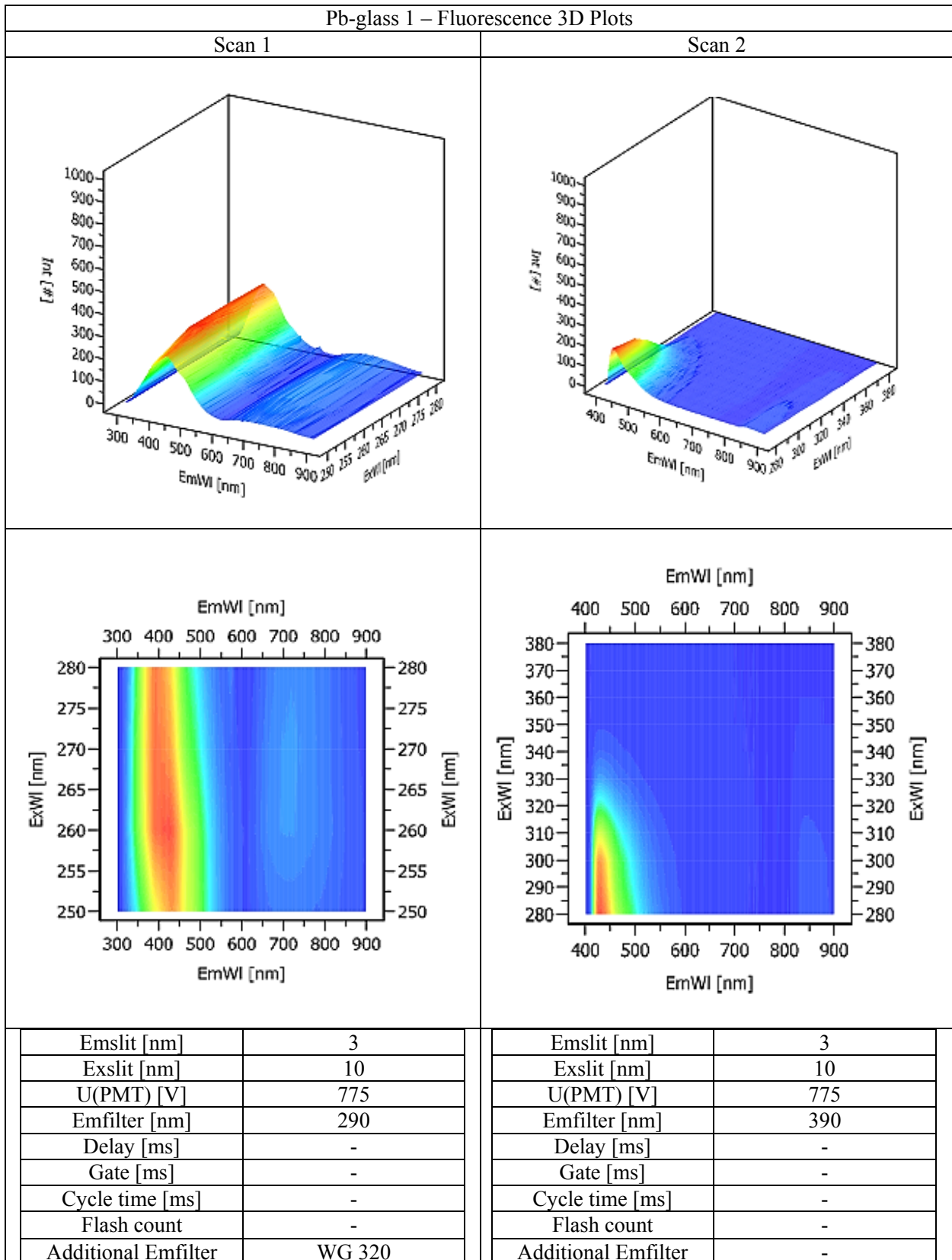


Figure 112: Pb-glass 1 fluorescence 3D spectra

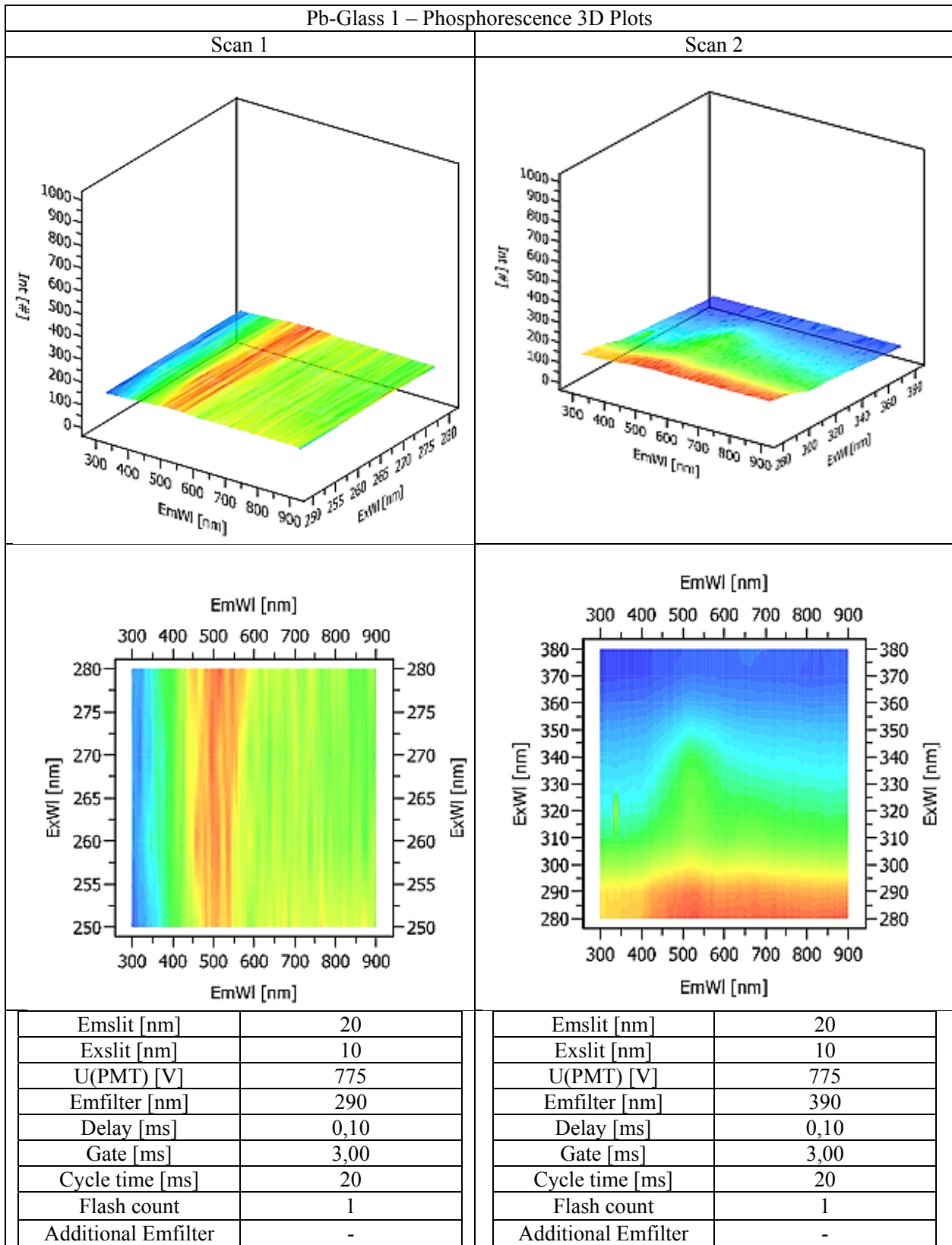


Figure 113: Pb-glass 1 phosphorescence 3D spectra

3.2.4 Decay curves

The experimental results indicated that the fluorite sample showed no measurable emission at a delay time of 0,10 ms and gate time of 3,00 ms. To investigate the possibilities for decay measurements with the LS 55, the gate time was varied from the smallest possible setting of 0,01 ms to 0,05 ms where no emission could be observed any more. The measured spectra are plotted in figure 114.

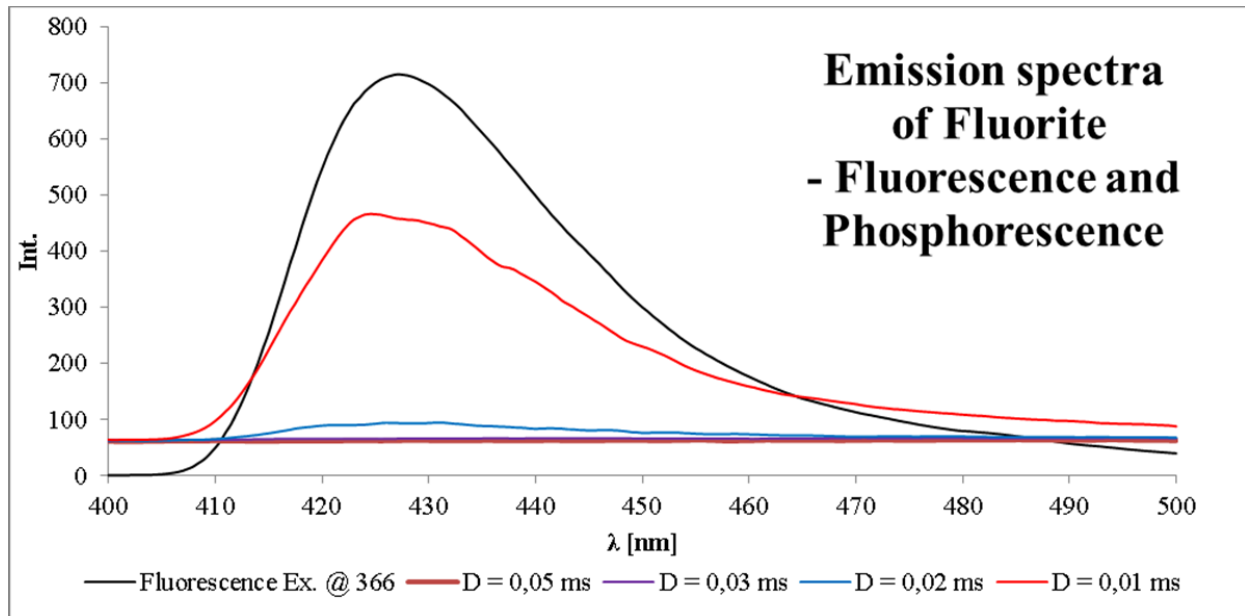


Figure 114: Fluorite spectra - raw data for the decay curves

In the phosphorescence mode different values for the y-axis offset were observed. This offset values were subtracted from the maxima at a wavelength of 424 nm.

Table 53: Decay experiment – results and method parameters

Measurement mode	Fluorescence	Phosphorescence	Phosphorescence	Phosphorescence	Phosphorescence
Delay [ms]	0	0,05	0,03	0,02	0,01
Exc. WL [nm]	366	366	366	366	366
Emslit [nm]	6	6	6	6	6
Exslit [nm]	10	10	10	10	10
U(PMT) [V]	775	775	775	775	775
Emfilter [nm]	390	390	390	390	390
Delay [ms]	-	0,05	0,03	0,02	0,01
Gate [ms]	-	3,00	3,00	3,00	3,00
Cycle time [ms]	-	20	20	20	20
Flash count	-	1	1	1	1
Additional Emfilter	-	-	-	-	-
Peak height. @ 424 nm	714,73	0,97	3,37	32,15	402,43

The results for the peak height at the wavelength of 424 nm in as a function of delay time are presented in figure 115.

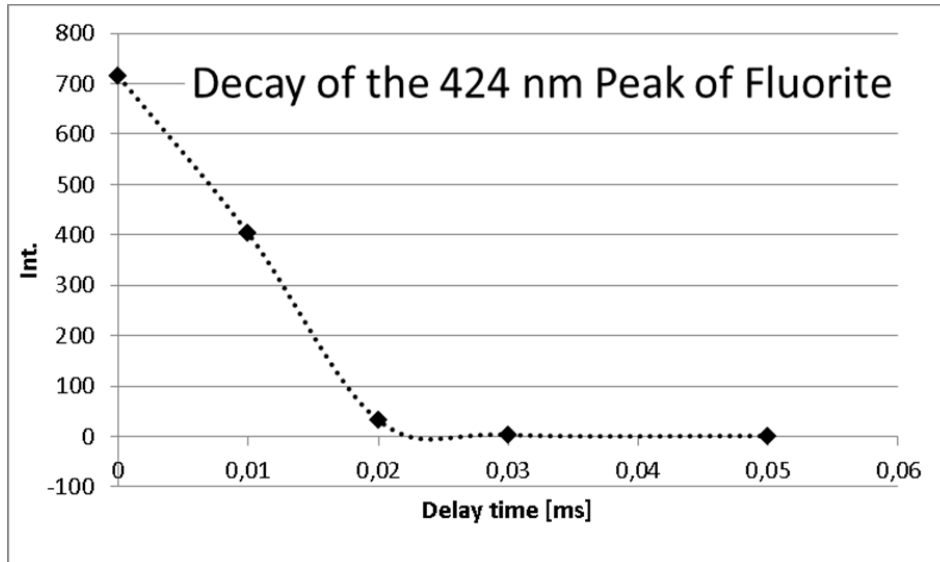


Figure 115: Peak height at 424 nm vs. delay time

However, the Eu^{2+} emission at 424 nm has a reported decay time of 600 – 800 ns and should not be observed in the LS 55 system in the phosphorescence mode [125]. It must be mentioned that there is a mismatch between the reported decay times of Eu^{2+} in the literature and the measured decay times. This mismatch is presently unresolved.

4 Conclusion

Preparation for the samples for the optical measurements was achieved by cutting and polishing. The purity of mineral phases can be assessed by tests with the Raman spectroscopy of the project partner MUL.

The NIR-reflection measurements of the chosen mineral samples (Bauxite, Magnesite, Talc, Fluorite, Calcite, Chalcedony and Barite) show good discrimination possibilities for those minerals, when the first and second derivatives of the spectra are compared. Data produced with the L950 system are of good quality and can serve as a base for implementation in UV, VIS, NIR reflection or transmission sensor sorting systems. However, the reflection measurements are more time consuming than the measurements with industrial sensor systems. Some bands in the reflection spectra were interpreted according to the literature. Often occurring OH-combinations and overtones at around 1400 nm and 1900 nm can be increased and identified if the samples are wetted with H₂O. An easy to use standard method and analysis procedure for the measurement of reflection spectra was defined.

It was shown that a discrimination via the emission spectrum of a mineral with the LS 55 is possible, if a suitable activator is present in the mineral, e.g. Mn²⁺ in Calcite or Eu²⁺ in Fluorite. The emission features recorded in the spectrofluorimeter allow to set discriminators for sorting purposes. Crucial information can be obtained either in the fluorescence or phosphorescence spectra. It is a major problem of the LS 55 that life time of excited states can lead to problems in detection of the activators. An attempt to assess fluorescence intensity with a straightforward approach was made. While taking the photographs under UV light, it turned out that the use of a 15 W shortwave UV-lamp is highly recommended for good photograph quality with standard digital cameras. For all the examined minerals and glasses (Fluorite, Calcite, Magnesite, Chalcedony, CAB 15 and a PbO reference glass) bands in the emission spectra could be measured. A silicon piece of very high purity was used as a blank standard for fluorescence. In a hypothetical sorting experiment, all the mentioned samples can be distinguished from one another. Due to the life time problem emission measurements are more complex than reflection measurements. However, easy to use methods for emission measurements with the present system were worked out. An emission correction function for the emission side of the LS 55 was recorded according to the recommended BAM standards.

The illumination situation in the LS 55 spectrofluorimeter was assessed with radiometric measurements and the use of a chemical actinometer. This illumination situation was compared to the irradiance values for commercial available laser illumination systems. In the LS 55 irradiance values in the range of 10⁻⁵ – 10⁻⁴ W/cm² could be measured. The glass sorting systems from Binder + Co work with irradiances of 10⁻² – 10⁻³ W/cm². Laser systems recommended for LIF-sorting applications are in the order of 10⁻³ – 10³ W/cm². LIF lab-scale systems work with irradiances of about 10⁹ – 10¹¹ W/cm².

A database and literature search was carried out. It is important to have reference data to compare spectra of actual samples to find activators and spectroscopically active species in the minerals. The three most important databases available in the internet are: USGS for reflection spectra of minerals, Mindat for general information on Minerals and Fluomin for fluorescence spectra. The literature research on fluorescent minerals showed that there are three books of great importance for the field, the works of: Marfunin [154], Gorobets & Rogojine [155] and Gaft, Reisfeld & Panczer [76].

5 Literature

- [1] Wills, B.A.; *Wills' Mineral Processing Technology – An Introduction to the Practical Aspects of Ore Treatment and Mineral Recovery*; Elsevier, 2011; pp 203-377
- [2] Kieler, M.; *Optische Erkennung bleioxidhaltiger Gläser in Recyclingglasscherben*, Diploma Thesis at Graz University of Technology, 2009
- [3] Infomation brochure „CLARITY lead“ of Binder + Co available on http://www.binder-co.com/downloads/Produktblatt-CLARITY_lead_deu.pdf accessed on 1.10.2012
- [4] Ohnewein, G.; *Verwendbarkeit des UV-Cut-Off Verfahrens als optisches Sortierkriterium im Altglasaufbereitungsprozess*, Diploma Thesis at FH Joanneum, 2006
- [5] Ören, E; *Sorting of Fluorescent Minerals by Using a Multi Sensor Sorter (MIDAS)*, Diploma Thesis at the Istanbul Technical University – Institute of Science and Technology in cooperation with RWTH Aachen, 2007
- [6] Wotruba, H. , Kleine, C.; *New Developments in Sensor-Based Sorting*, Proceedings of the XII International Mining Symposia, Turkey: Hacettepe University – Department of Mining Engineering, 2010
- [7] Wotruba, H.; Robben, M.; Kleine, C. In *Applications of Sensor-based Sorting in the Raw Material Industry*; Nienhaus, K., Ed., Petz, T., Ed., Wotruba, H., Ed.; Shaker Verlag: Germany, 2011, pp. 8 – 13
- [8] Okrusch, M., Matthes, S. *Mineralogie – Eine Einführung in die spezielle Mineralogie, Petrologie und Lagerstättenkunde*; 8. Ed., Springer: Berlin, Heidelberg, New York, 2009, p. 1
- [9] Brauns, R, Chudoba, K.F. *Allgemeine Mineralogie – Sammlung Göschel Band 29/29a*; Walter de Gruyter & Co: Berlin 1968, pp 139 - 150
- [10] Okrusch, M., Matthes, S. *Mineralogie – Eine Einführung in die spezielle Mineralogie, Petrologie und Lagerstättenkunde*; 8. Ed., Springer: Berlin, Heidelberg, New York, 2009, p. 4
- [11] Jones, W.R. *Minerals in Industry*; Penuin Books: New York 1943, p.10
- [12] Brauns, R, Chudoba, K.F. *Allgemeine Mineralogie – Sammlung Göschel Band 29/29a*; Walter de Gruyter & Co: Berlin 1968, p. 5
- [13] Okrusch, M., Matthes, S. *Mineralogie – Eine Einführung in die spezielle Mineralogie, Petrologie und Lagerstättenkunde*; 8. Ed., Springer: Berlin, Heidelberg, New York, 2009, p. 34
- [14] Okrusch, M., Matthes, S. *Mineralogie – Eine Einführung in die spezielle Mineralogie, Petrologie und Lagerstättenkunde*; 8. Ed., Springer: Berlin, Heidelberg, New York, 2009, pp. 4-5
- [15] Kettle, S.F.A. *Symmetry and Structure – Readable Group Theory for Chemists*; 3rd Ed., Wiley: West Sussex – England, 2007, p. 11

- [16] Hook, J.R., Hall, H.E. *Solid State Physics*; 2nd Ed., Wiley: West Sussex, 1991, pp. 2 -7
- [17] Askeland, R.D. *The Science and Engineering of Materials*; 2nd Ed., Chapman and Hall: London, New York, Tokyo, Melbourne, Madras, 1990, pp. 52 – 53
- [18] Hook, J.R., Hall, H.E. *Solid State Physics*; 2nd Ed., Wiley: West Sussex, 1991, pp. 7 - 8
- [19] Atkins, P.W., Frieman, R. *Molecular Quantum Mechanics*; 5th Ed., Oxford University Press: Oxford, 2011, pp. 125 – 131
- [20] Hollemann, A.F., Wiberg, E. *Lehrbuch der Anorganischen Chemie*; 101th Ed., Walter de Gruyter: Berlin, New York, 1995, pp. 173 – 178
- [21] Massa, W. *Kristallstrukturbestimmung*; 6th Ed., Vieweg + Teubner: Wiesbaden, 2009, pp. 59 – 76
- [22] Machlin, E. *An Introduction to Aspects of Thermodynamics and Kinetics Relevant to Materials Science*, 3rd Ed., Elsevier: Amsterdam, 2007, pp. 185 – 205
- [23] Askeland, D. R., Pradeep, P. F., Wright, W. J. *The Science and Engineering of Materials*, 6th Ed., Cengage Learning: Stamford, 2011, pp. 113 – 121
- [24] Askeland, D. R., Pradeep, P. F., Wright, W. J. *The Science and Engineering of Materials*, 6th Ed., Cengage Learning: Stamford, 2011, pp. 122 – 131
- [25] Askeland, D. R., Pradeep, P. F., Wright, W. J. *The Science and Engineering of Materials*, 6th Ed., Cengage Learning: Stamford, 2011, p. 84
- [26] Pauling, L. *J. Am. Chem. Soc.* 1929, 51, 1010 – 1026
- [27] Elliot, S. *The Physics and Chemistry of solids*, Wiley and Sons: Chichester, New York, Weinheim, Brisbane, Singapore, Toronto, 1998, p. 151
- [28] Kröger, F.A., Vink, H.J. In *Solid State Physics*, Vol. 3, Seitz, F. and Turnbull, D. Ed.; Academic Press Inc: New York, 1956, pp. 273 – 301
- [29] Ong, J.N. *J. Electrochem. Soc.* 1967, 114 (10), pp. 1080 – 1083
- [30] Strunz, H., Nickel, E.H. *Strunz Mineralogical Tables*, E. Schweizerbart'sche Verlagsbuchhandlung (Nägele u. Obermiller): Stuttgart, 2001, pp. 1 – 27
- [31] <http://en.wikipedia.org/wiki/File:Electromagnetic-Spectrum.png> (looked up on 15.10.2012)
- [32] Solé, J.G., Bausá, L.E., Jaque, D. *Optical Spectroscopy of Inorganic Solids*, Wiley: West Sussex (England), 2005, pp. 2 – 3
- [33] Solé, J.G., Bausá, L.E., Jaque, D. *Optical Spectroscopy of Inorganic Solids*, Wiley: West Sussex (England), 2005, pp. 4 – 5
- [34] Günzler, H., H.M. Heise *IR-Spektroskopie – Eine Einführung*, 3rd Ed., Wiley – VCH: Weinheim (Germany), 1996, pp. 26 – 29

- [35] Ruan, H.D., Frost, J.T. Klopprogge, L., Duong, L. *Spectrochem. Act.*, Part A, 2001, 58, pp. 265 - 272
- [36] Nakamoto, K. *Infrared and Raman Spectra of Inorganic and Coordination Compounds*, 2nd Ed., Wiley: New York, Chichester, Brisbane, Toronto, Singapore, 1986, pp. 20 – 25
- [37] Nakamoto, K. *Infrared and Raman Spectra of Inorganic and Coordination Compounds*, 2nd Ed., Wiley: New York, Chichester, Brisbane, Toronto, Singapore, 1986, p. 4
- [38] Atkins, P.W. *Quanta – A Handbook of Concepts*, 2nd Ed., Oxford University Press: Oxford, New York, Toronto, 1991 pp. 404 – 405
- [39] Günzler, H., H.M. Heise *IR-Spektroskopie – Eine Einführung*, 3rd Ed., Wiley – VCH: Weinheim (Germany), 1996, Vpp. 15 – 17
- [40] Atkins, P.W. *Physikalische Chemie*, 3rd Ed., Wiley – VCH: Weinheim (Germany), 2001, pp. 337 – 356
- [41] Atkins, P.W. *Physikalische Chemie*, 3rd Ed., Wiley – VCH: Weinheim (Germany), 2001, p. 347
- [42] Solé, J.G., Bausá, L.E., Jaque, D. *Optical Spectroscopy of Inorganic Solids*, Wiley: West Sussex (England), 2005, pp. 235 - 252
- [43] Kettle, S.F.A. *Symmetry and Structure – Readable Group Theory for Chemists*; 3rd Ed., Wiley: West Sussex – England, 2007, pp. 349 – 355
- [44] Solé, J.G., Bausá, L.E., Jaque, D. *Optical Spectroscopy of Inorganic Solids*, Wiley: West Sussex (England), 2005, p. 237
- [45] Atkins, P.W. *Physikalische Chemie*, 3rd Ed., Wiley – VCH: Weinheim (Germany), 2001, p. 482
- [46] Atkins, P.W. *Physikalische Chemie*, 3rd Ed., Wiley – VCH: Weinheim (Germany), 2001, p. 487
- [47] <http://symmetry.otterbein.edu/common/images/flowchart.pdf> looked up on 18.10.2012
- [48] Solé, J.G., Bausá, L.E., Jaque, D. *Optical Spectroscopy of Inorganic Solids*, Wiley: West Sussex (England), 2005, pp. 240 – 251
- [49] Atkins, P.W., Jones, L. *Chemie - einfach alles*, Wiley: Weinheim (Germany), 2005, pp. 742 – 744
- [50] Kettle, S.F.A. *Symmetry and Structure – Readable Group Theory for Chemists*; 3rd Ed., Wiley: West Sussex – England, 2007, p. 41
- [51] Atkins, P.W. *Physikalische Chemie*, 3rd Ed., Wiley – VCH: Weinheim (Germany), 2001, p. 1069
- [52] Atkins, P.W. *Quanta – A Handbook of Concepts*, 2nd Ed., Oxford University Press: Oxford, New York, Toronto, 1991 pp. 360 – 362
- [53] Atkins, P.W. *Molecular Quantum Mechanics*, 5th Ed., Oxford University Press: Oxford, New York, 2011, pp. 218 – 219

- [54] Atkins, P.W. *Molecular Quantum Mechanics*, 5th Ed., Oxford University Press: Oxford, New York, 2011, pp. 243 – 247
- [55] Gatterer, K. *Solid State Spectroscopy – Lecture Notes*, Summer Term 2012
- [56] Shudeman, C. L. B., *Journal of the Franklin Institute*, 1937, 224(4), pp. 501 – 518
- [57] Gray, N. M., Wills, L. A. *Phys. Rev.*, 1931, 248(38), pp. 248 – 254
- [58] Hesse, M, Meier, H., Zeeh, B., *Spektroskopische Methoden in der organischen Chemie*, 7th Ed, Thieme: Stuttgart, New York, 2005
- [59] http://en.wikipedia.org/wiki/Morse_potential looked up on 22.10.2012
- [60] Günzler, H., Heise, H.M. *IR-Spektroskopie*, Wiley-VCH: Weinheim, 1986 p. 29
- [61] Nakamoto, K. *Infrared and Raman Spectra of Inorganic and Coordination Compounds*, 2nd Ed., Wiley: New York, Chichester, Brisbane, Toronto, Singapore, 1986, p. 8
- [62] Thimm, L., *FT-IR und FT-NIR spektroskopische Untersuchung in Kombination mit chemometrischen Auswertalgorithmen zur Charakterisierung der chemischen Zusammensetzung von Straßenbaubitumen*, Dissertaion an der Universität Duisburg-Essen, 2009, pp. 11 – 15
- [63] Perkin Elmer Hardware Guide *High-Performance Lambda Spectrometers*, 2007, p. 27
- [64] Perkin Elmer Hardware Guide *High-Performance Lambda Spectrometers*, 2007, pp. 27 – 29
- [65] Gauglitz, G., Vo-Dinh, T., *Handbook of Spectroscopy*, 2003, Wiley-VCH: Weinheim, p. 40
- [66] Gauglitz, G., Vo-Dinh, T., *Handbook of Spectroscopy*, 2003, Wiley-VCH: Weinheim, p. 70
- [67] Hering, E.; Martin, R. *Photonik – Grundlagen, Technologie und Anwendungen*; Springer: Berlin – Heidelberg – New York, 2006; pp 57 – 61
- [68] Personal communication Prof. Karl Gatterer, July 2012
- [69] Ishida, H., Tobita, S., Hasegawa, Y., Katoh, R., Nozaki, K. *Coord. Chem. Ref.*, 2010, 254, 2449 – 2458
- [70] <http://sales.hamamatsu.com/index.php?id=13226752> looked up on 29.10.2012
- [71] Lakhowitz, J.R.; *Principles of Fluorescence Spectroscopy*; 3rd edition, Springer Science+Business Media, LLC: 2006; pp. 51 – 54
- [72] Standard Operation Procedure (SOP) for use of CERTIFIED REFERENCE MATERIALS BAM-F001, BAM-F002, BAM-F003, BAM-F004 and BAM-F005 Calibration Kit SPECTRAL FLUORESCENCE STANDARDS (Fluka 97003)
- [73] Lakhowitz, J.R.; *Principles of Fluorescence Spectroscopy*; 3rd edition, Springer Science+Business Media, LLC: 2006; pp. 52 – 53

- [74] McNaught, I. J., *J. Chem. Ed.* 1980, 57, 2, 101 – 105
- [75] Ören, E.; *Sorting of Fluorescent Minerals by using an Multi Sensor Sorter (Midas)*; Diploma Thesis at the Istanbul Technical University – Institute of Science and Technology in Cooperation with the Aachen University of Technology
- [76] Gaft, M., Reisfeld, R., Panczer, G.; *Modern Luminescence Spectroscopy of Minerals and Materials*; Springer; Berlin Heidelberg; 2010
- [77] Gaft, M., Reisfeld, R., Panczer, G.; *Modern Luminescence Spectroscopy of Minerals and Materials*; Springer; Berlin Heidelberg; 2010
- [78] Gorobets, B.S., Rogojine, A. R.; *Luminescent Spectra of Minerals*; RPC VIMS; Moscow; 2002, 14- 35
- [79] Gorobets, B. S., Portnov, A. M., Rogozhin, A.A.; *Rad. Meas.* 1995, 4, 485 – 491
- [80] Strunz, H., Nickel, E.H. *Strunz Mineralogical Tables*, E. Schweizerbart'sche Verlagsbuchhandlung (Nägele u. Obermiller): Stuttgart, 2001
- [81] Diploma Thesis Contract from 13.12.2011 between Binder + Co GmbH (Gleisdorf Austria) and Johannes Hofer from 13.12.2011
- [82] Schneider, S.: *Collecting Fluorescent Minerals*; Schiffer Pub. Co; 2011
- [83] Schneider, S.: *The world of Fluorescent Minerals*; Schiffer Pub. Co; 2006
- [84] Wilson, W.: *Fluorescence and Luminescence in Minerals*
- [85] Weingrill, G., Hofer, J.; *Minutes of Meeting for the MINEXX Plus Meeting on 31.3.2012*; 2012
- [86] Personal communication Prof. K. Gatterer on 20.3.2012 in the context of a theory meeting concerning the ongoing diploma thesis
- [87] http://jp.hamamatsu.com/products/semicon-fpd/pd284/pd410/c9920/index_en.html; (status of 26.6.2012)
- [88] http://photonics.intec.ugent.be/education/ivpv/res_handbook/v2ch24.pdf; looked up on 28.8.2012
- [89] Ohno, Y.; *OSA Handbook of Optics, Vol. III Visual Optics and Vision – Chapter of Photometry and Radiometry*; available under <http://web.archive.org/web/20100705033930/http://www.ecse.rpi.edu/~schubert/More-reprints/1999%20Ohno%20%28OSA%20handbook%20of%20optics%29%20Photometry%20and%20radiometry.pdf>; looked up on 11.7.2012
- [90] Taylor, B.N.; *The International System of Units (SI)*; NIST Special Publication 330; 2001 Edition; available under <http://www.checklist.org.br/d/internationalsystemofunits.pdf>; looked up on 11.7.2012
- [91] Hering, E.; Martin, R. *Photonik – Grundlagen, Technologie und Anwendungen*; Springer: Berlin – Heidelberg – New York, 2006; pp 61 – 62

- [92] http://photonics.intec.ugent.be/education/ivpv/res_handbook/v2ch24.pdf; looked up on 28.8.2012
- [93] Hering, E.; Martin, R. *Photonik – Grundlagen, Technologie und Anwendungen*; Springer: Berlin – Heidelberg – New York, 2006; p. 58
- [94] Hering, E.; Martin, R. *Photonik – Grundlagen, Technologie und Anwendungen*; Springer: Berlin – Heidelberg – New York, 2006; p. 60
- [95] <http://www.lepla.edu.pl/en/modules/Activities/m07/m07-theo.htm>; looked up on 29.8.2012
- [96] Quote for LS 55 Fluorescence Spectrometer received at 21.12.2011
- [97] Technical Specifications for the LS 55 and the LS 45 Fluorescence Spectrometers; documentation provided by Perkin Elmer, 2006
- [98] LS 55 User's Guide (2000) p. 178
- [99] Gaft, M.; Reisfeld, R.; Panczer, G.; Blank, Ph.; Boulon, G.; *Laser-induced time-resolved luminescence of minerals*; Spectrochim. Act. P. A 54 (1998) 2163-2175
- [100] Gaft, M.; Reisfeld, R.; Panczer, G.; Uspensky, E.; Varrel, B.; Boulon, G.; *Luminescence of Pr³⁺ in minerals*; Opt. Mat. 13 (1999) 71-79
- [101] G. Panczer; Gaft, M.; Reisfeld, R.; Shoval, S.; Boulon, G.; Champagnon, B.; *Luminescence of uranium in natural apatites*; Journ. Of All. and Comp. 275-277 (1998) 269-272
- [102] Bozelee, J. B.; Anupam K. M.; Sharma, S.; Ingram, M.; *Remote Raman and fluorescence studies of mineral samples*; Spectrochim. Act. P. A 61 (2005) 2342-2348
- [103] Quanta-Ray Pro Series Pulsed Nd: YAG Lasers – Specifications; available under http://www.newport.com/Quanta-Ray-Pro-Series-Pulsed-Nd-YAG-Lasers/368168/1033/info.aspx#tab_Specifications; looked up on 12.7.2012
- [104] Personal communication, Karl Leitner (Binder + C, R&D department), 1.7.2012
- [105] Demtröder, W.; *Laserspektroskopie – Grundlagen und Techniken*; Springer: Berlin – Heidelberg – New York, 1993; pp. 214 – 223
- [106] Ou, Z.Y.; Pereira, S.F.; Polzik, E.S.; Kimble, H.J.; *85% efficiency for cw frequency doubling from 1.08 to 0.54 μm*; Optics Letters, Vol. 17, No. 9; May 1, 1992 (available on <http://authors.library.caltech.edu/3191/1/OUZol92.pdf>)
- [107] Personal communication, Prof. K. Gatterer 30.8.2012
- [108] Personal communication, Prof. S. Landgraf 26.7.2012
- [109] Lakhowitz, J.R.; *Principles of Fluorescence Spectroscopy*; 3rd edition, Springer Science + Business Media, LLC: 2006; p. 31
- [110] Lakhowitz, J.R.; *Principles of Fluorescence Spectroscopy*; 3rd edition, Springer Science + Business Media, LLC: 2006; pp. 31 – 34

- [111] Lakhowitz, J.R.; *Principles of Fluorescence Spectroscopy*; 3rd edition, Springer Science + Business Media, LLC: 2006; p. 33
- [112] Technical specifications of Hamamatsu Photomultiplier tubes R928 and R955; released by Hamamatsu in July 2006; available under http://sales.hamamatsu.com/assets/pdf/parts_R/R928_R955_TPMS1001E07.pdf, looked up in Oct. 2012
- [113] LS 55 User's Guide (2000) p. 177
- [114] Okrusch, M., Matthes, S. *Mineralogie – Eine Einführung in die spezielle Mineralogie, Petrologie und Lagerstättenkunde*; 8. Ed., Springer: Berlin, Heidelberg, New York, 2009, pp. 97 - 98
- [115] Hering, E.; Martin, R. *Photonik – Grundlagen, Technologie und Anwendungen*; Springer: Berlin – Heidelberg – New York, 2006; p. 60
- [116] Rahn, R.O.; *Potassium Iodide as a Chemical Actinometer for 254 nm Radiation: Use of Iodate as an Electron Scavenger*; Photochem. Photobiol. 66(4) (1997) 450-455
- [117] Rahn, R.O.; Gerstenberg, H.M.; Vavrina, G.A.; *Dosimetry of ionizing radiation using an iodide/iodate aqueous solution*; Applied Radiation and Isotopes 56 (2002) 525-534
- [118] Sommersacher, P.; *Planung, Bau, Inbetriebnahme und Vermessung eines Coronareaktors*; Diploma Thesis at the Graz University of Technology (Institute of Chemical Engineering and Environmental Technology); 2010
- [119] Rahn, R.O.; *Use of Potassium Iodide as a Chemical Actinometer*; Photochem. Photobiol. 58(6) (1993) 874-880
- [120] Gaft, M., Reisfeld, R., Panczer, G.; *Luminescence Spectroscopy of Minerals and Materials*; Springer Science + Business Media, Berlin Heidelberg 2010, p. 36
- [121] Broicher, H.F.; *Nutzung der Analyse der laser-induzierten Fluoreszenz zur Online-Einzelkornsortierung*; consulting report form Rock ID Consulting for the Binder + Co AG, 2012
- [122] Okrusch, M., Matthes, S. *Mineralogie – Eine Einführung in die spezielle Mineralogie, Petrologie und Lagerstättenkunde*; 8. Ed., Springer: Berlin, Heidelberg, New York, 2009, pp. 91-93
- [123] Okrusch, M., Matthes, S. *Mineralogie – Eine Einführung in die spezielle Mineralogie, Petrologie und Lagerstättenkunde*; 8. Ed., Springer: Berlin, Heidelberg, New York, 2009, pp. 343 – 345
- [124] Tipler, A., T., Mosca, G. *Physik – Für Wissenschaftler und Ingenieure*; 2nd Ed., Elsevier Spektrum akademischer Verlag: München, 2004, pp. 1103 - 1106
- [125] Gaft, M., Reisfeld, R., Panczer, G.; *Luminescence Spectroscopy of Minerals and Materials*; Springer Science + Business Media, Berlin – Heidelberg, 2010, pp. 58 -59
- [126] Riedel, E. *Anorganische Chemie*; de Gruyter, Berlin – New York, 2004, p. 216
- [127] Gauglitz, G., Vo-Dinh, T., *Handbook of Spectroscopy*, 2003, Wiley-VCH: Weinheim, pp. 78 – 79

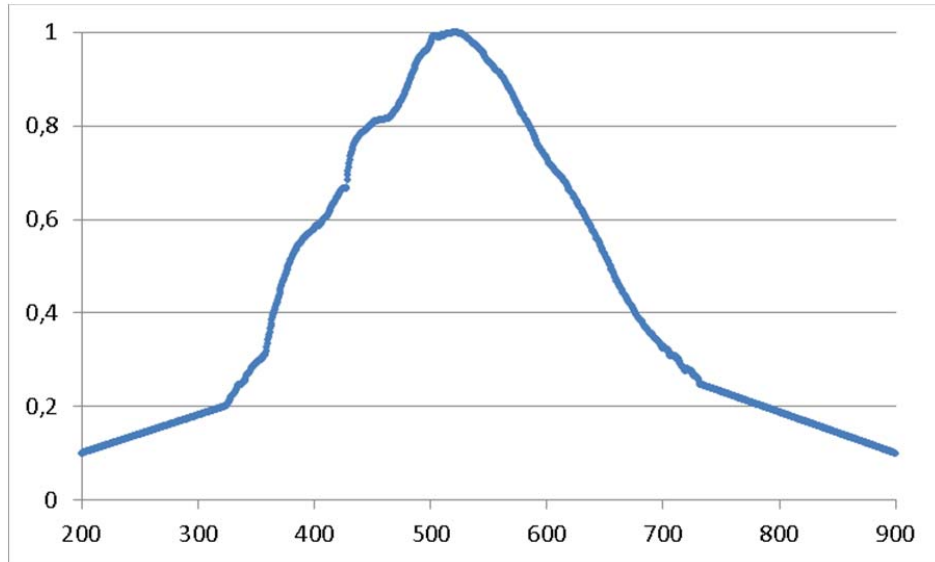
- [128] http://speclab.cr.usgs.gov/PAPERS_calibration_tutorial/ looked up on 13.11.2012
- [129] Frezzotti, M. L., Tecce, F., Casagli, A., *Raman Spectroscopy for fluid inclusion analysis*, J. Geochem. Expl., 112 (2012) pp. 1 – 20
- [130] Atkins. P.W. *Physikalische Chemie*, 3rd Ed., Wiley – VCH: Weinheim (Germany), 2001, p. 565
- [131] Atkins. P.W. *Physikalische Chemie*, 3rd Ed., Wiley – VCH: Weinheim (Germany), 2001, p. 563 – 565
- [132] Gatterer, K. *Solid State Chemistry*, lecture notes winter term 2011/12
- [133] http://home.gwu.edu/~xqiu/qiu_thesis/node39_ct.htm looked up on 14.11.2012
- [134] <http://ocw.nctu.edu.tw/course/ch-inorganic-phosphors/dieke-diagram-for-res.pdf> (looked up on 14.11.2012)
- [135] LS 55 User's Guide (2000) p. 176
- [136] LS 55 User's Guide (2000) p. 177
- [137] LS 55 User's Guide (2000) p. 178
- [138] Huckins, S, Personal Communication, 10.10.2012
- [139] Okrusch, M., Matthes, S. *Mineralogie – Eine Einführung in die spezielle Mineralogie, Petrologie und Lagerstättenkunde*; 8. Ed., Springer: Berlin, Heidelberg, New York, 2009, pp. 120 – 121
- [140] Strunz, H., Nickel, E. H.; *Strunz Mineralogical Tables*; 9 th. edition, E. Schweizerbart'sche Verlagsbuchhandlung (Nägele u. Obermiller): Stuttgart, 2001, p. 238
- [141] Strunz, H., Nickel, E. H.; *Strunz Mineralogical Tables*; 9 th. edition, E. Schweizerbart'sche Verlagsbuchhandlung (Nägele u. Obermiller): Stuttgart, 2001, p. 239
- [142] Strunz, H., Nickel, E. H.; *Strunz Mineralogical Tables*; 9 th. edition, E. Schweizerbart'sche Verlagsbuchhandlung (Nägele u. Obermiller): Stuttgart, 2001, p. 235
- [143] Strunz, H., Nickel, E. H.; *Strunz Mineralogical Tables*; 9 th. edition, E. Schweizerbart'sche Verlagsbuchhandlung (Nägele u. Obermiller): Stuttgart, 2001, p. 193
- [144] Strunz, H., Nickel, E. H.; *Strunz Mineralogical Tables*; 9 th. edition, E. Schweizerbart'sche Verlagsbuchhandlung (Nägele u. Obermiller): Stuttgart, 2001, p. 286
- [145] Strunz, H., Nickel, E. H.; *Strunz Mineralogical Tables*; 9 th. edition, E. Schweizerbart'sche Verlagsbuchhandlung (Nägele u. Obermiller): Stuttgart, 2001, p. 663
- [146] Okrusch, M., Matthes, S. *Mineralogie – Eine Einführung in die spezielle Mineralogie, Petrologie und Lagerstättenkunde*; 8. Ed., Springer: Berlin, Heidelberg, New York, 2009, p. 147
- [147] Strunz, H., Nickel, E. H.; *Strunz Mineralogical Tables*; 9 th. edition, E. Schweizerbart'sche Verlagsbuchhandlung (Nägele u. Obermiller): Stuttgart, 2001, p. 153

- [148] Okrusch, M., Matthes, S. *Mineralogie – Eine Einführung in die spezielle Mineralogie, Petrologie und Lagerstättenkunde*; 8. Ed., Springer: Berlin, Heidelberg, New York, 2009, pp. 79 – 80
- [149] Strunz, H., Nickel, E. H.; *Strunz Mineralogical Tables*; 9 th. edition, E. Schweizerbart'sche Verlagsbuchhandlung (Nägele u. Obermiller): Stuttgart, 2001, p. 286
- [150] Okrusch, M., Matthes, S. *Mineralogie – Eine Einführung in die spezielle Mineralogie, Petrologie und Lagerstättenkunde*; 8. Ed., Springer: Berlin, Heidelberg, New York, 2009, pp. 95 – 97
- [151] Strunz, H., Nickel, E. H.; *Strunz Mineralogical Tables*; 9 th. edition, E. Schweizerbart'sche Verlagsbuchhandlung (Nägele u. Obermiller): Stuttgart, 2001, pp. 204 – 205
- [152] Okrusch, M., Matthes, S. *Mineralogie – Eine Einführung in die spezielle Mineralogie, Petrologie und Lagerstättenkunde*; 8. Ed., Springer: Berlin, Heidelberg, New York, 2009, p. 161
- [153] Strunz, H., Nickel, E. H.; *Strunz Mineralogical Tables*; 9 th. edition, E. Schweizerbart'sche Verlagsbuchhandlung (Nägele u. Obermiller): Stuttgart, 2001, pp. 204 – 205
- [154] Marfunin, A.S.; *Spectroscopy, Luminescence and Radiation Centers in Minerals*; Springer: Berlin – Heidelberg – New York, 1979
- [155] Gorobets, B. S, Rogojine, A. A.; *Luminescent Spectra of Minerals – Reference Book*; VIMS (All-Russia Institute of Mineral Resources Moscow), 2001
- [156] Palmer, S. J., Raddy, J., Frost, R. L.; *Spectr. Chim. Act.*; A 71 (2009) 1814 – 1818
- [157] Nakamoto, K. *Infrared and Raman Spectra of Inorganic and Coordination Compounds*, 2nd Ed., Wiley: New York, Chichester, Brisbane, Toronto, Singapore, 1986, p. 255
- [158] Takahashi, K, Miyahara, J, Shibahara, Y, *Journ. Electrochem. Soc.*, 132, 6, 1985, pp. 1492 – 1494
- [159] Gaffey, S. J., *Americ. Min.*, 71, 1986, pp. 151 – 162
- [160] Lawson, K. E., *J. Chem. Phys.*, 44, 11, 1965, pp. 4159 - 4166
- [161] Rao, J.L., Narendra, G. L., Sreedhar, B, Lakshman, V. J., *Phys. Stat. Sol.*, b, 153, 1989, pp. 257 - 262
- [162] Satyanarayana, N, Radhakrishna, S, *Physica*, 138B, 1986, pp. 97 – 102
- [163] Gruen, D. M., *J. Am. Chem. Soc.*, 76, 8, 1954, pp. 2117 – 2120
- [164] <http://www.fluomin.org/uk/fiche.php?id=29&name=FLUORITE>, looked up on 20.11.2012
- [165] <http://www.fluomin.org/fr/fiche.php?id=157&name=CALCITE>, looked up on 20.11.2012
- [166] <http://www.fluomin.org/fr/fiche.php?id=475&name=MAGNESITE>, looked up on 20.11.2012
- [167] <http://www.fluomin.org/uk/fiche.php?id=784&name=chalcedony>, looked up on 20.11.2012

- [168] Okrusch, M., Matthes, S. *Mineralogie – Eine Einführung in die spezielle Mineralogie, Petrologie und Lagerstättenkunde*; 8. Ed., Springer: Berlin, Heidelberg, New York, 2009, p. 108

6 Appendix

6.1 Emission Correction function for the LS 55 with R955 PMT



x	y	x	y	x	y	x	y
200,0	0,10000001	210,5	0,10851153	220,5	0,11661773	231	0,12512925
200,5	0,10040532	211	0,10891684	221	0,11702304	231,5	0,12553456
201,0	0,10081063	211,5	0,10932215	221,5	0,11742835	232	0,12593987
201,5	0,10121594	212	0,10972746	222	0,11783366	232,5	0,12634518
202	0,10162125	212,5	0,11013277	222,5	0,11823897	233	0,12675049
202,5	0,10202656	213	0,11053808	223	0,11864428	233,5	0,1271558
203	0,10243187	213,5	0,11094339	223,5	0,11904959	234	0,12756111
203,5	0,10283718	214	0,1113487	224	0,1194549	234,5	0,12796642
204	0,10324249	214,5	0,11175401	224,5	0,11986021	235	0,12837173
204,5	0,1036478	215	0,11215932	225	0,12026552	235,5	0,12877704
205	0,10405311	215,5	0,11256463	225,5	0,12067084	236	0,12918235
205,5	0,10445842	216	0,11296994	226	0,12107615	236,5	0,12958766
206	0,10486373	216,5	0,11337525	226,5	0,12148146	237	0,12999297
206,5	0,10526904	217	0,11378056	227	0,12188677	237,5	0,13039828
207	0,10567435	217,5	0,11418587	227,5	0,12229208	238	0,13080359
207,5	0,10607966	218	0,11459118	228	0,12269739	238,5	0,1312089
208	0,10648497	218,5	0,11499649	228,5	0,1231027	239	0,13161421
208,5	0,10689028	219	0,1154018	229	0,12350801	239,5	0,13201952
209	0,1072956	219,5	0,11580711	229,5	0,12391332	240	0,13242483
209,5	0,10770091	220	0,11621242	230	0,12431863	240,5	0,13283014
210	0,10810622	220,5	0,11661773	230,5	0,12472394	241	0,13323545

x	y	x	y	x	y	x	y
241,5	0,13364076	262	0,15025849	282,5	0,16687621	303	0,18349393
242	0,13404608	262,5	0,1506638	283	0,16728152	303,5	0,18389924
242,5	0,13445139	263	0,15106911	283,5	0,16768683	304	0,18430455
243	0,1348567	263,5	0,15147442	284	0,16809214	304,5	0,18470986
243,5	0,13526201	264	0,15187973	284,5	0,16849745	305	0,18511517
244	0,13566732	264,5	0,15228504	285	0,16890276	305,5	0,18552048
244,5	0,13607263	265	0,15269035	285,5	0,16930807	306	0,18592579
245	0,13647794	265,5	0,15309566	286	0,16971338	306,5	0,1863311
245,5	0,13688325	266	0,15350097	286,5	0,17011869	307	0,18673641
246	0,13728856	266,5	0,15390628	287	0,170524	307,5	0,18714172
246,5	0,13769387	267	0,15431159	287,5	0,17092931	308	0,18754703
247	0,13809918	267,5	0,1547169	288	0,17133462	308,5	0,18795234
247,5	0,13850449	268	0,15512221	288,5	0,17173993	309	0,18835766
248	0,1389098	268,5	0,15552752	289	0,17214524	309,5	0,18876297
248,5	0,13931511	269	0,15593283	289,5	0,17255055	310	0,18916828
249	0,13972042	269,5	0,15633814	290	0,17295586	310,5	0,18957359
249,5	0,14012573	270	0,15674345	290,5	0,17336117	311	0,1899789
250	0,14053104	270,5	0,15714876	291	0,17376648	311,5	0,19038421
250,5	0,14093635	271	0,15755407	291,5	0,17417179	312	0,19078952
251	0,14134166	271,5	0,15795938	292	0,17457711	312,5	0,19119483
251,5	0,14174697	272	0,15836469	292,5	0,17498242	313	0,19160014
252	0,14215228	272,5	0,15877	293	0,17538773	313,5	0,19200545
252,5	0,14255759	273	0,15917531	293,5	0,17579304	314	0,19241076
253	0,1429629	273,5	0,15958062	294	0,17619835	314,5	0,19281607
253,5	0,14336821	274	0,15998593	294,5	0,17660366	315	0,19322138
254	0,14377352	274,5	0,16039124	295	0,17700897	315,5	0,19362669
254,5	0,14417883	275	0,16079655	295,5	0,17741428	316	0,194032
255	0,14458414	275,5	0,16120187	296	0,17781959	316,5	0,19443731
255,5	0,14498945	276	0,16160718	296,5	0,1782249	317	0,19484262
256	0,14539476	276,5	0,16201249	297	0,17863021	317,5	0,19524793
256,5	0,14580007	277	0,1624178	297,5	0,17903552	318	0,19565324
257	0,14620538	277,5	0,16282311	298	0,17944083	318,5	0,19605855
257,5	0,14661069	278	0,16322842	298,5	0,17984614	319	0,19646386
258	0,147016	278,5	0,16363373	299	0,18025145	319,5	0,19686917
258,5	0,14742131	279	0,16403904	299,5	0,18065676	320	0,19727448
259	0,14782663	279,5	0,16444435	300	0,18106207	320,5	0,19767979
259,5	0,14823194	280	0,16484966	300,5	0,18146738	321	0,1980851
260	0,14863725	280,5	0,16525497	301	0,18187269	321,5	0,19849041
260,5	0,14904256	281	0,16566028	301,5	0,182278	322	0,19889572
261	0,14944787	281,5	0,16606559	302	0,18268331	322,5	0,19930103
261,5	0,14985318	282	0,1664709	302,5	0,18308862	323	0,19970634

x	y	x	y	x	y	x	y
323,5	0,20011165	344	0,27098808	364,5	0,38958679	385	0,53759317
324	0,20051696	344,5	0,27272521	365	0,39465402	385,5	0,54023968
324,5	0,20092226	345	0,27451492	365,5	0,39950708	386	0,54260126
325	0,2034528	345,5	0,27663126	366	0,40321924	386,5	0,54406027
325,5	0,20570801	346	0,28014678	366,5	0,40767384	387	0,54580438
326	0,20677937	346,5	0,28280938	367	0,41256686	387,5	0,54666203
326,5	0,20820061	347	0,28489587	367,5	0,41673705	388	0,5475196
327	0,2103469	347,5	0,28581903	368	0,42030611	388,5	0,54860876
327,5	0,21265122	348	0,28704701	368,5	0,42381573	389	0,551424
328	0,21535717	348,5	0,2888714	369	0,4276312	389,5	0,55413936
328,5	0,21906251	349	0,29013199	369,5	0,43193139	390	0,556395
329	0,22190914	349,5	0,29068276	370	0,43613679	390,5	0,55811897
329,5	0,22332472	350	0,29137388	370,5	0,44120732	391	0,55982424
330	0,22444821	350,5	0,29168005	371	0,44696633	391,5	0,56015285
330,5	0,22529732	351	0,29412418	371,5	0,45215014	392	0,5604616
331	0,22705676	351,5	0,29500368	372	0,45626969	392,5	0,56114823
331,5	0,22899056	352	0,2961787	372,5	0,46018622	393	0,5627038
332	0,23046834	352,5	0,29786687	373	0,46391011	393,5	0,56447851
332,5	0,23420472	353	0,29841641	373,5	0,46741315	394	0,56568783
333	0,23673219	353,5	0,29926625	374	0,47044079	394,5	0,56679893
333,5	0,23922888	354	0,29934965	374,5	0,47386883	395	0,56799433
334	0,24224858	354,5	0,29980367	375	0,47777377	395,5	0,5690261
334,5	0,24407307	355	0,30126526	375,5	0,48138786	396	0,56988992
335	0,24637838	355,5	0,30262296	376	0,48518823	396,5	0,57093013
335,5	0,24699068	356	0,30485276	376,5	0,48944603	397	0,57238438
336	0,24674729	356,5	0,30712108	377	0,49308434	397,5	0,57405921
336,5	0,24690098	357	0,30832527	377,5	0,49650027	398	0,57549005
337	0,24673058	357,5	0,30925625	378	0,49981999	398,5	0,57639572
337,5	0,24743407	358	0,31015041	378,5	0,50291958	399	0,57710501
338	0,24913003	358,5	0,3109769	379	0,5059637	399,5	0,57808952
338,5	0,25045434	359	0,31727008	379,5	0,50897114	400	0,57865093
339	0,25207383	359,5	0,32770717	380	0,51200589	400,5	0,58057339
339,5	0,25276749	360	0,33482331	380,5	0,51484288	401	0,58326454
340	0,25382909	360,5	0,34157204	381	0,5171204	401,5	0,58521477
340,5	0,25550544	361	0,3474406	381,5	0,52088679	402	0,5860436
341	0,25768244	361,5	0,35334695	382	0,52449703	402,5	0,58693623
341,5	0,26051461	362	0,35916011	382,5	0,52674102	403	0,58688598
342	0,26442875	362,5	0,3653456	383	0,52944066	403,5	0,58607038
342,5	0,26768002	363	0,37183722	383,5	0,53180678	404	0,58532537
343	0,26932547	363,5	0,3781978	384	0,53385068	404,5	0,58601984
343,5	0,27018697	364	0,38436703	384,5	0,53533448	405	0,58772221

x	y	x	y	x	y	x	y
405,5	0,58944827	426	0,66414191	446,5	0,79548678	467	0,82158747
406	0,59140093	426,5	0,66520221	447	0,79682371	467,5	0,82352636
406,5	0,59392884	427	0,66496217	447,5	0,79803538	468	0,82546253
407	0,59599784	427,5	0,66552291	448	0,79926821	468,5	0,82785093
407,5	0,59775415	428	0,66794234	448,5	0,80040362	469	0,82993148
408	0,59902748	428,5	0,68302737	449	0,80151945	469,5	0,83159755
408,5	0,60090672	429	0,69501163	449,5	0,80278414	470	0,83258149
409	0,60261968	429,5	0,70308327	450	0,80392216	470,5	0,83413407
409,5	0,60313574	430	0,71100454	450,5	0,80516185	471	0,83588835
410	0,60411906	430,5	0,71917382	451	0,80640996	471,5	0,83767926
410,5	0,60430931	431	0,72749589	451,5	0,80749873	472	0,83980136
411	0,60508474	431,5	0,73429696	452	0,80845294	472,5	0,84239036
411,5	0,60653795	432	0,73956165	452,5	0,8088953	473	0,84468121
412	0,60889189	432,5	0,74363971	453	0,80917446	473,5	0,84707523
412,5	0,61255725	433	0,74851582	453,5	0,80981581	474	0,84873752
413	0,61509797	433,5	0,75342301	454	0,81018165	474,5	0,85142303
413,5	0,61711483	434	0,75756286	454,5	0,81037631	475	0,85350273
414	0,61982829	434,5	0,76089671	455	0,81070277	475,5	0,85585692
414,5	0,62185286	435	0,7642031	455,5	0,81101202	476	0,85835267
415	0,62459071	435,5	0,76636456	456	0,8114193	476,5	0,86131364
415,5	0,62756784	436	0,7683568	456,5	0,81140988	477	0,86376876
416	0,63025455	436,5	0,7694038	457	0,81154456	477,5	0,86677686
416,5	0,63303692	437	0,77156028	457,5	0,81205189	478	0,86941082
417	0,63438445	437,5	0,77336645	458	0,81215328	478,5	0,87248389
417,5	0,63609817	438	0,77497163	458,5	0,81212197	479	0,87527903
418	0,63753225	438,5	0,77677324	459	0,81253141	479,5	0,87779526
418,5	0,63984394	439	0,77842128	459,5	0,81278389	480	0,88059277
419	0,64344801	439,5	0,78025927	460	0,813136	480,5	0,88359554
419,5	0,64621152	440	0,78231565	460,5	0,81345345	481	0,88634683
420	0,64804053	440,5	0,78351898	461	0,81384278	481,5	0,88967538
420,5	0,65070405	441	0,78458577	461,5	0,81449844	482	0,89308983
421	0,65252769	441,5	0,78519551	462	0,81495622	482,5	0,8965421
421,5	0,65364521	442	0,78596309	462,5	0,81516916	483	0,90033388
422	0,65496565	442,5	0,78692342	463	0,81526757	483,5	0,90367248
422,5	0,65810709	443	0,78764464	463,5	0,8154997	484	0,90711665
423	0,66072169	443,5	0,78868584	464	0,81559412	484,5	0,90981903
423,5	0,66173749	444	0,78986865	464,5	0,81626277	485	0,91247787
424	0,66329449	444,5	0,79075931	465	0,81723603	485,5	0,91546812
424,5	0,66446492	445	0,79172027	465,5	0,81817732	486	0,91908887
425	0,66458841	445,5	0,7929377	466	0,81916644	486,5	0,92271361
425,5	0,66428902	446	0,7942865	466,5	0,8200904	487	0,92639404

x	y	x	y	x	y	x	y
487,5	0,92932888	508	0,98957074	528,5	0,99338588	549	0,93929354
488	0,93261875	508,5	0,99182092	529	0,99291063	549,5	0,93822099
488,5	0,93499035	509	0,99261146	529,5	0,99186082	550	0,9370588
489	0,9371212	509,5	0,99260836	530	0,99059967	550,5	0,93580876
489,5	0,93961043	510	0,99290366	530,5	0,9897766	551	0,93434914
490	0,94210943	510,5	0,99248663	531	0,98899595	551,5	0,93372238
490,5	0,94448909	511	0,99123934	531,5	0,98730991	552	0,93273088
491	0,94640872	511,5	0,99186143	532	0,98623749	552,5	0,93147543
491,5	0,9476274	512	0,99296395	532,5	0,98548104	553	0,93069876
492	0,94991885	512,5	0,99402527	533	0,98524476	553,5	0,93007349
492,5	0,95153587	513	0,99477048	533,5	0,98500265	554	0,92816125
493	0,952717	513,5	0,99591097	534	0,98431891	554,5	0,92614182
493,5	0,95428916	514	0,99617767	534,5	0,98322941	555	0,92428908
494	0,95562412	514,5	0,99570785	535	0,98165809	555,5	0,92192555
494,5	0,95662233	515	0,99515938	535,5	0,97939523	556	0,92022152
495	0,95765247	515,5	0,99563943	536	0,97734214	556,5	0,91908409
495,5	0,95822546	516	0,99589975	536,5	0,97595005	557	0,9181633
496	0,95923085	516,5	0,99554797	537	0,97501676	557,5	0,91678182
496,5	0,96025009	517	0,99588712	537,5	0,97498493	558	0,91560898
497	0,96133252	517,5	0,99616987	538	0,97444204	558,5	0,91489905
497,5	0,96288895	518	0,99623492	538,5	0,97343923	559	0,91439865
498	0,96496044	518,5	0,99678348	539	0,97265007	559,5	0,91312885
498,5	0,96664175	519	0,99775986	539,5	0,97150879	560	0,91257552
499	0,96917266	519,5	0,99863138	540	0,96965826	560,5	0,91088185
499,5	0,97119241	520	0,99946674	540,5	0,96846323	561	0,90870027
500	0,97403768	520,5	0,999917	541	0,96696707	561,5	0,90672681
500,5	0,97826891	521	0,99994357	541,5	0,96616944	562	0,9045347
501	0,98330085	521,5	1	542	0,96453189	562,5	0,90265292
501,5	0,98582558	522	0,99948841	542,5	0,96274395	563	0,90172423
502	0,98802851	522,5	0,99904763	543	0,96191734	563,5	0,8999268
502,5	0,98970453	523	0,99879539	543,5	0,96061479	564	0,89807896
503	0,99109571	523,5	0,99849626	544	0,95920872	564,5	0,89510217
503,5	0,9906279	524	0,99807468	544,5	0,95825909	565	0,89271822
504	0,99054831	524,5	0,99758524	545	0,95639883	565,5	0,89024962
504,5	0,99159303	525	0,99734422	545,5	0,95510199	566	0,88701336
505	0,99220256	525,5	0,99720147	546	0,95313426	566,5	0,88475604
505,5	0,99051946	526	0,99655815	546,5	0,95108829	567	0,88351098
506	0,99001876	526,5	0,99609374	547	0,94895015	567,5	0,881133
506,5	0,98959168	527	0,99598566	547,5	0,94652785	568	0,87921986
507	0,9890121	527,5	0,99537412	548	0,94416624	568,5	0,87763952
507,5	0,98856745	528	0,9946039	548,5	0,94177078	569	0,87627495

x	y	x	y	x	y	x	y
569,5	0,87473392	590	0,77461699	610,5	0,69647516	631	0,61546999
570	0,87198433	590,5	0,77208583	611	0,69592488	631,5	0,61346841
570,5	0,86936626	591	0,76937811	611,5	0,69293872	632	0,61157311
571	0,86694708	591,5	0,76670762	612	0,69083567	632,5	0,60926058
571,5	0,86381157	592	0,76229151	612,5	0,68975422	633	0,60757064
572	0,86103442	592,5	0,75941551	613	0,68907131	633,5	0,60614211
572,5	0,85876809	593	0,75710474	613,5	0,68849249	634	0,60382029
573	0,85607276	593,5	0,7549342	614	0,68862091	634,5	0,60151119
573,5	0,85353594	594	0,75240077	614,5	0,68534709	635	0,59908909
574	0,85028439	594,5	0,75101202	615	0,68214134	635,5	0,59540083
574,5	0,84679051	595	0,74934642	615,5	0,68147713	636	0,59164515
575	0,84414396	595,5	0,747443	616	0,68098258	636,5	0,59065795
575,5	0,84316124	596	0,74517542	616,5	0,67809951	637	0,58967585
576	0,84128642	596,5	0,74432215	617	0,67553139	637,5	0,58766428
576,5	0,83853238	597	0,74240549	617,5	0,67378072	638	0,58506191
577	0,83496869	597,5	0,74107856	618	0,6717841	638,5	0,58134794
577,5	0,83165409	598	0,7402797	618,5	0,66720925	639	0,57768402
578	0,8292567	598,5	0,73638311	619	0,66360967	639,5	0,57582908
578,5	0,82650169	599	0,73481973	619,5	0,66189848	640	0,57482352
579	0,82427942	599,5	0,73368828	620	0,66095916	640,5	0,57298523
579,5	0,8240997	600	0,73228161	620,5	0,6593932	641	0,57083314
580	0,82259124	600,5	0,72925532	621	0,65848722	641,5	0,57011501
580,5	0,81944556	601	0,72662252	621,5	0,65743958	642	0,56866488
581	0,81617982	601,5	0,72231519	622	0,65571756	642,5	0,56391976
581,5	0,81358714	602	0,71893299	622,5	0,65349849	643	0,55975168
582	0,81253161	602,5	0,7178324	623	0,65113899	643,5	0,55827537
582,5	0,81092228	603	0,71774234	623,5	0,64779128	644	0,55696742
583	0,80918959	603,5	0,71715464	624	0,64540404	644,5	0,55486183
583,5	0,80835986	604	0,71606747	624,5	0,64356557	645	0,55290461
584	0,80724644	604,5	0,71335187	625	0,64184439	645,5	0,54954845
584,5	0,80434819	605	0,71118451	625,5	0,64051255	646	0,54643536
585	0,80118419	605,5	0,71070014	626	0,63930243	646,5	0,54365787
585,5	0,79840197	606	0,71056614	626,5	0,63698865	647	0,54084088
586	0,79638309	606,5	0,70805009	627	0,6337415	647,5	0,53808688
586,5	0,79412478	607	0,70471279	627,5	0,63020066	648	0,53535218
587	0,79180315	607,5	0,70337348	628	0,62751887	648,5	0,53276871
587,5	0,78946722	608	0,70231882	628,5	0,62591307	649	0,52995311
588	0,78687961	608,5	0,69917919	629	0,62428808	649,5	0,52835212
588,5	0,7834166	609	0,69665487	629,5	0,62365497	650	0,52735027
589	0,78064497	609,5	0,69691986	630	0,62280069	650,5	0,52354548
589,5	0,77808803	610	0,69712509	630,5	0,6195407	651	0,51949896

x	y	x	y	x	y	x	y
651,5	0,51762594	672	0,41996585	692,5	0,34662317	713	0,30334257
652	0,51493878	672,5	0,418343	693	0,34395031	713,5	0,30195234
652,5	0,51220786	673	0,41617892	693,5	0,34439339	714	0,29943126
653	0,51000472	673,5	0,41387729	694	0,34466448	714,5	0,29655853
653,5	0,50712114	674	0,41153193	694,5	0,34370933	715	0,29113679
654	0,50346637	674,5	0,40833641	695	0,34262399	715,5	0,28940514
654,5	0,50154226	675	0,40579048	695,5	0,34126215	716	0,28929235
655	0,49965706	675,5	0,404173	696	0,33865475	716,5	0,28647343
655,5	0,49560226	676	0,40213725	696,5	0,33758003	717	0,28403835
656	0,49217514	676,5	0,39955626	697	0,33665644	717,5	0,2845175
656,5	0,49125604	677	0,39776025	697,5	0,33393246	718	0,28383367
657	0,48978098	677,5	0,39586873	698	0,33085498	718,5	0,27950783
657,5	0,48645855	678	0,39403116	698,5	0,32864257	719	0,27567601
658	0,48296907	678,5	0,39290018	699	0,32679873	719,5	0,27682827
658,5	0,47929994	679	0,39158957	699,5	0,32551716	720	0,27857326
659	0,47519963	679,5	0,38886871	700	0,3249992	720,5	0,27911966
659,5	0,47200553	680	0,38645026	700,5	0,32658129	721	0,28064649
660	0,46916755	680,5	0,38466472	701	0,32777531	721,5	0,2800922
660,5	0,46740837	681	0,3827873	701,5	0,32725236	722	0,27894781
661	0,46657649	681,5	0,38205699	702	0,32632654	722,5	0,27751121
661,5	0,46307351	682	0,38183135	702,5	0,32327231	723	0,27724215
662	0,45970032	682,5	0,37871574	703	0,32027738	723,5	0,27536396
662,5	0,45808897	683	0,37554937	703,5	0,32136386	724	0,27331927
663	0,45650031	683,5	0,37428823	704	0,32237538	724,5	0,2744369
663,5	0,45516194	684	0,37266022	704,5	0,31993323	725	0,27536169
664	0,45314005	684,5	0,37068274	705	0,31571837	725,5	0,26972396
664,5	0,45088701	685	0,36971031	705,5	0,31343651	726	0,26518003
665	0,44895068	685,5	0,36801031	706	0,31128361	726,5	0,26733064
665,5	0,4448571	686	0,36646342	706,5	0,30895477	727	0,26843919
666	0,44096362	686,5	0,36517155	707	0,30890841	727,5	0,26527322
666,5	0,43991595	687	0,36398455	707,5	0,31018955	728	0,26357003
667	0,43932909	687,5	0,36234075	708	0,31108616	728,5	0,26367556
667,5	0,43758499	688	0,36084495	708,5	0,3093768	729	0,26394444
668	0,4358635	688,5	0,35749145	709	0,30743201	729,5	0,26346416
668,5	0,43399499	689	0,35449607	709,5	0,30719473	730	0,26164468
669	0,43074921	689,5	0,35492102	710	0,30566761	730,5	0,25998896
669,5	0,42871658	690	0,35580121	710,5	0,30642759	731	0,25600533
670	0,42738076	690,5	0,35489473	711	0,30754561	731,5	0,25182393
670,5	0,424096	691	0,35363693	711,5	0,30359769	732	0,24759435
671	0,42175227	691,5	0,35156672	712	0,30058804	732,5	0,24715566
671,5	0,42118099	692	0,3492493	712,5	0,30223054	733	0,24671639

x	y	x	y	x	y	x	y
733,5	0,24627712	754	0,22826711	774,5	0,2102571	795	0,19224709
734	0,24583785	754,5	0,22782784	775	0,20981783	795,5	0,19180782
734,5	0,24539858	755	0,22738857	775,5	0,20937856	796	0,19136856
735	0,24495931	755,5	0,2269493	776	0,2089393	796,5	0,19092929
735,5	0,24452004	756	0,22651004	776,5	0,20850003	797	0,19049002
736	0,24408078	756,5	0,22607077	777	0,20806076	797,5	0,19005075
736,5	0,24364151	757	0,2256315	777,5	0,20762149	798	0,18961148
737	0,24320224	757,5	0,22519223	778	0,20718222	798,5	0,18917221
737,5	0,24276297	758	0,22475296	778,5	0,20674295	799	0,18873295
738	0,2423237	758,5	0,22431369	779	0,20630369	799,5	0,18829368
738,5	0,24188443	759	0,22387443	779,5	0,20586442	800	0,18785441
739	0,24144517	759,5	0,22343516	780	0,20542515	800,5	0,18741514
739,5	0,2410059	760	0,22299589	780,5	0,20498588	801	0,18697587
740	0,24056663	760,5	0,22255662	781	0,20454661	801,5	0,1865366
740,5	0,24012736	761	0,22211735	781,5	0,20410734	802	0,18609733
741	0,23968809	761,5	0,22167808	782	0,20366807	802,5	0,18565807
741,5	0,23924882	762	0,22123881	782,5	0,20322881	803	0,1852188
742	0,23880955	762,5	0,22079955	783	0,20278954	803,5	0,18477953
742,5	0,23837029	763	0,22036028	783,5	0,20235027	804	0,18434026
743	0,23793102	763,5	0,21992101	784	0,201911	804,5	0,18390099
743,5	0,23749175	764	0,21948174	784,5	0,20147173	805	0,18346172
744	0,23705248	764,5	0,21904247	785	0,20103246	805,5	0,18302245
744,5	0,23661321	765	0,2186032	785,5	0,20059319	806	0,18258319
745	0,23617394	765,5	0,21816393	786	0,20015393	806,5	0,18214392
745,5	0,23573467	766	0,21772467	786,5	0,19971466	807	0,18170465
746	0,23529541	766,5	0,2172854	787	0,19927539	807,5	0,18126538
746,5	0,23485614	767	0,21684613	787,5	0,19883612	808	0,18082611
747	0,23441687	767,5	0,21640686	788	0,19839685	808,5	0,18038684
747,5	0,2339776	768	0,21596759	788,5	0,19795758	809	0,17994758
748	0,23353833	768,5	0,21552832	789	0,19751832	809,5	0,17950831
748,5	0,23309906	769	0,21508906	789,5	0,19707905	810	0,17906904
749	0,2326598	769,5	0,21464979	790	0,19663978	810,5	0,17862977
749,5	0,23222053	770	0,21421052	790,5	0,19620051	811	0,1781905
750	0,23178126	770,5	0,21377125	791	0,19576124	811,5	0,17775123
750,5	0,23134199	771	0,21333198	791,5	0,19532197	812	0,17731196
751	0,23090272	771,5	0,21289271	792	0,1948827	812,5	0,1768727
751,5	0,23046345	772	0,21245344	792,5	0,19444344	813	0,17643343
752	0,23002418	772,5	0,21201418	793	0,19400417	813,5	0,17599416
752,5	0,22958492	773	0,21157491	793,5	0,1935649	814	0,17555489
753	0,22914565	773,5	0,21113564	794	0,19312563	814,5	0,17511562
753,5	0,22870638	774	0,21069637	794,5	0,19268636	815	0,17467635

x	y	x	y	x	y	x	y
815,5	0,17423708	836	0,15622708	856,5	0,13821707	877	0,12020706
816	0,17379782	836,5	0,15578781	857	0,1377778	877,5	0,11976779
816,5	0,17335855	837	0,15534854	857,5	0,13733853	878	0,11932852
817	0,17291928	837,5	0,15490927	858	0,13689926	878,5	0,11888925
817,5	0,17248001	838	0,15447	858,5	0,13645999	879	0,11844999
818	0,17204074	838,5	0,15403073	859	0,13602073	879,5	0,11801072
818,5	0,17160147	839	0,15359147	859,5	0,13558146	880	0,11757145
819	0,17116221	839,5	0,1531522	860	0,13514219	880,5	0,11713218
819,5	0,17072294	840	0,15271293	860,5	0,13470292	881	0,11669291
820	0,17028367	840,5	0,15227366	861	0,13426365	881,5	0,11625364
820,5	0,1698444	841	0,15183439	861,5	0,13382438	882	0,11581437
821	0,16940513	841,5	0,15139512	862	0,13338511	882,5	0,11537511
821,5	0,16896586	842	0,15095585	862,5	0,13294585	883	0,11493584
822	0,16852659	842,5	0,15051659	863	0,13250658	883,5	0,11449657
822,5	0,16808733	843	0,15007732	863,5	0,13206731	884	0,1140573
823	0,16764806	843,5	0,14963805	864	0,13162804	884,5	0,11361803
823,5	0,16720879	844	0,14919878	864,5	0,13118877	885	0,11317876
824	0,16676952	844,5	0,14875951	865	0,1307495	885,5	0,11273949
824,5	0,16633025	845	0,14832024	865,5	0,13031023	886	0,11230023
825	0,16589098	845,5	0,14788097	866	0,12987097	886,5	0,11186096
825,5	0,16545171	846	0,14744171	866,5	0,1294317	887	0,11142169
826	0,16501245	846,5	0,14700244	867	0,12899243	887,5	0,11098242
826,5	0,16457318	847	0,14656317	867,5	0,12855316	888	0,11054315
827	0,16413391	847,5	0,1461239	868	0,12811389	888,5	0,11010388
827,5	0,16369464	848	0,14568463	868,5	0,12767462	889	0,10966462
828	0,16325537	848,5	0,14524536	869	0,12723536	889,5	0,10922535
828,5	0,1628161	849	0,1448061	869,5	0,12679609	890	0,10878608
829	0,16237684	849,5	0,14436683	870	0,12635682	890,5	0,10834681
829,5	0,16193757	850	0,14392756	870,5	0,12591755	891	0,10790754
830	0,1614983	850,5	0,14348829	871	0,12547828	891,5	0,10746827
830,5	0,16105903	851	0,14304902	871,5	0,12503901	892	0,107029
831	0,16061976	851,5	0,14260975	872	0,12459974	892,5	0,10658974
831,5	0,16018049	852	0,14217048	872,5	0,12416048	893	0,10615047
832	0,15974122	852,5	0,14173122	873	0,12372121	893,5	0,1057112
832,5	0,15930196	853	0,14129195	873,5	0,12328194	894	0,10527193
833	0,15886269	853,5	0,14085268	874	0,12284267	894,5	0,10483266
833,5	0,15842342	854	0,14041341	874,5	0,1224034	895	0,10439339
834	0,15798415	854,5	0,13997414	875	0,12196413	895,5	0,10395412
834,5	0,15754488	855	0,13953487	875,5	0,12152486	896	0,10351486
835	0,15710561	855,5	0,1390956	876	0,1210856	896,5	0,10307559
835,5	0,15666634	856	0,13865634	876,5	0,12064633	897	0,10263632

x	y
897,5	0,10219705
898	0,10175778
898,5	0,10131851
899	0,10087925
899,5	0,10043998
900	0,10000071